CRANFIELD UNIVERSITY

College of Aeronautics

Flow Control and Prediction Technology Group
Engineering Doctorate

Academic Year 1998-1999

Andrew Shires

Analysis and prediction of the low speed flow over a highly swept wing

Academic supervisor: Dr K P Garry
DERA supervisor: Prof J L Fulker

November 2000

Acknowledgements

I wish to thank friends and colleagues at DERA Bedford for their assistance and support in producing this thesis; in particular Mr John Fulker and Dr Pat Ashill for their guidance, ideas and support; Mr John Betterton for his optics expertise, workshop staff and 13ft x 9ft wind tunnel technicians; and the Ministry of Defence for funding the work.

Additionally, I would like to thank my tutor Dr Kevin Garry for his patience and guidance; Mr Andrew Bytheway and Dr Robina Chatham of the Cranfield School of Management for their assistance in writing the non technical aspect of this thesis.

Finally, my sincere gratitude to my wife Phillippa, for her moral and practical support.

Summary

A combined experimental and theoretical study is described of the low speed flow over a highly swept and cambered wing that simulates the flow features of a transonic manoeuvre condition. The thesis is divided into two parts:

Part I examines the research objectives from a customer perspective, with background information on the project history and funding sources. Since the research is aimed at improving the aerodynamic performance of low observable configurations, stealth technologies are discussed and their implications for combat aircraft wing flows. The management chapter of the thesis then discusses the influences affecting the decision making process for the acquisition of weapon systems in the UK.

Part II describes the design of a highly swept and cambered wing that generates strong adverse pressure gradients near the trailing edge, leading to three-dimensional separations in this region. Using surface flow visualisation the nature of these flows is defined, indicating how the position of a separated streamline moves forward with increasing angle of incidence. These observations are confirmed by flow predictions using the SAUNA Computational Fluid Dynamics (CFD) method that solves the Reynolds Averaged Navier-Stokes equations, employing a two-equation turbulence model. The mechanism of the flow separation is also predicted using CFD, indicating that a separated stream surface reattaches at the wing trailing edge, forming a 'tunnel' of separated flow. To the authors knowledge this represents the first time that the main physical features of such a complex three-dimensional separated flow has been modelled using a CFD method. From an evaluation of the CFD methods employed, a design process has been proposed by which a wing designer can determine if wing flows over similar configurations remain attached.

Additionally, the velocity magnitudes within parts of the separated shear layers and the wake are obtained using an optical non-intrusive measurement technique and give good agreement with the theory.

Contents

PART I – A customer perspective

List of Tables

List of Figures

Notation

Symbols

A_T	cross-sectional area of wind tunnel
c	wing chord
C_D	drag coefficient
C_f	local skin friction coefficient
C_L	lift coefficient
C_p	pressure coefficient
D	dimension of the first grid point from the surface of the wing
K	kinetic turbulent energy
M	Mach number
Re_c	Reynolds number, based on wing chord
s	wing semi-span
S	wing area
t	wing thickness
V	freestream speed
x, y, z	cartesian co-ordinates (see figure 7-1)
u, v, w	velocity components in the x, y, z cartesian directions
Vm	wind tunnel model volume
y^+	non-dimensional boundary layer dimension normal to the wing surface
α	angle of incidence
β	$=\sqrt{1-M^2}$
β_i	angle between freestream and inviscid flow directions
β_v	angle between inviscid and viscous flow directions

Δ	incremental part of
Λ	wing leading-edge sweep
ν	kinematic viscosity
ε_1	wind tunnel solid blockage factor
ε_2	wind tunnel wake blockage factor
μ	laminar viscosity
μ_t	turbulent viscosity
θ	angular deflection of the wing section camber line
∞	conditions far upstream

Abbreviations

2D	two-dimensional
3D	three-diemsional
BAe	British Aerospace Plc.
CFD	Computational Fluid Dynamics
DERA	Defence Evaluation and Research Agency
MoD	Ministry of Defence
OFF	offset
SAUNA	Structured and Unstructured Numerical Analysis
TE	trailing edge
UK	United Kingdom
VFPST	Viscous Full-Potential method for swept and Tapered wings
VII	Viscous-Inviscid Interaction procedure

PART I – A customer perspective

1 Customer requirements

1.1 The Future Offensive Air System

For the period post 2015 a continuing need is foreseen to deliver weapons on to surface targets from airborne platforms. The Tornado GR4 currently fulfils the long-range offensive role but is scheduled for withdrawal from service by 2015-2018 due to a combination of attrition, fatigue and supportability. The Future Offensive Air System (FOAS) will be tasked with similar roles to the Tornado GR4, to complement those of the Typhoon (Eurofighter), *i.e.*;

- Air Interdiction
- Battlefield Air Interdiction
- Offensive Counter Air
- Anti-Surface Warfare
- Suppression of Enemy Defences
- Tactical Reconnaissance
- Close Air Support

The UK Ministry of Defence (MoD) has launched a £35 million feasibility study, following the endorsement of Staff Target ST(A) 425 describing the primary attributes and broad requirements of FOAS for an in service date of 2017. Possible concepts that could fulfil the FOAS role under consideration are;

- Development of a new manned aircraft
- Development of an unmanned air combat vehicle (UCAV)
- Off-the–shelf aircraft
- Conventional air launched cruise missiles (CALCM) released from a large, non-penetrating aircraft

The MoD has requested the Defence Evaluation and Research Agency (DERA) and industry to assess key technologies to support the next generation of combat air system for both the Royal Air Force (*i.e.* FOAS) and Royal Navy (a Future Carrier Borne Aircraft). In particular, all aspects of stealth and agility need to be improved and platforms will require increased range to facilitate tactical/deception routing and enable longer-range targets to be attacked. Additionally, all offensive aircraft will need to be capable of operating, to some degree, in the air defence role. Stealth considerations are pervasive to this research, and trade-offs between stealth characteristics and aerodynamic range and performance are considered.

1.2 The work programme

The majority of work described in this thesis has been funded by the MoD Applied Research Programme (ARP), package 7b, research objective 3 on 'Combat Aircraft Wing Flows'[1]. The research package is part of the FOAS feasibility study, aimed at providing enabling technologies, particularly for stealthy wings with high leading and trailing edge sweep, and is divided into the following assignments;

- Study and control of leading-edge flows on highly swept wings
- Study and control of trailing-edge flows on highly swept wings
- Study of the buffeting characteristics of combat aircraft wings
- The study of scale effects on moderately swept leading and trailing edges
- The study of stealthy lateral controls

The assignment on highly swept trailing edge flows began in April 1995 with the design and manufacture of a variable sweep panel wing model and finished in February 1998. The ARP involved experimental and theoretical studies of flows around this wing aimed at understanding the flow mechanism, attempts to predict the onset of trailing edge separation and methods of controlling flow breakdown. The work on controlling separation using vortex generators is not within the scope of this thesis and is reported elsewhere[2]. The ARP identified a complex, three-dimensional flow regime in the trailing edge region of the model that provided a challenging test case to state of the art Computational Fluid Dynamics (CFD) methods. Subsequently, an MoD Corporate Research Programme (CRP) assignment on the 'Validation of CFD', which began in April 1998, included a study of the flow about this wing and part funded the work described in this thesis[3]. Unlike the ARP, the CRP is aimed at providing MoD with basic or underpinning research that is not linked to specific procurement programmes. The CRP has provided flow field velocities using a novel non-intrusive measurement technique to validate CFD calculations performed under both ARP and CRP programmes Since April 1999, the author has also been responsible for the project management of the CRP assignment.

1.3 The need for stealth technologies

Before the first airstrike of the gulf war by ten F-117A tactical fighters, a US Air Force pilot remarked: 'Bats were the first visual proof I had that stealth really worked..... In the morning we'd find bat corpses scattered around our airplanes inside open hangers'[4]. Stealth technology proved just as effective against SAM defensive radar as it was against that of the bats. The F-117A could release its laser guided bomb at 20km whereas its maximum detection range is 17km giving an obvious advantage over conventional aircraft. Stealth research arose from a Pentagon meeting in July 1975 which discussed Russian technical advances in early-warning radar systems. Russia deployed 16 different missile systems, capable of detecting intruding aircraft from hundreds of miles away, and able to engage both low flying attack fighters and cruise missiles at the same time. This compared to the 2 defensive ground-to-air systems operated by the US. Most alarming was that Russia was exporting its advanced non-nuclear defensive systems around the world. During the 1973 Yom Kippur war, the Israelis, equipped with the latest and most advanced attack fighters from the US, and with highly trained pilots, lost 109 aircraft in 18 days, mostly to radar-guided ground-to-air missiles and anti-aircraft batteries manned by relatively under trained Egyptian and Syrian personnel. Understandably, this was a major concern for the US administration.

A solution provided by the Skunk Works (the Lockheed Advanced Development Company), was to make the amount of electromagnetic energy reflected from a target infinitesimally small, so as to be virtually invisible on radar. The Skunk Works designed an aircraft, the 'Have Blue', composed entirely of flat angular surfaces (effectively a diamond shape, bevelled in four directions). The prototype, from which the F-117A was derived, first flew in

December 1977. Although some benefits are gained by using composite materials that can absorb radar, a significant factor to the F-117A's success is its unorthodox geometry (figure 1-1).

1.4 Aerodynamic considerations

The external shape of aircraft has traditionally been defined by aerodynamic considerations and the requirements for available internal volume, structural integrity and effective control surfaces. The advent of stealth introduced aircraft shapes that would never be considered on the grounds described previously. For example, the multiple flat facets covering the F-117A significantly increase the risk of flow separation at the facet edges. At the time the F-117 was designed, the governing Maxwell equations could only be solved for flat surfaces due to limitations in computer capability. Nowadays, Maxwell's equations can be solved for smooth, curved surfaces, hence the US B-2 bomber depicted in figure 1-2. Despite its smooth shape, the B-2 with its highly swept leading and trailing edges, wing-body blending and lack of fins poses considerable aerodynamic and control challenges.

The research described in this thesis is focused on theoretical and experimental studies of flows over a stealthy wing planform with leading and trailing edge sweeps that differ from those currently used. These configurations represent a high risk from the aerodynamic standpoint in that the flows are complex, prone to boundary layer separation and susceptible to scale or Reynolds number effects. Consequently, at present, the full-scale characteristics of stealthy aircraft cannot be predicted with confidence either by Computational Fluid Dynamics (CFD) or from wind-tunnel tests. The likelihood of such separation increases if trailing-edge flaps are deployed or, more generally, if wing camber is increased. In addition, the problem is exacerbated at high subsonic speeds by the presence of a shock wave on the upper surface. These separations will increase drag significantly and degrade the buffet characteristics of the aircraft. Wing efficiency governs the combat performance of aircraft, consequently improvements in wing design will lead to significant reductions in aircraft drag and improved buffet performance. These improvements are only achieved by research aimed at developing an understanding of complex wing flows, by exploring experimentally, the fundamental mechanisms of wing flows and the experimental validation of CFD techniques to identify where the modelling of the flow physics is inadequate. This research is aimed at gaining significant improvements in both buffet and drag characteristics of wings, thus allowing better payload fraction/range and/or enhanced aircraft agility.

In addition to the military implications of this research, to increase the productivity of conventional civil aircraft, especially on long range routes, an increase in cruise Mach number is required (currently aiming for about 0.9)[5]. From an aerodynamic standpoint, this implies an increase in wing sweep. The trailing-edge sweep of civil aircraft is restricted by the need to ensure that the flow is attached at all critical design points and that there are sufficient margins before significant separation occurs at off-design points. Since trailing edge sweep would, by necessity, be more highly swept than current aircraft, this area of the wing flow needs to be studied in detail if the potential for a significant increase in aircraft cruise speed is to be exploited. Concepts are often borrowed from the study of two-dimensional flows to predict separations, which can lead to erroneous results. Therefore, a more detailed

understanding of these flows and the capability of CFD methods to predict these flows are required.

2 Strategic analysis of the cost problem of future weapon systems for the UK armed forces *(management chapter).*

2.1 Introduction

This management chapter examines the influences affecting the decision making process for acquiring weapon systems. In the present post cold war scenario the lack of a direct threat to national security makes the acquisition of new equipment for the armed forces hard to justify in the face of competition from other areas of public spending, and also the requirements more difficult to define. The government spends large sums of public funds on the acquisition of weapon systems each year for which it must be accountable. Therefore, the ability to review strategic directions, the decision making process and how procurement strategies are implemented must be managed effectively. The management of UK defence procurement strategies is the responsibility of the Defence Council of the Ministry of Defence (MoD) which is chaired by the Secretary of State for Defence. The stated aim of defence procurement is "to meet the operational requirements of the armed forces in the timescale in which the equipment is needed, and at minimum overall cost to the defence budget."

The acquisition process should involve the three sequential stages depicted in the table below, showing the key factors that need to be understood at each stage[6]:

Strategic analysis	Strategic choice	Strategic implementation
♦ The environment ♦ Culture and stakeholder expectations ♦ Resources and strategic capability	♦ Identifying strategic options ♦ Evaluating options ♦ Selecting strategy	♦ Planning and allocating resources ♦ Organisation, structure and design ♦ Managing strategic change

Strategic analysis is concerned with understanding the position of the UK government in terms of its military obligations to NATO, the United Nations (UN) and its citizens; its budgetary constraints; the relationships between its numerous stakeholders; and the strength of its defence industrial base (DIB), amongst other factors. The aim of strategic analysis is to form a view of the key influences on the present and future procurement requirements and, therefore, on the choice of strategy for acquiring them.

The government has a number of options open to it in procuring military equipment for its forces; purchasing from its domestic industrial base; licensed production from outside the country; international collaboration and international competition. The arguments for local procurement tends to be more political than economic in nature, in order to protect its domestic industrial base, for security reasons or to ensure guaranteed supply. This has become

increasingly difficult for countries to justify and economic considerations now tend to out weigh many political and military arguments previously used to support procurement strategies. Countries such as France (Rafale), Sweden (Gripen) and the US (F-117, F-22, B-2 etc) have traditionally developed and produced combat aircraft using their domestic industrial bases, though escalating costs will probably prohibit such strategies for the next generation of combat aircraft, even in the US. The UK, along with many other European nations, (Tornado, Typhoon) has moved towards international collaboration in order to share development and production costs. China has licensed the production of the Flanker from Russia due to its lack of technical capability, despite the long-term threat this poses to Russia. World-wide a number of alternative strategic directions are evident, not all of which are sustainable. The strategy will depend on the commercial, economic, political, technological, cultural and social environment and the capabilities of its industrial base. Once these factors are clearly understood various options can be formulated and evaluated.

Procuring weapon systems can be extremely complex to implement, involving large numbers of resources, with lead times of up to 30 years and high technical risk. Managing this process and ensuring that quality, costs and time-scales are maintained poses many problems. Governments are likely to change during the procurement process bringing different viewpoints and therefore, changes in strategic direction. For example, the rise to the fore of the Green party in the re-unified Germany threatened the future of its procurement programme for the EF2000, consequently affecting its procurement within partner nations, including the UK.

This chapter will focus on the strategic analysis of the issues pertinent to the UK, particularly for the procurement of combat aircraft such as FOAS. It will examine the environment and the complex relationships between various stakeholders; the armed services, politicians and civil servants, scientists and engineers, foreign governments and its own citizens. Additionally, it will consider the capabilities of its domestic industrial base and research establishments. To conclude, the author will attempt to justify the present strategic direction of the UK government and suggest how this might change for the procurement of next generation weapon systems. Although this chapter draws on authoritative documents, the views expressed are those of the author and may not correspond with MoD policy.

2.2 Strategic environment

Before examining the environmental issues, it is necessary to consider the historical events that have shaped defence procurement in the UK and its current positioning in the world export market.

2.2.1 Historical perspective

Prior to the Second World War, the MoD was self-reliant in terms of the control and management of its equipment procurement, requiring a large staff of civilian and military personnel. This was justified, mainly for reasons of security and a lack of external expertise. Much development, testing and verification work was carried out in-house using establishments such as the Royal Aircraft Factory, the predecessor to the Defence Evaluation and Research Agency (DERA). The management style of the era did little to promote

competition, contracts were issued on a cost plus basis and all procurement programmes and supporting services were manned and managed by MoD staff. Industry's role was solely that of producer, with contract arrangements providing no incentive to limit expenditure and allowing the MoD to interfere and make changes to the specification during a project. After the Second World War, adjustments to peacetime levels of demand led to over-capacity and the inevitable rationalisation of the industry resulting in the formation of a small number of large company's better able to benefit from economies of scale.

During the period 1950's to 1970's equipment was still tailored specifically to the needs of the UK armed forces in countering the soviet-threat. The size of defence orders was of a magnitude that justified their development and government was able to afford the required costs of development. There was also a pervasive culture of secrecy surrounding government decision-making processes, giving a lack of public and parliamentary oversight. However, in 1965 the cancellation of the TSR-2 programme due to spiralling costs marked the start of a new relationship between the MoD and industry, introducing competition to defence procurement and close collaboration. This resulted in several mergers within Britain and an increasing pressure to allow foreign firms to bid for UK defence contracts. In the early 1980's a value for money initiative tried to impose a free-market philosophy on defence procurement, encouraging increased private funding of research through 'spin-off' technologies, relaxing government regulation of exports and, most particularly, removing the anomaly of a national monopoly of defence suppliers.

These competitive procurement policies of the 1980's, combined with the peace dividend in the 1990's, resulted in shrinking orders and questions over the future survival of the UK's defence industrial base. Globally, defence budgets fell from $1.2T in 1985 to $868B in 1993[7]. The reasons for the level of expenditure on equipment in the past was easier to explain due to the need for the British armed forces to fulfil their national and NATO alliance defence roles in the face of a clearly identifiable and capable Soviet threat. Following the end of this threat, government studies such as 'Options for Change', 'Defence Cost Studies' and the 'Strategic Defence Review' have resulted in the size of the British armed forces being reduced by around 30%, with expenditure reduced to about 2.8% of the national GDP in 1998 from a high of 5.2% in 1985[7].

UK involvement in the Gulf war and UN peacekeeping missions have increased the emphasis on force projection, the ability to deploy relatively small combat units anywhere in the world at short notice. This represents a very different threat from that posed by an intensive campaign in Western Europe against large numbers of soviet armour. Though the requirements of the UK armed forces in fulfilling this new role are changed, the need for state of the art weaponry has not abated, particularly with an increased public expectation on weapon capabilities, such as improved accuracy and survivability of the weapon platforms. Consequently, annual expenditure on equipment procurement is currently about £8.5B, representing nearly 40 % of the total defence budget[7].

Despite reductions in the procurement of UK weapon systems, the MoD Defence Export Services Organisation (DESO) expects the export market to expand from US$37.1 billion in 1996 to US$50.3 billion by the year 2000, showing a potential expansion in the world market. The figures for world market share, shown in the tables below, indicate that UK defence

exports account for 20% of the world market, of which 22% is from sales of airborne weapon systems. In the UK, defence exports represent 2.5% of GDP, 9% of manufacturing output and 2% of all exports. Of the total sales of £14 billion, exports represent 40% of total output[7].

World's defence export market share	
50%	US
20%	UK
12%	France
16%	Other

Distribution of UK defence exports	
22%	Air
14%	Naval
9%	Land systems
55%	Other

This has led industry to tailor its products to meet the additional needs of export customers as well as to exploit dual-use and spin-off technologies in civil markets.

The present high standing of the UK in aerospace defence is due to the high levels of research and development investment over the past 10 to 20 years. The Scientific Advisory Council speculates that the gestation time between research and production is generally 10 to 15 years with some projects *i.e.* the Typhoon (Eurofighter) taking up to 30 years. However, investment is reducing in the UK (for aerospace) in contrast to increasing research budgets in competing nations. Rationalisation of government research facilities, combining establishments responsible for weapon systems associated with the traditional air, sea, land and electronics sectors into the DERA, have reduced duplication of research effort. The introduction of best management practices have also brought about efficiency gains. But government policy for the private sector to make up the shortfall is unsustainable and may lead to an accelerated decline with a loss of world market share.

The UK defence industry has undergone continuous change since World War II. Mergers in the sixties, nationalisation in the seventies and re-privatisation and aggressive cost control in the eighties has led to a reduction in the major players (BAe, GEC, RR, VSEL and Hunting). These five companies account for 31% of UK expenditure on defence[7]. Similar changes in the US are leading to a few very large companies with the necessary economies of scale to survive in what has become a very competitive market. This has placed increased pressure on UK industry to restructure, creating strategic alliances within Europe and with the US, to remain competitive.

2.2.2 External influences

History has shown that changes in the political/legal, economic, socio-cultural and technological environment since the end of the Second World War have had a considerable impact in shaping procurement processes. Therefore, a study of these environmental issues, or PEST analysis, is a useful starting point in determining what influences are prevalent today and how the changing environment may affect future procurement policy.

Political

Since the end of the cold war and the collapse of the former Soviet Union, the loss of a readily identifiable enemy has led to the perception of a lesser threat to world peace. However, the Soviet threat has been replaced by a variety of other threats such as the proliferation of weapons of mass destruction, regional conflicts and tensions, civil wars and terrorism. These 'new' threats pose no less of a requirement on the UK armed forces. The UK has obligations, not only to defend and protect national security, but also of its members of the commonwealth and through its alliances with NATO, the UN and the European Union. The UK has signed a European Union treaty giving provisions for a common foreign and security policy that might in time lead to a common defence force. It is expected that the UK will play an increasing role within the EU, as defence resources are pooled and collaboration with European partners on defence procurement increases. Participation in United Nations peacekeeping operations, such as in Bosnia, Yugoslavia, Cambodia, Angola, Cyprus etc., will continue, though support missions such as these are already stretching the resources of the armed forces. Britains unique relationship with the United States will ensure that the US is an integral part of the UK's defence policy, though this may reduce as an affinity with Europe grows. This relationship could also be threatened by escalating trade conflicts between the US and Europe. The intense rivalry between Boeing and Airbus has already impacted on limiting defence collaboration between the US and the UK to specific technology areas.

The economic growth of China through foreign investment, attracted by a mass potential market and cheap production, will lead to better integration with the outside world, making it more dependant on trade to sustain an increasingly urban population and reduce unemployment. Central and South America has seen the demise of military regimes and the strong growth of democracy, though economic growth has not matched that of the Asian economies. The transformation in Russia from the old repressive regime to a democracy with a free market has seen slow economic growth, political mismanagement and high social costs, but is expected to continue along this path. Russian armed forces are even assisting with UN peacekeeping missions in Bosnia and Yugoslavia. In the Middle East and North Africa, the terrorist threat from Islamic Fundamentalists continues to pose problems. In counties such as Iran, Iraq and Libya, poverty and poor government has led to social unrest and instability. However, the need for better integration of regional economies may reduce the likelihood of military conflicts. For much of the region, the influence of oil revenues, establishment of democracies and continued peace negotiations have led to relative stability.

The adoption of a capitalist market system is prompting more countries to adopt democratic principles and the number of democracies in the world is growing steadily. Since historically, democracies do not tend to go to war with each other this is a very positive sign for world peace. The profound political, economic and social changes likely to take place over the next decade or so will promote a more peaceful world and reduce the UK's political importance within it.

At home, the increasing need for cost-effective weapon systems has led to changes in foreign trade regulations and monopolies legislation to improve competitiveness. The government has also reduced bureaucratic regulations within the MoD, introducing new management systems

and rationalising the MoD Procurement Executive, its research establishments and its defence industrial base.

Economic

In 1994, President Clinton stated that "we recognise that trade, as much as troops, will increasingly define ties that bind nations in the 21st century". The growing interdependence between national economies, prompted in part by the growth of major world trade groupings, are factors which are likely to promote harmony between nations and contribute to a reduction in conflict. As more countries develop open market economies in an attempt to improve their competitiveness, wealth and the livelihood of their citizens so they will be forced by fear of adverse market reaction to renounce violence. All nations will have to come to terms with the dominant power of the financial markets over governments, and the shift in the political and economic centre of emphasis from Europe to Asia and the Pacific, surpassing the economic strength of the United States.

Figure 2-1 compares tension factor with the percentage GDP spent on defence[8], clearly showing a direct relationship between the two. The expected improvements in international relations discussed above will lead to large reductions in defence spending across the developed world. However, an export market will be maintained by countries with growing economies requiring a defence capability. This will in turn level the playing field in terms of military capability. By the year 2020, estimates indicate that the UK will have moved from 8th position in the world league (in terms of GDP) to 14th position, compromising the UK position as a leading world economic and military power, and as a permanent member of the UN Security Council[8]. The financial pressures of coping with an ageing population combined with budgetary pressures to improve other public services such as health will contribute to a decline in the percentage GDP spent on defence. This will have a significant impact of the UK's defence industries and force them into closer collaboration with companies in other countries. Experience has shown that countries with strong aerospace industries benefit from the systematic appreciation of their currency. Therefore, there is also pressure on governments to protect their defence industrial base, enabling it to compete in the world defence export market, providing 'spin-off' technologies to be exploited by civil markets and to create employment opportunities.

Socio-cultural

Throughout the developed world birth rates are declining and longevity is increasing. Social trends indicate that by 2011 the size of the working population will have diminished, yet the financial burden of pensions, social security and health service costs will increase dramatically[8]. UK citizens are primarily concerned with their own economic welfare and will wish to see taxes spent on education, health care and pensions in preference to defence. In addition, as integration with the EU continues there will be further pressure on the government to increase spending on education and healthcare to be in line with most other EU countries.

Despite the general support for the armed services by the majority of the nation and the moral obligation felt towards protecting the oppressed, economic issues at home will prevail. The expectation on other nations to make a bigger contribution to peacekeeping activities will increase.

Technological

The UK has the capability to design, develop and manufacture a range of high-technology products including aircraft, missiles, submarines and tanks. The defence industry also has a good track record, selling mainly on superior technology and increasingly on operating performance. A number of studies have shown that innovation and technology have a significant impact on GDP and economic growth with a tendency for the nation to experience systematic appreciation of their currency.

The present high standing of the UK in aerospace defence is due to the high levels of research and development investment over the past 10 to 20 years. The Defence Evaluation and Research Agency is the custodian of the defence technology base for the MoD with a remit to gain access to science and technology through its own research and international collaborations, to transfer technologies to UK industry, exploit dual-use technologies and operate several strategic facilities. In recent years rationalisation of DERA and the implementation of best management practices has improved its cost effectiveness. However, the strong emphasis on developing non-MoD income to supplement its decreasing MoD budgets and developing strong commercial awareness has soured relations with industry. Government policy for the private sector to make up the shortfall is unsustainable and if MoD investment in new technologies continues to fall, it may lead to an accelerated decline with a loss of world market share.

The rate of technology obsolescence that forces technological developments and improvements in performance has led to escalating unit costs. The unit cost for a World War II fighter, of about US$10,000 compares with a U$100 million price tag for the latest F-22 fighter[9]. This increase, by a factor of 10,000 over 50 years, makes mid-life upgrades an attractive alternative to buying new aircraft. The development costs for a World War II fighter might be $50,000 and take six months (*i.e.* the production cost of five aircraft). A modern fighter takes at least six years and costs about $10 billion to develop (*i.e.* the production costs of 200 aircraft). The combination of high development and production costs and relatively small production runs represent a significant increase in acquisition costs. The high unit cost means fewer aircraft can be afforded and governments may be reluctant to use such valuable assets.

Another technological issue is the improved access to technology in developing countries through sponsoring students at western universities, the sale of technologies by countries with struggling economies such as Russia, and the migration of highly trained personnel. This poses an increased potential threat from nuclear, biological and chemical weapons.

2.2.3 Competitive environment

In addition to considering the external influences of the environment it is useful to analyse the competitive environment of the defence industrial base so as to understand the five competitive forces *i.e.* the threat of potential entrants, the power of buyers and suppliers, the threat of substitutes and competitive rivalry.

Threat of entry

For the manufacture of most weapon systems and particularly military aircraft, the opportunities for new market entrants are small. The capital requirements to build the necessary infrastructure such as production, test and evaluation facilities are immense. Dwindling orders for new weapon systems are forcing most defence contractors to merge to benefit from economies of scale. The accessibility of domestic and export markets will depend on government policy towards its domestic industrial base and its legislation on export licences. Without high levels of research and development, a new entrant is unlikely to be innovative and produce a system that has sufficient differentiation to gain competitive advantage.

An exception is governments that license production from overseas, requiring no research and development whilst gaining access to new technologies and creating a skilled workforce. Time-scales for the introduction of equipment into service are short since the technology is proven and low risk. This approach can only be justified if large quantities are to be manufactured, benefiting from economies of scale, though exporting items manufactured under licence is difficult. Costs are usually high since the licensee will want to recoup development costs and component suppliers are often sourced in the country of origin. For example, when the Australian government produced the F-18 fighter under licence from the US, it cost 27% more than a direct purchase. Manufacturers of civil aircraft who have the infrastructure and economies of scale could also compete in defence markets, particularly with products that are easily adapted to military roles *i.e.* military transport and surveillance aircraft.

Power of buyers

Since the government is usually the main and possibly only customer for its domestic defence products, it has a significant amount of power. Due to low production volumes defence contractors may only decide to proceed with the development and manufacture of new weapon systems once firm domestic and export orders have been received.

Power of suppliers

Rationalisation of the aerospace industry created fewer component suppliers. In general, their products tend to be highly specialised and fully integrated with the complete system, preventing prime defence contractors from switching suppliers without significant costs. The move towards concurrent engineering has led towards closer working relations between manufacturers and suppliers. Commonality and standardisation of components reduces in-service costs of the weapon system. In spite of the increasing complexity and capability of combat aircraft, there has been a marked improvement in reliability, mostly as a consequence of greater improved component reliability.

Threat of substitutes

Emerging technologies can often produce an alternative and more cost effective solution to a particular staff requirement. For example, the anti-armour role could be fulfilled by main battle tanks, attack helicopters, fighter aircraft or unmanned combat air vehicles etc. Though there are strategic reasons for having more than one solution, there is a significant threat that a weapon system can become superfluous before its time, resulting in cancelled orders.

Competitive rivalry

Competitive rivalry is greatest when the threat of new entrants or substitute systems is high and buyers and suppliers exercise control. From this analysis of the defence industry it is clear, therefore, that the production of weapon systems is a highly competitive industry. For these reasons, mergers in the aerospace industry have left a small number of dominant defence contractors world-wide. Due to the large investments in specialist plant and a trained workforce and a reliance on a relatively small product range, exit barriers are high. High R&D expenditure ensures that defence products remain innovative and different from those of competitors. As the life cycle cost of weapon systems becomes an increasingly important factor, there is an increased emphasis on defence contractors to provide in-service support to the armed services.

2.2.4 Competitive position

The auditing of environmental influences and competitive forces provides an indication of key factors that will effect the positioning of the UK industrial base. The next step is to analyse the competition, consider how the market is segmented and determine the UK's competitive position. A detailed analysis of foreign defence industrial bases and the product ranges that come under the umbrella of weapon systems will not be covered in this report, though some discussion of competitive positioning is made in the following sections.

2.3 Resources and capabilities

For a government to pursue a particular strategic direction it must ensure that it has the capability of sustaining that strategy. An understanding of the countries strategic capability is achieved through the resource analysis of its industrial base and research facilities, thereby identifying its core competencies.

2.3.1 Resource audit

Physical

The development, production and verification of weapon systems requires significant amounts of infrastructure, from research facilities such as high-speed wind-tunnels and super-computing centres, to production machinery and tooling, to evaluation and testing facilities such as airfields and weapon test ranges. Major facilities for R&D and test and evaluation are government owned, being the responsibility of DERA, with some facilities operated by industry. Many facilities were built during the period of the cold war and are now ageing and in need of modernisation. Without the additional income generated by non-MoD business these facilities will be degraded and it may become necessary to look to overseas alternatives where security issues may be of concern. The prediction of aerodynamic loads and structural integrity require state of the art computing facilities and numerical methods. These are generally available to scientists and engineers and benefit from close collaboration between industry, DERA and academia. The production facilities operated by UK industry are of a high standard, though production can be geographically diverse due to an increased reliance on European collaborative programmes.

Human

A key requirement is the skills base of the country. The UK has a well educated population providing specialised skills in a number of specific fields; science and engineering, project management, pilots etc. This skills base needs to be a sustained resource. Lack of funding in defence R&D and further rationalisation will result in the migration of skilled personnel to the civil sector or abroad. However, the movement of personnel between civil and defence sectors can benefit both markets through the transfer of new ideas. Security considerations usually limit personnel working in the defence sector to UK citizens.

Financial

The discussion on political, economic and socio-cultural influences described how relative political stability and increasing pressure from other areas of public spending is reducing defence budgets.

Intangible

Government and industry will own a substantial number of patents for new technologies that have been developed with defence funding.

2.4 Culture and stakeholder expectations

This section will identify the organisational structure of the MoD and the various departments responsible for decision making. It will also discuss reasons for acquiring weaponry and the acquisition process before considering the relationships between various stakeholders.

2.4.1 Organisational structure

In 1964 the MoD to the Admiralty, the War Office, and the Air Ministry were amalgamated into a unified MoD, and in 1971 the Ministry of Aviation Supply was incorporated. The MoD is the Department of State responsible for the formulation and execution of defence policy, it is the central operational and administrative headquarters of the armed forces and steers the body that procures their equipment. The department is headed by the Secretary of State for Defence and chairs the Defence Counsel, the legal body for controlling the three services. The Secretary of State answers to Parliament for the actions of the department and the armed forces. The MoD is headed by a senior service officer, the Chief of Defence Staff (CDS), and a senior civil servant, the Permanent Under Secretary (PUS). The structure of the top levels of the MoD is given in the table below with definitions of the core headquarters functions[7].

Members of the Defence Council					
		Secretary of State			
		CDS		PUS	
Chief of Defence Intelligence	Chief of Defence Procurement	Second PUS	Chief Scientific Advisor	Vice CDS	Single Service Chiefs of Staff

Defence Intelligence	Procurement Executive	Office of Management and Budget (OMD)	Defence Scientific Staff	Defence Staff	Single-Service Executive Staffs
Identify future operation environments	Cost effective equipment procurement	Financial management and authorisation	Advise OMB on policy and research objectives	Define operational requirements, policy formulation, and planning	Management/ administration of their respective services

2.4.2 The procurement cycle

Prior to the 1950's defence procurement was rather ad hoc; "technology was limited, equipment performance was inadequate, virtually all the expertise resides inside government establishments, industry was used mainly for production, and costs were low". In 1969, the Downey report made recommendations to the MoD on how it should procure equipment. The procurement process was divided in several stages each of which had to be completed and formally accepted as being satisfactory before funds could be committed for the next stage.

Preliminary study	The Procurement Executive conducts a preliminary study to investigate the feasibility of an initial idea and gain an indication of costs.
Staff target	Defence Staff issue a statement of the operational requirements, approved by the Equipment Approvals Committee of the MoD and by government Ministers.
Feasibility study	Establishes whether current technology is capable of meeting the staff target and to outline the most promising technical approaches, including initial cost/life-cycle estimates, generally conducted by government research establishments and industry. The feasibility study can account for about 1% of the total development costs, but can be higher where technical risks are high.
Staff requirement	A comprehensive statement of the requirements. It provides the development team with all necessary details, including relevant standards, specifications and assessment methods. Sets out project costs, time-scales, and justifications of the requirement.
Project definition	Intended to highlight areas of particular technical difficulty and risk. Involves planning, design and engineering work necessary to detail the

	costs and duration of the programme. Normally conducted by industry, with a contractor selected by competitive tendering. Project definition examines trade-offs between cost and performance.
Full development	Development of all engineering processes, trials and tests to establish a final design, sufficient to allow production to begin. Conducted by industry, it usually includes the manufacture of prototypes. Detailed evaluation and trials are conducted and logistic support implemented, including reference documentation, spare-parts, training and simulators etc. If problems occur, and the in-service date is delayed or expected production costs and increase beyond defined margins, approval to continue must be sort from the government.
Production	Before accepting the equipment, it will be evaluated for conformance with the staff requirements, unless purchasing commercial-off-the-shelf items or from overseas. This is usually undertaken by a government agency such as DERA and/or the armed forces. Production and testing may overlap due to the long lead times required for acquiring materials and tooling for the production process. Major changes at this stage can increase project risk and cause prohibitive delays and cost increases.

Although the Downey cycle brought regulation to the defence procurement process, ensuring equipment was well engineered and to a high standard, significant problems remained. In 1986 the National Audit Office examined deficiencies in the MoD control of its contractors and the development of new equipment. Three-quarters of cases examined incurred substantial cost or delay problems related to non-compliance of the required procedures. Both the MoD and contractors were found to underestimate technical risk and development costs, particularly during the project definition stage, consequently, few projects were cancelled. Procedures were found inadequate for developing large sophisticated software systems and proved over-complicated and expensive for purchasing small numbers of items. MoD staff neglected to make adequate independent evaluations of development cost estimates and poor management by contractors resulted in few if any penalties. Nowadays, competition and fixed price contracts have encouraged contractors to put adequate management procedures in place. The rigid scrutiny required at nearly every step of the Downey cycle and accompanying approval procedures were a main cause of lengthy delays.

For certain procurement programmes, the Cardinal point specification system is more efficient, since more emphasis is put on industry to define a research and development (R&D) programme. MoD communicates what equipment characteristics it would like to have in the future and industry states what it is proposing to export as a consequence of market research, effectively replacing the feasibility study of the Downey procedure. Any similar technology areas are thereby identified and attempts to align R&D programmes can be made. The Cardinal points procedure lists desired characteristics, which unlike staff requirements are not normally mandatory, and industry is then invited to tender on a fixed price basis. The tender evaluation, by MoD/DERA considers how well the requirements are met, time-scales and of course cost. The system requires four prime conditions to be met;

- industry is aware of the likely future requirements of the armed services
- the export market will be the major source of trade for the items developed

- industry will assess levels of technological risk and will design and manufacture accordingly
- the equipment produced is suitable for local and overseas customers with little or no modifications allowing for economies of scale.

The cardinal points specifications has resulted in much shorter procurement time scales, improved financial stability as a result of fixed pricing, lower costs through increased competition and less rigid specifications. The responsibility for R&D, with its inherent costs and risks, has switched from the MoD to industry. The MoD research base is still essential for applied research unsuited to industry due to security implications or lack of commercial potential and for assessing bids/products from industry for compliance with staff requirements. DERA is also responsible for undertaking basic or underpinning research that can be transferred to industry to support future work programmes.

In 1991 the Buckley report recommended substantial changes to the procurement process to include a cost-effectiveness analysis in support of key decisions on defence acquisitions. It introduced a Combined Operational Effectiveness and Investment Appraisal (COEIA) mechanism to ensure the rigorous and objective qualification of the operational benefits of the competing options as well as the traditional investment appraisal of their costs.

The COEIA involves selecting alternative procurement options, defining assumptions, examining the cost breakdown structures, discounting the expected cash flow and analyzing risks and uncertainties. The mechanism has played a central part in UK defence equipment selection for approximately six years and has brought considerable improvements to the decision-making process. A range of different classes of military equipment, such as main battle tanks, attack helicopters or ground attack aircraft are all compared in an investment appraisal, against the ability to meet the demands of defined defence roles. The financial benefit provided by a new class of equipment is difficult to define, requiring an analysis of expected life-cycle costs as well as acquisition costs. The studies are structured to provide guidance on the most appropriate mix of equipment classes, likely to generate the most effective military capability. A major constraint on the study is the amount of money available in the defence budget for the year when the procurement is anticipated. This defines the numbers of assets in the different equipment classes that can be afforded. Thus a further study is required to identify the most cost-effective equipment type. Supporting documentation to the COEIA will include a requirement definition from each of the armed services, and justification of the project validity and affordability. Documents are approved by the MoD Equipment Approval Committee, who make recommendations to ministers on the preferred procurement option. The COEIA is performed before each major milestone or decision point that involves either a commitment of substantial funds or the irrevocable abandonment of a procurement option.

Possible recommendations from a COEIA study might include, in order of increasing costs;
- continue using existing equipment
- refurbish existing equipment to extend life
- procure or lease new/second-user off-the-shelf equipment with similar capabilities
- upgrade existing equipment to enhance capability

- request industry to suggest a mechanism for meeting an operational requirement by means of the Private Finance Initiative (equivalent to the Cardinal Points Procedure described above)
- procure or lease new/second-user off-the-shelf equipment to improve capability
- fund the development and production of new equipment.

2.4.3 Stakeholder expectations

The process of procuring weapon systems involves the attitudes and expectations of a large number of stakeholders with quite diverse skills and qualities. These include members of the armed services, politicians and civil servants, scientists and engineers, managers and shareholders, foreign governments and its own citizens. Whether a system is innovative, represents value for money or is more lethal or reliable, will depend on the stakeholders vested interests. The attitudes and expectations in other countries can also be important, particularly within the present climate of international mergers, acquisitions and collaborations.

UK citizens, the commonwealth, international alliances and the EU

The beneficiaries of the services provided by the armed forces want a well equipped and capable force with accurate weapons, that minimise collateral damage, and enhance survivability. UK tax payers will want value for money in terms of weapon acquisition and in-service costs and full accountability for procurement decisions.

Armed services

Members of the armed services, as the users of the weapon systems, will wish to see that any new or upgraded equipment offers an enhanced capability over current equipment, not only in terms of performance, but also its reliability, ease of use/maintainability and particularly its survivability.

Improved technology can benefit soldiers by reducing workloads, for example, modern avionics now perform many of an aircraft's management functions, though technology can also make humans redundant *i.e.* navigators and flight engineers. Therefore, there is a perceived threat that the work of engineers and scientists is reducing their military role to one of resource management.

There is also considerable rivalry between the three services; the Army, Navy and Air Force. Single service procurement decisions are sometimes incompatible with the requirements of the other two services. For example, both the Navy and the RAF fly Harrier aircraft though developments of the land and carrier based variants have occurred independently of each other.

Previous governments have been broadly content for each service to determine its own role and equipment requirements depending on affordability, with insufficient scrutiny of the justification. More recently, government has created several initiatives to improve the co-ordination of joint procurement programmes. However, there remain vested interests of single

service Chiefs of Staff in protecting their own service rather than providing the most cost-effective defence.

Ministry of Defence

Government ministers, civil servants and members of the armed services, responsible for the management of weapon system procurement programmes, are ultimately interested in cost effectiveness. With limited defence budgets and pressure from other areas of public spending, they will prefer relatively low cost options of mid-life upgrades or off-the-shelf purchases to the development and production of new systems. A successful procurement strategy can also boost the career of a desk officer, civil servant or minister. Hence there will be an emphasis on managing and reducing risk, possibly at the expense of innovative technologies. At the same time, MoD has a vested interest in maximising the capability of its armed forces and protecting its industrial base and its research and evaluation capabilities within DERA.

Possible conflicts of interest may arise from a military desk officers' sense of urgency, and the civil servants' preoccupation with financial approval and political sensitivities. Conflicts may arise between technical staff within the Procurement Executive, who supervise development and production, and those in the Office of Management and Budget, responsible for financial scrutiny of expenditure.

The perception is that the MoD is bureaucratic, with endless committees, difficulties in establishing responsibilities, slow in decision making and not organised for effective management.

Department of Trade and Industry

Another government department to benefit from military R&D is the Department of Trade and Industry (DTI) which aims to maximise the exploitation of 'dual-use' and 'spin-off' technologies from military R&D to benefit the country's civil markets. In the 1950's and 1960's military R&D accounted for most of the high-technology R&D being undertaken. In some market segments this trend has now reversed with civil R&D leading the industry *i.e.* information technology and materials. It is very difficult to measure 'spin-off' effects due to the large uncertainties and time lags associated with R&D. A 'spin-off' example is the US space programme which claims to have pushed forward the state of electronics, materials, computer software, and synthetic substances *i.e.* Kevlar. Another argument is that resources spent on military development reduces that available for civil exploitation, resulting in a loss of overall competitive advantage. Some countries such as Japan have highly integrated defence and civil R&D activities and question the effectiveness of the 'spin-off' mechanism, looking more towards 'spin-in' technologies from civil to military markets *i.e.* Japans FSX fighter. Despite doubts over its effectiveness, most evidence indicates that 'spin-off' theory does lead to substantial exploitation benefits in the civil market. There is an increasing trend towards dual use technologies that encourage funding from both sources. However, although this may be beneficial in the short term, a reliance on this strategy could degrade longer term defence capability since civil markets can have very different internal and external influences. There are concerns that the commercial success of 'dual-use' technologies may threaten national security with technology going to the highest bidder.

Defence, Evaluation and Research Agency

The stakeholders within DERA are scientists and engineers with a vested interest in researching and developing highly innovative solutions to defence problems. Scientists have an intense interest in their own field which may prejudice their advice, suffering from the 'not invented here' syndrome. DERA has several roles to play;

- Underpinning or corporate research to provide a future capability
- Applied research on specific procurement programmes
- Independent and impartial technical advice to MoD
- Operation of major test and evaluation facilities
- Defence analysis studies
- To generate income from non-MoD sources

Policies of procuring off-the-shelf systems or enhancing existing equipment reduce DERA's traditional role in the development cycle, of transferring research into new hardware. UK funding for research and development has been severely depleted compared with other nations and could have a serious impact on the future role of DERA. Though rationalisation and the introduction of best management practices have increased efficiencies within DERA it has to generate more income from civil markets. This is best achieved through the exploitation of 'dual-use' technologies and MoD corporate research programme proposals are now assessed for wealth creation potential. New civil/defence link programmes identify key defence technologies that are crucial to maintaining world market share through the exploitation of parallel technologies in both markets. Foresight techniques are used to identify emerging technologies. DERA is having to prioritise research agendas to maximise cost effectiveness, with R&D effort targeted at areas that offer value for money.

DERA's increasing reliance on civil markets has caused suspicion within industry and could prejudice the ability for DERA to offer independent and impartial advice to MoD. In general, closer collaboration between DERA, MoD and industry has created a better understanding of customer needs and research programmes have been tailored accordingly. However, the future role of DERA needs to be better defined if it is to continue with innovative defence research to sustain the UK defence industrial base.

Defence Industrial Base

The main industrial stakeholders are its shareholders whose main interests are in maximising the profits of the company. The industrial workforce will also expect company profits to sustain jobs. Declining sales and fixed price contracts have forced the industry to rationalise and improve management processes, particularly in the reduction of risk. Collaborative programmes share development costs and reduce technical and financial risk. Industrial stakeholders also expect some level of government protection, getting preference over foreign competition for the home market.

Academia

The research performed in UK universities is specifically aimed at underpinning future capabilities. Participation in applied research, on specific procurement programmes, is unlikely due to security concerns. MoD ensures that a proportion of its research budget is spent in academia, with research programmes usually managed by DERA or industry.

Universities also play an important role in educating future scientists and engineers, providing a skilled workforce to sustain the defence industrial base.

Export customers

Foreign governments have similar requirements to those of the UK government in acquiring cost effective weapon systems. They may have additional objectives such as gaining access to technological knowledge or creating a domestic industrial base by licencing production. Much will depend on foreign policy, international relations and a good track record. As the export market makes a significant contribution to the UK economy, it is an important consideration in developing acquisition policies.

2.5 Strategic change

By comparing positive and negative aspects of the procurement industry's ability to react to various potential environmental changes the author has identified the following scenarios:

- The UK is able to maximise the potential benefits of emerging technologies such as stealth, through its capable resources, ability to innovate and ability to spin off technology to the civil sector.
- International relations with countries such as the US and a closer affinity with Europe allows for closer collaborations and alliances, sharing the burden of development costs and reducing production costs through economies of scale.
- Efficient procurement processes such as the Combined Operational Effectiveness and Investment Appraisal (COEIA) and closer working relationships between MoD/DERA and industry give the MoD better accountability and demonstrate that the UK is getting value for money.
- The increasing cost of pensions, social services and health care is reducing the amount government is prepared to spend on defence. To retain an adequate capability, MoD will need the cost savings afforded by international development programmes, increased foreign competition or consider cheaper alternatives such as mid-life upgrades and off-the-shelf purchases.
- Increased international political stability coupled with a decline in the economic ranking of the UK will reduce international expectations of the UK armed forces. The ability of the UK defence industrial base to produce innovative, cost effective weapon systems coupled to a good track record will sustain a healthy export market.

2.6 Summary

History has shown that the UK defence industry, MoD and its research establishments have had to adapt to large changes in the environment since the Second World War. The huge financial and technological resources required to design and develop a new combat aircraft, coupled with declining defence budgets following the end of the Cold War and increased budgetary pressure from other public services have forced governments into cost effective acquisition programmes. Policies of self sufficiency to protect the domestic industrial base, guarantee supply and for reasons of national security can no longer be justified. Instead, governments maintain capabilities in critical technology areas, such as high speed wind tunnel test facilities, whether or not there is an immediate requirement. Rationalisation, effective

project management, particularly in terms of managing risk, competitive tendering and better alignment with industry have resulted in efficiency gains for both the MoD and industry. Joint service procurement policies ensure effective defence solutions are acquired avoiding duplication of resources. The Joint Strike Fighter being developed in the US is unprecedented in that, at the design stage, it is already intended for all three branches of the armed services. The prospect of an air force with a single fighter type has logistic and cost attractions, but should the aircraft be grounded due to technical problems the air force could be left in-operative.

The UK defence industrial base remains an important player in the world export market, achieved largely through superior products employing innovative technologies. A lack of investment in defence R&D and an over-reliance on dual-use and spin-off technologies for generating additional income from civil markets could limit future innovation and therefore the competitiveness of UK defence products.

Britain has realised the benefits to be gained by international collaboration with participation on European acquisition programmes such as the Tornado and Typhoon. Since the unilateral cancellation by one nation is an unattractive position due to the cost of compensation to other partners, the political stability of the alliance is assured. Although these European collaborations increase overall programme costs, the cost per partner is significantly lower. Cost savings are realised through technological synergies and economies of scale that are not offered by the separate operating companies.

1990		1995	
Company	Revenue $bn	Merged company	Revenue $bn
Lockheed	8.0	Lockheed Martin	19.7
Martin Marietta	5.5		
GE Aerospace	5.8		
Loral	1.9		
General Dynamics	8.7		
Boeing	6.1	Boeing	18.2
Rockwell	3.9		
McDonnell Douglas	10.1		
GM Hughes	6.0	Raytheon	12.0
E-Systems	1.9		
Raytheon	5.8		
Texas Instruments	2.3		
Northrop	5.8	Northrop Gruman	6.5
Westinghouse	3.9		
Grumman	3.7		

In contrast, the table above[10] shows that recent mergers have left the US with four major aircraft manufacturers. To compete in an increasingly competitive export market, Europe will need to move towards big cross-border mergers to combine economies of scale and operating efficiencies from a single operating company. Sir Richard Evans, BAe's chief executive said "To take on the might of the US, Europe's aerospace industry will need to unite into one huge company or it could die within five years".

This study has identified several key factors; external influences of the political, economic and social environment, capabilities of the defence industrial base and DERA, and relationships between the diverse range of stakeholders involved, that contribute to determining the strategic direction of UK weapon system procurement. The strategic analysis has indicated several initiatives that will shape future policies and which are currently being adopted by MoD and UK prime contractors. There are concerns over the funding of defence R&D required to maintain or improve world market share in defence exports and the significant wealth this generates for the UK economy.

References (I)

1 'Combat Aircraft Wing Flows – Project Management Plan.' J L Fulker, DERA/HWA/CN/MP/.

2 'An experimental study of the control of separated flow on a wing with high trailing-edge sweep.' A Shires and J I Broadley, DERA/AS/HWA/CR97013, February 1997.

3 'Validation of CFD – Project Management Plan.' A Shires, DERA/HWA/CN/MP/97010/2, June 1999.

4 '21st century fighters.' W B Scott, article in 'aviation week & space technology', August 1998.

5 "British Airways' requirements for a new large airliner." Capt R J L Acton, 'The new large aircraft', RAeS conference proceedings, October 1993.

6 'Exploring Corporate Strategy.', G Johnson and K Scholes, third edition, 1993.

7 'Defence research and development: it's vital role in sustaining the UK defence industry base.' Grp Capt S H Anderton, RMCS report R/97/509, 1997.

8 'UK defence foresight - A scenario for 2011.' M N Hill, RMCS report R/96/779, 1996.

9 'Aircraft design integration and affordability.' L Campos, AGARD-R-826, November 1998.

10 'The relationship between policy, doctrine, concepts, operational requirements and procurement.' Mjr L Tuson, RMCS report R/98/1203, 1998.

Bibliography (I)

'21st century fighters.' W B Scott, article in 'aviation week & space technology', August 1998.

'The armed forces of the European Union – Section 3.15: United Kingdom.', Jane's, July 1999.

'FOAS new working practices.' Dr H A Smith, DERA/AS/SID/CR980314, February 1999.

'Aeronautical research and technology – a strategic imperative for Europe.', Confederation of European Aerospace Societies, Position Paper, June 1997.

'DRA: Air systems sector business plan.' M Earwicker, DRA/AS/BP96, January 1996.

'Defence research and development: it's vital role in sustaining the UK defence industry base.' Grp Capt S H Anderton, RMCS report R/97/509, 1997.

'The management of defence procurement.' Mjr A K T Faithful, RMCS report R/97/782, 1997.

'The relationship between policy, doctrine, concepts, operational requirements and procurement.' Mjr L Tuson, RMCS report R/98/1203, 1998.

'Weapons procurement decision making in the United Kingdom.' Mjr A J Walker, RMCS report R/98/1205, 1998.

'An evaluation of strategic planning in the Royal Air Force.' Wg Cdr A W Madge, RMCS report R/97/529, 1997.

'UK defence foresight - A scenario for 2011.' M N Hill, RMCS report R/96/779, 1996.

'Aircraft design integration and affordability.' L Campos, AGARD-R-826, November 1998.

'Strategic management of the cost problem of future weapon systems - Skunk works lessons learned.' L M Nicolai, from proceedings on 'Strategic management of the cost problem of future weapon systems ', AGARD-CP-602, September 1997.

'Cost effectiveness in UK defence procurement: the COEIA', Dr A J Lindop, from proceedings on 'Strategic management of the cost problem of future weapon systems ', AGARD-CP-602, September 1997.

'The future for combat aircraft design – An industrial view.' L Skorczewski, from proceedings on 'Strategic management of the cost problem of future weapon systems ', AGARD-CP-602, September 1997.

'The value of S & T in affordability.' J D Lang, B Birchfield, C R Saff and G Shumaker, from proceedings on 'Strategic management of the cost problem of future weapon systems ', AGARD-CP-602, September 1997.

'Technology – Solution of the next generation of affordable strike fighters.' F C Schwartz, from proceedings on 'Strategic management of the cost problem of future weapon systems ', AGARD-CP-602, September 1997.

'Reorganisation of evaluation and research to support defence procurement.' R Cadwallader, from proceedings on 'Strategic management of the cost problem of future weapon systems ', AGARD-CP-602, September 1997.

'Cost reduction strategies in acquiring aircraft weapon systems at "Pax River".' P F Zalesak, from proceedings on 'Strategic management of the cost problem of future weapon systems ', AGARD-CP-602, September 1997.

PART II – Investigation of the low speed flow over a highly swept wing

3 Overview

3.1 Summary of literature review

The review of available literature initially considers the historical development of swept wings since the Second World War. With the advent of the jet engine, aircraft were able to attain higher speeds, resulting in regions of locally supersonic flow over the wings. It was realised towards the end of the war that sweepback could alleviate the effects of compressibility. Nowadays, an important driver for sweeping wings is to reduce observability by aligning all edges to one common angle of between 40° and 50°, thereby increasing chances of survivability. A review of stealth technologies is included that considers the capabilities of other sensors used in defensive systems and alternative means of reducing reflected radar energy.

Wings with highly swept leading and trailing edges increase the possibility of three-dimensional separation, particularly if trailing edge flaps are deployed or, more generally, if wing camber is increased. Therefore, a review of separation mechanisms in three-dimensional flows has been undertaken. Research of swept wing flows has thus far focussed on experimental studies, based on measurements of forces, moments and surface pressures and some surface flow visualisation studies. Additionally, most research activity has considered the problem of leading edge separations over slender swept wings. However, a number of researchers have identified possible mechanisms for flow breakdown as a result of studies of flows in adverse pressure gradients and over swept bodies. The application of non-intrusive flowfield measurement techniques or flow predictions using Computational Fluid Dynamics (CFD) methods has not been attempted for verifying the three-dimensional nature of these flows.

The literature review concludes by examining a number of methods for calculating turbulent boundary layers. These range from relatively simple integral methods, based on semi-empirical relationships, to solutions of the Navier-Stokes equations. The review identifies the need to determine the required detail of the flow physics for a particular application. This will then determine the level of mathematical complexity required to approximate this physical behaviour of the turbulent flow. For highly swept wing flows with strong adverse pressure gradients, significant streamline curvature and flow separation, a solution of the Reynolds Averaged Navier-Stokes equations is recommended, employing a two-equation turbulence model.

3.2 Research aims

Since the 1960's there has been little research interest in highly swept wings with trailing edge separations. However, the need to design aircraft with lower observability has renewed

interest in the aerodynamic behaviour of these wings. With the emergence of new technologies such as optical non-intrusive measurement techniques and advances in computer hardware and flow prediction algorithms it is now possible to explore the flow breakdown mechanism in more detail. In particular, these methods allow the behaviour of the separated stream-surface to be understood. Therefore, the research described in this thesis aims to investigate the aerodynamic characteristics at low speeds of a highly swept trailing edge model using experimental and theoretical methods. A wind tunnel model has been designed that features a complex three-dimensional flow on the wing upper surface with flow separation near the trailing edge. The study aims to firstly, characterise the nature of the flow breakdown using a combination of experimental and theoretical methods and secondly, by evaluating the capabilities of existing CFD methods and turbulence models in order to assess their suitability as design tools for engineers involved in the evaluation of combat aircraft wing flows

3.3 Overview of thesis

Following a review of the available literature in chapter 4, the numerical methods that have been applied in designing the wing section and for predicting the flow development over the wing are described in chapter 5. Chapter 6 discusses the process of designing a wind tunnel model for a low speed study that simulates the pressure distribution typical of a transonic manuoevre condition. The wind tunnel facility is also described and methods of measuring and correcting data. Experimental techniques for visualising the flow development on the wing surface and in the field are discussed and an optical non-intrusive measurement technique for measuring flowfield velocity components. An analysis of the experimental data is given in chapter 7, indicating trends in lift, drag and flow development with wing sweep, freestream velocity and angle of incidence. The chapter also describes results from an integral boundary layer method for calculating the turbulent shear layers and solutions of the Reynolds Averaged Navier-Stokes equations. A discussion of these results explains the flow mechanism and assesses the level of flow detail that CFD can be expected to predict in chapter 8. Finally, concluding remarks and recommendations for future work are discussed in chapters 9 and 10 respectively.

Some of the work described in this thesis has additionally been described in reports for the MoD customer in references 1 to 5. The author has also presented the work at two international conferences[6, 7].

4 Literature review

A review of the literature relevant to the scope of this thesis is given below. It begins with an historical look at the developments of swept wings and the operational and technological influences. Since the primary driver for wing sweeps of between 40° and 50° degrees is the desire for low observability, we shall also consider how stealth shaping fulfils this requirement and what alternative technologies are available to the wing designer. The following sections will then examine our understanding of the behaviour of three-dimensional boundary layers and particularly their development over swept wings. We shall then consider the development of numerical models for the prediction of separated wing flows and in particular, the two key requirements; a suitable calculation method for modelling the physics of turbulent boundary layers and the requirements of the grid in resolving turbulent structures.

4.1 The development of swept wings

The trend for increased aircraft speed was given an impetus towards the end of the Second World War with the development of the jet engine. The higher speeds in turn demanded advances in aerodynamics to alleviate the effects of compressibility on stability, control and the rapid drag rise. To some extent these effects were reduced by the use of thinner wings, but this compromised the wing strength, weight and fuel volume. The use of sweepback to reduce drag at transonic/supersonic speeds was first proposed by Busemann in 1935 though the application of sweepback to the aircraft of that era was not thought practical. Betz[8] (1940) realised that the immediate benefit of sweep is to delay to a higher speed the occurrence of regions of supersonic flow and hence the drag rise. Towards the end of the war Germany was producing aircraft with swept wings, most notably the Me262 jet fighter with a leading edge sweep of 18.5°. At the end of the war much of the German research was discovered and put to use in other countries, as shown by the Russian MiG-15 and the US F-86 Sabre.

There are however, a number of penalties with sweepback; reduced lift at a fixed angle of incidence, increased induced drag (unless measures are taken to provide an elliptical loading, by twisting the wing for example), increased roll due to sideslip, tip stalling, reduced effectiveness of high-lift devices and structural problems. The problem of tip-stalling effected many of the early swept wings, featuring flow separation at the tips that spread inboard with increasing incidence. Boundary layer fences or notches were employed to reduce the inboard spread of separation.

Wing designs have generally adopted leading edge sweeps of less than 35° to minimise the adverse effects of three-dimensional bubble type separations, or sweeps of greater than 53° with relatively sharp leading edges, near which a steady vortex sheet is shed with the beneficial effect of augmenting lift. The development of civil and military aircraft, designed to operate in the transonic flow regime, have generally produced wings with leading edge sweeps of about 30°. Supersonic fighters on the other hand, have led to delta or thin swept wings with a leading edge sweep greater than about 53°. Since some designs of combat aircraft have to encompass both the benefits of a supersonic dash with transonic loiter/cruise capabilities, some (fixed) wings have compromised with wing sweeps between these

generalised limits. However, the main driver for wings with leading edge sweeps in the range 40°-50°, with its inherently poor aerodynamic and structural characteristics, has been the need to reduce the aircraft observability from opposing radar systems and, therefore, enhance its chances of survivability.

4.2 The LO requirement for swept wings

The concept of stealth[9-13] (i.e. designing an 'invisible' aircraft) in the context of this thesis, is predominantly concerned with reducing the radar signature of an airborne target. A weaker radar signature not only creates a diminished target for hostile defence systems, but also aids many electronic warfare measures to confuse hostile defences. By reducing the radar cross-section (RCS) of a target, the power of the defensive radar would, by necessity, be increased, making it more visible over a wider range and easier to be avoided or destroyed by antiradiation missiles. The principal technique is to shape the exterior profile of the aircraft such that energy incident from the viewing radar is not scattered back towards it. This is only possible for a limited range of viewing angles hence, priority is given to the directions corresponding to the largest threats i.e. the head-on aspect, paramount for early warning detection. How far a radar can detect or track a target depends on its transmitters power, antenna size, receiver sensitivity, environmental conditions and the RCS of the target. The only parameter within the aircraft designers control being the RCS of the aircraft. Although radar absorbing materials (RAM) can reduce radar signature, many RAM's are bad conductors that consequently increase the thermal signature. However, RAM coatings and structures are used to overcome the limitations of shaping, for example, the operational airframe of the F-22 comprises 40% composites.

The degree of stealth depends on several other means of detecting targets; using infra-red sensors to detect thermal signatures, electronic surveillance measures to detect the targets own electromagnetic signature, optical sensors for visual detection and sonar sensors to detect the acoustic signatures. Radar can detect airborne objects at much longer distances than infrared, acoustic or ultraviolet, and is not as dependent on weather conditions. Thus radar is currently the primary sensor used in defensive systems.

On the other hand, designers of defensive systems can employ various countermeasures against low-observable (LO) targets. Though an aircraft may be stealthy in the head-on aspect when illuminated by a monostatic radar (i.e. with a combined transmitter and receiver), multistatic radars can be used to collect radar echos away from the transmitter source. These systems have the added advantage that receiver and operating crew are not jeopardised by antiradiation missiles. Alternately, airborne or spaceborne radar can look down on an aircraft at an angle not optimised for low observability. Finally, stealth shaping becomes inconsequential for low frequency radiation as in over-the-horizon radar, using wavelengths of the same order as the size of the target. The relative costs of developing these technologies is still unclear, so stealth shaping and the consequent trade-offs with aerodynamic and structural needs are still relevant to future military aircraft specifications.

To understand the requirements for stealth shaping, we must firstly understand the mechanisms of radar defensive systems. Consider a plane wave from a monostatic radar impinging onto the swept leading-edge of a wing. Figure 4-1 indicates that the reflections are diffuse, depending on the surface finish, with a specula peak. Clearly, it is advisable to direct this specula peak away from the incident path, so that a monostatic radar sees only the (small) diffuse reflection. This is achieved through highly swept leading-edges (i.e. between 40° and 50°), resulting in either a delta wing planform or highly swept trailing-edges. Surface discontinuities, such as wing/body junctions should also be avoided using blending. Cavities act as specula reflectors, producing a considerable contribution to the RCS of a target. Furthermore, incident and reflected radiation will combine by successive constructive and destructive interference's as a function of the aspect angle, creating an image defined by 'hot-spots' which can identify the target type. For this reason engine intakes are hidden from ground based radar using S-shaped intake ducts leading to buried engines, and/or positioning intakes on the upper surface of the aircraft, and cockpits need to be specially coated with RAM. Other general requirements are for tail fin stabilisers canted inward or outward and the internal carriage of all stores.

Detection range varies with the fourth root of the RCS. Comparing the RCS figure for a conventional fighter with that for an F-117A fighter given in Table 1, we see that stealth technology reduces detection range by about 30%. The table also indicates that RCS is not simply dependent on target size, but also on the curvature of its contours.

4.3 Separation mechanisms

Following the 'discovery' of the boundary layer by Prandtl[14] in 1904, a number of early studies were mainly concerned with understanding two-dimensional separations. Schubauer[15] (1935) investigated laminar separation of the flow about elliptic cylinders using the hot-wire anemometry technique to measure velocity profiles in the boundary layer. Later, Schubauer and Klebanoff[16] (1951) used the technique to provide data for two-dimensional turbulent boundary layers. After the Second World War interest in swept wing flows led to investigations of the mechanism of three-dimensional separation. Jones[17] (1947) compared experimental studies of oblique viscous flows over circular wires and wings. He described the essential characteristic of three-dimensional flow over wings, that pressure gradients exist in the transverse direction as well as the freestream direction and will create crossflows in the boundary layer which, if sufficiently large lead to three-dimensional separation. He observed that whilst the oblique flow about a wire follows two-dimensional theory, the same does not hold for the wing. Sears[18] (1948) discussed the concept of 'limiting streamlines' in laminar boundary layers on yawed cylinders. He described a streamline just above the surface of the body as a limiting streamline if it possesses the same direction as a skin friction line or surface shear-stress trajectory. The limiting streamlines typically originate from an attachment line and after circumscribing the body surface, merge into a single line. Sears noted that this limiting streamline will act as a barrier to adjacent streamlines but did not refer to it as a separation line. Eichelbrenner and Oudart[19, 20] (1955) subsequently proposed that the converging limiting streamlines formed a three-dimensional separation.

Kuchemann[21] (1953) described the need for experimental data such as off-surface velocity measurements and flow visualisation methods in order to understand the mechanism of 'mixed flows' over swept wings. In summarising a series of experiments on swept wings at the RAE, Kuchemann[22] (1955) remarked "flow separations have come to stay, and it has been said that we must learn how to live with them and how to organise them to our best advantage". Kuchemann also describes the beneficial effects of leading edge vortex sheet separations in providing vortex lift. During the 1950's a number of experiments[23-31] examined the effects of various swept wing sections and planforms on aerodynamic forces and moments and surface pressure distributions. Maltby[32] (1962) had shown that using an oil-streak visualisation technique, the direction indicated by a streak of oil on the model surface is very close to the direction of the skin friction lines through the point (i.e. the limiting streamlines). Using this technique, Maskell[33] (1955) identified two main types of separated flow structures; a bubble type and a free shear-layer type (see figures 4-2 and 4-3). He observed that fluid accumulating at a three-dimensional separation line, which in general is oblique to the direction of the external inviscid flow field, leaves the separation line usually as a free shear layer and rolls up in the process of passing downstream. Maskell hypothesised that limiting streamlines from upstream and downstream of the separation line merge and leave the surface as a surface of separation. Although Maskell's hypothesis was challenged by Legendre[34, 35] (1956, 1965) and Oswatitsch[36] (1957) with mathematical models for the behaviour of limiting streamlines, Lighthill[37] (1963) showed that the behaviour of skin friction lines supported Maskell's theory.

Further experimental work was aimed at visualising the flow separation mechanism and using yawmeters and wake surveys to derive boundary layer information. Most theoretical work up to this point relied on experimental measurements of the boundary layer to develop empirical relationships. In particular, Black[38] (1952) visualised the surface flow over a 44° slender swept wing using a paraffin and lampblack mixture and studied how the leading edge separation develops with incidence. Similarly, Gregory and Love[39] (1965) used oil flow experiments to visualise the primary and secondary separation and attachment lines over a slender delta wing. Bebner[40] (1954) and Brebner and Wyatt[41] (1960) used yawmeters and wake surveys over 45° and 55° swept wings to show that crossflows induced by the wing sweep result in a thicker boundary layer near the trailing edge than would be expected from an unswept wing. Winter and Moss[42] (1974) showed that the effect of increasing Reynolds number for a 55° swept wing, was to reduce boundary layer thickness at the trailing edge and delay separation.

Most low speed experimental and theoretical studies since the 1960's have concentrated on highly swept wings ($\Lambda > 55°$) with thin slender sections giving rise to leading edge separations. The recent need for LO wings swept between 40° and 50°, that are relatively thick to facilitate the internal carriage of stores, has renewed interest in predicting and controlling trailing edge separations. Additionally, for wings with leading edge flaps deployed and/or at high subsonic speeds, there is a decreased tendency for leading edge separation. The emphasis is then on understanding and controlling trailing edge separation in the region of the adverse pressure gradient over the aft part of the wing, downstream of any shock waves.

However recent studies of such wings, particularly for lambda and diamond wing planforms, are generally of a sensitive nature and are unavailable for review.

4.4 Calculation methods for turbulent boundary layers

A review of the methods available for predicting the development of turbulent boundary layers has identified a number of approaches detailed below. These range from relatively simple integral boundary layer methods to the complexity of time accurate solutions of the Navier-Stokes equations. The choice of prediction method will depend on the complexity of the viscous flow anticipated for a particular application.

4.4.1 Integral boundary layer methods

Initial attempts at predicting separation position were limited to models of laminar boundary layers i.e. Von Karman and Millikan[43] (1934). Towards the end of the War, theoretical work focused on an analysis of experimental data for two-dimensional turbulent boundary layers to determine fundamental variables that control their development. Von Doenhoff and Tetervin[44] (1943) found two key variables; the ratio of a non-dimensional pressure gradient to the local skin friction coefficient and the shape of the boundary layer. An empirical equation was developed in terms of these parameters, that when used with the momentum equation and skin friction relation, allows turbulent boundary layers to be predicted up to the onset of separation. Further contributions to deriving empirical relationships for a shape parameter and velocity profile were made by Tetervin and Lin[45] (1951), and initial attempts to extend these ideas to three-dimensional flows by Cooke[46] (1958).

Integral methods for predicting the behaviour of turbulent boundary layers in two-dimensional and axisymmetric flows have been used for some time by the aeronautical industry. They are reliable and accurate for attached boundary layers and for limited regions of separated flow. Methods of this sort may be coupled with a solution of the Euler or Potential flow equations for the inviscid flow outside the boundary layer and wake, and a suitable method for predicting the laminar shear layers upstream of a specified transition position. Such viscous-inviscid interaction (VII) techniques iteratively derive a pressure distribution for the equivalent inviscid flow about an aerofoil, which is used for the laminar and turbulent calculations of a new boundary layer and wake to thus update the inviscid procedure (see section 5.4).

An approach originally based on the entrainment method of Head[47] (1956) and Green[48] (1972) is the lag-entrainment method of Green[49] *et al.* (1973) that defines a boundary layer in terms of three independent parameters; momentum thickness, shape parameter and entrainment coefficient. For a given pressure distribution, these values are predicted by forward integration of three simultaneous ordinary differential equations; the momentum integral, entrainment and a rate equation for the entrainment coefficient (*i.e.* the 'lag' equation) derived from the turbulent kinetic energy equation. Thus the lag equation contains terms for the advection, production, diffusion and dissipation of turbulent kinetic energy. The calculation method is extended past the trailing edge for wake flows with skin friction coefficient set equal to zero.

Approaches for extending these ideas for three-dimensional wing flows and adjustments to the entrainment relationship are discussed in the following chapter.

4.4.2 Turbulence modelling

The physical phenomenon of turbulence can be described as a cascade effect in which large-scale forcing transfers kinetic energy to smaller and smaller scales through non-linearities of fluid motion, until eventually at the molecular scale, viscosity causes the energy to be dissipated as heat. Thus, turbulence is inherently a three-dimensional and time dependent phenomenon, characterised by the presence of a large range of excited lengths and timescales. The inherent three-dimensionality means there are no satisfactory two-dimensional approximations and this is one of the reasons turbulence remains the most noteworthy unsolved scientific problem of the twentieth century.

The Navier-Stokes equations were derived in 1845, extending the Euler equations by including the effects of viscosity, giving five coupled partial differential equations that represent the conservation of mass, energy and the three components of momentum. The difficulty in solving these equations is in the ability to predict the rate of dissipation of kinetic energy due to the turbulent diffusion of large-scale eddies into heat through molecular viscosity. Additional equations to solve for these turbulent stresses result in there being more unknown correlation's than there are equations and hence a problem of closure. For virtually all flows of practical engineering interest there is a non-linear relationship between the inertial and viscous forces that govern Reynold stresses and, therefore, the rate of viscous dissipation (*i.e.* for Reynolds numbers greater than unity).

The ability to generate a mathematical model for turbulent stresses that approximates the physical behaviour of turbulent flows is a key element of CFD. An ideal model should introduce the minimum amount of complexity whilst capturing the essence of the relevant physics. We should expect the complexity of the mathematics needed for a given application to increase as the amount of required flow field detail increases. For example, if all we require is skin friction for a flow with mild pressure gradients, a simple mixing length model may suffice. On the other hand, if we desire complete time history of every aspect of a turbulent flow, only a direct numerical solution (DNS) of the complete Navier-Stokes equations will suffice. A number of approaches are available and will very much depend on the application.

4.4.3 Reynolds Averaged Navier Stokes (RANS)

For most practical applications a complete time-history of a turbulent flow is unnecessary. Thus statistical methods are used that time-average the turbulent fluctuations, using assumptions about the cascading process described above. The time-averaged approach to solving the Navier-Stokes equations originated with work by Reynolds[50] in 1895 with his pioneering research on turbulence. Due to the importance of this research, the standard time-averaging process is commonly referred to as Reynolds averaging. The methods of turbulence closure approximations to the RANS equations are generally categorised by the number of additional equations required and are given by, in order of increasing complexity;

1. Algebraic (zero-equation) models
2. One-equation models
3. Two-equation models
4. Second-moment closure models

Following the revolution in computer technologies since the 1960's, much development of all four categories of turbulence model has occurred, resulting in a vast number of models to choose from. The following sections attempt to describe some of the main developments and assess the applicability of the methods.

Algebraic (zero-equation) models

In 1877 Boussinesq[51] produced the earliest attempt at a mathematical representation of turbulent stresses (Reynolds stresses) with the concept of an eddy viscosity. Neither Reynolds nor Boussinesq attempted a solution of the RANS equation since the physics of viscous flows near bodies was not understood until Prandtl's discovery of the boundary layer[14] in 1904. In 1925 Prandtl[52] introduced the mixing length hypothesis for calculating the eddy viscosity. The Reynolds stress tensor is computed as the product of an eddy viscosity and the mean strain rate tensor. Eddy viscosity is evaluated for a mixing length proportional to the distance from the solid surface within the viscous sub-layer (elsewhere, eddy viscosity is proportional to boundary layer thickness). This concept formed the basis of virtually all turbulence modelling research for some time thereafter, with contributions from von Karman[53]. Van Driest[54] (1956) devised a viscous damping correction for the mixing-length model that is used in most algebraic models today. Cebeci and Smith[55] (1974) refined the model for attached boundary layers. To avoid defining the mixing-length scale as a function of boundary layer displacement thickness, Baldwin and Lomax[56] (1978) proposed an alternative scheme that is widely used today. Both of the latter schemes are relatively simple to implement (except for complex geometries) and are reasonably reliable for attached boundary layer flows. Johnson and King[57] (1985) devised a half-equation model that uses an extra ordinary differential equation for the maximum Reynolds shear stress, by adjusting the eddy viscosity in the outer part of the boundary layer. This method is more reliable in adverse pressure gradients and for predicting flow separation.

One-equation models

In 1945, Prandtl[58] postulated a model in which eddy viscosity depends on the kinetic energy of the turbulent fluctuations, k. An additional differential equation is solved to approximate for k, thereby introducing an historical influence on eddy viscosity. However, these one equation models still require a length scale characteristic of eddy size, usually the boundary layer displacement thickness. For separated boundary layers and free shear layers this mixing length is not as simple to define. Therefore, these methods have not proved popular with few benefits over algebraic models, though an implementation by Bradshaw, Feriss and Atwell[59] (1967) did show some improvements[60].

Two-equation models

In 1942 Kolmogorov[61] produced the first complete model of turbulence though it was several years later before computers were capable of solving its non-linear differential equations. In

addition to the model of kinetic energy of the turbulent fluctuations, k, Kolmogorov introduced another parameter, "the rate of dissipation of energy in unit volume and time", ω. This model incorporates the term $\sqrt{k}/\omega$ defining a mixing length scale and like k, ω was derived by solving a differential equation. With the advent of more powerful computers, many researchers have derived two-equation models, most notably Launder and Spalding[62] (1972). Launder produced a k-ε model, where ε is proportional to the product of k and ω, though this model has been shown inadequate for flows with adverse pressure gradients[63, 64]. For most two-equation turbulence models the application of a no-slip boundary condition to solid surfaces and the integration through the laminar sub-layer gives unsatisfactory results. A low Reynolds number approach to the problem is to introduce viscous damping factors, though these viscous corrections slow convergence and require tuning for different applications. Therefore, they do not represent much of an improvement over algebraic models. At high Reynolds numbers wall functions are used to match values of k and ω or ε to satisfy the no-slip condition. The use of wall functions avoids the need for extra viscous damping terms and allows larger near-wall cells, resulting in larger time-steps and faster convergence. Another problem with two-equation models is that the second equation (in terms of ω, ε or other parameter) has many approximations, resulting in a large number of models.

Independently of Komogorov, Saffman[65] (1970) also developed an improved k-ω model that could be integrated through the laminar sub-layer (without any special viscous corrections) and is suitable for adverse pressure gradients. A number of authors[66-69] have produced improved variations of this model, most notably that of Wilcox[64] (1988). Menter[70] (1993) replaced the relatively complex wall matching procedure of the Wilcox k-ω model with a simple wall boundary condition for ω and added a cross-diffusion term to the ω-equation to reduce an over sensitivity to free-stream ω. Another enhancement by Menter was a 'shear-stress transport' modification that uses a limiter on eddy viscosity which has improved predictions for separated flows.

In replacing unknown correlations with algebraic expressions involving known turbulence and mean flow properties, all two-equation models have closure coefficients. These are defined by the developer using assumptions such as homogeneous turbulent flow and boundary layer properties, and may need tuning for particular applications. Although two-equation models are considerably more complex than algebraic or one-equation models, some are more suited to applications requiring the prediction of viscous flows in adverse pressure gradients, or with separation, particularly the Wilcox k-ω model with Menters' modifications. Additionally, two-equation models can be easier to implement for complex geometry's than algebraic models.

The inadequacies of the Boussinesq eddy viscosity assumption limit the capability of two-equation models for complex flows, for example; flows over highly curved surfaces or with separation. By adding extra terms to the eddy viscosity formulation that are non-linear with respect to strain rate tensor, improvements in flow modelling can be found. These non-linear eddy viscosity models are relatively simple to implement and when used with k-ε or k-ω models can provide improvements, particularly for flows with high streamline curvature[71, 72].

Second-moment closure models

In 1951, Rotta[73] introduced a differential equation describing the Reynolds stress tensor to replace the eddy viscosity assumption. This required an additional seven equations to be solved, six for the components of the Reynolds stress tensor and one for a length scale. Further improvements in computer performance in the 1970's accelerated the development of differential Reynolds stress models[74, 75] particularly by Launder, Reece and Rodi[76] (1975) with improvements by Gibson and Launder[77] (1978), using an ε length scale. Further contributions by Lumley[78] (1978), Speziale[79] (1987) and Reynolds[80] (1987) were made to improve the closure process. As with the two-equation k-ε models, these second-order models cannot be integrated through the viscous sub-layer, requiring wall functions or viscous damping functions. Craft, Launder and Suga[81] (1996) have developed an ε based model that does not have these restrictions, though it is very complex. Alternatively, the Wilcox multiscale model[82] (1988) uses the ω length scale, is relatively simple and can be integrated through the laminar sub-layer without the need for wall/viscous damping functions. The model borrows a pressure-strain correlation from the Launder, Reece and Rodi model[76]. Although these models have demonstrated improved capabilities, particularly for flows with high streamline curvature, they are highly complex to implement and require substantial testing to ensure they are numerically stable and without errors.

4.4.4 Direct Numerical Simulation (DNS)

Although complete time-dependent solutions of the Navier-Stokes equations have been performed[83] for simple applications, the computer resources required are immense. The extent of the computational domain must be sufficient to accommodate the largest turbulence scales, whilst the grid must be fine enough to resolve the smallest turbulent scales, particularly near solid bodies, resulting in a very large grid. Additional problems of imposing boundary conditions at outer boundaries and of numerical accuracy have restricted the DNS approach to be mostly for steady two-dimensional problems.

4.4.5 Large Eddy Simulation (LES)

The principle of LES is to compute the large-scale time dependent turbulence structures directly (DNS), whilst modelling the small scales. The largest eddies possess most of the turbulent energy and are affected by boundary conditions. On the other hand, small scale eddies are more isotropic and have more universal characteristics and are thus easier to model. Also, because these small eddies are modelled, the grid resolution required can be relaxed. The unresolved (sub-grid scale) turbulent features are generally modelled using an eddy viscosity model similar to those described in section 4.4.3 though unlike RANS methods, the models should be applicable to a greater range of applications.

For flows of most interest at high Reynolds number, the unresolved scales can be anisotropic, particularly near solid walls, requiring more complex sub-grid scale models[84, 85] incorporating wall functions[86] to avoid expensive grid refinement and thus the direct simulation of eddies in

this region. At present, computer resources are still not sufficient to apply LES to industrial flows and are thus relatively untried.

5 Review of prediction methods

5.1 Opportunities for CFD

During the last decade, aeronautical Computational Fluid Dynamics (CFD) has made a substantial contribution in the development of both civil and military aircraft. CFD has now reached a point of maturity where it has become an essential tool for the design and development of aerodynamic configurations. Indeed, it is in the design and development of wings where rapid prototyping is of the essence, that CFD has its most obvious benefits. For most flow regimes, CFD can provide reliable results that are more affordable and within a shorter response time, relative to the cost and time-scales of the manufacture and testing of wind-tunnel models. Experimental aerodynamics remains, however, essential for final design verification and the evaluation of CFD methods to ensure reliable results, particularly for modelling complex three-dimensional flows where the capabilities of CFD remain largely inadequate.

Modern aircraft designed to operate at a particular condition or combination of conditions, at transonic speeds, will inevitably have shock waves. This transonic flow regime creates particular problems for numerical modelling. Additionally, although viscosity may be negligible for much of the flow it can have a significant effect on the global flow pattern. A moderate increase in the angle of attack of an aircraft, induced by a sudden gust or a high lift manoeuvre for example, could cause the boundary layer to separate causing a radical change in the flow including a sudden loss of lift, ultimately leading to a stall. The importance of non-linearity within these flows prevents the omission of non-linear terms from the governing flow equations and makes a numerical solution of the problem more complex.

The shock waves and their interaction with the boundary layer will define the performance boundaries of the aircraft in terms of drag rise, buffet onset and buffet penetration. CFD has made it possible to exploit the benefits of designing for subsonic and transonic flows, by examining trade-offs between geometric shapes necessary for low observability and aerodynamic performance for example. The incentive for wing designers to improve aerodynamic efficiency by reducing drag, yielding significant savings in operational costs due to reduced fuel burn, or improvements in the buffet performance to extend the flight envelope, is substantial.

5.2 Evaluation of CFD

The evaluation of a CFD code[87] must:

- ensure the user is confident that results are acceptably free from non-physical or numerical inaccuracies,
- make certain that the method behaves in a reliable and consistent manner,
- identify which physical processes the code can model in a practical sense,
- determine whether the code can be used on radically new geometries with confidence,
- be economical in terms of computer time and effort.

Therefore, the evaluation of a code must be based on a careful exercise of comparing CFD results with parameters measured in a wind-tunnel environment or from flight tests. Confidence in a methods capability can only occur when (a) the accuracy and limitations of, for example an experiment, are thoroughly understood, and (b) the code achieves consistency and the limitations of the physical modelling of the flow are understood. This should be achieved for a range of geometries and flow conditions for which the code is intended to be used. An evaluation exercise may show that a CFD code is not sufficiently accurate to be used in isolation, but using empirical data from experimental studies, for example to define input boundary conditions, can be used as an effective design tool. Often CFD codes are run as 'free-air' simulations and comparisons made with experimental data which are corrected for tunnel interference. Frequently, these correction techniques are based on more approximate and less appropriate methods than those being evaluated.

CFD evaluation must ensure that measured data are sufficiently detailed to be consistent with CFD modelling requirements on flow-field boundaries as well as geometric surfaces, and flow visualisation is used to fully understand complex flows. It is essential that wind tunnel model contours are accurately measured to ensure there are no geometric deviations from the theoretical co-ordinates and that aeroelastic effects are considered in a CFD simulation.

CFD modelling inaccuracies can be divided into four categories;

- The grid generation stage will be influenced by the accuracy of body surface representation as well as resolution of the geometry and interpolation techniques used to compute flow variables.
- The choice of governing equations and the assumptions made *i.e.* in the modelling of viscous and rotational effects and of enthalpy changes. Also, empirical models may be used, based on similar geometries and flow conditions. Theoretical models may not be capable of accurately modelling the transition from laminar to turbulent flow or of predicting differing degrees of flow separation with the same accuracy.
- Discretisation of the governing equations is the source of many errors due to the assumptions made e.g. truncation errors, choice of differencing scheme used, treatment of flow-field discontinuities and schemes to enhance the stability and convergence rates.
- Definition of boundary and initial conditions, depending on whether 'free-air' or 'in-tunnel' conditions are being modelled.

Details of the CFD codes used in this investigation, either as design tools or in evaluation studies, are given below;

5.3 Methods available

In principle, it is possible to perform direct numerical simulations using the full equations for fluid motion including time accurate viscous effects *i.e.* the Navier-Stokes equations. In practice, considerable difficulties exist in representing the viscous terms accurately and in modelling turbulence. As technological advances in computer hardware and algorithm development have evolved, the scope of CFD methods to extend the range of flight conditions that can be reliably predicted has increased as we have seen from the previous chapter. Table

2 indicates which assumptions to the governing equations are used to simplify the numerical solution and their range of applicability.

In order to model the types of flow that we are primarily concerned with in this thesis we need to examine the capabilities of VII methods and solutions of the Navier-Stokes equations. Since the development of new algorithms was beyond the scope of this work, existing industrial CFD methods readily available to DERA, have been assessed for their suitability. This and the computational resources available limit the Navier-Stokes solution methodologies to time-averaged solutions of the problem using a turbulence model for closure *i.e.* RANS methods. Detailed descriptions of the VII (VFPST) and RANS (SAUNA) methods are given below. Additionally, a transonic aerofoil code (BVGK) and a turbulent boundary layer method (TAPERBL), both based on the VII principle, were used in the design of the wing section and are described below.

5.4 VII methods

5.4.1 BVGK

The transonic aerofoil CFD code, BVGK[88], has been used to calculate flow characteristics for highly cambered aerofoils for angles of incidence/Mach number up to separation. The code has become the UK standard for predicting the aerodynamic drag of aerofoil sections, and is known to give good agreement with experiment[89]. Based on the viscous-inviscid interaction (VII) procedure, this method combines a numerical solution of the exact potential-flow equations for the equivalent inviscid flow with integral methods to solve the shear-flow equations.

The original method of Garabedian and Korn[90-92] (1971) used a finite difference scheme for solving the full potential equations for subsonic and transonic flows about aerofoils. Therefore, the method assumes steady, irrotational and isentropic inviscid flow. A conformal mapping procedure first transforms the aerofoil into a circle and then the external flow domain onto the interior of the circle such that the centre of the circle corresponds to all points that are an infinite distance from the aerofoil surface in the physical plane (see figure 5-1). This generates a uniform computational or parametric polar grid with grid refinement close to the aerofoil surface in the physical grid, sufficient to resolve the larger velocity gradients found in this region. Using this discretisation, the full-potential equations are solved iteratively on 'coarse' (80x16) and 'fine' (160x31) grid levels. In the transformed plane, both u and v-velocity components are set to zero at the trailing edge to satisfy the Kutta condition. At the aerofoil surface (outer boundary of the parametric polar grid) the v-velocity component is set to zero and at the outer boundary (the centre of the parametric polar grid), u and v-velocity components are given free-stream values.

Since the potential equations are of an elliptic form in regions of subsonic flow and hyperbolic in supersonic regions, two differencing schemes are employed. In subsonic flow, where flow is dependent on both upstream and downstream influences, a central differencing scheme is used of second order accuracy. In supersonic regions, where there is no dependence on

downstream influences, a forward differencing scheme is used that is first or second order accurate, depending on the amount of artificial viscosity introduced. With a minimum level of artificial viscosity the scheme is second order accurate, but is numerically unstable. This form of differencing permits the formation of steep pressure rises, equivalent to shock waves. Since the method was intended for supercritical aerofoil design, that typically features weak upper surface shock waves, the isentropic nature of the potential flow equations is assumed to be preserved. However, where local Mach number exceeds about 1.3, shock waves are deemed sufficiently strong to make this assumption invalid. Since the flow across these 'pressure waves' experiences a loss of momentum in this potential flow solution, conservation of momentum is not satisfied across subsonic and supersonic domains. Therefore, this differencing scheme is referred to as non-conservative.

Collyer[93, 94] (1977) developed a viscous version of the Garabedian and Korn (VGK) method, based on the VII technique, for fully attached boundary layers. VGK uses the previous method, with a few modifications, to solve the full-potential equations for the inviscid regions of the flow. This is coupled with the calculation method of Thwaites[95] (1949), with a modification for compressibility effects by Stewartson[96] (1949), for the laminar shear layers and the lag-entrainment method described in section 4.4.1 for the turbulent shear layers. Boundary-layer transition at the specified location is assumed to occur discontinuously but boundary-layer momentum thickness is taken to be continuous at transition. This flow model has been found to be preferable for the prediction of drag to an alternative model in which boundary-layer displacement thickness is assumed constant across transition.

- An inviscid flow-field is generated before calculating shear layers. The inviscid pressure distribution on the aerofoil surface and wake centreline is adjusted to account for curvature effects of the aerofoil and wake on the normal pressure gradients within the shear layers.
- A boundary layer and wake are then calculated for each surface downstream of the stagnation point to obtain shear layer displacement thickness and momentum thickness. To account for the mass deficit/addition as the shear layers grow and reduce, the boundary condition for the 'equivalent inviscid flow' must be modified. By specifying a distribution of sources and sinks (*i.e.* in the form of transpiration velocities) at grid points on the aerofoil surface and along the rear dividing streamline in the wake, this boundary condition ensures that mass is conserved. Also, to match the pressure change across the wake in both viscous and inviscid flows, a boundary condition imposes a jump in tangential velocity.
- Since the conformal mapping is singular at the trailing edge it is not possible to define the wall transpiration velocities there. Therefore, a trailing edge pressure is extrapolated from upstream and downstream pressure distributions in the shear layers, and on both surfaces. The four extrapolated pressures are thus averaged to give a unique trailing edge pressure that satisfies the Kutta condition. It is necessary to subsequently smooth the upstream and downstream pressure distributions on each surface away from this mean trailing edge pressure. Since the shear layers are calculated in the physical plane, the close proximity of grid points at the trailing edge can lead to difficulties in obtaining converged solutions. Therefore, it is necessary to omit three grid points upstream and downstream of the

trailing edge (on the finest grid level) from the shear layer calculations, and to interpolate transpiration velocities at these omitted points for the boundary conditions to the inviscid procedure.

- The non-conservative finite differencing scheme used in solving the potential equations is also modified to allow conservation of mass, though not momentum, across subsonic/supersonic domain boundaries. However, in practise a differencing scheme somewhere between the two approaches appears to predict the expected shock strength and position. Thus, VGK provides a parameter that allows the user to specify to what degree mass is conserved, giving a 'partially-conservative' differencing scheme.

The above inviscid/viscous procedure is repeated until the maximum change in velocity potential between successive iterations is less than a prescribed level for convergence.

Though the VGK method gives good agreement with experiment[89, 94, 97], it has been found to under-predict boundary layer growth as separation is approached. Therefore, for flows with strong adverse pressure gradients it is necessary to include higher-order Reynolds stresses and flow curvature effects in the lag-entrainment method. Ashill *et al.*[88] (1987) made a number of improvements to the implementation to produce the BVGK method used today;

- The integral equations for the conservation of mass and momentum included second-order Reynolds stress terms and allowances for streamline curvature on turbulence structure.
- An improved shape parameter relationship suitable for flows with trailing-edge separation.
- A modification to the skin-friction relationship for low Reynolds number.
- The turbulent shear layers are calculated using an inverse procedure suitable for flows with separation, retaining a direct procedure for the laminar shear layers (thus BVGK is 'semi-inverse'). From an assumed distribution of boundary layer thickness, the lag-entrainment equations are solved for streamwise velocity, momentum thickness and entrainment coefficient. To match this inverse solution with that of the equivalent inviscid flow, a refined displacement thickness distribution (and therefore, transpiration velocity distribution) is generated for the next inviscid cycle.
- As a consequence of the inverse procedure for the turbulent shear layers, an alternative method is required for determining the pressure at the trailing edge, necessary to satisfy the Kutta condition. Instead of determining a mean pressure at the trailing edge, the displacement surface curvature and angle of the wake centre line, relative to the chord, are adjusted until the upper and lower surface pressures at the trailing edge are equal and the displacement surface is smooth.

For flows approaching separation or with separation close to the trailing edge, BVGK gives significant improvements compared with VGK.

5.4.2 TAPERBL

TAPERBL is used for calculating the three-dimensional boundary layer behaviour on an infinite and tapered swept wing from a specified static-pressure distribution. The code utilises a similar procedure for calculating laminar and turbulent shear layers as VGK, though only

one calculation is performed since the pressure distribution is fixed. The laminar shear layers are corrected for the effects of cross-flows using the method of Cooke[98] (1960) and the lag-entrainment equation is modified by Smith[99, 100] (1972, 1974) for infinite yawed wings. The code also includes corrections for low Reynolds number and streamline curvature on turbulence, similar to those implemented in BVGK.

5.4.3 VFPST

The Viscous Full-Potential method for Swept and Tapered wings (VFPST) is an extension of the VGK aerofoil method to three-dimensional wing and wing/body flows by Forsey and Carr[101]. The conformal transformation is similar to that of VGK with the mapping of the flow field domain to the inside of a cylinder. The method can also include a simple fuselage, of fixed circular cross-section, that is first mapped to a slit in the plane of symmetry, so leaving a distorted wing in this 'intermediate space', and is subsequently mapped to the inside of the cylinder (see figure 5-2).

The potential flow equation in non-conservative form is approximated by a set of finite difference equations and is solved by an iterative process on a uniform mesh in the computational space using a successive line relaxation procedure. The turbulent shear layers are calculated using the lag-entrainment method, extended to three-dimensions by Smith[99, 100]. Modifications by Ashill and Smith[102] (1985) include an allowance for tapered wings and a semi-inverse coupling procedure, similar to that used in BVGK, that is more suitable for flows near separation. This method uses the assumption that the flow is locally similar to that around an infinite tapered wing, and thus, is restricted to wings having isobars lying close to the spanwise generators. For high aspect-ratio wings, with streamwise pressure distributions that vary slowly across the span, this assumption is generally satisfied. 'Higher-order' terms, such as those included in the BVGK code, which are known to be important for flows close to or with small amounts of separation are not included in the VFPST code.

5.5 RANS method

5.5.1 SAUNA

The SAUNA[103-105] (Structured And Unstructured Numerical Analysis) system employs body-conforming grids for complex three-dimensional geometries and combines this with a solution of the Reynolds Averaged Navier-Stokes or Euler equations. Although SAUNA has a capability to embed regions of unstructured grid to accurately define regions of geometric complexity, only structured grids have been used in this study due to the relative simplicity of the geometry. There are several stages to obtaining a fully structured grid suitable for a solution of the RANS equations, that are depicted in figure 5-3.

The entire flow field between the configuration surface and a user defined far-field boundary is divided into sub-domains that are topologically equivalent to cuboidal blocks, commonly referred to as the 'Multi-block' method[106]. The blocks contain a structured non-overlapping hexahedral grid system that are patched together to form the global grid, ensuring that grid lines are constrained to pass between blocks with continuity of position, slope and curvature. The decomposition of the flow domain into blocks, the block-to-block connectivities and the distribution of grid points on these block edges is defined by the user, providing some grid control at an early stage. To manually specify this data for a complex configuration can require a large amount of effort, hence an algorithm automates the topology generation process[107]. From a simple user-defined schematic of the configuration and interactive prompts, a component adaptive block structure is produced. In particular, sub-regions can be identified in which the resulting grid has a structure that is compatible with particular geometric characteristics *i.e.* to embed a 'c' grid topology about a leading-edge. This part of the system also identifies which boundary conditions (see table 3) apply to each surface and whether grid refinement is required for modelling viscous effects.

Since flow properties depend on the surface curvature of solid boundaries, it is important to obtain an accurate representation of the geometry. In general, the geometry is known to the user as a set of discrete points rather than a closed analytical expression. Thus to recreate each surface from the discrete data patches of bi-cubic splines[108] are formed. The physical geometry is initially transformed into two-dimensional parametric co-ordinates, representing the normalised surface distances along and across cross-sections of geometry points. Where a discontinuity in surface slope exists, for example at a wing crank, the bi-cubic patching is constrained to maintain this slope discontinuity. Once all surface patches exist, intersections between relevant surfaces (*i.e.* wing and body) are calculated.

The quality of surface grids will strongly influence the subsequent generation of field grids and flow behaviour near solid boundaries. Therefore the user has a significant amount of control over this part of the system. Surface grids are generated in the two-dimensional parametric space and are then mapped, via the bi-cubic patches, back to curvilinear co-ordinates in physical space. Their generation requires the solution of a set of elliptic equations[109] containing source terms to position grid points where solution activity is high and thus control quality. These source terms are derived from specified point distributions along

block edges[110]. Since the distribution of grid points along all block edges would require a large amount of effort, an algorithm distributes points automatically to form an initial grid. These initial point distributions will be sensitive to local grid topology and the position of intersecting components. Once surface grids have been generated, examination of the grids may indicate that changes to the underlying topology are required, to increase a block-edge dimension for example, or to edit a particular feature of a surface grid.

To ensure surface grids are of a high quality, a graphical interactive surface grid editor[111] allows the user to make a number of changes to the parametric grid such as; moving the position of block corners, re-distributing points, straightening block edges etc. There are a number of reasons why a grid may need editing:

- Grids generated by solving elliptic equations have a tendency to fold over, requiring a fix by the user to resolve the problem
- The automatic point distribution algorithm can be insensitive to geometric slope discontinuities, such as at wing cranks, and it may be necessary to move block boundaries such that they improve the definition of the discontinuity.
- Local grid topologies, such as embedded 'c' grids, can produce undesirable features in the global grid, particularly near singularities, that need to be controlled.
- A high quality parametric grid may not represent a high quality grid in the physical space, usually due to a poor geometry definition, and may need editing to remove these discrepencies.

The edits performed are automatically saved for use in subsequent applications. Once the user has finished editing any number of surfaces, surface grids are re-generated using the previous algorithm. It is usually necessary to perform the edit/re-generation loop several times before satisfactory grids on all surfaces are attained.

Field grids are generated in a similar manner to the development of surface grids. Elliptic differential equations are solved iteratively using a point over-relaxation scheme. Constraints on the field grid can be imposed by the generation of control planes, to prevent grid distortion problems (for example at the wing tip). These control planes are generated as 'surface' grids which cross the domain, with one physical co-ordinate approximately constant. For RANS calculations, a field grid suitable for inviscid flow (Euler) is first calculated and is then refined in the surface normal direction within selected blocks using a transfinite interpolation scheme. By this means, sufficient grid resolution is achieved in regions where shear layers, wall bounded or free, are expected to form as part of the viscous flow solution. The magnitude of the initial grid spacing normal to these selected surfaces is a critical parameter in determining solution accuracy and is therefore specified by the user.

Although the multiblock method allows better automation and control over the grid generation process, it can create a large number of blocks leading to poor performance on vector processing machines. Therefore, the block structure is processed ahead of the flow simulation to form a set of large computational regions or 'super-blocks'. Each super-block is composed of several ordinary blocks, either in total or in part, and is formed with information necessary to communicate with other super-blocks, in a manner transparent to the user. Additionally, within the structured grid generation system there exists a rapid grid re-generation module

'remesh'[112] that can be used following minor design changes to the baseline geometry. Providing the re-design does not require global changes to a grid such as a redefinition of block dimensions or a new grid topology, the remesh module provides a means for an efficient design optimisation study.

The Euler/RANS flow solver, uses a Jameson-type flow algorithm[113, 114], in which an explicit time-marching, finite volume technique is used to solve the equations at each grid vertex from some initial conditions to a steady state solution. The time dependent form of the equations, in conservative form, are solved by balancing the mass, momentum and energy fluxes for control volumes within the flow-field. For a given vertex, a control volume is defined as the sum of the cells which meet at the vertex. For the Navier-Stokes equations, additional viscous terms use a control volume defined by the centroids of each cell that comprise the Euler control volume. The flux balance is evaluated as the sum of the normal fluxes across the external faces of a control volume by averaging variables at adjacent nodes. The RANS equations can be solved for all control volumes within the grid, or a zonal strategy can be used to solve the RANS equations in blocks adjacent to viscous shear layers and the Euler equations for the inviscid part of the flow. Since the Baldwin-Lomax[115] and Johnson-King[116] algebraic models are not suited for separated flow with high streamline curvature, this thesis will concentrate on the k-ω two-equation model[117] and the Wilcox multi-scale model[117]. An LES model is currently being implemented within the SAUNA system[118] and may be evaluated in future work.

On the wing surface, a no-slip boundary condition is applied with Riemann invariant conditions on all farfield boundaries except the plane of symmetry, which has a flow tangency condition. For the two-equation turbulence models, k, ε or ω are fixed at constant freestream conditions on the inflow boundary and are extrapolated at the outflow boundary. It is necessary to specify two constants, C_1 and C_2:

$$k_\infty = C_1 U_\infty^2$$

$$C_2 = \left[\frac{\mu_t}{\mu}\right]_\infty$$

where C_1 sets the freestream turbulence intensity, k_∞, and C_2 gives the freestream ratio of eddy-viscosity to laminar viscosity. Both k-ω and k-ε models impose a lower limit on ω or ε to prevent negative values, based on the Schwarz inequality[117].

The mean flow equations are augmented by the addition of second and fourth order artificial dissipation to reduce oscillations near shock waves and to prevent odd-even decoupling. To prevent the artificial dissipation from swamping the real viscous effects in regions of high grid aspect ratio, an anisotropic formulation is used. In addition, a modification is applied near surfaces in order to reduce the dissipation and enhance the accuracy of the prediction of sensitive quantities such as skin friction. Fourth order artificial dissipation alone is added to the turbulence model equations to smooth turbulence quantities, though this is reduced near

solid walls. Dissipation terms are constructed as a combination of approximations to Laplacian and biharmonic operators via loops over edges in the grid and are scaled relative to the local maximum wave speeds[114].

The discretised turbulence equations are marched in time to a steady state simultaneously with the mean flow equations, employing a five-stage explicit Runge-Kutta scheme. A stable time-step for the mean flow equations is determined from a von Neumann stability analysis of both the convective and diffusive terms. A similar approach is used for the turbulence equations, with an allowance for the presence of source terms. For the mean flow equations, a W-cycle multi-grid technique is used to accelerate convergence, with turbulence variables evaluated on the finest grid level only. The rate of convergence of the scheme is further improved by using implicit residual smoothing for the mean flow equations.

5.6 Post-processing tools

An important element in any CFD system is the ability to visualise the vast amounts of data that are generated. Forces and moments are obtained using the SAUNA post processing facility, by integrating surface pressures. SAUNA post processing also extracts contour data, such as chordwise pressure distributions. The Ensight software package has allowed visualisation of the three-dimensional flowfield around the wing, including stream traces within the calculated shear layers and wing surface streaklines to analyse the flow development.

6 Model design, manufacture & wind-tunnel testing

6.1 Aerofoil section design

The wing section used in this study was derived from the supercritical aerofoil, RAE5225, which has been extensively used for CFD validation and is an AGARD test case[119]. The RAE5225 section has a 14% thickness/chord ratio, a trailing-edge thickness of 0.5% chord, and was designed with significant rear camber to study viscous effects on flows over aerofoils with severe adverse pressure-gradients. Therefore, RAE5225 is an ideal baseline geometry for the present investigation.

Although this is purely a low speed study, the pressure distribution generated by the wing is designed to be typical of that for a landing or transonic manoeuvre condition where flaps may be deployed to increase wing lift. Therefore, the camber distribution along the RAE5225 section was modified to increase the rear adverse pressure gradient. However, to ensure the flow remains attached over the forward part of the aerofoil at high incidence, the nose was drooped to reduce leading-edge suction peaks and provide a more favourable pressure gradient in this region. To promote boundary layer separation on the upper surface, trailing edge droop is also applied. This is achieved by firstly splitting the baseline geometry into thickness and camber distributions, then modifying the camber distribution using the formula for a circular arc,

$$\Delta Z_{FORWARD} = -\frac{(X_F - X).(1-\cos\theta_F)}{\sin\theta_F} \qquad for\ X < X_F$$

$$\Delta Z_{REAR} = -\frac{(X - X_R).(1-\cos\theta_R)}{\sin\theta_R} \qquad for\ X > X_R$$

the camber line upstream of a chordwise position, x_F is drooped by an angular deflection, θ_F. Similarly, the camber line is drooped aft of position, x_R by an angular deflection θ_R. To determine suitable locations for the forward and rear positions and angular deflections, a parametric study was undertaken. By varying these four parameters, geometries were generated by combining the thickness and modified camber distributions. For each section, the BVGK aerofoil code (see section 5.4.1) was used to calculate pressure distributions over a range of angles of incidence at a two-dimensional Mach number of 0.15. These pressure distributions, section geometry and flow conditions were transformed to equivalent three dimensional values on a swept un-tapered wing using the following relationships[120]:

$$C_{p\,3D} = C_{p\,2D}\cos^2\Lambda, \quad Z_{3D} = Z_{2D}\cos\Lambda, \quad M_{3D} = M_{2D}\sec\Lambda, \quad C_{L\,3D} = C_{L\,2D}\cos^2\Lambda$$

At the three wing sweeps considered, Λ = 30°, 40° and 50°, the TAPERBL boundary layer method (see section 5.4.2) was used to calculate a 3-D turbulent boundary layer on an infinite swept wing, given the transformed pressure distributions. This enables the streamline curvature within the boundary layer to be evaluated. Figure 6-1 shows how the angle between

the local boundary layer direction and the free-stream flow direction varies across the wing chord. The aim of the study was to define a wing section for which the limiting streamline is parallel to the trailing-edge over the rear of the section at each sweep angle. In this way, the values; $x_F = 0.30$, $\theta_F = 15°$ and $x_R = 0.60$, $\theta_R = 30°$ were chosen to define the new wing section, designated 2337. Additionally, it was found necessary to smooth the upper and lower surface geometry to reduce discontinuities in surface curvature at the forward and rear droop locations. The geometric co-ordinates defining the un-swept (2-D) wing section are given in Appendix A.

Pressure distributions at a fixed lift coefficient, $C_L = 0.89$, and aerofoil profiles for the RAE5225 and 2337 sections are shown in figure 6-2. The distributions show that the increased camber of the 2337 section gives a more relaxed pressure-gradient over the forward part of the aerofoil, significantly reducing the suction peak level, whereas a more adverse gradient is achieved near the trailing edge.

6.2 Wing model design & manufacture

Using the co-ordinates for the 2337 wing section derived above, a constant chord (*i.e.* un-tapered and un-twisted) wing was designed and manufactured, capable of being swept aft from 0° to 60° in 5° intervals. The wing has a streamwise chord of 2ft (0.61m) and a semi-span of 6ft (1.83m) at 0° sweep. Three tip sections were manufactured that when attached, allow streamwise tips at 30°, 45° and 60° wing sweeps. The model was machined from solid aluminium and hand finished to give a smooth surface. Grooves machined in both surfaces for pressure tubing are filled with resin. The wing has a detachable section over the rear 25% of the chord to facilitate the study of other trailing edge sections, should it be required. After manufacture the wing was inspected and differences from the nominal z-ordinate, shown in figure 6-3, are relatively small.

Figure 6-4 shows the model mounted on the floor of the 13ft x 9ft low speed wind tunnel at DERA Bedford. The model is shown swept at 40° with the 45° swept tip attached, giving a tip section inclined at 5° to the freestream direction. To prevent the relatively thick boundary layer that grows on the tunnel floor from disturbing the wing root flow, which could propagate out towards the tip, a splitter plate is used (see figure 6-4). The flat plate is mounted horizontally onto the working section turntable, 0.15m above the wind tunnel floor and is not in physical contact with the wing. A seal is used in the wing root region to prevent flow from below the splitter plate passing through the gap. Originally a brush seal was planned, but when fitted was found to exert a measurable force on the wing (since the wing is 'live' and the splitter plate is not) which would thus affect repeatability of force and moment measurements. Eventually a foam-rubber seal (draught excluder tape) was found to provide an adequate seal between the wing and splitter plate, whilst not interfering with the wing *i.e.* if a force is exerted on the wing, the balance measurements always return to their initial state after the force is removed.

The wing is pressure plotted at 5 spanwise stations, each station having 36 upper surface and 16 lower surface static pressure holes. As the wing sweeps of most interest are between 40°

and 50°, pressure tappings are inclined at 45° to the leading-edge sweep, giving almost streamwise pressure distributions at the main sweep, Λ = 40°. The pressure holes are concentrated near the leading and trailing edges where pressure gradients are highest.

6.3 The wind-tunnel facility

The 13ft x 9ft tunnel (figure 6-5) is a closed circuit, continuous operation atmospheric low speed facility[121]. The large contraction ratio between the settling chamber and working section and four screens in the settling chamber provide excellent flow quality (rms fluctuations in longitudinal velocity are below 0.04% of the mean velocity at 61m/s). The working section has good optical access for the flow visualisation techniques described below. The working section is rectangular, being 13ft (4m) wide and 9ft (2.7m) high with corner fillets. A six bladed fan (30ft diameter) is driven by a 1500 HP 1100rpm DC motor, giving a maximum working-section speed of 91 m/s.

A significant advantage of this tunnel is its short start-up and shutdown times (advantageous for oil flow visualisations where many, very short runs are needed). Static and dynamic loads on the model can be measured, though only static data were recorded during the present test.

The model was mounted on the half model rig via a mounting block, which also provided the ability to change sweep angles. This mounting block is fixed to a mechanical balance suspended below the turntable. Turntable rotation is the only attitude change that can be applied to the model, giving pitch angles in the range ±180° (measured to within ±0.01°), depending on model size and in the first test, the lengths of pressure tubing from tunnel wall holes to the pressure recording system positioned on the mounting block.

6.4 Transition fixing

It is necessary to 'trip' or 'fix' the boundary layer on the model to ensure that the position of transition from laminar to turbulent flow is defined and the boundary layer behaviour is representative of flight conditions. The trips should fix transition with a minimum disturbance to the flow and should be applied in a consistent manner. To be effective, the trip must be upstream of the position of natural transition of the model, which will depend on;

- tunnel turbulence and noise levels and the test Reynolds number.
- pressure gradients and leading edge suction peaks.
- sweep instability of swept wings due to turbulent contamination or amplification of disturbances along the attachment line and cross flows within the boundary layer.
- surface roughness.
- deviations in model temperature.

Transition is generally fixed on wings using a sparse distribution of three-dimensional excrescencies. For swept wings this method is more effective than a two-dimensional trip (*i.e.* a wire), being insensitive to flow direction. For the test series, Carborundum grit is attached to the model surface using a thin film of epoxy resin. Careful attention to the process is required to ensure repeatability of results, by obtaining a consistent and repeatable density of particles.

Various criteria are available to determine the minimum height needed to fix transition with three-dimensional excrescencies of this type. Of these the Van Driest and Blumer criteria[122], based on experiments on flat plates, is most appropriate and is defined in Appendix B. At a given transition position, the local velocity and boundary layer parameters calculated by the TAPERBL method are used to determine particle height. Consequently, grade 46 Carborundum particles were selected and embedded in Araldite adhesive in a 5mm wide band at 5% chord on both upper and lower surfaces. One trip geometry should suffice for a wide range of angles of incidence at low free-stream Mach numbers and at a given Reynolds number.

A number of techniques are available to check the effectiveness of the transition trip such as liquid crystals or infra-red techniques. For this study, initial oil flow patterns were examined for the presence of natural transition upstream of the trip, visualised as a series of turbulent wedges. As a result of this the initial transition position (at 10% chord) was moved further upstream to 5% chord. Oil flows also indicated that the particle height was sufficient for fully developed turbulence downstream of the trip and that relaminarisation did not occur.

6.5 Force and surface pressure measurements

The mechanical balance records four components that are processed by the off-line analysis described below to give model forces and moments.

Model surface pressures are measured by a pressure transducer mounted in a multi-port scanning head (*i.e.* a scanivalve). Seven scanivalves were used in the test, with 42 of the 48 ports on each scanivalve connected to either wing or tunnel wall static-pressure tappings. The other six ports recorded the settling chamber stagnation pressure, working section reference pressure and a calibration pressure (set to -1.0psi). Of the 7 scanivalves, 5 used 5psi (34.4KPa) range transducers and 2 had 2.5psi (17.2KPa) range transducers. The basic accuracy of the pressure measurements depends on a number of factors; the accuracy of the gauge used to measure calibration pressure, non-linearity and hysteresis characteristics of the transducer (minimised by choosing the transducer to suit the pressure range), and carry-over between pressure ports. Scanivalves are located beneath the turntable to minimise tubing and therefore, lag effects, and each pressure tapping was leak checked prior to testing. The transducers are driven and scanned together under computer control, scanning all 48 ports in about 30 seconds. To avoid carry-over between pressure ports, the data is sampled to ensure that the pressure is steady before moving on to the next port. The calibration pressure is referenced to the working section reference pressure and provides a gain factor for each transducer that is used to correct for any instrumentation drifts during on-line data reduction. A calibration pressure is produced by a self contained generator unit. The above techniques allow pressure to be measured to within 0.05% of the transducer full scale and pressure coefficients to an accuracy of $\Delta Cp = \pm 0.002$[123].

6.6 Data reduction methods

Raw data measured in the wind tunnel, such as angles of incidence, pressures, forces and moments, must be corrected to account for instrumentation drifts and effects of constraining

the flow over a model in a solid wall wind tunnel. The process of reducing raw pressure measurements to pressure coefficients whilst allowing for instrumentation drift was discussed above. Further data corrections can be divided into four stages;

Firstly, the on-line reduction[124] of the four measured balance components, namely normal force, axial force, pitching moment and root bending moment, to non-dimensional loads on the model by the following five steps;

1 Isolating net aerodynamic loads by subtracting the raw data recorded during a 'wind-off' test. The 'wind-off' tests are made whilst the tunnel is shutdown, prior to the first 'wind-on' test of each new configuration within the current test series. 'Wind-off' data is taken over the full range of incidences needed for the test to allow a simple linear interpolation to be used at the appropriate 'wind-on' model attitudes. Also, before the start of each 'wind-on' test, a single data point is recorded for zero incidence. The balance readings for subsequent data points are subtracted by those for the 'set zero' data point. At the end of a run, a final 'set zero' is taken to determine whether any significant drifts in either of the four balance components has occurred. One source of balance drift is if temperature gradients exist within the balance, though these effects tend to be limited to high speed testing. Another source of balance drift could occur if the 'live' wing is fouled by the foam seal.

2 The net aerodynamic readings are converted to dimensional loads using linear interpolation of a previous tunnel calibration that assumes no interactions between components. As mentioned above, data is subsequently corrected 'off-line' to account for second order component interactions. A tunnel calibration should include a flow survey of the working section since corrections to incidence vary with working section geometry and wall boundary layer development.

3 Loads are converted to non-dimensional coefficients using the working section dynamic pressure and appropriate dimensions, relative to the balance axis system.

4 Coefficients are transformed relative to the model datum axes if the x-axis is offset from the balance x-axis.

5 Since the balance and model rotate together in pitch, a final transformation is required to convert coefficients relative to the stability or wind axes system.

The second stage can include corrections for second order component interactions and for any balance drift between the start and end of the run.

The final two stages attempt to infer the equivalent free-air flow over the model from the constrained-air flow data recorded in the tunnel. As described above, this is necessary for comparison with flight test data and, more significantly for this investigation, for validating free-air CFD results. Whilst the previous two stages are performed by existing data reduction methods it was necessary to implement the following stages for this project.

The third stage determines a blockage constraint factor using the 'classical' method described in reference 125. More recent methods have been developed which use measurements of changes in flow quantities at or near the tunnel walls between empty and model-present tunnel runs[126]. Static pressure coefficients were recorded at about 9 streamwise stations along the roof and side walls for each run (including a tunnel empty run), to provide sufficient data for these methods to be used. However, results presented in this thesis are corrected using classical theory, whereby the model is replaced by singularities and the walls with a set of images. The blockage correction consists of contributions due to model volume (solid blockage) and due to the wake, given by;

$$\varepsilon_1 = 0.000456\left[1+1.2\frac{t}{c}\right]\frac{V_m}{\beta^3} \qquad (\textit{solid blockage})$$

$$\varepsilon_2 = \frac{C_D S}{4A_T\beta^2} \qquad (\textit{wake blockage})$$

where, V_m is the model volume, $\beta = \sqrt{1-M^2}$ and A_T is the cross-sectional area of the wind tunnel. A modification can be applied to the wake blockage for models with separated flows, proposed by Maskell[125]. However, there is evidence that maximum lift coefficient is underestimated for models with partially separated flow and thus has not been used[126]. The following corrections are made using these blockage factor contributions;

$$M = M + (1+0.2M^2).(\varepsilon_1+\varepsilon_2) \qquad C_p = C_p + (2-(2-M^2).C_p).(\varepsilon_1+\varepsilon_2)$$

$$C_L = C_L - (2-M^2).(\varepsilon_1+\varepsilon_2) \qquad C_D = C_D - (2-M^2).(\varepsilon_1+\varepsilon_2)$$

In solid wall wind tunnels, a fourth stage in the data reduction is required to correct for an additional lift constraint associated with the images of vortices on the wing and in the wake, inducing an upwash in the region of the wing. Therefore, the corrections derived by Acum[127] are made, given by;

$$\alpha = \alpha + \lambda_\alpha S.C_L + \Delta\alpha_{OFF} \qquad C_D = C_D + \left[\frac{\pi}{180}\right]\lambda_\alpha S.C_L^2$$

where λ_α is defined by empirical data in the tunnel reference manual for a swept un-cranked wing mounted on the tunnel floor. The correction for angle of incidence includes a term, $\Delta\alpha_{OFF}$, to account for errors in aligning the model in the wind tunnel and is deduced in the next chapter.

6.7 Flow visualisation

Previous sections have described how measurements such as pressure, lift and drag are obtained, though these quantities give only a limited amount of information on the flow

development. Variations of pitching moment, lift and drag coefficients with angle of incidence identify trends and static pressure measurements give valuable information at a few discrete points on the model surface. Comparisons with these results give a quantitative indication of the accuracy of CFD flow solutions. However, to understand fully the nature of the flow, particularly for complex three-dimensional flows, and to determine qualitatively if CFD methods are modelling the correct flow physics, visualisation of the flow is necessary. This section describes a number of techniques that could or have been used to study the flow mechanism within the boundary layer and in the separated shear layers off the model surface.

6.7.1 Surface oil flows

During the initial wind tunnel tests it was important to study the flow visually from oil flow patterns to give an early indication of the flow mechanism and ensure that any root and tip effects have little influence on the flow development. Additionally, wool tufts were stuck to the top surface of the splitter plate to ensure that the flow was attached over the forward part of the plate and that the seals were effective.

There is good reason to expect that the flow of a thin layer of oil under a boundary layer will be in the direction of limiting streamlines[128]. An exception is in the immediate neighbourhood of separated flow where oil tends to collect. The main problems in the experimental technique are firstly in selecting a suitable oil medium and pigment for the prevailing test conditions, that can be photographed with consistently good quality and secondly, interpreting the patterns in terms of the three-dimensional flow structure. Ideally, the 'paint' should not begin to run until the desired tunnel speed is reached, and after a convenient time, be sufficiently dry to be unaffected by gravity after tunnel shutdown.

The major factors affecting the rate of flow are oil viscosity and skin friction. Previous experience at DERA has shown that kerosine or light diesel oil are ideal for use in the 13ft x 9ft tunnel, depending on tunnel speed. In the initial test, diesel oil was used at all but the lowest speed (*i.e.* 40m/s) which used a kerosine mixture having a lower viscosity. However, during the first test, when the ambient temperature increased by about 7°C, the kerosine mixture evaporated before a flow pattern could be established, after which diesel was used for all speeds.

The stiffness of the paint and the formation of streaks depend on the size of the particles in the pigment as well as oil viscosity. Experience has shown that 'Dayglo' pigments (used in the manufacture of fluorescent paints and printing inks) are ideal, having a particle size of about one micron. The patterns they create are clearly visible in natural light and photograph very well in ultra-violet light. Still photographs of oil flows were taken, whilst a video camera was used to record initial attempts. This involved blacking out the tunnel windows and illuminating the model with an ordinary u-v lamp, using an exposure time of about 75 seconds.

Photographs of oil flows were scanned using a flatbed colour scanner and digitally enhanced to sharpen traces and improve contrast where necessary. Because of the size of the model,

each oil flow pattern was recorded on two photographs and attempts to match the two scanned images, particularly in the trailing edge region, result in some images being skewed and notches in the leading edge.

6.7.2 Vapour screens

The vapour or smoke screen technique involves seeding the flow with a sufficient concentration of particles that when illuminated by a laser light sheet, scatter light in regions where particles accumulate such as vortex cores. The difficulty is in producing a vapour that is uniform, dense, luminescent and non-toxic. Traditionally a mineral oil such as Kerosine is vapourised to produce a white mist that is injected into the free stream flow just upstream of a region of interest. However, at all but very low speeds it is difficult to generate enough smoke to visualise the flow. An alternative technique is to generate a Bromonaphthalene mist that has a tenfold improvement in luminosity over Kerosine smoke. Unfortunately, the process requires specialised apparatus to generate the mist and the mist is toxic.

If water is sprayed in the wind tunnel settling chamber to increase the ambient humidity, certain flow features such as vortex cores can be visualised if there is a sufficient drop in temperature to cause the water vapour to condense. However, it is difficult to obtain the required ambient conditions for this to occur, particularly in low speed tunnels such as the 13ft x 9ft tunnel and injecting large quantities of water is not always permissible.

Although the vapour screen method (using a water soluble 'disco fog' and a 2W Argon-Ion laser) was attempted, the vapour density at the speeds of interest was insufficient to allow any qualitative assessment of the flow mechanism to be made.

6.8 Non-intrusive flow field measurement techniques

Recent advances in laser optics and computational resources have allowed techniques such as Laser Doppler Anemometry and Particle Image Velocimetry to be developed to obtain valuable in-flow measurements, essential for the evaluation of CFD methods and particularly for complex viscous flows.

6.8.1 Laser Doppler Anemometry

Laser Doppler Anemometry (LDA) is a non-intrusive optical measurement technique for the investigation of velocities at a point in the flow. The technique has advantages over other in-stream velocity measurement methods, such as hot wires or pitot probes, in that the only flow intrusion is that of the seeding particles used. As an established technique, LDA has remained primarily within universities and their small-scale research facilities. The application of the technique in large scale commercial wind tunnels does bring about technical problems, some of which are addressed in this thesis. The present study commissioned the LDA technique in the 13ft x 9ft wind tunnel for measuring three component velocities to compare with CFD predictions.

The LDA technique measures the velocity components of particles suspended in the air flow. Since velocity measurements are based on the scattering of light from these seeding particles, their properties need consideration. Large particles scatter a greater proportion of light than small ones, hence there is a lower particle size limit below which they can no longer be detected. On the other hand, the seeding particles must follow fluctuations in the fluid velocity. It has been shown that for free-stream speeds of up to Mach 2, spherical oil droplets with diameters less than 2μm will follow the air flow direction without significant deviation[129].

The measuring volume is defined by the intersection region of two coherent laser beams. Figure 6-6 shows that within this intersection volume, the beams will interfere, producing a fringe pattern *i.e.* the wavelength of the reflected light is shifted slightly due to the Doppler effect. The distance between the fringes, δ_f, will depend on the wavelength, λ, and the angle between the incident beams, θ. The intensity of light scattered from a particle moving through the measuring volume will vary with a frequency proportional to the magnitude of the velocity vector normal to the fringe pattern (*i.e.* the x-direction in figure 6-6). The majority of light is scattered in the direction away from the transmitting laser. Therefore, in the early days of LDA forward scattering was commonly used, requiring the receiving optics to be positioned opposite the transmitting aperture. Advances in technology now permit the detection of the much weaker back-scattered signals, allowing for the integration of the transmitting and receiving optics in a common housing, eliminating the need to align separate units. Thus nowadays, backwards scattering is the most common measurement method for LDA.

Though laser intensity may vary with time and temperature, its wavelength is constant and high quality optics ensures that the beam intersection angle will also remain fixed. Thus measured frequency will vary linearly with particle velocity and can be calculated directly without the need for a calibration.

The schematic in figure 6-7 shows the laser beam split into parallel beams of approximately equal intensity. Refraction in the front lens causes the two beams to intersect at the focal point of the lens, creating a roughly cigar shaped measurement volume. The 8" diameter, 2500mm focal length front lens used gives a measurement volume with an approximate diameter of 200μm and length of 10mm. This small diameter ensures high spatial resolution in the plane normal to the incident beams (*i.e.* the x and y-directions in figure 6-7), while resolution in the direction of the beam is somewhat lower.

Light scattered back towards the transmitter is collected by the front lens and enters an optic fibre before reaching the receiver. Filters prevent ambient light from reaching the receiver and reduces signal noise. The receiver converts the optical signal into an electrical signal that is amplified and measured.

A constraint on the technique is the relative density of seeding particles. A sparse distribution may result in insufficient sampling whereas too many particles could prevent tracking in highly turbulent/high speed flows.

Using three pairs of interrogation laser beams of differing wavelength (*i.e.* colour), correctly orientated and illuminating a single measurement volume, it is possible to obtain three orthogonal velocity vectors in each of the Cartesian directions. The photograph in figure 6-8 shows the three pairs of beams being calibrated. Optical filters separate the three Doppler signals which can then be directed to separate receivers. Also, by mounting the LDA probes on a traverse it is possible to measure flow velocities at a number of points in a plane.

The LDA system chosen for this research is based on commercially available equipment configured for a large-scale industrial facility. Due to the financial constraints of operating the wind-tunnel it is necessary to achieve high data measurement rates, requiring an Argon-Ion laser with a continuous output power of at least 20W and an excellent beam quality. This study used a 25W laser hired from a London University. Fibre optics delivered laser light to two probes configured to receive the back scattered Doppler signal. A schematic of the LDA set-up (figure 6-9) shows the two probes mounted on a three-axis traverse located behind a large float glass observation window. The traverse is orientated such that the common probe axis is at 16° to the normal of the window in order to;

1. allow measurements to be made downstream of the observation window in the wake region of the model.
2. reduce the reflections of ambient light from the window surface entering the collection optics.
3. reduce the angle between the incident beams and the model surface, thereby reducing the intensity of scattered light from the model surface.

Ideally, the received Doppler signal is large compared to background light levels. When laser light hits the model surface it is absorbed and reflected as specular and diffuse light. The degree to which it is absorbed or reflected will depend on the surface material and finish. Unfortunately, a non-intrusive surface finish that can absorb laser light is unavailable. A mirror finish to the model will preserve the narrow, directional qualities of the incident beam creating specular reflections that, by careful positioning, can be directed away from the LDA probes. However, because the surface of the metal model has a dominant structure similar in size to the wavelength of the laser light, a diffuse reflection generally occurs. Thus, when the LDA measurement volume is close to the model surface, diffusive reflections can obscure the Doppler signal and reduce data quality. Although the model was polished before the experiment to try to minimise diffuse reflections and while the surface appeared shiny to the eye, it retained a dominant surface structure capable of diffuse reflection of the laser beam. This prevented measurements close to the model surface indicated by results presented in section 7.3.7.

Seeding particles were produced by a commercial six jet oil atomiser from food grade white oil. A stream of particles was introduced into the free-stream flow approximately 5m upstream of the LDA measurement region, sufficient to give an adequate density. Particle diameter was approximately 0.5μm to 2μm, *i.e.* within the acceptable tolerances discussed above.

For the application of LDA in large wind-tunnels, the location of the measurement volume is a significant distance from the probe heads, giving a small subtended angle between incident beams. This lengthens the measurement region and reduces data rates. To measure Reynolds shear stresses in the flow, the Doppler signal received by each of the three velocity channels must correspond to an individual seeding particle in order to determine velocity cross moments. This requires very precise alignment of the three pairs of incident beams (to within ±0.0002°). These factors coupled with the non-uniformity of the observation window refractive index, precluded the measurement of Reynolds shear stresses. Therefore, only standard time averaged velocity measurements were taken.

6.8.2 Particle Image Velocimetry

The main limitation of the LDA technique is that it is a point measurement method, giving low data rates. In order to cover a reasonable area of interest the instrumentation must be traversed to each new position, which can take some time to achieve. The Particle Image Velocimetry (PIV) technique on the other hand, provides quantitative flow field turbulence information at hundreds of positions on a 2-D slice through the flow field in an instant by comparing two consecutive images of a pulsed laser light sheet and interrogating the seeding paths. Recent advances in computer hardware and software have made this method a more attractive measurement technique compared with LDA. PIV attains much greater data rates with a less complicated instrumentation set-up. However, the technology is not yet available in the 13ft x 9ft wind tunnel.

7 Results and data analysis

7.1 Experimental results

During the first test series (see table 4), wing force, moment and surface pressure measurements were made at sweep angles of 30°, 40° and 50° over a range of freestream speeds and angles of incidence. A number of surface oil flow patterns were also recorded to identify the flow mechanisms. The second test series concentrated on flow control techniques using vortex generators and are described elsewhere[130]. The last test only considered two angles of incidence at which flowfield velocities were measured using the LDA technique at a wing sweep of 40°, and freestream speed of 60m/s.

The x, y and z cartesian co-ordinates adopted for all experimental and theoretical studies are indicated in figure 7-1. Additionally, u, v and w velocity components are defined along x, y and z axes respectively.

7.1.1 Aerodynamic forces and moments

The effect of increasing wing sweep is to reduce overall lift at a given angle of incidence (figure 7-2). This comes about, first, because local lift is reduced owing to the reduction in streamwise camber and thickness, and second because the span (or aspect ratio) of the wing becomes smaller.

Increasing wing sweep at a given lift coefficient has a similar, though somewhat more complicated effect on drag. First, the reduced aspect ratio increases the induced or trailing vortex drag. Second, the reduction in streamwise camber and thickness reduces the adverse pressure gradients over the rear of the section, reducing boundary-layer drag. However, increasing wing sweep increases the probability of three-dimensional separation owing to the crossflows within the boundary layer. This will cause an increase in the boundary layer drag. Figure 7-3 provides some support for these ideas by showing that sweep reduces drag at low lift, where the induced drag is small and trailing edge separation is avoided, and increases it at higher lift coefficients.

7.1.2 Surface flow visualisation

Figures 7-4 to 7-8 show photographs of oil flow patterns over a range of incidence for a freestream speed of 60m/s and a wing sweep, Λ = 40°. Gridlines have been drawn on the wing, parallel to, and at a angle of 45° to leading and trailing edges to help resolve flow directions. The flows are characterised by both the oil flows and pressure distributions, and indicate a complex three-dimensional separation, with the separation line moving forward with increasing incidence. The surface flow direction over the forward part of the wing is almost normal to the leading edge. However, the angle between the surface streamlines and freestream direction increases over the rear section where pressure gradients (and therefore crossflows) are most severe, until the streamlines run almost parallel to the trailing edge.

Streamlines originating from different spanwise locations merge into a single limiting streamline from which the flow separates into a stream-surface of separated flow surrounded by mainstream air. Oil flows indicate that downstream of this limiting streamline, there is a region of reversed flow where streamlines curve outboard towards the tip due to the crossflows, forming an aft limiting streamline. This results in a secondary separation which appears to coalesce with the main separation. Between the forward and aft limiting streamlines there is a region of stagnant flow where oil collects. Consequently, when the wind is turned off this oil can run and obscure some of the flow details.

Although the shear layers are highly three-dimensional due to the large crossflows, the flow is essentially that of an infinite swept wing except near tip and root regions. A vortex is shed from the tip leading edge that reduces surface streamline curvature, and delays the separation until further downstream in this region. Also, the crossflow gradients in the root region are relatively small, resulting in smaller deviations in streamline curvature, also delaying separation. A better understanding of the nature of the separated shear layers is gained through LDA measurements and CFD predictions and is described in section 7.3.7.

If we compare oil flows for the same incidence ($\alpha = 8.9°$) and wing sweep ($\Lambda = 40°$), at three freestream speeds, V = 40, 60 and 80m/s (figures 7-9, 7-7 and 7-10 respectively), we see similar flow patterns. The separation line occurs in a similar position for each freestream speed though the size of the stagnant region, between the forward and aft limiting streamlines, reduces with increasing speed. At the lower speed, the amount of oil that collects in this region has obscured most of the full pattern downstream of the separation line. Comparing flow development for each wing sweep, $\Lambda = 30°$, 40° and 50° (figures 7-11, 7-7 and 7-12 respectively), at the same speed (V = 60m/s) and incidence ($\alpha = 8.9°$) we again see similar flow patterns. Although the perspective of these pictures is quite different, the flow patterns indicate similar locations for separation lines and flow mechanisms. At the lowest sweep, the oil has again run after the tunnel has shut down disguising some of the flow pattern. Had comparisons been made at the same lift coefficient for each wing sweep, increasing sweep would require the angle of incidence to be increased and the limiting streamline would have moved further forward.

7.1.3 Surface pressure distributions

Measured pressure distributions over a range of angles of incidence are shown in figures 7-13 and 7-14 ($\Lambda = 40°$, $V_\infty = 60$m/s, $Re_c = 4.2 \times 10^6$). Pressure distributions on the lower surface are represented by a dashed line. As angle of incidence is increased the lower surface leading-edge suction peaks are reduced and upper surface suction levels increase as would be expected. These suction levels peak at about 60% chord, which might be thought to correspond to the 'hinge-line' of a deflected trailing edge flap. There is an adverse pressure gradient downstream of this position that is responsible for the crossflows observed in oil flow patterns. For angles of incidence above about 2.5°, oil flows indicate that the flow is separated downstream of a limiting streamline. This region is characterised by a region of almost

constant pressure. Figures 7-13 and 7-14 show that trailing edge pressure coefficient reduces with increasing angle of incidence for attached and separated flows.

By interpolating a value of pressure coefficient at the trailing edge it is possible to infer boundaries for separation onset. For attached flows, pressure coefficient would be expected to increase linearly with angle of incidence. However, as the flow approaches separation, the trailing edge pressure coefficient tends to increase more rapidly with increasing angle of incidence, as shown in the sketch in figure 7-15. It has been shown that the onset of separation occurs when this deviation in pressure coefficient from the linear C_{pTE}/α curve becomes greater than 0.05[131], although it is not clear if this criteria can be applied to wings of high sweep. The variation of trailing-edge pressure coefficient with angle of incidence (Λ = 40°, V_∞ = 60m/s) is shown in figure 7-16 for each of the five spanwise stations. An algorithm was written to interrogate these curves and determine the angle of incidence corresponding to the separation onset using the above criterion. By repeating the task at all freestream speeds and wing sweeps, the buffet boundaries indicated in figure 7-17 are derived. As might be expected, the angle of incidence for buffet onset increases with increasing speed and reducing sweep.

Although previous sections have discussed the effect of sweepback on flow development, the following descriptions will focus on a wing sweep of 40° and a freestream wind tunnel speed, V_∞ = 60m/s (M_∞ = 0.178). From the flow breakdown boundaries in figure 7-17, separation is expected to occur for angles of incidence above 5° at this condition. However, the oil flow pattern in figure 7-4 suggests that separation onset will be closer to about 2.5°.

7.1.4 Flowfield velocity measurements

The third test series commissioned the LDA non-intrusive flowfield measurement technique (described in section 6.8.1) in the 13ft x 9ft wind tunnel. Three velocity components (i.e. u, v and w) were measured on a streamwise plane located approximately mid-span, near the trailing edge region. Velocity magnitudes are compared with CFD predictions in section 7.3.7.

7.2 VII predictions using VFPST

From the nominal ordinates used to define the wing section for model manufacture, a wing geometry was created at 40° sweep with the same aspect ratio as the wind tunnel model (though the theoretical model has a streamwise tip). The CFD method VFPST described in section 5.4.3 was initially used to calculate wing flows and assess its capability for predicting separated flows.

Figures 7-18 and 7-19 compare experimental pressure distributions with those predicted using VFPST at angles of incidence, α = -6°, -4°, -2°, 0°, 1° and 2°, for Λ = 40°, V_∞ = 60m/s, and a Reynolds number (based on wing streamwise chord), $Re_c = 4.2 \times 10^6$. We have previously defined the corrected experimental angle of incidence as,

$$\alpha = \alpha_u + \Delta\alpha_c(C_L) + \Delta\alpha_{OFF}$$

where α_u is the uncorrected angle of incidence, $\Delta\alpha_c(C_L)$ is the correction (defined in section 6.6) and is a function of the lift coefficient, and $\Delta\alpha_{OFF}$ is the offset in angle of incidence due to errors in model alignment. At this stage of the analysis the offset ($\Delta\alpha_{OFF}$) had not been determined. Preliminary assessments indicated that a best match of pressure distributions was achieved by performing calculations at the uncorrected angle of incidence. This suggests that in the range of angles of incidence considered, the offset angle is of the same order and of opposite sign to the correction to angle of incidence due to wall constraints. At higher angles of incidence, that were subsequently used for calculations using SAUNA, this was no longer valid. The issue is discussed in more detail in section 7.3.6. Both measured and calculated pressure distributions are in close agreement, including the strong adverse pressure gradients over the rear of the sections. However, VFPST predicts a higher pressure at the trailing edge and therefore, a better pressure recovery than was measured. A converged solution could not be attained for higher angles of incidence.

At the highest angle of incidence, $\alpha = 2°$, the variation across wing chord of boundary-layer streamline curvature, relative to the local inviscid flow, β_v, is shown in figure 7-20 at five spanwise stations. The local flow direction of the inviscid flow, β_i, relative to the freestream direction is not readily available from the VFPST output, though infinite yawed wing theory would indicated that $\beta_i = 0$ at the trailing edge. Therefore, the boundary-layer flow direction, relative to the freestream direction (*i.e.* $\beta_i + \beta_v$) is about 35° at the trailing edge. The oil flow pattern in figure 7-4 at $\alpha = 2.52°$, indicates therefore that VFPST underestimates streamline curvature. Additionally, swept wing boundary layer calculations using TAPERBL, during the design of the wing section (figure 6-1) indicated that the local freestream direction, $\beta_i + \beta_v \approx 90°$ near the trailing edge at this angle of incidence.

The lag-entrainment method used to calculate turbulent boundary layers in VFPST is based on empirical formulations derived from two-dimensional experimental data. Although the method includes the effects of crossflows, VFPST has been tuned for flows typical of civil transport wings with moderate sweep and relatively benign boundary layer development. Therefore, it is not surprising that VFPST is unable to model the flow in the trailing edge region of a highly swept and cambered wing. A calculation method that models the turbulent fluctuations that develop in these crossflows is required. Section 4.4 indicates that a solution of the Reynolds Averaged Navier-Stokes equations using a two-equation turbulence model for closure would be more appropriate for this application.

7.3 RANS predictions using SAUNA

7.3.1 Initial wing grids

An initial structured multi-block grid was generated for the model at a wing sweep of 40° with refinement near the wing surface suitable for a solution of the RANS equations. A C-H topology was chosen for the wing, with the C-grid embedded around the leading edge, extending outboard of the wing tip to the outer boundary. Since the wing is represented topologically as a planar object, this results in the trailing edge and tip being closed to a slit by averaging upper and lower surfaces. The accuracy of the tip modelling is unlikely to affect the

main flow development, and the base thickness is relatively small, so the influence of these simplifications to the grid is likely to be negligible. The topology of 130 blocks is depicted in the schematic in figure 7-21. This topology gives a finest grid of $369x10^3$ cells (designated grid 1 in table 5). A plane of symmetry is assumed at the wing root with a flow tangency boundary condition. Other far-field boundaries have Reimann boundary conditions imposed and the wing has a no-slip boundary condition. Control planes are generated to improve field grid quality; constant y-planes through the wing tip and a z-plane downstream of the trailing edge. An intersection calculation between the wing and the plane of symmetry allows the user to distribute grid points around the wing section and to cluster towards the leading and trailing edges. Experience has shown that the quality of a refined Navier-Stokes grid is highly dependant on the quality of the original Euler grid. For this reason, much effort is spent in improving surface grid quality through editing, to ensure field grids are not skewed or stretched.

Additional geometric components are defined that shadow features of the configuration on far field boundaries or within the grid. This is preferable to editing block corners and edges on far field boundaries, to mirror the wing planform for example. Wing 'shadow planes' on OMIN and OMAX (i.e. the domain floor and roof) reduce the number of edits required to improve grid quality. The wing shadow planes have extension geometries upstream of the leading edge, by about 40% of wing chord, to position block boundaries for controlling C-grids about the wing leading edge. A wing extension plane geometry (WIEX) is also specified to extend the wing tip section to the outer boundary, OSYM. This geometry, which is reduced to a zero-thickness plane when the tip is closed to a slit, provides a significant amount of control to field grids outboard of the tip, particularly for highly swept wings. The wing, wing extension and shadow plane geometries are depicted in figure 7-22.

The sketch in figure 7-23 shows how grids around the singularities formed by C-grids are controlled on y-control planes and SYMM/OSYM farfield boundaries. Since editing the actual position of the 5-point singularities and the gridlines emanating from the singularities can over-constrain the grid, control is imposed on a boundary just upstream of the singularities. The boundary AE in the sketch is fixed as a straight line to remove bowing, and the block corners at positions B, C and D are located to control the position of the singularities. The shadow extension geometries described above fix this boundary 40% chord upstream of the leading edge which, experience has found, prevents grid around the singularity becoming 'squashed'. Grid points are re-distributed along the AE boundary to avoid discontinuities in cell size and to cluster grid points toward the singularity points. These and other edits ensure the cells surrounding the singularities are not stretched/skewed and that subsequent refinement of the 'C-blocks' for viscous modelling results in high quality grids.

The extent of the boundaries for the flow domain were chosen to represent the 13ft x 9ft wind tunnel dimensions so that subsequent 'in-tunnel' calculations could be compared on a similar sized grid. Figure 7-24 shows surface grids on the wing, wing extension, plane of symmetry, downstream boundary and floor of the domain. The grids are clearly clustered towards the wing surface in all directions and show good orthagonality. A close up of where the wing

leading edge intersects the plane of symmetry is shown in figure 7-25, after the edits described above have been applied to control the singularity position.

The initial spacing of the grid points away from the surface of a component is important for the correct prediction of the boundary layer and viscous effects. For low Reynolds number turbulence models, a reasonable first point spacing would be of the order $y^+ \approx 1$-2. For high Reynolds number turbulence models with wall functions, a reasonable first point spacing would be of the order $y^+ \approx 50$. y^+ can be approximated by the equation,

$$y^+ \approx D.\mathrm{Re}\sqrt{\frac{C_f}{2}}$$

where, D is the physical dimension of the first grid point from the wing surface, Re is the Reynolds number based on a unit geometry length and C_f, the local skin friction coefficient. The ideal grid is now dependent on the Reynolds' number (unlike Euler grids) and the user must 'tune' the spacing parameters to the particular application, although deficiencies in grid density may only become apparent in the post-processing analysis of an initial flow simulation. Four values of the physical distance, D, from the component to the first neighbouring grid point are specified at each of the four extremities of the component in parametric space; the leading edge root and tip and the trailing edge root and tip. By approximating the turbulent flow to that over a flat plate, the local skin friction coefficient is estimated using the 7th power velocity distribution law of Schlichting[132],

$$C_f = 0.0576\left[\frac{U_\infty x}{\nu}\right]^{-\frac{1}{5}}$$

Thus, assuming a length scale equal to the wing chord (*i.e.* x = c) a target of $y^+ \approx 1$, for low Reynolds number implementation, at the trailing edge requires first point distances, D_3 and D_4, of the order 10^{-5}. Leading edge distances, D_1 and D_2, are generally slightly smaller than those at the trailing edge. However, these parameters were relaxed to $D_1 = D_2 = 3\text{x}10^{-5}$ and $D_3 = D_4 = 6\text{x}10^{-5}$ to avoid convergence problems encountered refining the grids.

A two-equation k-ω turbulence model is used for closure, with user specified constants C_1 = 100 and C_2= 10 (see section 5.5). Unlike the VII method, transition position is not specified since the growth in calculated turbulent viscosity from freestream values, is determined by the turbulence model employed. Three levels of grid are produced allowing the W-cycle multi-grid convergence acceleration technique to be used. Initial calculations matched uncorrected experimental angles (see section 7.2) since the resulting predicted local lift coefficients were closer to measured values. The reasons for this discrepancy are described below. Convergence is determined by the reduction in maximum residual calculated for each time step. An overall reduction of about three orders of magnitude is required for convergence, with residuals reaching a steady state. In general, this requires approximately 500 medium grid cycles followed by 1000 fine grid cycles.

A SAUNA calculation was performed at a freestream Mach number, M = 0.178 (V = 60m/s), α = 6° and a Reynolds number based on wing chord, $Re_c = 4.2x10^6$. A comparison of measured and predicted pressure distributions at five stations on the wing are shown in figure 7-26. Although there is good agreement on both upper and lower surfaces, there are a number of oscillations in predicted pressure, particularly near the trailing edge and at about 30% chord on the upper surface. Additionally, the leading edge suction levels at the most inboard station are higher than those measured. However, the adverse pressure gradients over the rear of the wing and trailing-edge pressure coefficients are in good agreement.

Since there will be no boundary layer growth on the plane of symmetry, the predicted flow development near the wing root may differ to that of the experiment and explain why suction levels on the inner wing leading-edge are high. Therefore, a further grid was produced with an attempt to model viscous effects on an end-plate. Grids were additionally refined normal to the surface of the end-plate to resolve turbulent features and a no-slip boundary condition was imposed. The end-plate was bullet shaped with a similar width and forward extent to the splitter plate used in the experiment and had zero thickness (lying on the plane of symmetry). The geometry of the wing and end-plate are shown in figure 7-27. However, the resulting pressure distribution (figure 7-28) shows little improvement over the previous solution and since there is a significant increase in grid size in order to model this end-plate, it is neglected in all further calculation.

7.3.2 Wing smoothing

The design of the wing section involved increasing the local camber of a baseline geometry (section 6.1) that resulted in a discontinuity in surface curvature. Therefore, to reduce the pressure oscillations on both surfaces of the wing, smoothing of the z-ordinate (at the i^{th} node) was applied across the chord of the wing using the formula,

$$z_i^{n+1} = \frac{z_{i-2}^n + 3z_{i-1}^n + 6z_i^n + 3z_{i+1}^n + z_{i+2}^n}{14}$$

for a number of iterations, n. The result of this smoothing on the surface curvature distribution can be seen in figure 7-29. Since the curvature discontinuities are much reduced by the smoothing, a new grid was generated for a wing with the smoothed section, based on the previous topology. Calculations were performed at six angles of incidence in the range –3.55° to 10.35° ($M_\infty = 0.178$, $Re_c = 4.2x10^6$). Figures 7-30 and 7-31 show that although there are still oscillations in the trailing-edge pressure coefficient, the distributions are generally smooth. However, this smoothing has influenced flow development over the forward part of the section, giving poor agreement with experimental suction levels. Although calculations have not matched experimental local lift coefficients and are generally at a higher lift, trends are well represented with good agreement of lower surface pressure distributions. SAUNA also predicts the adverse pressure gradient over the rear section reasonably well and the pressure plateau near the trailing edge indicating the region of separated flow at higher angles

of incidence. The separated regions are clearly evident from figure 7-32 which shows how pressure coefficient contours (in intervals of 0.05), at a cut through the field grid at y/s = 0.5, vary with angle of incidence. Figure 7-32 shows a decreasing number of contours over the rear of the section on the upper surface corresponding to a flattening of the pressure gradient as indicated in figures 7-30 and 7-31. Figure 7-32 also appears to show that a vortical flow pattern is established at the trailing edge once the flow separates which increases in strength with increasing incidence. Also, the chordwise separation location at y/s = 0.5 derived from oil flow patterns is specified at point 'S' in figures 7-32c to 7-32e, and compares well with the expected separation location from pressure contours.

7.3.3 Grid refinement

Though a graphical inspection of the smoothed and nominal ordinates reveals little differences, smoothing has actually created a significant discrepancy in both upper and lower surface z-ordinate. The discrepancy results in the poor flow modelling over the forward part of the wing section described above. Further SAUNA calculations using the original nominal ordinates reveal that pressure oscillations are avoided by a refinement of the grid in this region.

A similar topology was used as for the previous case, with some block dimensions increased to give 90% more grid points distributed around the wing section (designated grid 2 in table 5). The same first point spacings and number of points normal to the surface were used as before to refine the embedded C-grid blocks near to the surface. Surface grids are compared for grids 1 and 2 in figure 7-33.

A calculation was performed at an angle of incidence, $\alpha = 6°$ ($M_\infty = 0.178$, $Re_c = 4.2 \times 10^6$). Wing pressure distributions are compared in figure 7-34 for this grid (grid 2), and the previous grid based on nominal ordinates (grid 1) and experiment. The grid 2 solution shows that this refinement has removed the oscillations, except near the trailing edge. Therefore, additional calculations were performed for grid 2 at angles of incidence, $\alpha = 2°$ and $10°$ and pressure distributions are compared with measured values in figure 7-35. Unlike the smoothed wing results presented in section 7.3.2, the present calculations have not modelled the separated flow near the trailing edge. At $\alpha = 6°$ and $10°$ the predicted trailing edge pressure is significantly higher than the measured value, and the pressure plateau over the rear of the section is not predicted.

7.3.4 Wind tunnel modelling

In addition to the 'free-air' calculations described in the previous section, an attempt to model the 'in-tunnel' flow was made to verify experimental corrections for wall constraints. The octagonal cross-section of the wind tunnel requires extra blocks in the y-ordinate direction, resulting in a topology containing 182 blocks compared with 130 blocks for the 'free-air' case. The wing is rotated about the mid-chord position to give an angle of incidence of 6° and the extension plane is twisted so that it has zero angle of incidence on the tunnel roof (*i.e.*

OSYM). Geometry components for the tunnel walls, floor and shadow planes are also defined, resulting in the twenty three geometry components pictured in figure 7-36.

Reference 133 recommends that upstream and downstream boundaries are a sufficient distance from the wing to ensure uniform flow variables are obtained on these boundaries. Figure 7-37 shows pressure coefficient contours (in intervals, $\Delta Cp = 0.05$), from an initial calculation, on a cut through the centreline of the tunnel and indicates that any pressure gradients near the upstream and downstream boundaries are negligible and, therefore, that the boundaries are suitably located. The boundary conditions on these surfaces also differ from the standard Riemann invariant conditions set for free-air simulations. It is recommend[133] to use 'nozzle-type' conditions, specifying the inflow boundary as a jet fan face and the outflow boundary as a surface of constant stagnation pressure (Rudy-Strikwerda boundary). These boundary conditions require special initialisation in the flow solver: the specification of a jet pressure ratio, temperature ratio and Mach number at the inflow boundary. Surface grids for the wing and tunnel walls (without the roof and a sidewall) are shown in figure 7-38.

However, comparisons of the predicted in-tunnel and measured (at an uncorrected angle of incidence of 6°) pressure distributions show that SAUNA predicts a significantly higher local lift coefficient than was measured. Therefore, corrections for wall constraint do not account for the angle of incidence discrepancy.

7.3.5 Grid enhancement

Since the free-air calculations described in section 7.3.3 did not predict the measured trailing-edge pressure at high angles of incidence and, therefore, did not model separation, enhancements to the grid were made to improve quality. In particular, it was noticed that maximum residuals, on which convergence is monitored mainly occurred close to the wing tip surface and spanwise pressure variations were oscillatory in this region. Additionally, by fixing far field boundaries to match the locations of the tunnel walls, freestream conditions could not be assumed on these boundaries. Therefore, the enhancement strategies involved (1) more representative modelling of the wing tip and (2) increasing the physical size of the flow domain. To avoid closing the wing tip to a slit, a C-topology was embedded around the tip as well as the leading edge. Although the wind tunnel model has a squared-off tip, the CFD wing tip was rounded to improve the quality of grid wrapping around the tip. As a consequence of these changes the wing extension plane is no longer necessary and the y-control plane through the wing tip must be moved inboard. Since the grid in the tip leading-edge region is complex, featuring embedded C-grids in both the x-z and y-z planes, extra control planes are required to control field grids. As well as an extra y-plane outboard of the tip, the z-control plane (in the plane of the wing) was extended upstream of the trailing edge to cross the whole domain. A particular problem was at the trailing edge of the tip, where a large number of points were clustered in a small region and grid edits downstream of the trailing edge were necessary to prevent grid crossover. As a consequence of these grid improvements it was also possible to reduce first point spacings normal to the wing, giving $y^+ \approx 1$ across the wing surface. The resulting grid (designated grid 3 in table 5) contained almost 10^6 cells.

7.3.6 Incidence correction

To determine the size of discrepancy between measured angle of incidence (corrected for tunnel wall interference) and that used for CFD calculations, comparisons were made of local lift-curve slopes. Lift coefficients were calculated by integrating the predicted and measured pressure distributions at each of the five spanwise stations. Figure 7-39 shows the variation of local lift coefficient with angle of incidence at y/s = 0.3, revealing that the slopes of both experimental and predicted curves are very similar, particular at low incidence. We can, therefore, infer an angular offset, presumably due to errors aligning the model in the wind tunnel. The angle of incidence corresponding to zero lift is interpolated/extrapolated from the lift-curve slopes and an average of all five stations determined (*i.e.* α_{OFF}). Further comparisons between experiment and CFD have matched an angle of incidence, α^*, where,

$$\alpha^* = \alpha - \alpha_{OFF}$$

There is a variation of $\Delta\alpha_{OFF} = 0.7°$ across the wing span from experimental data, giving a mean value, $\alpha_{OFF} = -5.3°$. Analysis of SAUNA results gives a smaller spanwise variation and a mean value, $\alpha_{OFF} = -6.5°$. Therefore, CFD calculations must be performed at an angle of incidence 1.2° lower than the corrected experimental angle of incidence to match lift.

Calculations were performed on the enhanced grid for angles of incidence, $\alpha^* = 0.5°$, 8.5°, 12.5° and 16.5° ($M_\infty = 0.178$, $Re_c = 4.2 \times 10^6$). Figures 7-40 and 7-41 compare the experimental and predicted pressure distributions. Unfortunately, these SAUNA calculations have not matched experimental corrected angles of incidence very well, generally being slightly higher. Therefore, predicted upper surface suction levels are slightly higher, though the adverse pressure gradients match reasonably well. However, SAUNA is still predicting a higher trailing edge pressure coefficient, particularly at $\alpha^* = 12.5°$ and 16.5°, and does not predict the plateau in pressure coefficient corresponding to the separated flow region. A further calculation using a Multiscale Reynolds Stress turbulence model (without wall functions), did not improve the modelling of the trailing edge flow at $\alpha^* = 8.5°$.

7.3.7 Further grid refinement

Previous grids have been refined around the wing section and close to the wing surface to capture the flow physics of the turbulent shear layers. Whilst these grids have given good agreement for attached flows, separated regions near the trailing edge are not modelled. Consequently, the Euler grids have been refined away from the wing surface in the z-ordinate direction. An additional block has been included in the topology above the wing upper surface, with a relatively large dimension along the block edge in the z-direction. This increases the grid size to about 1.55×10^6 cells (grid 4 in table 5). The surface grid on the y-control plane is compared with that for grid 3 in figure 7-42, to show the increased grid density above the wing surface. Calculations are performed at angles of incidence $\alpha^* = 10.0°$,

12.1°, 14.2° and 16.3° (M_∞ = 0.178, Re_c = 4.2x10^6). The predicted pressure distributions shown in figure 7-43 (α^* = 12.1° and 14.2°) are in good agreement with experiment in terms of upper surface suction levels and, therefore, local lift coefficients. Additionally, predicted trailing edge pressure and the level of the pressure plateau (corresponding to the region of separated flow) is in good agreement with measured values for α^* = 12.1°, though predicted pressure coefficients are somewhat higher for α^* = 14.2° in this region.

To determine the flow mechanism in separated regions off the surface, streamlines on a plane normal to the leading edge, positioned about mid-span, are plotted in figure 7-44 for each angle of incidence. These show that the separated shear surface reattaches at the trailing edge forming a closed bubble of circulatory flow. As incidence increases, the separation location moves upstream and the separated region grows in size. Since the flow is highly three-dimensional, the "Ensight" data visualisation package was obtained, allowing particles along streamlines in the boundary layer and the separated shear layers to be animated, giving a clear picture of the flow mechanism. Animations and images were transferred to VHS video and presented at the 23rd ICAS Congress in Melbourne, Australia, 1998. Whilst the video presentation has been copied onto CDROM, it has not been possible to submit this media as part of my thesis. However, the following figures present some of the images obtained.

Initially, stream ribbons in the inviscid part of the flow were obtained around the wing at an angle of incidence of α^* = 12.1°. Figure 7-45 shows that whilst there is some curvature of these stream ribbons towards the wing tip, deviations from the freestream direction are small compared with boundary layer curvature indicated by oil flows. The figure also shows the tip vortex that rolls up downstream of the trailing edge. To determine if SAUNA predicts the location of the limiting streamline and surface curvature, observed in oil flow patterns, equivalent surface streaklines were evaluated. These are shown in figures 7-46 and 7-47 for angles of incidence, α^* = 10.0° and 12.1° respectively, on the right hand side of the corresponding oil flow patterns. Note that no oil flow was recorded for an angle of incidence, α^* = 16.3°, so no comparison can be made with the CFD. Although the oil flow pictures are in perspective and the CFD images are in plan view, the similarity in terms of streamline curvature and separation line location appear very close. The predicted flows also show the effect of the tip leading-edge vortex on delaying separation in the tip region, though the predicted separation location appears too far aft when compared with experiment. However, it should be remembered that the wind tunnel model has a square tip inclined at 5° to the freestream direction and the CFD wing has a streamwise, rounded tip.

By animating the predicted surface streaklines (α^* = 12.1°), particles are observed accelerating over the forward part of the wing section, then decelerating downstream of about 60% chord, through the adverse pressure-gradient region. Because the particles have been constrained to follow near surface streakline paths, they do not leave the surface along the limiting streakline, but follow the limiting streakline towards the tip at a low speed relative to the freestream speed. These particles are joined by particles originating downstream of the limiting streakline that flow relatively slowly upstream until they reach the limiting streakline.

Thus, a large number of particles appear to collect along the limiting streakline, corresponding to the collection of oil in this stagnant region of the oil flow.

Streamlines were also traced on a cutting plane, normal to the leading edge, through the flow domain. Animation of particles along these streamlines shows relatively slow moving particles entrained in a circulatory region of separated flow near the trailing edge. Images of these particle animations along wing surface streaklines, and streamlines on the cutting plane are shown in figure 7-48 ($\alpha^* = 12.1°$). Vector arrows on this cutting plane are also shown in figure 7-49 in the region of the trailing edge (arrow length being proportional to the velocity magnitude). This figure indicates that the flow reattaches at the trailing edge, with a region of reverse flow upstream to the separation point (just outside the image), and a vortex core just above the model surface.

The flow development at the highest angle of incidence, $\alpha^* = 16.3°$, is depicted in figure 7-50. The view shows the upper surface of the outer wing and the development of surface streaklines on the wing surface and on a cutting plane normal to the leading edge. A relatively small secondary vortex is shown downstream of the trailing edge. Within the primary vortex, the reverse flow forms a small secondary separation bubble. Unfortunately however, there are no surface oil flow patterns at this angle of incidence to verify the predicted surface flow pattern. An oil flow pattern at a higher angle of incidence, $\alpha^* = 18.4°$, (figure 7-8) does not show any evidence of these secondary flows.

Figures 7-51 to 7-56 show colour shaded velocity contour plots which display comparisons between CFD data and experimentally obtained LDA measurements. The measured data pictured at the bottom of each figure is superimposed over a background indicating the freestream velocity component. What can be clearly seen for u and v velocity components at both angles of incidence, $\alpha^* = 14.2°$ and $16.3°$, is the general similarity of form between the CFD calculation and the LDA measurement. A lack of measured data close to the wing surface is due to the problem of back reflection or glare from the model surface discussed in section 6.8.1. However, downstream of the trailing edge where surface reflections are not a physical problem and away from the model surface, the quantitative accuracy of the measured LDA data is within $1.0 m/s^5$. For the flow conditions considered, both the SAUNA calculations and LDA measurements have determined flow separation over the rear of the wing section, with similar locations for the separated shear layers. In those regions where experimental data can be considered accurate both have produced remarkably similar results. The high values of the v-component within the separated region indicate that the dominant flow direction is along the wing span, towards the wing tip. The same observation was made from oil flow visualisation and CFD flow visualisation. A lack of reliable LDA measurements close to the wing surface implies that we cannot confirm that the shear layers reattach near the trailing edge, forming a closed separation bubble (in 2D) as predicted by CFD. For both angles of incidence, the measured w component appears to display an anomalous flow structure over the wing surface with significantly higher velocities than have been predicted. This could well be due to the longer measurement region in the w-direction that reduces data rates and, therefore, measurement accuracy (see section 6.8.1).

7.3.8 Grid sensitivity

The previous section described how careful grid refinement and enhancement strategies have produced a grid with sufficient resolution in both near wall and off-surface regions to compute the separated shear layers over the wing. However, the multi-block approach does not allow grid density to be increased locally without impacting on the global grid size. As a consequence, RANS solution on the previous grid takes about 4.5 days on one node of a Silicon Graphics Origin 200 (with 185MHz processors) workstation. Therefore, means of reducing the grid size are considered, that retain grid resolution in regions of the flow where solution activity is high. Ideally it would be possible to embed regions of structured or unstructured grid in regions off the wing surface to capture the separated shear layers. Whilst the hybrid approach within SAUNA allows unstructured (tetrahedral) cells to be embedded within a specified region of a structured multi-block grid, it is not currently possible to solve the RANS equations for such a grid. Additionally, it is not possible within the SAUNA system to have hanging nodes or overlapping grids that could increase local grid density.

Initially, the topology adopted for the generation of grids in section 7.3.7 was modified by simply reducing block edge dimensions in the x, y and z directions to reduce grid size. Field grids were subsequently generated using similar surface grid edits to the previous case, creating two further grids of 1.47×10^6 and 1.34×10^6 cells (grids 5 and 6 respectively). Calculations were performed on each grid for an angle of incidence, $\alpha^* = 14.2°$, $M_\infty = 0.178$, and $Re_c = 4.2 \times 10^6$. On the basis of comparing surface pressure distributions alone (figure 7-57), solutions for grids 5 and 6 show a higher trailing edge pressure than for the previous grid solution, indicating how sensitive these solutions are to grid density.

7.4 Solution adaptivity

Although surface grid editing allows grid points to be clustered towards regions identified as containing separated shear layers, there is a limit to how far block edges in the z-direction above the wing can be coarsened before grid control is lost. Therefore, a solution dependent procedure has been developed to constrain field grids to particular geometric regions. Traditional grid adaptive techniques resolve flow discontinuities in small volumes of the grid, such as shock waves. However, the region bounded by the separated shear layer represents a significantly large volume preventing such techniques being applied to this application. An alternative approach has been to generate geometry that is representative of the outer profile of the upper surface shear layers. By generating surface grids on this geometry component it has been possible to constrain field grids within the shear layers. It was intended that this technique could be adapted as flow conditions or wing geometry are changed.

In this instance, shear layer locations have been obtained by analysing an existing flow solution on a fine grid (for an angle of incidence, $\alpha^* = 14.2°$). The u-velocity component on several streamwise cuts through the domain is analysed to extract regions where local velocity component is less than 98% of the freestream value. These are depicted in figure 7-58 which shows colour shaded contours for the u-velocity component. Using geometric information about the wing, regions corresponding to leading edge stagnation points and lower surface

shear layers are excluded to leave the upper surface shear layers. A cubic spline is subsequently fitted to this outer boundary profile that is used to define a three-dimensional geometry. However, because the observed flow development is similar to that for an infinite swept wing, only the shear layer profile at a mid-span station is used for geometry definition in this case. The geometry is additionally translated by a small distance in the z-direction away from the wing surface to ensure subsequent grid refinement in blocks bounded by this geometry and the wing upper surface is sufficient to capture flow gradients at the edge of the shear layers.

The boundary geometry is represented as a constant z plane above the wing with a continuity boundary condition in the topology. Additional control planes are included to enable stretched cells in the region of the upper surface shear layers to be edited to improve orthogonality. Surface grids on the wing, boundary geometry and some control planes are shown in figures 7-59 for the tip region. The grid density between the boundary and wing surface, in the z-direction, is high, whilst there are no discontinuities in cell size. Without the bounding effect of the shear layer geometry, it would have been difficult to have reproduced a similar uniform grid density by editing surface grids alone. The refined field grid contains 806×10^3 cells, representing a 52% reduction over grid 4 described in section 7.3.7. However, although cpu times required to obtain a converged solution are significantly reduced, the pressure distribution shown in figure 7-60 for an angle of incidence, $\alpha^* = 14.2°$ ($M_\infty = 0.178$, and $Re_c = 4.2 \times 10^6$), indicates that predicted trailing edge pressure is not representative of the measured flow. Therefore, since this solution has failed to correctly model the trailing edge flow, further work is necessary to refine the adaptive grids to determine optimum grid densities using this novel technique.

8 Discussion

The research described in this thesis has been concerned with identifying the types of wing flow that may be prevalent for future military offensive aircraft, likely to feature wings with leading and trailing edge sweeps of between 40° and 50°. The primary driver for such wing sweeps is the need to reduce the amount of reflected radiation directed towards a monostatic radar system from the head on aspect. This reduces the opportunities for detection and thus increases the prospects of survivability of the aircraft. Although other detection systems are currently employed, radar remains the primary sensor for defensive systems due to its better range and all weather capability. However, these configurations represent a high risk from the aerodynamic standpoint in that the flows are complex, three-dimensional and prone to boundary layer separation resulting in increased drag, buffeting and loss of control.

In particular, if leading edge flaps are deployed at high subsonic speed, such as in a transonic manoeuvre, or at low speed in a landing/take-off configuration, there is an increased tendency for the flow to separate near the trailing edge. Most research activity has focussed on understanding leading edge separations for highly swept wings with slender wing sections. The understanding of three-dimensional flows featuring trailing edge separation is relatively limited. A number of studies in the 1950's (i.e. references 17 to 42) explored the flow mechanics experimentally. However, these early studies were based mainly on force, moment and surface pressure measurements and surface flow visualisation techniques. Although some studies used yawmeters and pitot probes to examine flow behaviour off the surface and in wakes, they were unable to determine any details about the mechanism of flow breakdown. Whilst more recent studies have explored the flow over wings of lambda and diamond planforms, featuring highly swept leading and trailing edges, the work is generally of a sensitive nature and is unavailable for review. Consequently, this study has employed a combination of experimental and theoretical methods to characterise the flow over a wing of 40° sweep.

8.1 Analysis of surface flow structure

For this study a wing has been designed with a significant amount of camber that can simulate the pressure distribution typical of a transonic manoeuvre condition, for analysis in a low speed wind tunnel facility. Initially trends were determined from the measurement of lift and drag for various wing sweeps (in the range 30° to 50°), freestream speeds and angles of incidence on wing lift and drag. These showed that a more highly swept wing, with a reduced streamwise thickness and camber distribution, generates less local lift. Coupled to the fact that aspect ratio is reduced, the overall lift of the wing is reduced. The measurements of overall drag are consistent with the fact that, at low lift where the flow is attached, wing sweep reduces the streamwise adverse pressure gradients and consequently the boundary-layer drag. They also indicate an increased drag at high lift, in agreement with the observation that increased sweep increases the crossflow in the boundary layer making rear separation more likely and with the fact that the spanwise load distribution deviates further from an ideal elliptical loading, thereby increasing induced drag.

The main objective of this investigation, however, has been to explore the mechanics of the flow breakdown on the wing upper surface, with the further aim of providing the designer with the means of predicting these flows. The surface flow development has been characterised by a combination of surface oil flow patterns and surface pressure measurements. We have seen that over the rear of the section, the adverse gradients in pressure coefficient induced by rear camber are relatively high and increase with increasing angle of incidence. These pressure gradients induce spanwise crossflows in the boundary layers *i.e.* a velocity component that is normal to the velocity vector just outside the boundary layer. Downstream of the suction peak, crossflow velocities will change sign and boundary layer streamlines within the adverse pressure gradient will twist towards the wing tip. This is illustrated in oil flow patterns (figures 7-4 to 7-12) where oil filaments follow near surface boundary layer paths. Since the pressure gradient normal to the surface can be ignored to a first approximation as in boundary-layer theory, particles close to the surface follow more highly-curved paths than the faster particles further out in order to conserve momentum. This is illustrated in figure 8-1 where a particle path near the surface is shown as a dashed line and a particle path away from the surface as a solid line. The most extreme situation occurs when two or more particle paths close to the surface merge or run close together. In this situation, three-dimensional separation is said to occur[22]. Streamlines originating from different spanwise locations along the attachment line will merge into a single limiting streamline as suggested by Sears[18] from investigations of flows over swept elliptical cylinders. Maskell[33] further suggested that from this cusped separation line there originates a stream-surface of separated flow (illustrated in figure 4-2). Downstream of the separation line chordwise pressure gradients are relatively small, corresponding to the pressure coefficient plateau in figure 7-14. Oil flows indicate that the dominant flow direction in this region is towards the wing tip with reverse flow towards the separation line. Aft limiting streamlines, originating from different spanwise locations along the trailing-edge merge into an aft separation line. The collection of oil in the region bounded by the forward and aft separation lines indicates that the surface flow in this region is stationary.

Although surface pressure measurements and oil flow patterns indicate the surface flow development is supportive of theories hypothesised by Sears and Maskell, they cannot explain the mechanism of the separated stream-surface(s). Maskell proposed two mechanisms for the separation of a three-dimensional boundary layer: a closed bubble type and a free vortical shear layer separation (see figure 4-3). However, this study has shown, through a combination of non-intrusive flowfield measurements and CFD predictions, that the separation near the trailing edge of a swept wing can lie somewhere in between these two mechanisms. The separated shear layer reattaches along the trailing edge of the wing as illustrated by the sketch in figure 8-2 (note that forward and aft limiting streamlines merge into a single line of separation in the sketch). However, the surface of separation does not form a closed bubble and is open at both the spanwise extents. Near the wing root there is inflow from the external stream that forms a vortical flow structure along the wing trailing edge, bounded by the wing surface below and the separated shear layer. The dominant flow direction of the vortex is spanwise towards the wing tip, where the outflow interacts with the vortex shed from the wing tip. Thus, the separation mechanism can be thought of as a 'tunnel separation', allowing flow within it to be transferred from root to tip.

8.2 Evaluation of CFD

First it is necessary to define what is meant by the evaluation of a CFD method. No numerical method can ever be fully validated against experimental or flight data since there will always be features of the flow that are not resolved sufficiently. Since an enormous amount of information is required to completely describe a physical turbulent flow, analytical models of turbulence can only approximate the magnitudes and length-scales of turbulent fluctuations. Thus, for a given turbulent flow problem we must pose the question: given a set of initial boundary conditions, how do we predict the physically meaningful properties of the flow ? Section 4.4 described how the amount of flowfield detail required for a given application will determine the complexity of the mathematics needed. For the present application, of understanding the upper surface flow in the trailing edge region of highly swept wings, the wing designer will need three key items of information. Firstly, at what conditions can flow separation be expected and secondly, what impact will separation have on the handling characteristics of the aircraft i.e. drag, buffet and controllability. Finally, the designer will want a reasonably accurate prediction of where on the wing upper surface the flow is separated. If flow breakdown occurs in a critical region of the flight envelop with a major adverse effect on aircraft performance the designer will need to modify the configuration geometry to avoid separation or delay the onset of separation to a less critical condition. Alternatively, a knowledge of the separation line location would additionally allow flow control techniques such as vortex generators or boundary layer suction to be employed.

Thus this study has been primarily concerned with evaluating CFD methods as a tool for the wing designer, although inferences with experiment are made regarding the physical structure of the separated region. The designer must be sure a CFD method has been properly evaluated before it can be used as a design tool. Reassurance will be needed that the wind-tunnel tests, on which the evaluation is based, are properly corrected for effects that are not present in free air or flight conditions. Thus corrections will need to be included for wind-tunnel wall constraint, as in the present study. Ideally, the evaluation should be performed at flight Mach number and Reynolds number. In this respect the fact that the present studies are performed at low speed and sub scale conditions (for a typical combat aircraft) may be regarded as an impediment. However, the present evaluation may be regarded as an important first step on the road to building confidence in the method. The comparisons in the present investigation between measurements of overall forces, surface pressures and off-surface velocities using LDA (properly corrected for wind-tunnel wall constraint) have shown that the SAUNA CFD method (using the strategy discussed below) predicts the essential features of the complex flows at the rear of highly–swept wings.

In the initial part of the study, wing sections were assessed using the BVGK and TAPERBL codes. BVGK was used to determine the pressure distribution for the equivalent 2D flow which were then transformed to 3D using a transformation for infinite yawed wings[120]. Using

these pressure distributions TAPERBL was used to compute the streamwise development of the boundary layer, again assuming infinite yawed-wing flow. Figure 6-1 shows that this approach predicts that the limiting streamline becomes perpendicular to the chord normal to sweep, i.e. the limiting streamline becomes parallel to the trailing edge, indicating three-dimensional separation. The wind tunnel experiment subsequently confirmed that these limiting streamline directions are approximately correct. Therefore, this tool represents a simple and quick method of assessing the possibility of separation for wing designs. However, because wing tip and root effects will affect flow development, further calculations are necessary to model the flow over the complete configuration to obtain the three-dimensional separation location.

Though VFPST is used extensively for analysing wing and wing/body flows, its main application thus far has been for the analysis of civil transport aircraft with moderately swept leading and trailing edges. For more highly swept wings, the pressure distributions in figure 7-19 have shown an inadequacy in predicting the pressure gradients over the rear of the wing section and the trailing edge pressure coefficient. VFPST underestimates the boundary layer cross flows in regions of adverse pressure gradients and, therefore, the boundary layer growth giving a lower boundary layer thickness at the trailing edge. This reduces the effective camber of the inviscid wing section resulting in a more favourable adverse pressure gradient and a higher trailing edge pressure. The lag-entrainment turbulent boundary layer calculation method is based on empirical relationships derived from measured two-dimensional turbulent boundary layers with modifications for the effects of crossflows encountered by wings of moderate sweep. Therefore, it is perhaps not surprising that VFPST cannot predict trailing edge separation on highly swept wings with strong adverse pressure gradients.

A review of turbulent calculation methods in chapter 4 indicated that a solution of the Reynolds Averaged Navier-Stokes equations, employing a two-equation turbulence model would be more appropriate for the prediction of the flow physics. However, this represents a significant increase in the amount of effort and computational resources required to compute these flows compared with the VFPST method. Calculations using the SAUNA system to generate grids and solve the governing equations using a standard k-ω turbulence model, have however provided solutions that are in good agreement with measured surface and field data. A significant amount of effort was spent refining and enhancing grids to enable the separated trailing edge flow to be predicted. Therefore, the study has identified a number of key guidelines:

- Farfield boundaries should be a sufficient distance from geometric surfaces (i.e. of the order of twice the wing semi-span)
- The wing tip should be modelled accurately and not be closed to a slit (as happens for a standard C-H wing topology)
- For low Reynolds number two-equation turbulence models, an initial point spacing normal to the wing surface of $y^+ \approx 1$ is required to resolve turbulent fluctuations in attached boundary layers.
- A sufficient number of grid points should be distributed around the wing chord to resolve flow gradients (i.e. more than 200 points).

- There must be sufficient resolution of the grids away from the wing surface, particularly in regions near the trailing edge upper surface, to resolve flow gradients in the separated shear layers. Clearly, the need for increased grid density in the field near the trailing edge will be greater if flow separation occurs in this region. Based on this study it is recommended that a simple procedure should be employed, similar to the one described above using BVGK and TAPERBL (both industry standard codes) to determine the degree to which care needs to be taken with grids in this region.

The careful generation of field grids using the above guidelines, coupled with a solution of the RANS equations using a k-ω two-equation turbulence model, will enable the wing designer to predict trailing edge separations and give a reasonably accurate location for the separation line. Though comparisons between predicted and measured forces have not been made the predicted lift and drag, derived from integrating wing surface pressures, should represent trends reasonably well. Therefore, in terms of the three criteria that have been suggested as a measure of a CFD methods capability, in the context of predicting the flow behaviour over highly swept and cambered wings, the SAUNA CFD system has proved to be an effective tool. However, these methods should be reassessed, by comparison with appropriate experimental or flight data, if they are to be used at higher Reynolds number and freestream Mach number or for more complex geometries with any confidence. Additionally, to the authors knowledge, this represents the first time that the main physical features of a complex three-dimensional separated flow has been modelled using a CFD method.

Wing design for next generation combat aircraft may require the assessment of many wing derivatives. This study has illustrated that such wings are likely to feature high sweep angles and three-dimensional flows. Therefore, viscous effects will play a dominant role in the flow development and cannot be ignored. With an increasing demand on overnight design capabilities and the use of numerical design optimisation methods, there is a considerable emphasis on reducing cpu times. Ideally, the designer would like to use a rapid 'black box' technique, probably using grid adaption. An attempt was made to develop such a technique in the present study without complete success. However, it is not clear that such a method can be implemented without having sufficient grid resolution in the region where the separation occurs in the first place. Furthermore, 'black box' methods need to be treated with some caution since there is no guarantee with such methods that the solution is acceptable on physical grounds. In the end the good judgement of the user will be tested. The present study has shown that, as long as simple rules are followed, it is possible to predict complex three-dimensional flows over highly swept wings with the SAUNA CFD code.

9 Conclusions

A combined experimental and theoretical study has been described of the low speed flow over a highly swept and cambered wing, that simulates the flow features of a transonic maneouvre condition. The following main conclusions can be drawn:

- A wing of 40° sweepback with a highly-cambered section generates strong adverse pressure gradients over the rear of the section, leading to three-dimensional separations in this region at high angles of incidence. Using surface flow visualisation the nature of these flows has been defined, indicating how the position of a separated streamline moves forward with increasing angle of incidence. These observations have been confirmed by flow predictions using a CFD method that solves the Reynolds Averaged Navier-Stokes equations, employing a two-equation turbulence model.

- The SAUNA CFD system has also predicted the flow behaviour in the separated shear layer regions off the wing surface. The separated stream surface forms a tunnel by reattaching at the wing trailing edge, allowing inflow and outflow at the inboard and outboard extremities of the tunnel separation respectively. To the authors knowledge this represents the first time that the main physical features of such a complex three-dimensional separated flow has been modelled using a CFD method.

- Additionally, the velocity magnitudes within parts of the separated shear layer and the wake have been obtained using an optical non-intrusive measurement technique and give good agreement with the theory. This again represents a significant contribution to the data available for wing flows of this type.

- From an evaluation of the CFD methods employed, a design process has been proposed by which a wing designer can determine: (1) if the wing design is susceptible to flow breakdown at certain flow conditions, (2) assess the likely impact of the separated regions on aircraft performance and (3) examine where the separated region lies so that measures to control and/or delay the onset of separation can be made. It is shown that a simple two-dimensional calculation, coupled with a three-dimensional boundary layer method for infinite swept wings, would provide a relatively quick and simple determination of limiting streamline shapes and hence an indication if flow separation is a probability. However, for a detailed analysis of the flow over the complete wing, a solution of the Reynolds Averaged Navier-Stokes equations, employing a two-equation turbulence model, is shown to give accurate predictions of the positions of separation lines and the extent of the separation.

10 Recommendations for future work

While the present study has led to definite conclusions there remain a number of aspects that need further attention.

The analysis of the LDA data showed that surface glare associated with the model surface finish prevented accurate data from being taken close to the model surface. It is proposed that further measurements with improved surface finishes and/or coatings be undertaken in an attempt to remedy this.

An important requirement for the future development of CFD is to improve productivity. Methods will only be used routinely for design purposes if they produce data within a working day, at most. From this point of view the concept of grid adaption is attractive since it avoids the need for grid refinement studies. Further work is needed in this area. An alternative strategy that might be worth exploring is to implement knowledge bases within the CFD code to aid the choice of grids, thus possibly saving a considerable amount of preliminary work.

Lastly, the present study needs to be extended to flows at higher subsonic Mach number and Reynolds number. It is expected that in some ways the problems may become more severe (e.g. the appearance of shock waves and shock/boundary-layer interactions and thinner shear layers which may be difficult to model without an inordinately large number of grid points) and in other ways they may become less severe (e.g. higher Reynolds number implies less severe viscous effects).

References (II)

1 'Preliminary studies of trailing-edge flows on highly-swept wings.' A Shires, DRA/AS/HWA/WP95131, August 1995.

2 'Initial studies of trailing-edge flows on highly-swept wings.' A Shires and J I Broadley, DRA/AS/HWA/CR96004, February 1996.

3 'An experimental study of the control of separated flow on a wing with high trailing-edge sweep.' A Shires and J I Broadley, DERA/AS/HWA/CR97013, February 1997.

4 'Trailing-edge flows on highly-swept wings.' A Shires, DERA/AS/HWA/CR980001, February 1998.

5 'Progress report on the second year of project on 'Validation of CFD'.' J G Betterton and A Shires, DERA/MSS/MSF2C/CR990103, June 1999.

6 'Trailing-edge flows on highly swept wings.' A Shires, AIAA-97-2319, 1997.

7 'Trailing-edge flows on highly swept wings.' A Shires, ICAS-98-3.8.1, 1998.

8 'Sonderaufgaben der aerodynamischen forschung.' A Betz, Schriften der deut akademie der luftfahrtforschung No. 1020/409, 1940.

9 'Inside the Skunk Works.' Popular Science, October 1994.

10 'Airframe contribution features necessary for stealth.' E Schweicher, Optronics & Microwaves Dept., Royal Military Academy, B-1040 Brussels.

11 'How to design an 'invisible' aircraft' J A Adam, IEEE Spectrum, April 1988, pp. 26-31.

12 'Radar cross section: engineering for stealth.' Electronic Engineering, February 1987, pp. 49-60.

13 'Stealth - the next step.' Flight International, April 1990, pp. 24-25.

14 'Uber flussigkeitsbewegung bei sehr kleiner reibung.' L Prandtl, Presented to Third Congress on Mathematicians, Heidelberg, Germany, 1904

15 'Air flow in a separating laminar boundary layer.' G B Schubauer, NACA Report 527, 1935.

16 'Investigation of separation of the turbulent boundary layer.' G B Schubauer and P S Klebanoff, NACA Report 1030, 1951.

17 'Effects of sweep-back on boundary layer and separation.' R T Jones, NACA Report 884, 1947.

18 'The boundary layer of yawed cylinders.' W R Sears, Journal Aeron. Sci., Volume 15, No. 1, 1948.

19 'Methode de calcul de la couche limite tridimensionelle – Application a un corps fusele incline sur le vent.' E A Eichelbrenner and A Oudart, ONERA Pub. No. 76, 1955.

20 'Le decollement laminaire en trois dimensions.' E A Eichelbrenner and A Oudart, La Recherche Aeronautique, No. 47, 1955.

21 'Types of flow on swept wings.' D Kuchemann, Journ. RAeS, Volume 57, pp 683-699, 1953.

22 'Flow with separations.' D Kuchemann, RAE TM Aero. 453, 1955.

23 'Low speed measurements of the pressure distributions and overall forces on wings of small aspect ratio and 53° sweepback.' J Weber, RAE TN Aero. 2017, 1949.

24 'Low speed characteristics of a 45° sweptback wing of aspect ratio 8 from pressure distributions and force tests at Reynolds numbers from 1,500,00 to 4,800,00.' R R Graham, NACA RM L51H13, 1951.

25 'Low speed tests on 45° sweptback wings, Part II: balance and pressure measurements on wings of different aspect ratio.' D Kuchemann, J Weber and G G Brebner, RAE R Aero. 2419, 1951.

26 'The longitudinal characteristics at Mach numbers up to 0.92 of a cambered and twisted wing having 40° of sweepback.' G G Edwards, B E Tinling and A C Ackerman, NACA RM A52F18, 1952.

27 'Some effects of flow separation on the overall force characteristics of thin wings of aspect ratio 2 to 4.' A L Courtney, RAE TM Aero. 2401, 1955.

28 'Some effects of flow separation on slender delta wings.' J Weber, RAE TM Aero. 2425, 1955.

29 'Low speed wind tunnel tests on a fully tapered wing with 81° leading edge sweep and a 6% thick RAE 101 section.' D A Kirby, RAE TM Aero. 449, 1955.

30 'Some observations of the flow over a delta winged model with 55° leading edge sweep at Mach numbers between 0.4 and 1.8.' E P Sutton, RAE TM Aero. 2430, 1955.

31 'Low speed tests on 45° sweptback wings.' J Weber and G G Brebner, RAE R Aero. 2374, 1951; RAE R Aero. 2419, 1951; ARC R&M 2882, 1958.

32 'Flow visualisation in windtunnels using indicators.' R L Maltby, AGARD AG-70, 1962.

33 'Flow separation in three dimensions.' E C Maskell, RAE R Aero. 2565, 1955.

34 'Separation de l'ecoulement laminaire tridimensionnel.' R Legendre, La Recherche Aeronautique, No. 54, pp 3-8, 1956.

35 'Lignes de courant d'un ecoulement continu.' R Legendre, Rech. Aerosp., No. 105, pp 3-9, 1965.

36 'Die ablosungsbedingung von grenzshichten.' K Oswatitsch, IUTAM Symposium on Boundary-Layer Research, Freiburg, 1957.

37 'Attachment and separation in three-dimensional flow.' M J Lighthill, 'Laminar Boundary Layers', Oxford Univ. Press, pp 72-82, 1963.

38 'A note on vortex patterns in the boundary layer of a sweptback wing.' J Black, Journal RAeS, Volume 56, pp 279-285, 1952.

39 'Some problems of flow laminarization on a slender delta wing.' N Gregory and F M Love, Recent developments in boundary-layer research, AGARDograph No. 97, 1965.

40 'Boundary layer measurements on wings of 45° sweep at low speed.' G G Brebner, RAE TN Aero. 2298, 1954.

41 'Boundary layer measurements at low speed on two wings at 45° and 55° sweep.' G G Brebner and L A Wyatt, RAE TN Aero. 2702, 1960.

42 'Measurements of pressure distributions on a half model wing body combination of 55° sweep over a wide range of Reynolds number.' K G Winter and J B Moss, RAE TR 74149, 1974.

43 'On the theory of laminar boundary layers involving separation.' T von Karman and C B Millikan, NACA Report 504, 1934.

44 'Determination of general relations for the behaviour of turbulent boundary layers.' A E von Doenhoff and N Tetervin, NACA Report 435 (ACR No. 3G13), 1943.

45 'A general integral form of the boundary-layer equation for incompressible flow with an application to the calculation of the separation point of turbulent boundary layers.' N Tetervin and C C Lin, NACA Report 1046, 1951.

46 'A calculation method of three-dimensional turbulent boundary layers.' J C Cooke, RAE TN Aero. 2576, 1958.

47 'Entrainment in the turbulent boundary layer.' Head M R, ARC R&M 3152, 1958

48 'Application of Head's entrainment method to the prediction of turbulent boundary layers and wakes in compressible flow.' Green J E, RAE TR72079, 1972

49 'Prediction of turbulent boundary layers and wakes in compressible flow by a lag-entrainment method.' J E Green, D J Weeks and J W F Brooman, ARC A&M 3791, 1973

50 'On the dynamical theory of incompressible viscous fluids and the determination of the criterion.' O Reynolds, Philosophical Transactions of the Royal Society of London, Series A, Volume 186, 1895.

51 'Theorie de l'ecoulement tourbillant.' J Boussinesq, Mem. Presentes par Divers Savants Acad. Sci. Inst. Fr., Volume 23, pp 46-50, 1877.

52 'Uber die ausgebildete turbulenz.' L Prandtl, ZAMM, Volume 5, pp 136-139, 1925

53 'Mechanische ahnlichkeit und turbulenz.' T Von Karman, Proc. Int. Congr. Appl. Mech., 3rd, Stokholm, Part 1, pp 85-105, 1930

54 'On turbulent flow near a wall.' E R Van Driest, Journal of the Aeronatical Sciences, Volume 23, pp 1007, 1956

55 'Analysis of turbulent boundary layers.' T Cebeci and A M O Smith, Ser. In Appl, Math. & Mech., Volume XV, Academic Press, 1974

56 'Thin-layer approximation and algebraic model for separated turbulent flows.' B S Baldwin and H Lomax, AIAA Paper 78-257, Huntsville, AL., 1978

57 'A mathematically simple turbulence closure model for attached and separated turbulent boundary layers.' D A Johnson and L S King, AIAA Journal, Volume 23, No. 11, pp 1684-1692, 1985

58 'Uber ein neues formelsystem fur die ausgebildete turbulenz.' L Prandtl, Nacr. Akad. Wiss. Gottingen, Math-Phys. Kl., pp 6-19, 1945

59 'Calculation of boundary layer development using the turbulent energy equation.' P Bradshaw, D H Feriss and N P Atwell , Journal of Fluid Mechanics, Volume 28, Part 3, pp593-616, 1967

60 'Computation of turbulent boundary layers – 1968.' D E Coles and E A Hirst, AFOSR-IFP-Stanford Conference, Volume II, Stanford University, CA., 1969

61 'Equations of turbulent motion of an incompressible fluid.' A N Kolmogorov, Izvestia academy of sciences, USSR; Physics, Volume 6, Nos. 1 and 2, pp 56-58, 1942

62 'Mathematical models of turbulence.' B E Launder and D B Spalding, Academic Press, London, 1972

63 'Scrutinising the k-ε turbulence model under adverse pressure gradient conditions.' W Rodi and G Scheuerer, ASME, Jornal f Fluids Engineering, Volume 108, pp 174-179, 1986

64 'Reassessment of the scale determining equation for advanced turbulence models.' D C Wilcox, AIAA Journal, Volume 26, No. 11, pp 1299-1310, 1988

65 'A model for inhomogeneous turbulent flow.' P G Saffman, Proc. Roy. Soc., London, Volume A317, pp 417-433, 1970

66 'A turbulence model for high speed flows.' D C Wilcox and I E Alber, Proc. of the 1972 Heat Trans. & Fluid Mech. Inst., Stanford Univ. Press, pp231-252, 1972

67 'Turbulence-model predictions for turbulent boundary layers.' P G Saffman and D C Wilcox, AIAA Journal, Volume 12, No. 4, pp 541-546, 1974

68 'A complete model of turbulence.' D C Wilcox and R M Traci, AIAA Paper 76-351, San Diego, CA., 1976

69 'Progress in turbulence modelling for complex flow fields including effects of compressibility.' D C Wilcox and M W Rubesin, NASA TP-1517, 1980

70 'Zonal two-equation turbulence models for aerodynamic flows.' F R Menter, AIAA 93-2906, 1993

71 'Turbulent boundary layers with large streamline curvature.' R M C So and G L Mellor, ZAMP, Volume 29, pp 54-74, 1978

72 'Development and application of a cubic eddy-viscosity model of turbulence.' T J Craft, B E Launder and K Suga, International Journal of Heat and Fluid Flow, Volume 17, pp 108-115, 1996

73 'Statistischa theorie ichthlomogener turbulenz.' J C Rotta, Zeitschrift fur Physik, Volume 129, pp 547-572, 1951

74 'Calculation of the turbulent shear flows through closure of the Reynolds equations by invariant modelling.' C duP Donaldson and H Rosenbaum, ARAP Report No. 127, Aeronautical Research Associates of Princeton, Princeton, NJ., 1968

75 'Transport equations in turbulence.' B J Daly and F H Harlow, Physics of Fluids, Volume 13, pp 2634-2649, 1970

76 'Progress in the development of a Reynolds-stress turbulence closure.' B E Launder, G J Reece and W Rodi, Journal of Fluid Mechanics, Volume 68, Part 3, pp 537-566, 1975

77 'Ground effects on pressure fluctuations in the atmospheric boundary layer.' N M Gibson and B E Launder, Journal of Fluid Mechanics, Volume 86, Part 3, pp 491-511, 1978.

78 'Computational modelling of turbulent flows.' J L Lumley, Adv. Appl. Mech., Volume 18, pp 123-176, 1978

79 'Second-order closure models for rotating turbulent flows.' C G Speziale, Q. Appl. Math., Volume 45, pp721-733, 1987

80 'Fundamentals of turbulence for turbulence modelling and simulation.' W C Reynolds, Lecture notes for von Karman Institute, AGARD Lecture Series No. 86, pp 1-66, New York: NATO, 1987

81 'Development and application of a cubic eddy-viscosity model of turbulence.' T J Craft, B E Launder and K Suga, Int. Journal of Heat and Fluid Flow, Volume 17, pp 108-115, 1996.

82 'Multiscale model for turbulent flows.' D C Wilcox, AIAA Journal, Volume 26, No. 11, pp 1311-1320, 1988.

83 'Turbulence statistics in fully developed channel flow at low Reynolds number.' J Kim, P Moin and R Moser, Journal of Fluid Mechanics, Volume 177, pp 133-166, 1987

84 'Large-eddy simulation of turbulent obstacle flow using a dynamics subgrid-scale model.' K-S Yang and J H Ferziger, AIAA Journal, Volume 31, No. 8, pp 1406-1413, 1993

85 'Numerical simulation of turbulent flows.' R S Rogallo and P Moin, Annual Review of Fluid Mechanics, Volume 16, pp 99-137, 1984

86 'An investigation of supersonic buffet using a large eddy simulation.' D L Hunt, PhD thesis, Queens Univ., Belfast, 1995

87 'CFD Requirements for Code Validation.' E G Waggoner, M Burt, S Lekoudis, U Kaynak, E H Hirschel, H Korner, 'A selection of experimental test cases for the validation of CFD codes', AGARD-AR-303, Vol. I, August 1994, pp. 5-16.

88 'An improved semi-inverse version of the viscous Garabedian and Korn method.' P R Ashill, R F Wood and D J Weeks, RAE Technical Report TR 87002, 1987.

89 'Validation of CFD methods for transonic aerofoil and wing flows.' J L Fulker and P R Ashill, RAE TM Aero. 2167, 1989.

90 'Analysis of transonic aerofoils.' P R Garabedian D G Korn, Comm. Pure App. Math., 24, 841, 1971.

91 'Numerical methods for solving the potential flow equations for two-dimensional aerofoils in subsonic and transonic flows.' ESDU Transonic Data Memorandum No. 79009, 1979.

92 'Methods for estimating the pressure distribution on a two-dimesional aerofoil in viscous transonic flow.' ESDU Transonic Data Memorandum No. 81019, 1982.

93 'An extension to the methods of Garabedian and Korn for the calculation of transonic flow past an aerofoil to include the effects of a boundary layer and wake.' M R Collyer, RAE Technical Report 77104, 1977.

94 'Improvements to the viscous Garabedian and Korn (VGK) method for calculating transonic flow past an aerofoil.' M R Collyer and R C Lock, RAE TR78039, 1978.

95 'Approximate calculation of the laminar boundry layer.' B Thwaites, Aero. Qu., Volume 1, No. 245, 1949.

96 'Correlated incompressible and compressible boundary layers.' K Stewartson, Proc. Roy. Soc., London, Volume 200, No. 84, 1949.

97 'Wind tunnel experiments on aerofoil models for the assessment of computational flow methods.' P R Ashill, D J Weeks and J L Fulker, RAE TM Aero. 2121, 1988.

98 'Boundary layers over infinite yawed wings.' J C Cooke, Aero. Qu. Volume 11, pp 333-347, 1960.

99 'A calculation method for the turbulent boundary layer on an infinite yawed wing in compressible, adiabatic flow.' P D Smith, RAE TR72193, 1972.

100 'An integral prediction method for three-dimensional compressible turbulent bounadry layers.' P D Smith, ARC R&M No. 3739, 1974.

101 'The calculation of transonic flow over three-dimensional swept wings using the exact potential equation.' C R Forsey, M P Carr, DGLR symposium transonic configurations, Bad Harzburg, DGLR paper 78-064, 1978.

102 'An integral method for calculating the effects on turbulent boundary-layer development of sweep and taper.' P R Ashill and P D Smith, Journal RAeS, February 1985.

103 'SAUNA: A system for grid generation and flow simulation using hybrid structured and unstructured grids.' P N Childs, J A Shaw, A J Peace and J M Georgala, First European Computational Fluid Dynamics Conference, Sept 1992.

104 'Validation and evaluation of the advanced aeronautical CFD system Sauna - a method developer's view.' J A Shaw, J M Georgala, P N Childs, C A McHugh, N E May and A J Peace, Paper 3, 1993 European Forum on Recent Developments and Applications in Aeronautical CFD, Sept 1993.

105 'Inviscid and viscous flow modelling of complex aircraft configurations using the CFD simulation system SAUNA.' A J Peace, N E May, M F Pocock and J A Shaw, 19th ICAS Congress Paper ICAS-94-2.6.3, 1994.

106 'Grid generation and flow calculations for complex aircraft geometries using a multi-block scheme.' N P Weatherill and C R Forsey, AIAA Paper 84-1665, 1984

107 'Automatic topology generation for multi-block grids.' J A Shaw and N P Weatherill, J Appl Math and Comps, 1993.

108 'Surfaces for computer aided design of space forms.' S A Coons, MIT MAC TR-41, 1967.

109 'Automatic numerical generation of body-fitted curvilinear coordinates systems for field containing arbitrary two-dimensional bodies.' J F Thompson, F C Thames and C M Mastin, J Comp Phys, Volume 15, pp 299-319, 1974.

110 'Direct control of grid point distribution in meshes generated by elliptic equations.' P D Thomas and J F Middlecoff, AIAA Journal, Volume 18, pp 652-656, 1980.

111 'A discussion on issues relating to multi-block grid generation.' J M Georgala and J A Shaw, AGARD CP-464, Paper 16, 1989.

112 'A method for attaining multi-block flow simulations rapidly following local design modifications to a baseline geometry.' C M Newbold and J A Shaw, ARA Memo 367, 1993.

113 'A vertex based multi-grid lgorithm for three-dimensional compressible flow calculations.' A Jameson, ASME Numerical methods for compressible flow symposium, 1989.

114 'Calculation of inviscid transonic flow over a complete aircraft.' A Jameson, T J Baker and N P Weatherill, AIAA-86-0103, 1986.

115 'A multi-grid Navier-Stokes method for block-structured grids.' A J Peace and N E May, ARA CR M237/8/4, 1996.

116 'Implementation of the Johnson-King turbulence model in the SAUNA flow code, including initial evaluation.' N E May and J A Chappel, ARA CR M264/18, 1996.

117 'Efficient implementation of two-equation and differential reynolds stress turbulence models into a cell-vertex, explicit time-marching Navier-Stokes flow code.' N E May, ARA CR M345/1, 1998.

118 'Large eddy simulation using the SAUNA CFD system – a feasibility study.' N E May and D L Hunt, ARA CR M345/6, 1998.

119 'Investigation of the flow over a series of 14%-thick supercritical aerofoils with significant rear camber.' P R Ashill, 'A selection of experimental test cases for the validation of CFD codes', AGARD-AR-303, Vol. II, August 1994, pp. A3(1-13).

120 'The aerodynamic design of section shapes for swept wings.' H H Pearcey, 'Advances in Aeronautical Sciences', Volumes 3-4, Pergamon Press Ltd., 1961.

121 'A guide to the DRA 13ftx9ft low speed wind tunnel facility.' M H Hunter, DRA Technical Report TR93014, April 1993.

122 'Effect of roughness on transition in supersonic flow.' E R Van Driest and C B Blumer, AGARD Report 255, 1960.

123 'Pressure Measurement techniques used in wind tunnel tests at DRA.' B L Welsh, P R Ashill, DRA Working Paper WP94070/1, May 1995.

124 'Functional specification of the half-model balance data reduction on-line to the 13ftx9ft tunnel.' C S Barnes, RAE internal document, November 1979.

125 'Subsonic wind tunnel wall corrections.' H C Garner, W E Rogers, W E A Acum, E C Maskell, AGARDograph 109, October 1966.

126 'A method for determining wall-interference corrections in solid-walled tunnels from measurements of static pressure at the walls.' P R Ashill, D J Weeks, AGARD-CP-335, pp1.1-1.12, 1982.

127 'Corrections for symmetrical swept and tapered wings in rectangular wind tunnels.' W E A Acum, R&M 2777, April 1950.

128 'The surface oil flow technique for use in low speed wind tunnels.' R L Maltby, R F A Keating, AGARDograph 70, part I.3, 1962.

129 'The application of CTA, LDA and PIV to set boundary conditions for the verification of CFD results.' F E Jorgensen, B M Madsen, D R McCluskey, Presented at the 4th World Conference in applied fluids Dynamics, computational and experimental methods, 7-11 June 1998, Freiburg, Germany.

130 'The control of trailing edge separation on highly swept wings using vortex generators.' J I Broadley, Cranfield University PhD thesis, 1998.

131 'A study of the factors influencing shock-induced separation on swept wings.' J L Fulker and P R Ashill, RAE TR83088, 1983.

132 'Boundary-Layer Theory.' H Schlichting, McGraw-Hill series in mechanical engineering, sixth edition, 1968.

133 'A further evaluation of the SAUNA CFD system for modelling the effects of solid wind tunnel walls.' C Lovell, ARA CR M334/2, 1998.

Bibliography (II)

'Design for air combat.' R Whitford, Jane's, London , 1987.

'Aircraft design, integration and affordability.' L M B C Campos, AGARD-R-826, 1998.

'Turbulence modelling for CFD.' D C Wilcox, DCW Industries Inc., 1993.

'A brief description of theoretical methods currently being applied to aerofoil and wing flows at the defence research Agency.' J I Broadley, DRA/AS/HWA/WP95164, 1995.

'Practical use of transport turbulence models in aerospace – CFD implementation and applications.' D L Hunt and N E May, AIAA-99-3137, 1999.

'Turbulence: a universal problem.' C L'Vov and I Procaccia, article from Physics World, August 1996.

'Essential elements of computational algorithms for aerodynamic analysis and design.' A Jameson, NASA/CR-97-206268, 1997.

'Boundary layers in three dimensions.' J C Cooke and M G Hall, RAE Report Aero. 2635, 1960.

'Three-dimensional interactions and vortical flows with emphasis on high speeds.' D J Peake and M Tobak, AGARDograph No. 252, 1980.

'Some examples of separation in three-dimensional flows.' W J Rainbird, R S Crabbe, D J Peake and R F Meyer, National Research Council of Canada, Report No. DME/NAE 1966(1), 1966.

'Three-dimesional boundary layers: a report on Euromech 2.' J H Horlock, J F Norbury and J C Cooke, Journal of Fluid Mechanics, Volume 27, Part 2, 1967.

'The prediction of separation of the turbulent boundary layer.' B S Stratford, Journal of Fluid Mechanics, Volume 5, 1958.

'Turbulent secondary flows.' P Bradshaw, Ann. Rev. Fluid Mech., pp 53-74, 1987.

Tables

Target	Approximate RCS (/m^2)
B-747	100
Car	100
Tank	50
Conventional fighter aircraft	2-6
Adult male	1
Cruise missile	0.8
F-117A	0.025
Bird	0.01

Table 1: Approximate RCS (Radar Cross Section) values of the head on aspect at microwave frequencies.

Navier-Stokes (DNS)	Unsteady viscous flow
Navier-Stokes (LES)	Viscous flow with time accurate solutions of large, dominant turbulent fluctuations and a turbulence model for small scale turbulence.
Navier-Stokes (RANS)	Viscous flow, with time averaging of turbulent fluctuations and a turbulence model for closure.
Euler	Inviscid flow, but will model entropy changes across a shock wave. (VII techniques give robust and reliable methods for approximating viscous effects).
Potential flow	Isentropic, inviscid, irrotational flow (VII techniques give robust and reliable methods for approximating viscous and compressibility effects).
Transonic Small-Perturbation	For flows with weak perturbations from freestream conditions.
Linearised	For low speed or supersonic flows, using first order theory.

Table 2: Indicating increasing complexity of CFD methods available.

Boundary condition	**Description**
Continuity	to model both inflow and outflow.
Flow tangency	at solid surfaces on which viscous effects are not to be computed the condition sets the velocity component normal to the surface to zero.
Riemann Invariants	applied at the farfield to model both inflow and outflow.
Rudy-Strikwerda	For a subsonic jet efflux crossing a farfield boundary (P_∞ condition).
No-slip	At solid surfaces on which viscous effects are to be computed a no slip condition is applied setting all velocity components equal to zero.
Jet fan inflow	For a subsonic jet inflow crossing a farfield boundary.

Table 3:* SAUNA *boundary conditions for flowfield predictions.

Test series	Date	Purpose
1	June 1995	Measurement of forces, moments and surface pressures and oilflow investigations at wing sweeps, $\Lambda = 30°, 40°, 50°$ and a range of freestream speeds and angles of incidence.
2	May 1996	Measurement of forces, moments and surface pressures and oilflow investigations of flow control techniques.
3	November 1998	Commission the LDA technique.
4	January 2000	Measurement of Reynolds stresses using LDA technique.

Table 4: Wind tunnel test history.

Grid	Wing section points	Points normal to surface	Grid cells (Euler)	Grid cells (NS)	D1, D2	D3, D4
1	121	41	181,632	368,896	0.00006	0.00003
2	217	41	374,400	758,784	0.00006	0.00003
3	233	41	532,000	982,000	0.00001	0.00001
4	233	41	1,074,000	1,550,000	0.00001	0.00001

Table 5: SAUNA grid sizes.

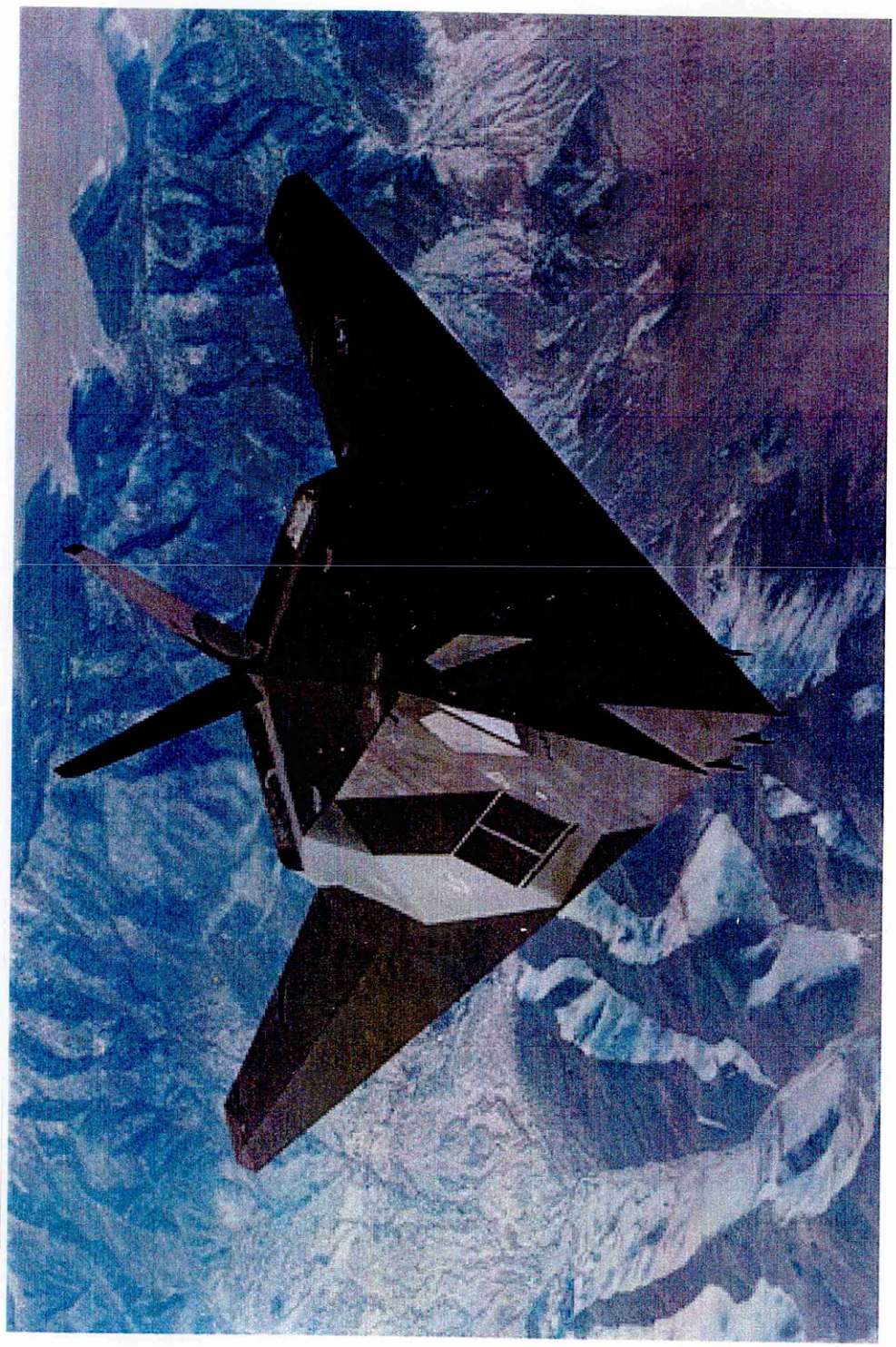

Figure: 1-1
Photograph of the F-117A aircraft.

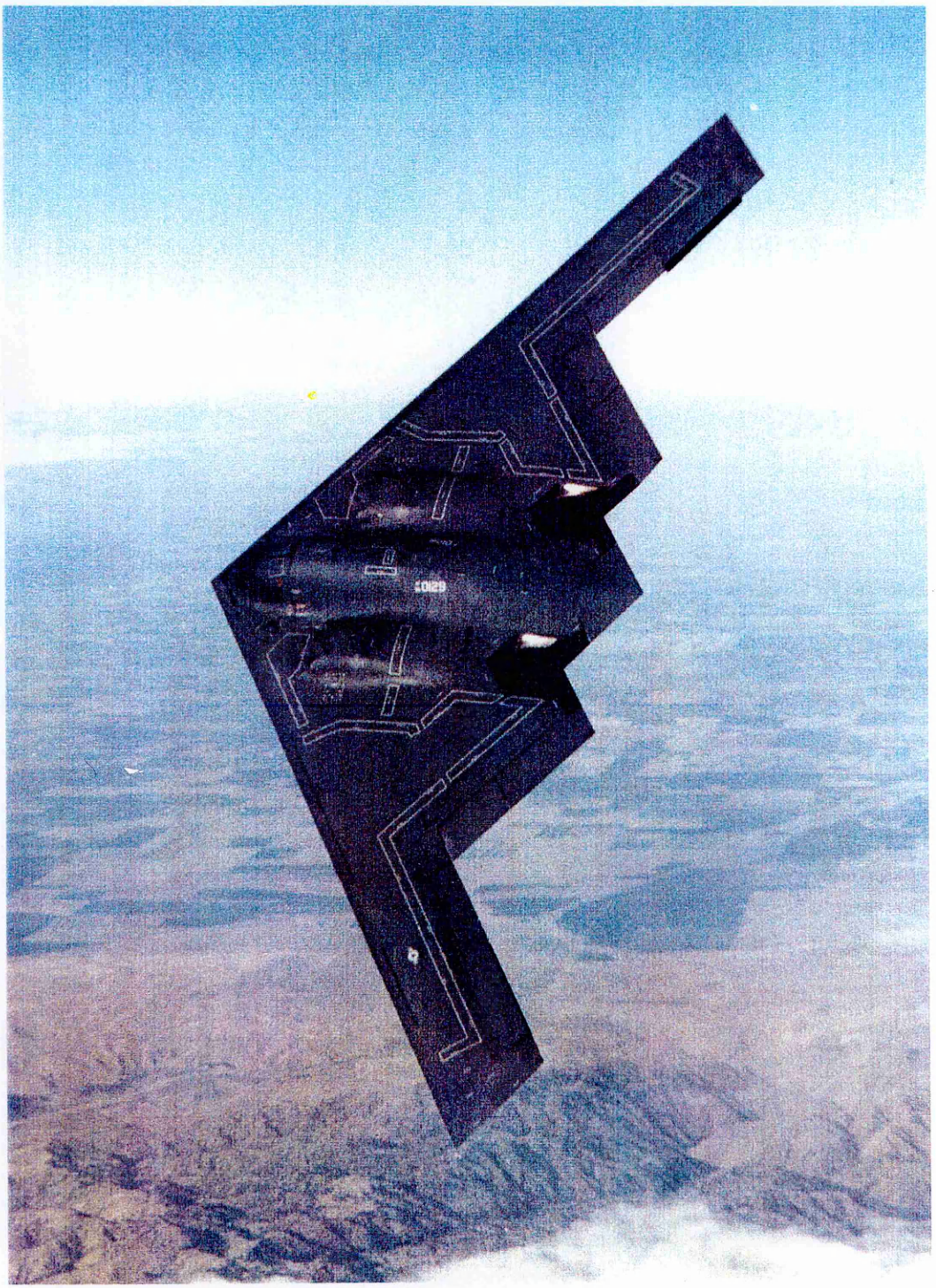

Figure: 1-2
Photograph of the B-2 aircraft.

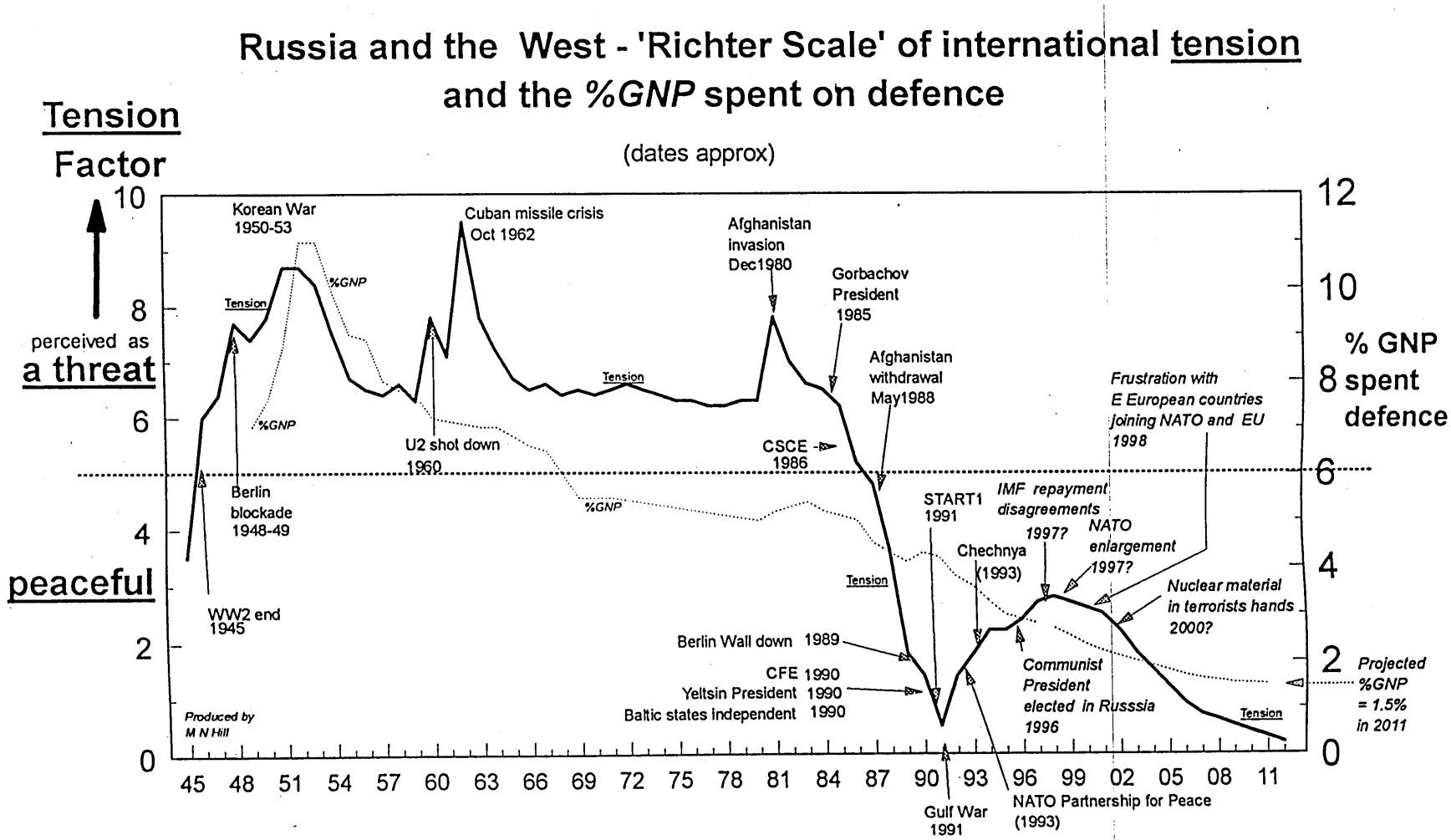

Figure: 2-1
Relation of tension factor with %GNP spent on UK defence.

Figure: 4-1
Mechanism of monostatic radar.

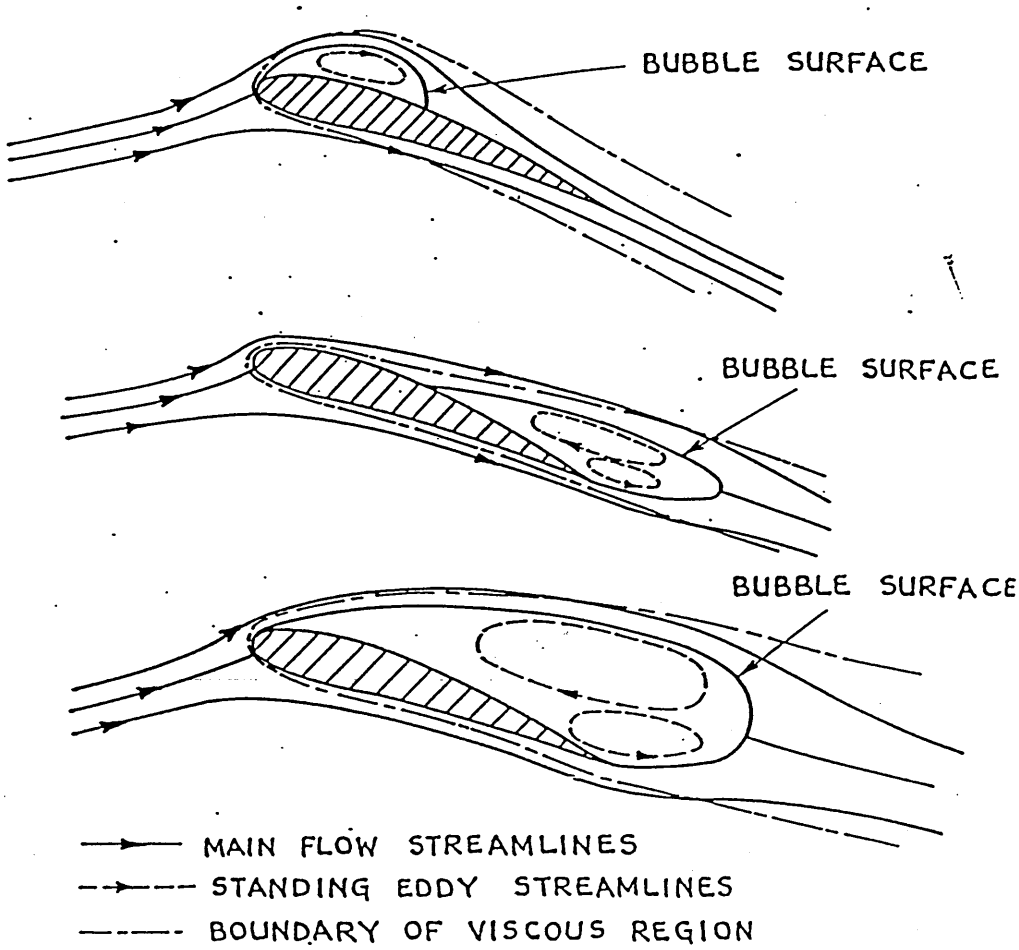

2D separation bubbles

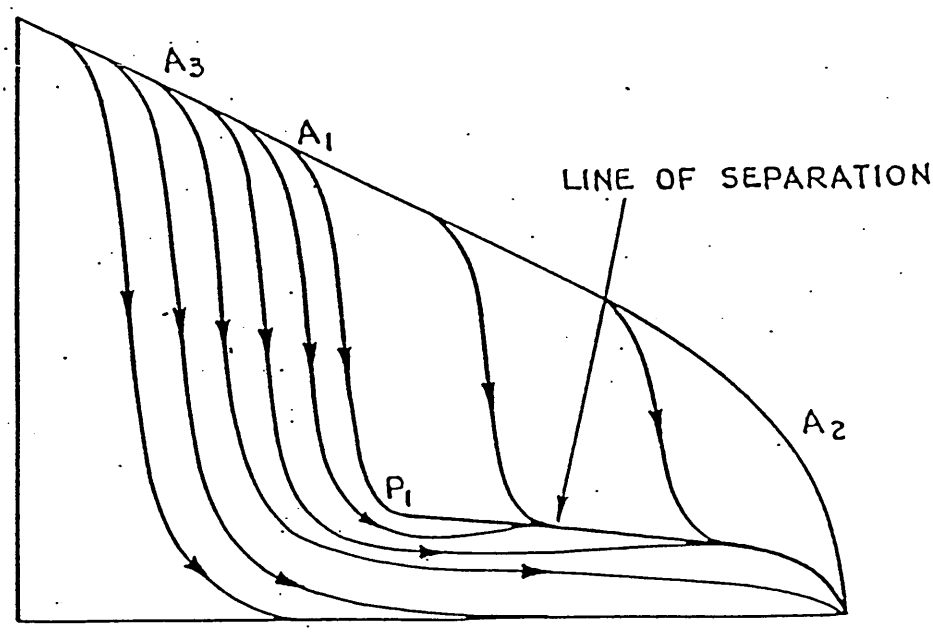

Figure: 4-2
Examples of flow separation (Maskell[33]).

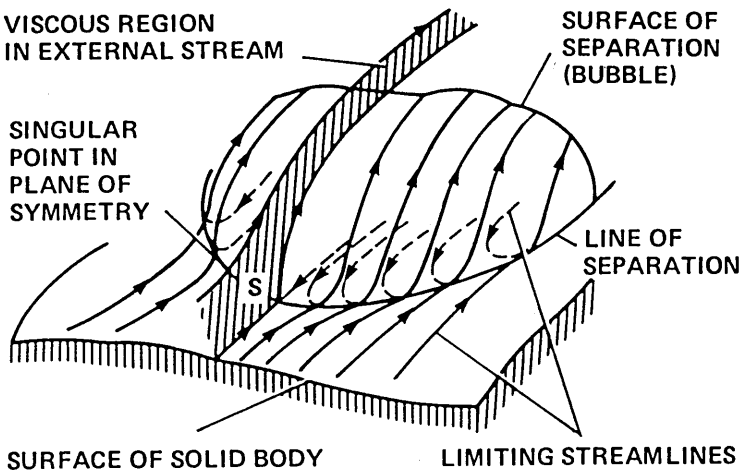

(a) BUBBLE

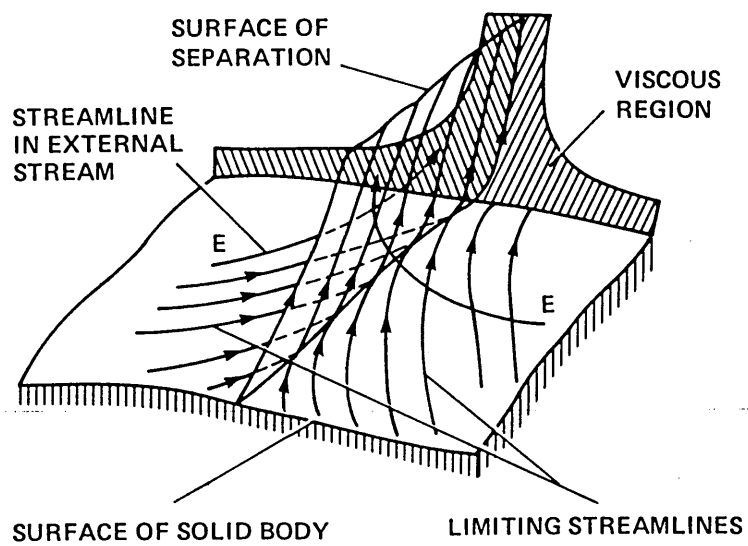

(b) FREE SHEAR LAYER

Figure: 4-3
Examples of flow separation (Maskell[33]).

Irregular grid in physical space

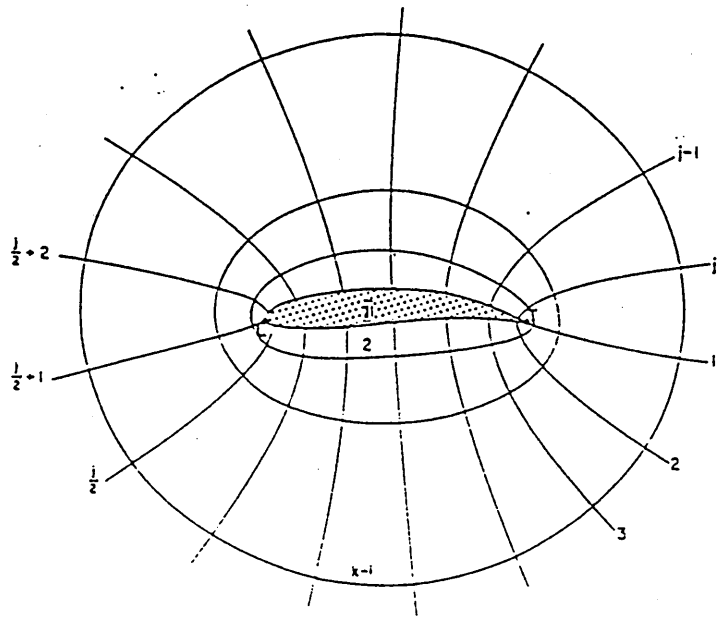

Regular grid in computational space

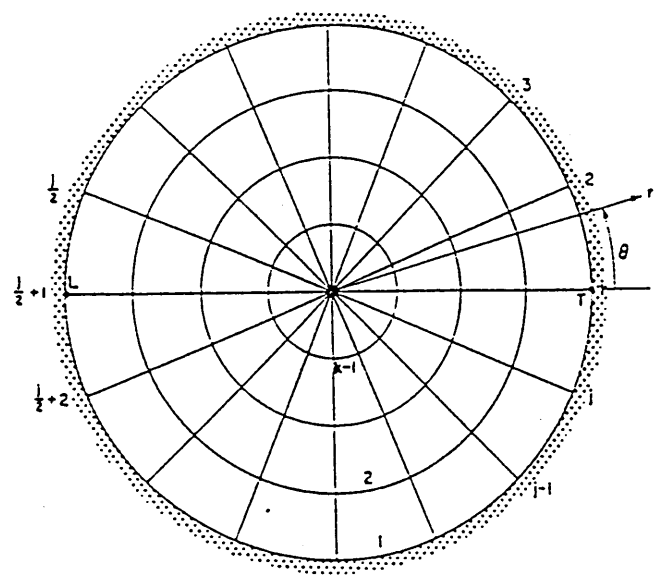

Figure: 5-1
VGK mapping procedure.

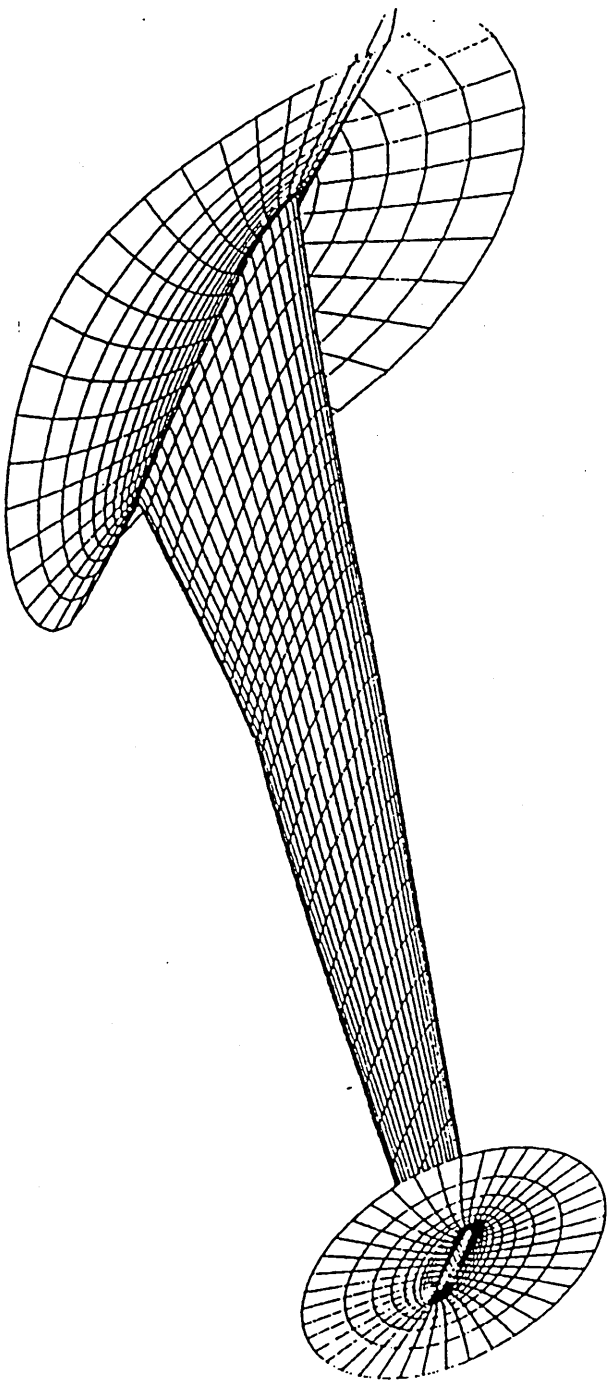

Figure: 5-2
VFP mapping procedure.

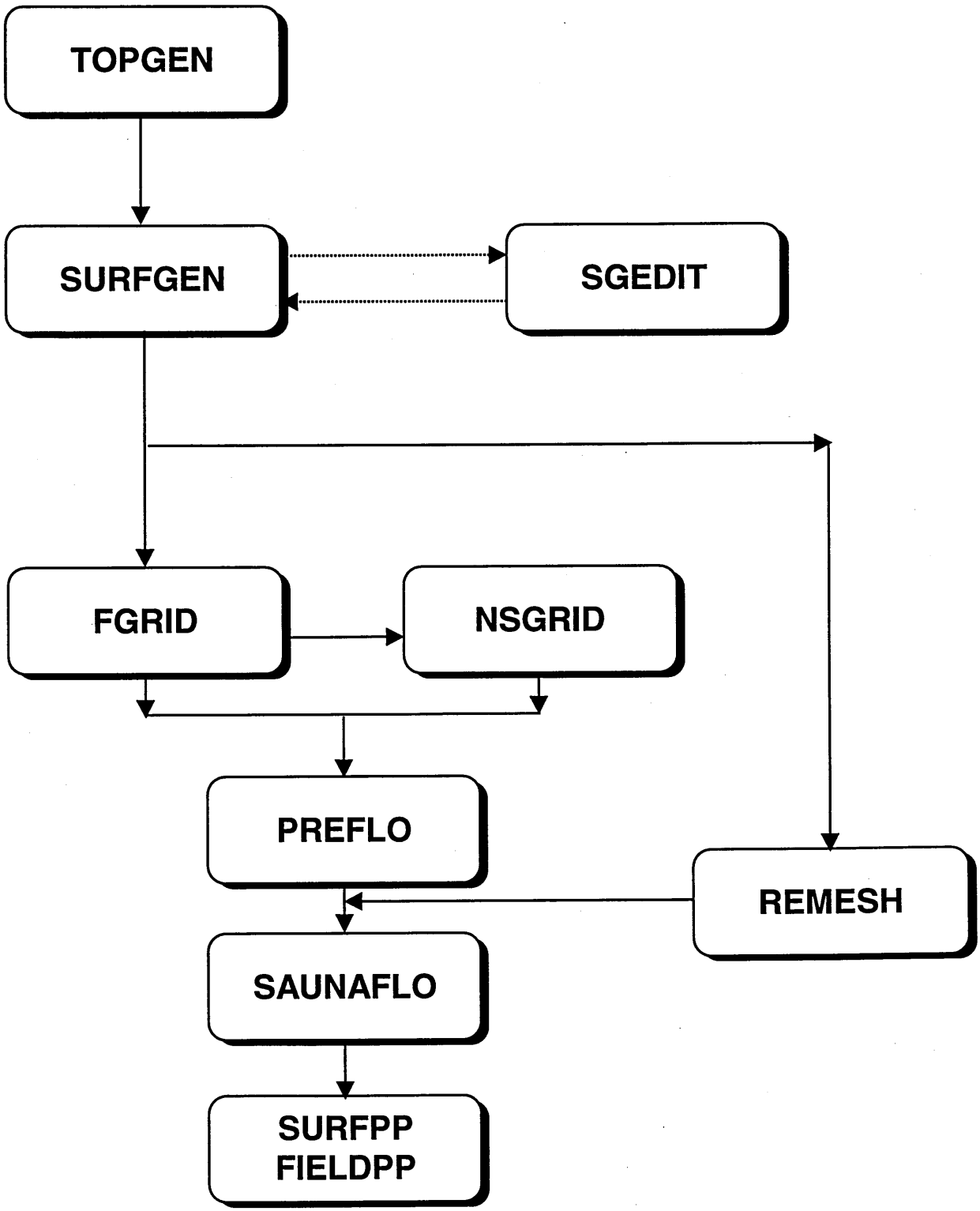

Figure: 5-3
SAUNA structure.

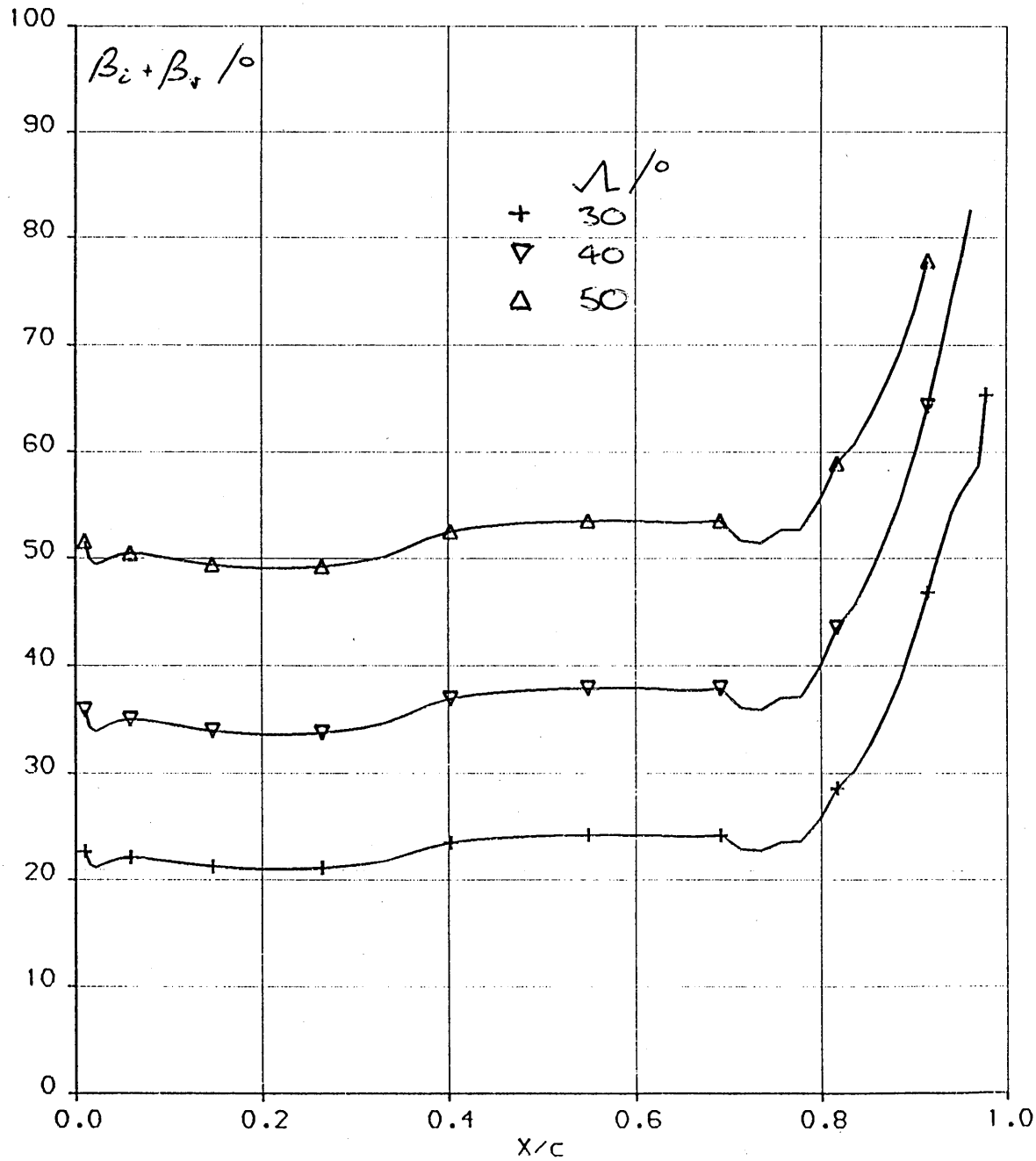

Figure: 6-1
Predicted boundary layer curvature, V = 60m/s, α=2 °.

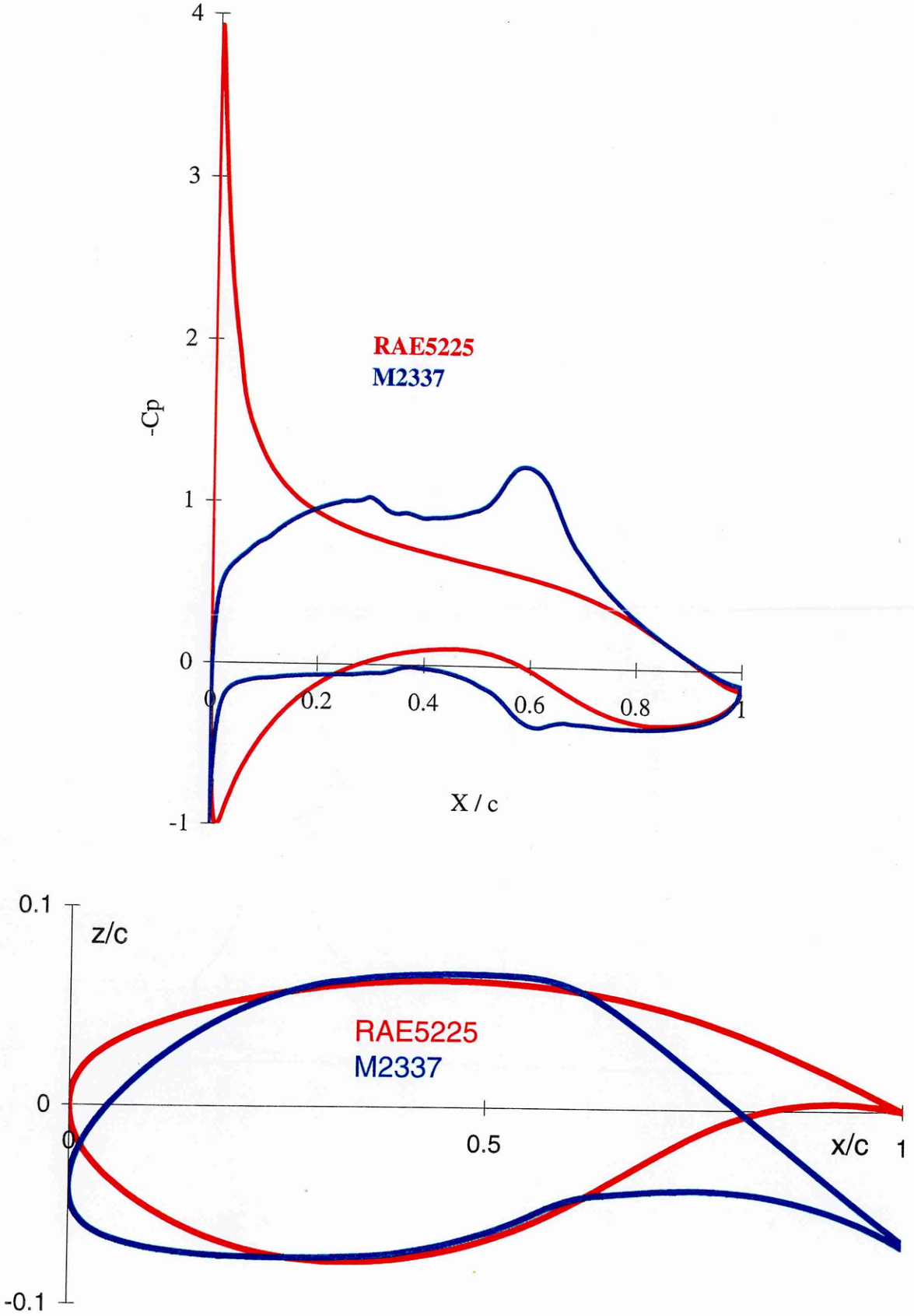

Figure: 6-2
BVGK pressure coefficient distributions and aerofoil sections.

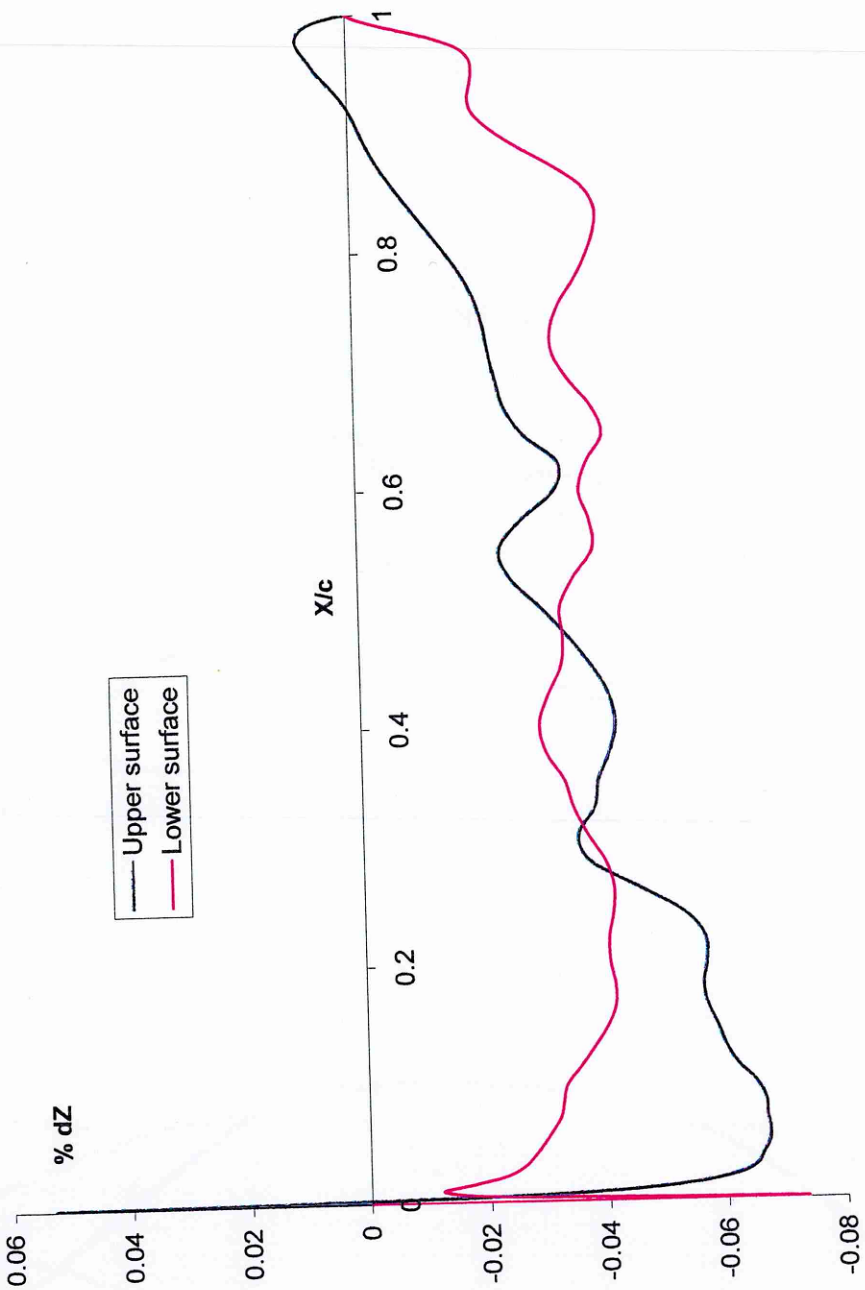

Figure: 6-3
Percentage difference between nominal and inspected z-ordinate.

Figure: 6-4
Model 2337 mounted on the floor of the 13ft x 9ft wind tunnel.

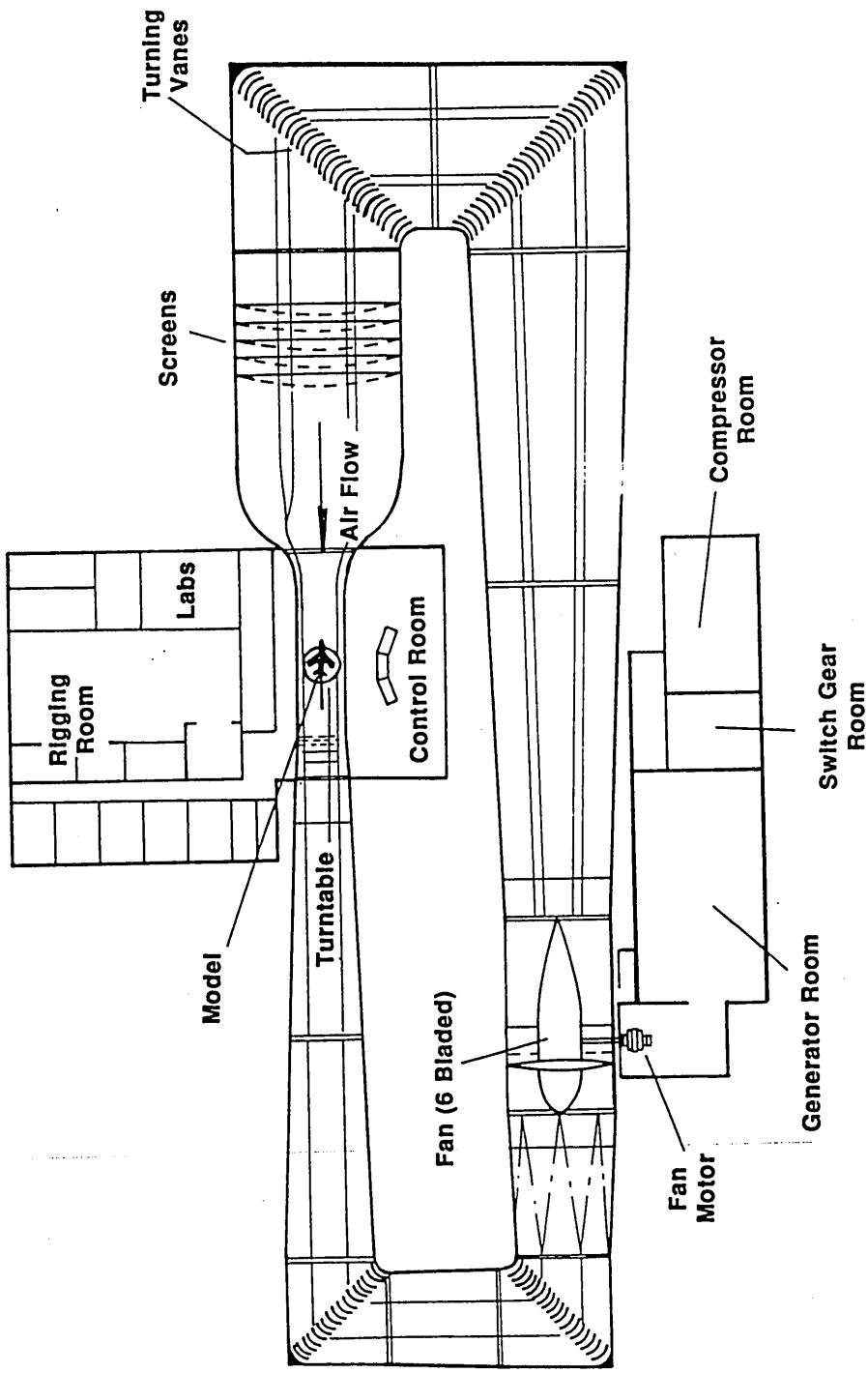

Figure: 6-5
13ft x 9ft wind tunnel circuit.

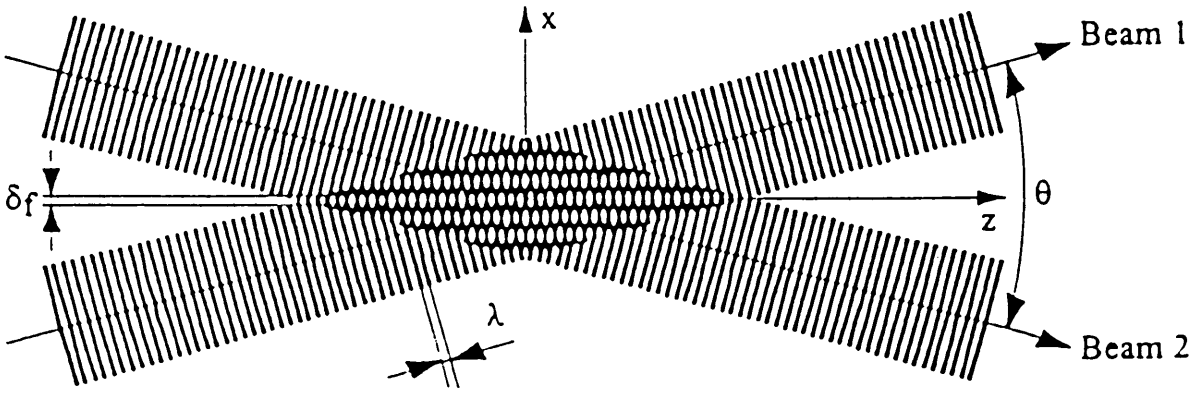

Figure: 6-6
Illustration of LDA measurement region.

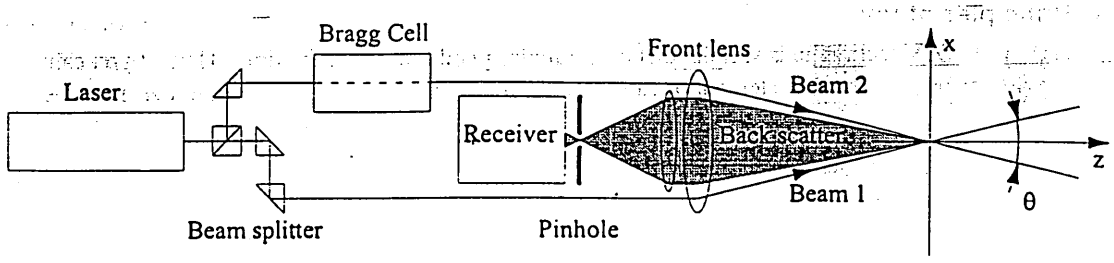

Figure: 6-7
Schematic of LDA technique.

Figure: 6-8
Photograph of LDA in use in the 13ft x 9ft wind tunnel.

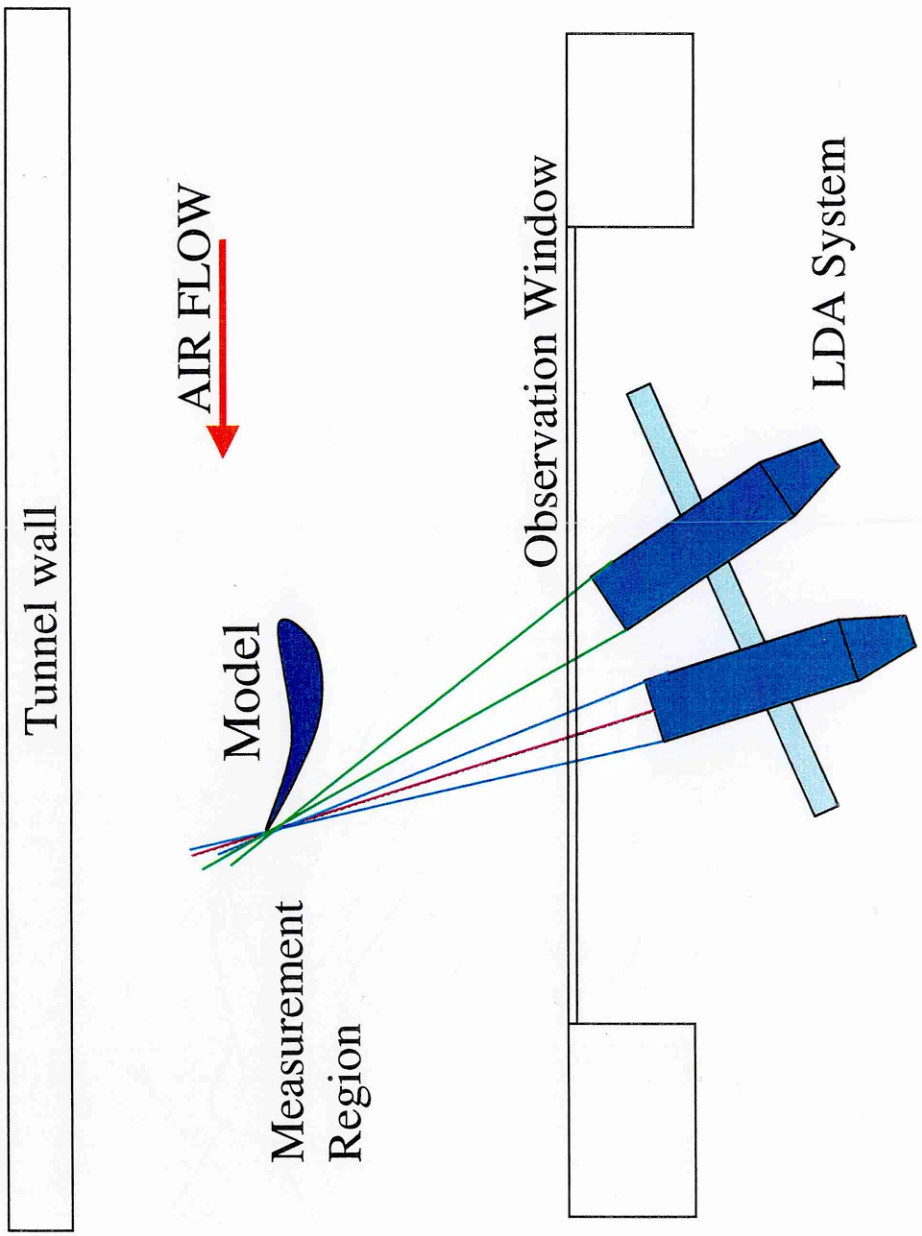

Figure: 6-9
Schematic of LDA system in 13ft x 9ft wind tunnel.

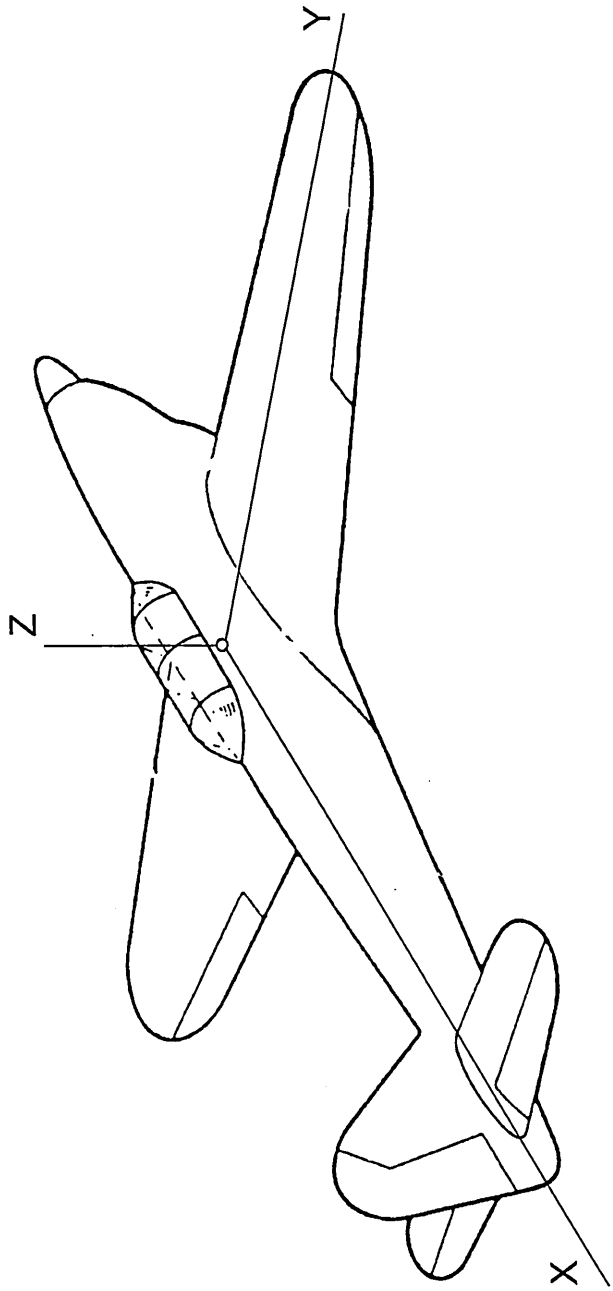

Figure: 7-1
Definition of the cartesian co-ordinate system.

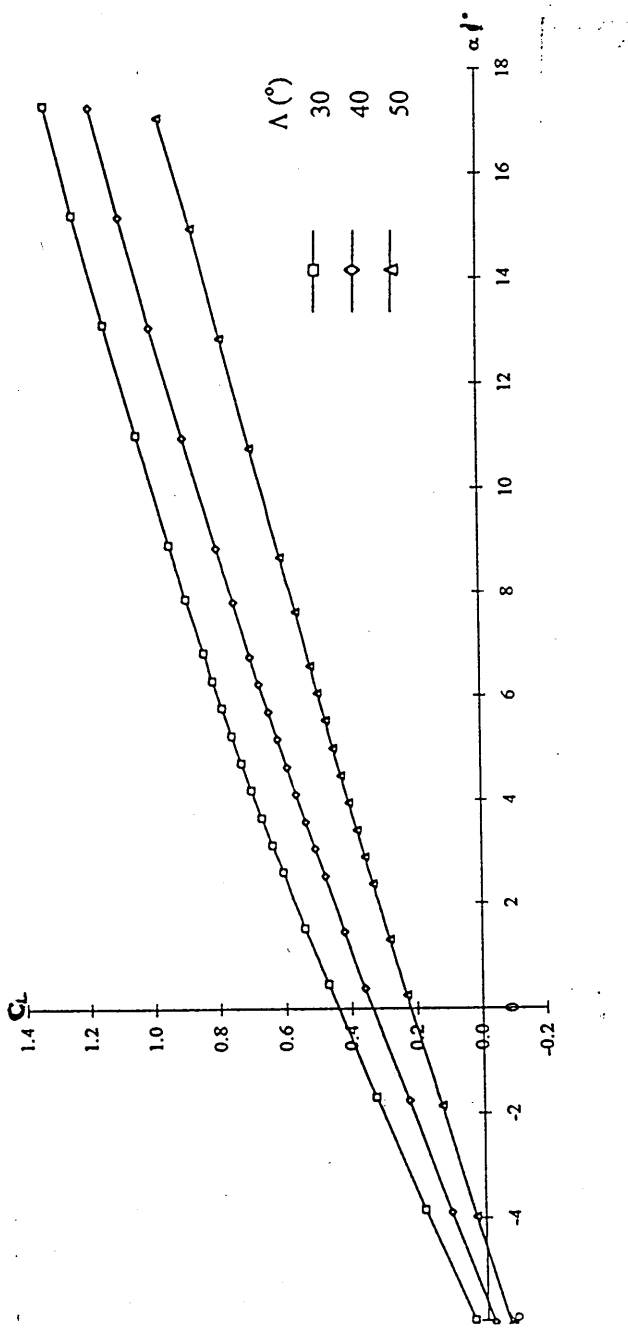

Figure: 7-2
Variation of measure lift coefficient with angle of incidence.

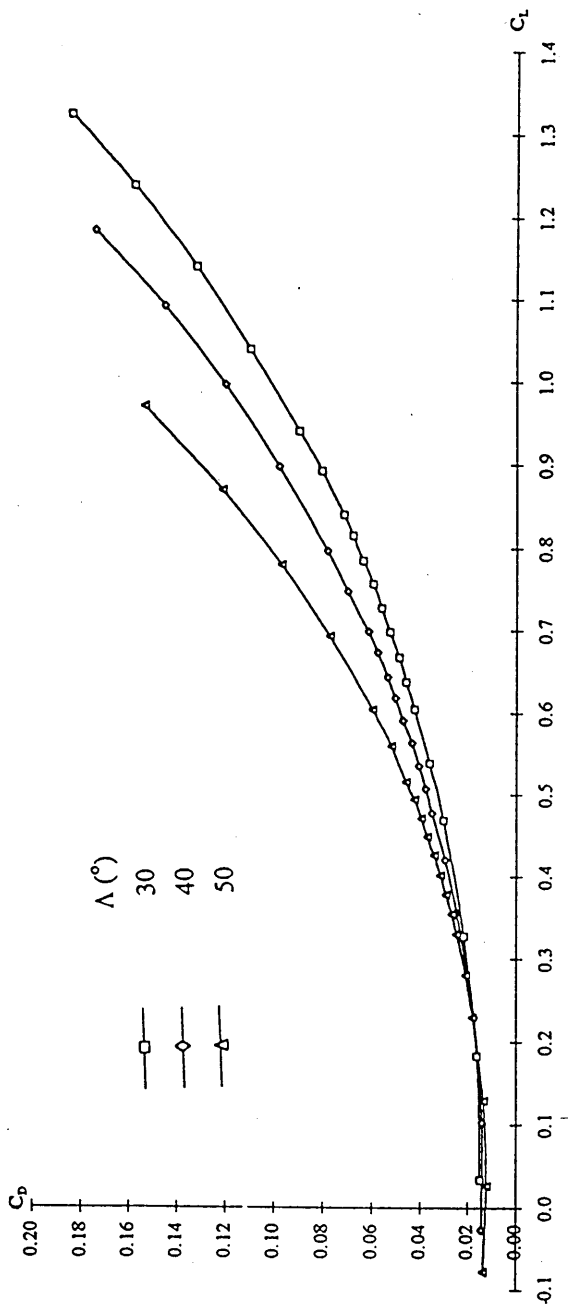

Figure: 7-3
Variation of measured drag coefficient with lift coefficient.

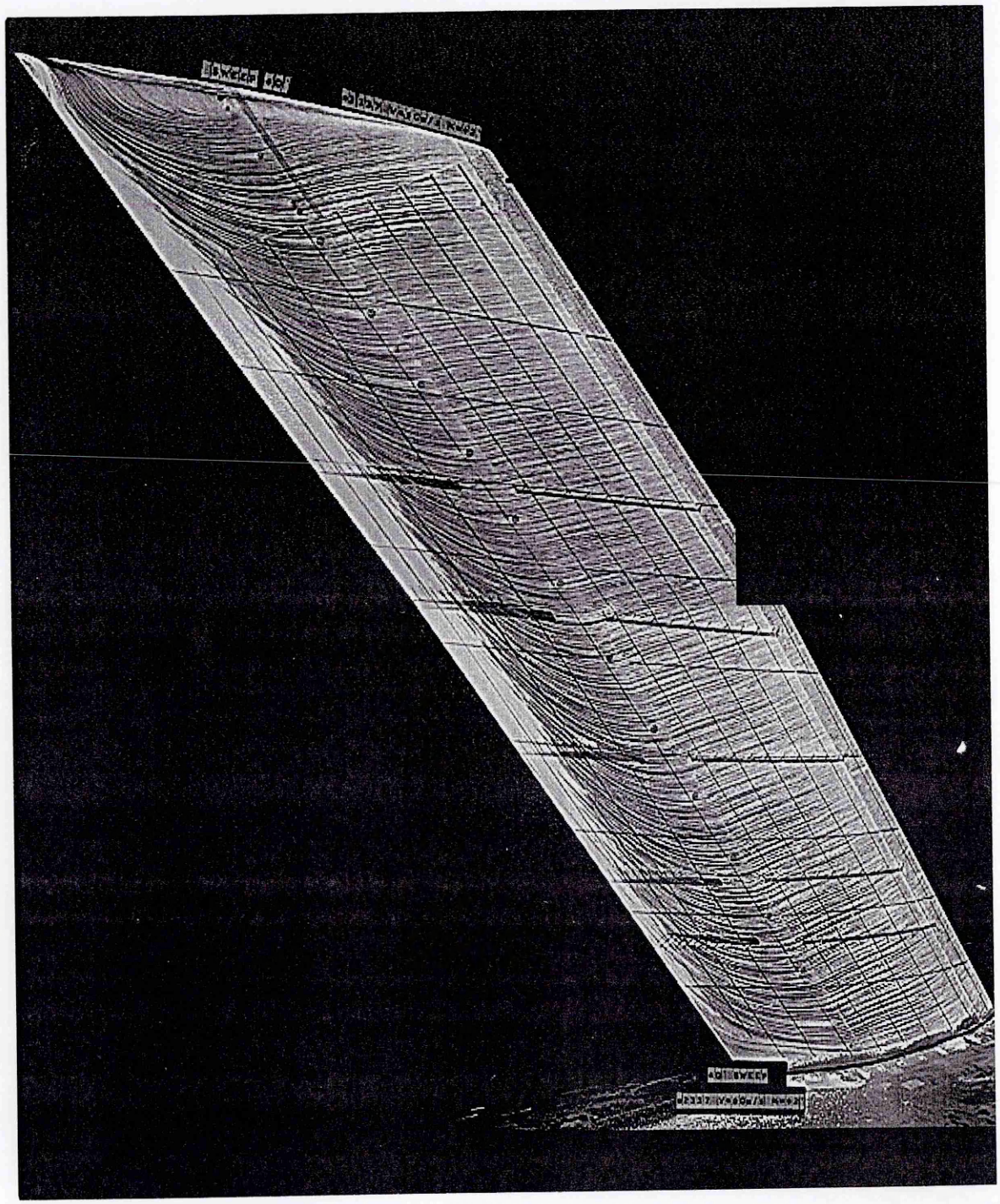

Figure: 7-4
Upper-surface oil flow pattern, $\Lambda = 40°$, V = 60m/s, α=2.5°.

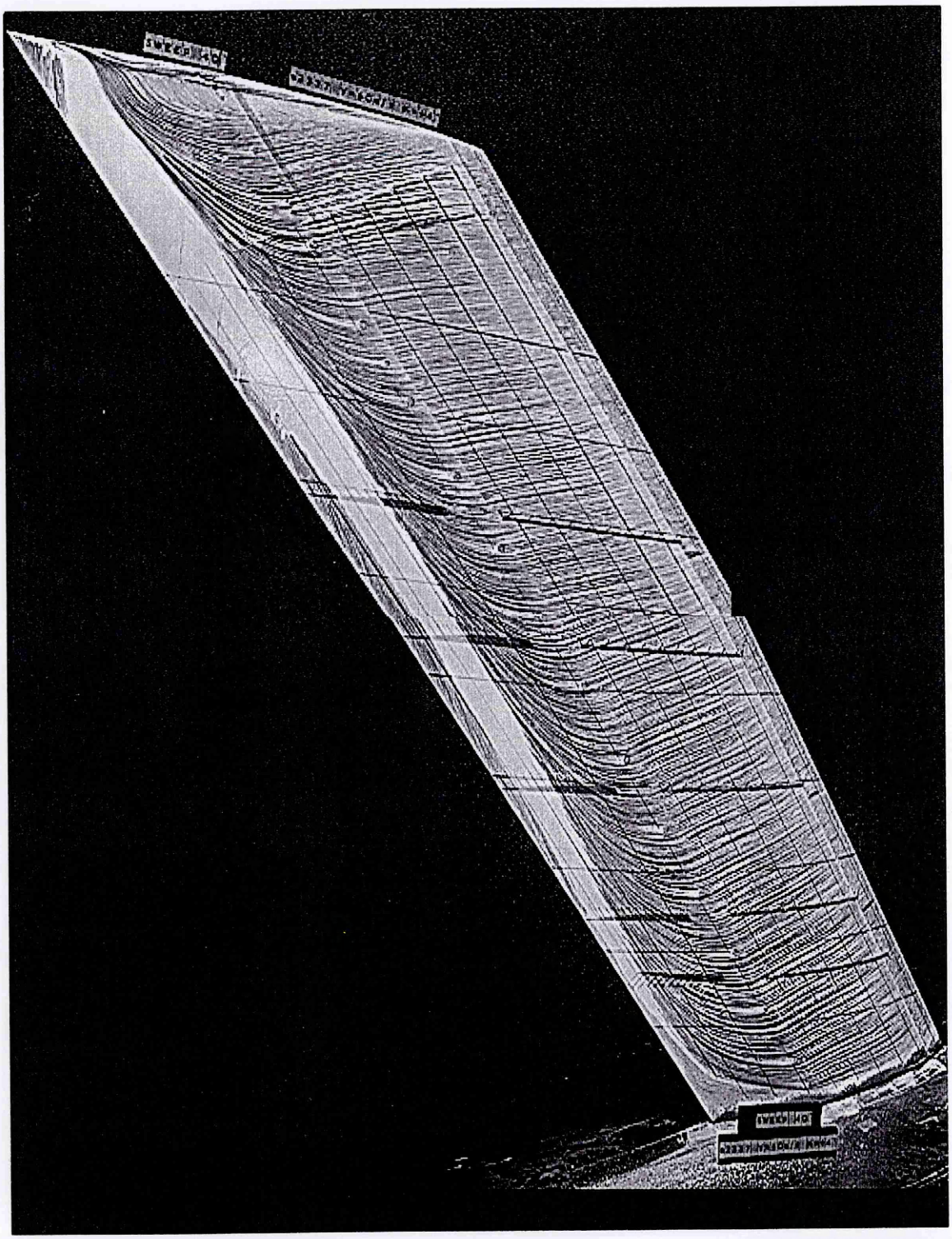

Figure: 7-5
Upper-surface oil flow pattern, $\Lambda = 40°$, V = 60m/s, α=4.6°.

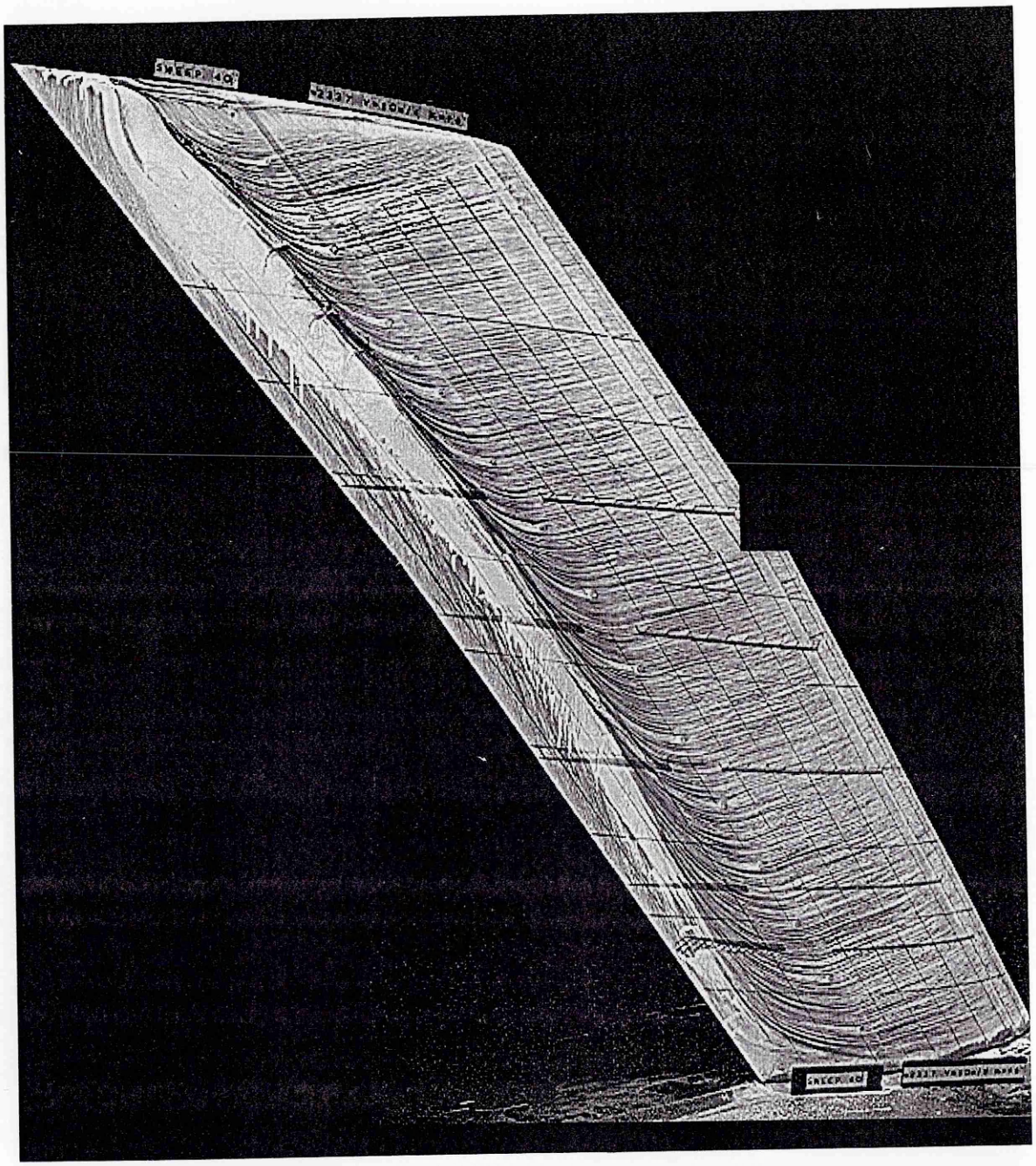

Figure: 7-6
Upper-surface oil flow pattern, $\Lambda = 40°$, V = 60m/s, α=6.8°.

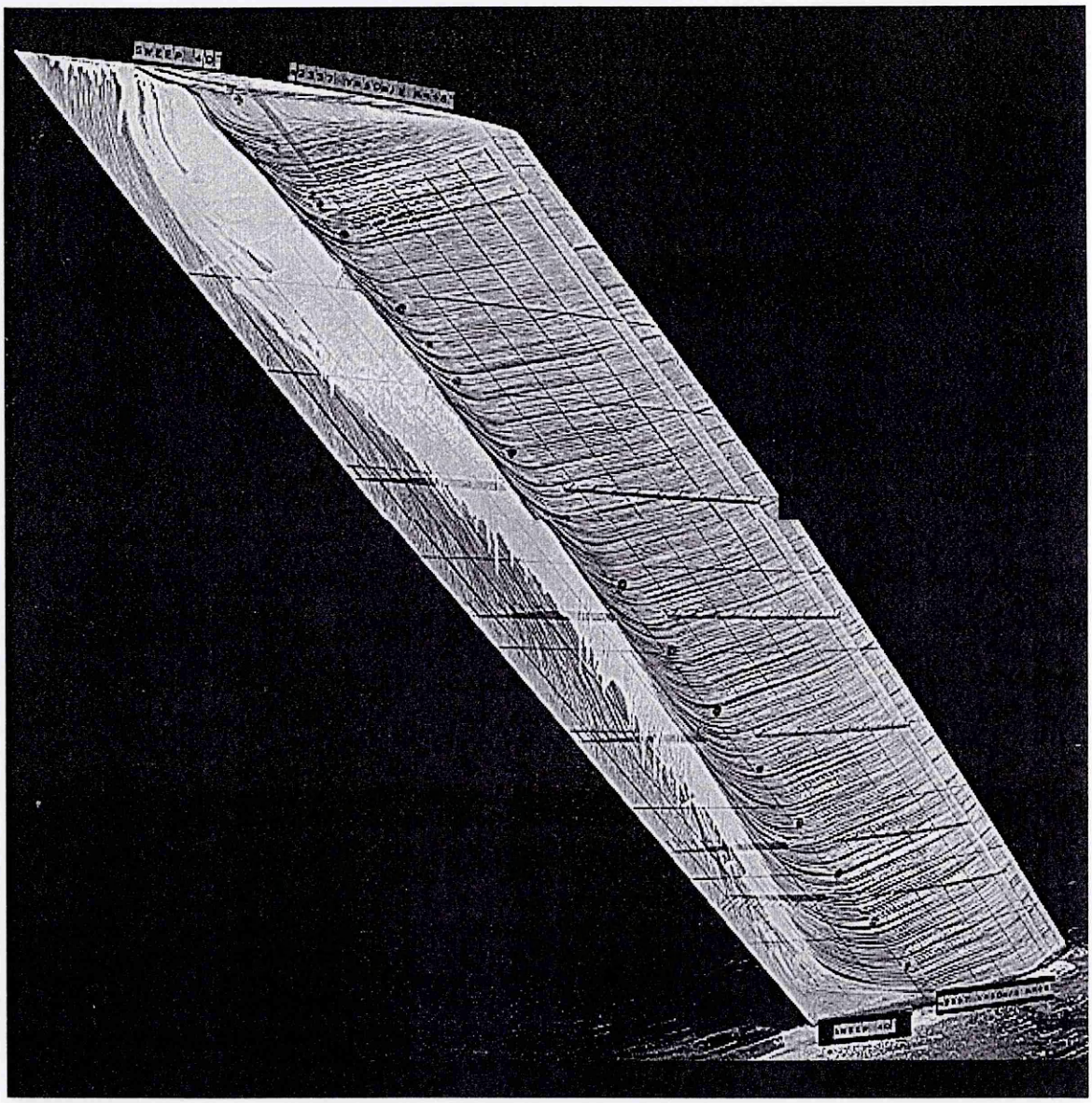

Figure: 7-7
Upper-surface oil flow pattern, $\Lambda = 40°$, V = 60m/s, α=8.9°.

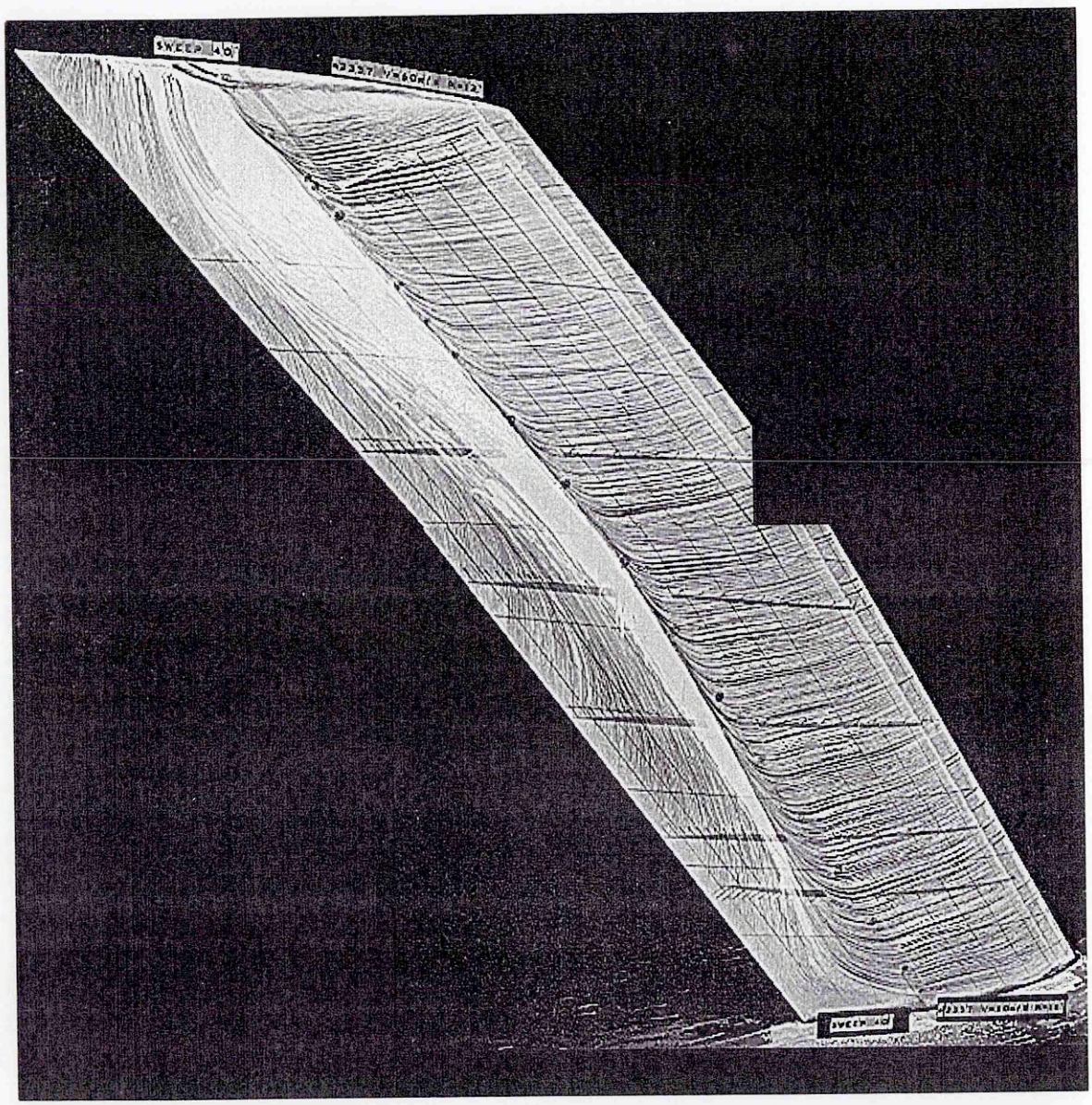

Figure: 7-8
Upper-surface oil flow pattern, $\Lambda = 40°$, V = 60m/s, α=13.1°.

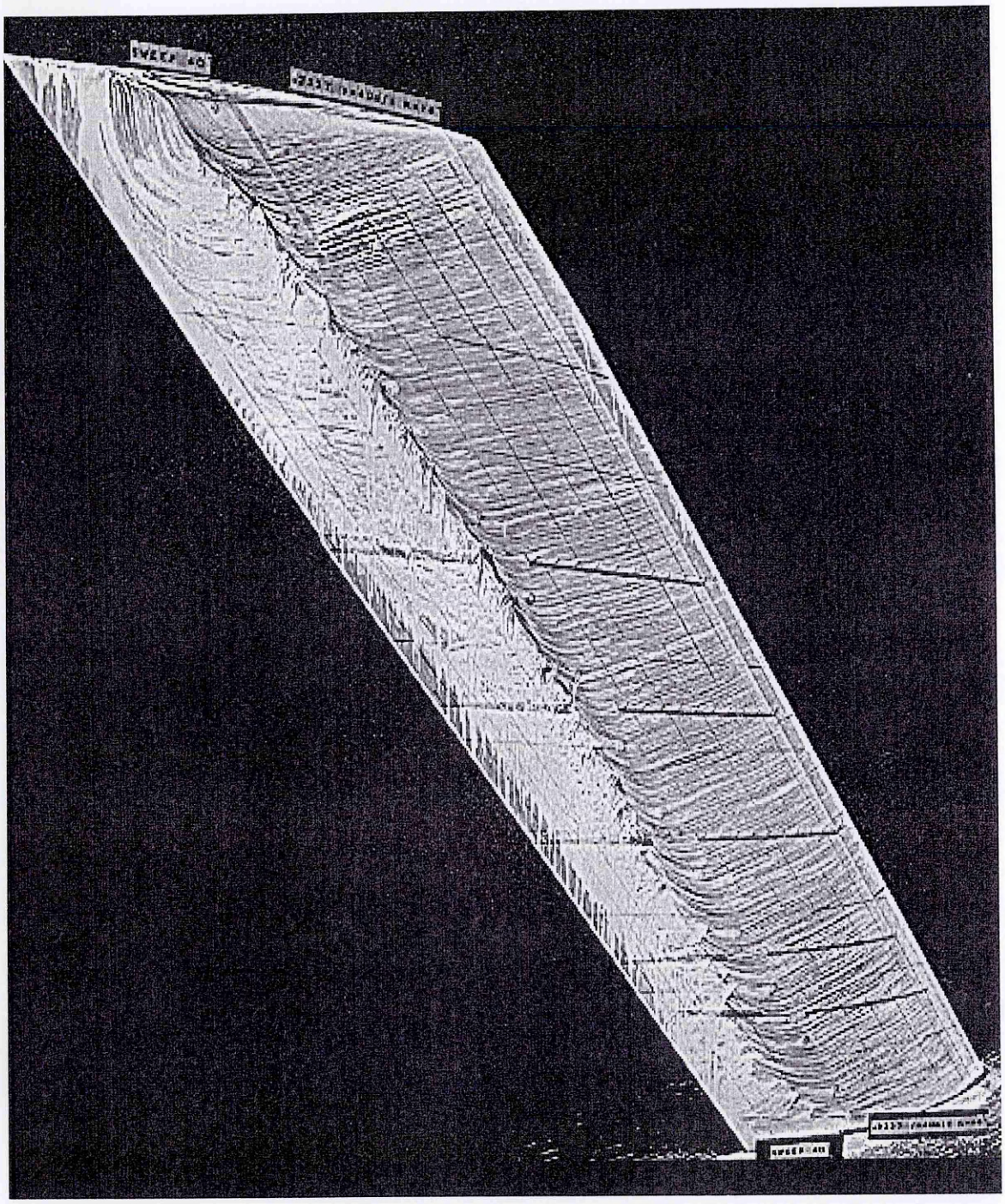

Figure: 7-9
Upper-surface oil flow pattern, $\Lambda = 40°$, V = 40m/s, α=8.9°.

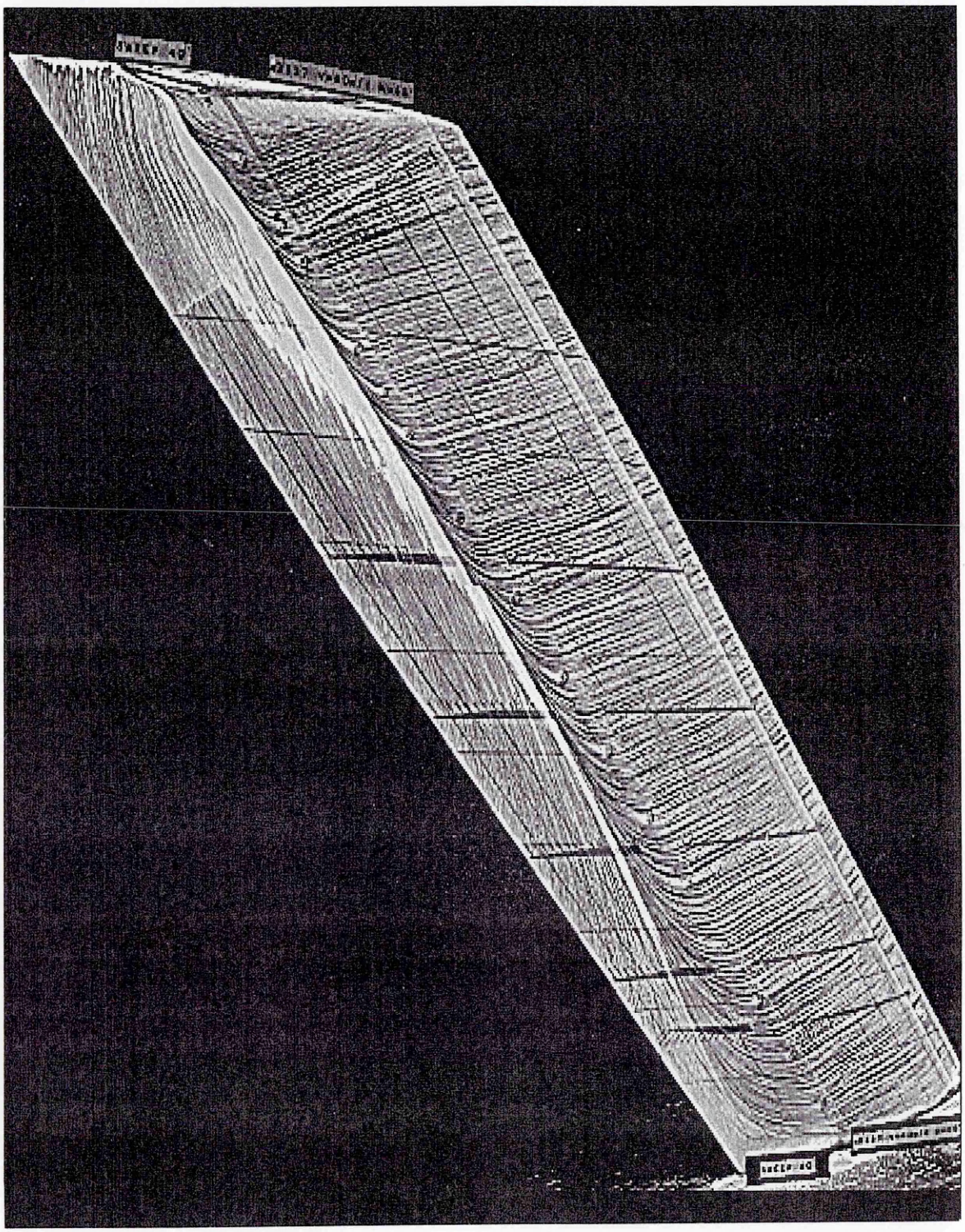

Figure: 7-10
Upper-surface oil flow pattern, $\Lambda = 40°$, V = 80m/s, α=8.9°.

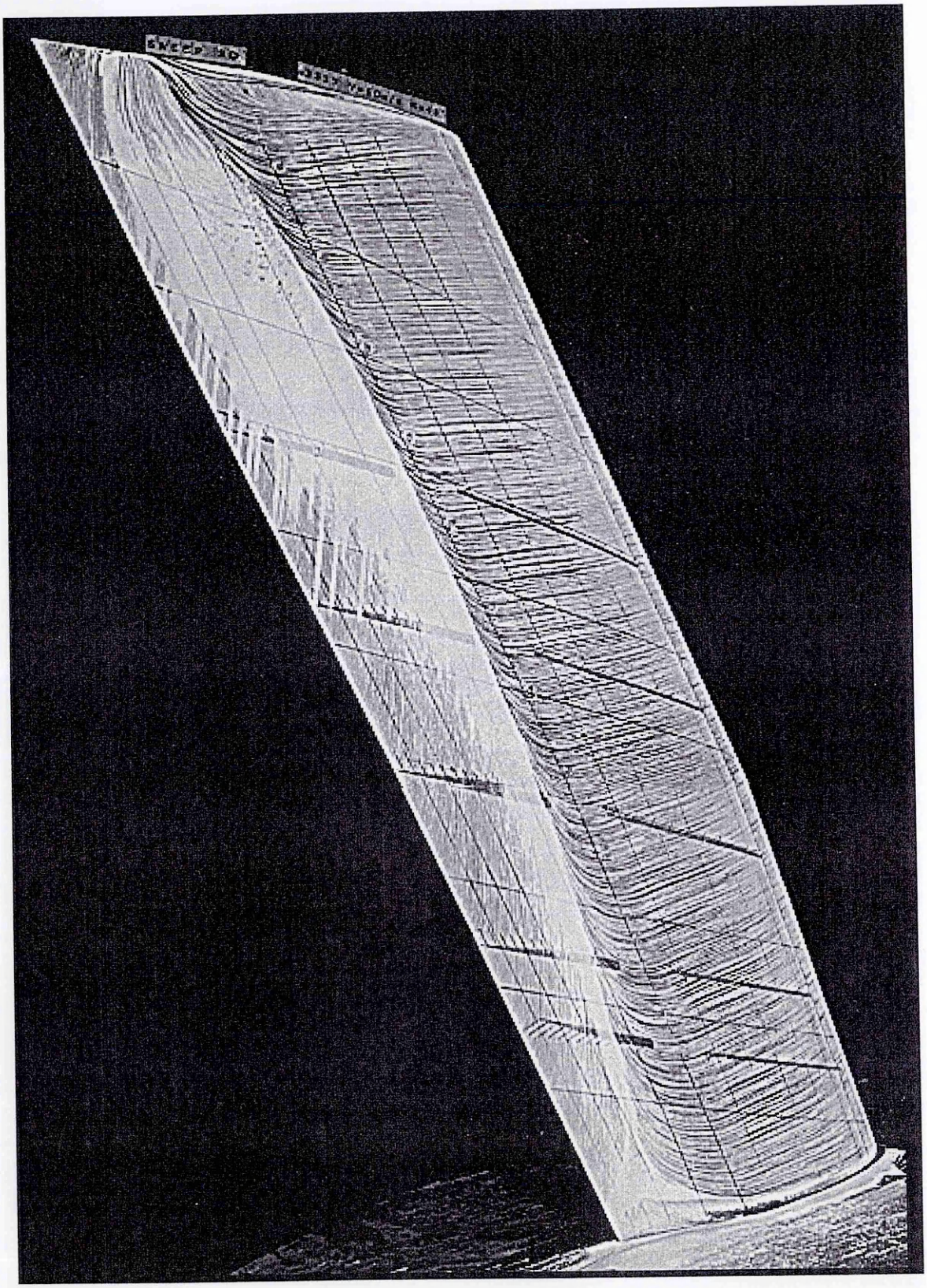

Figure: 7-11
Upper-surface oil flow pattern, $\Lambda = 30°$, V = 60m/s, α=8.9°.

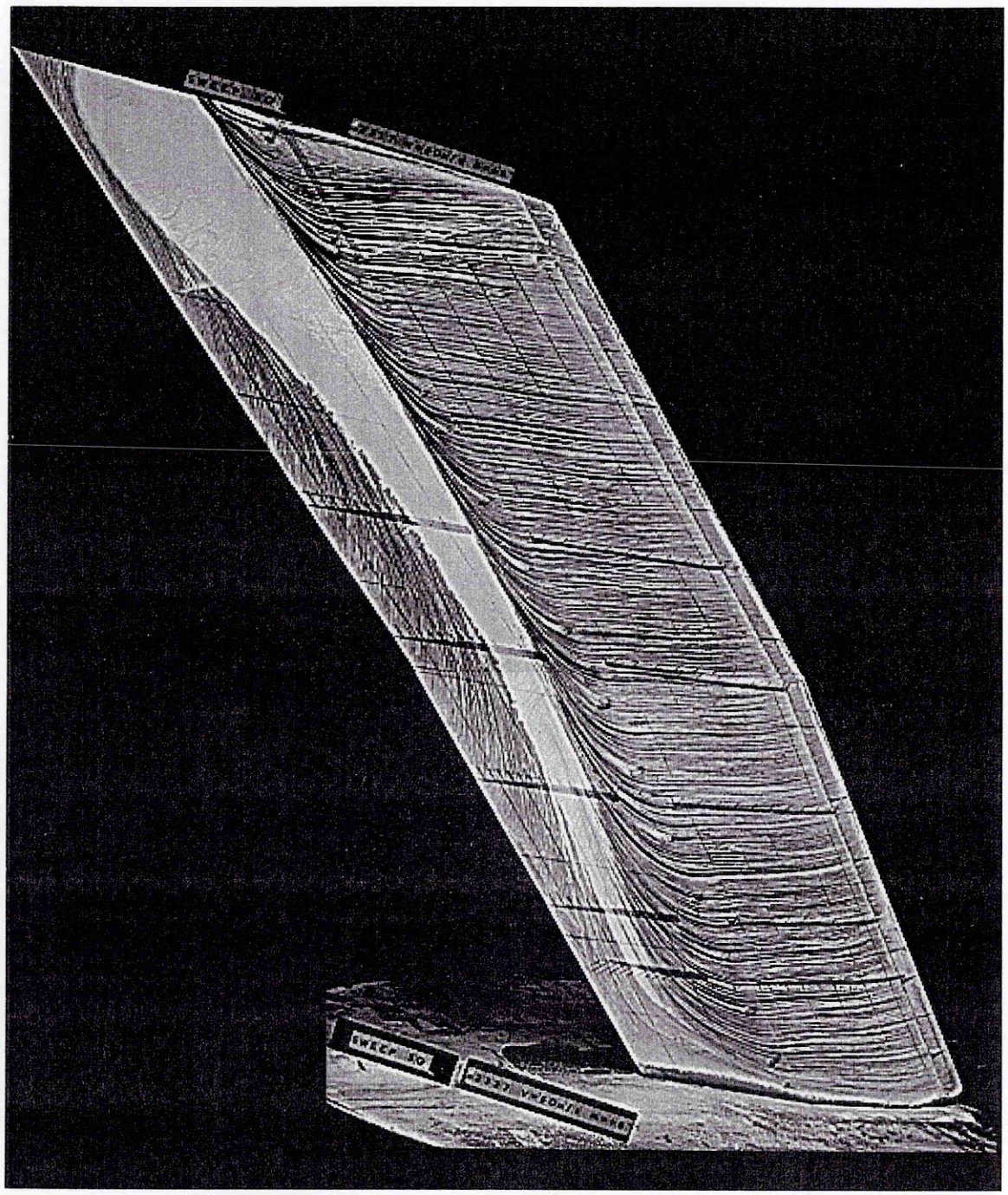

Figure: 7-12
Upper-surface oil flow pattern, $\Lambda = 50°$, V = 60m/s, α=8.9°.

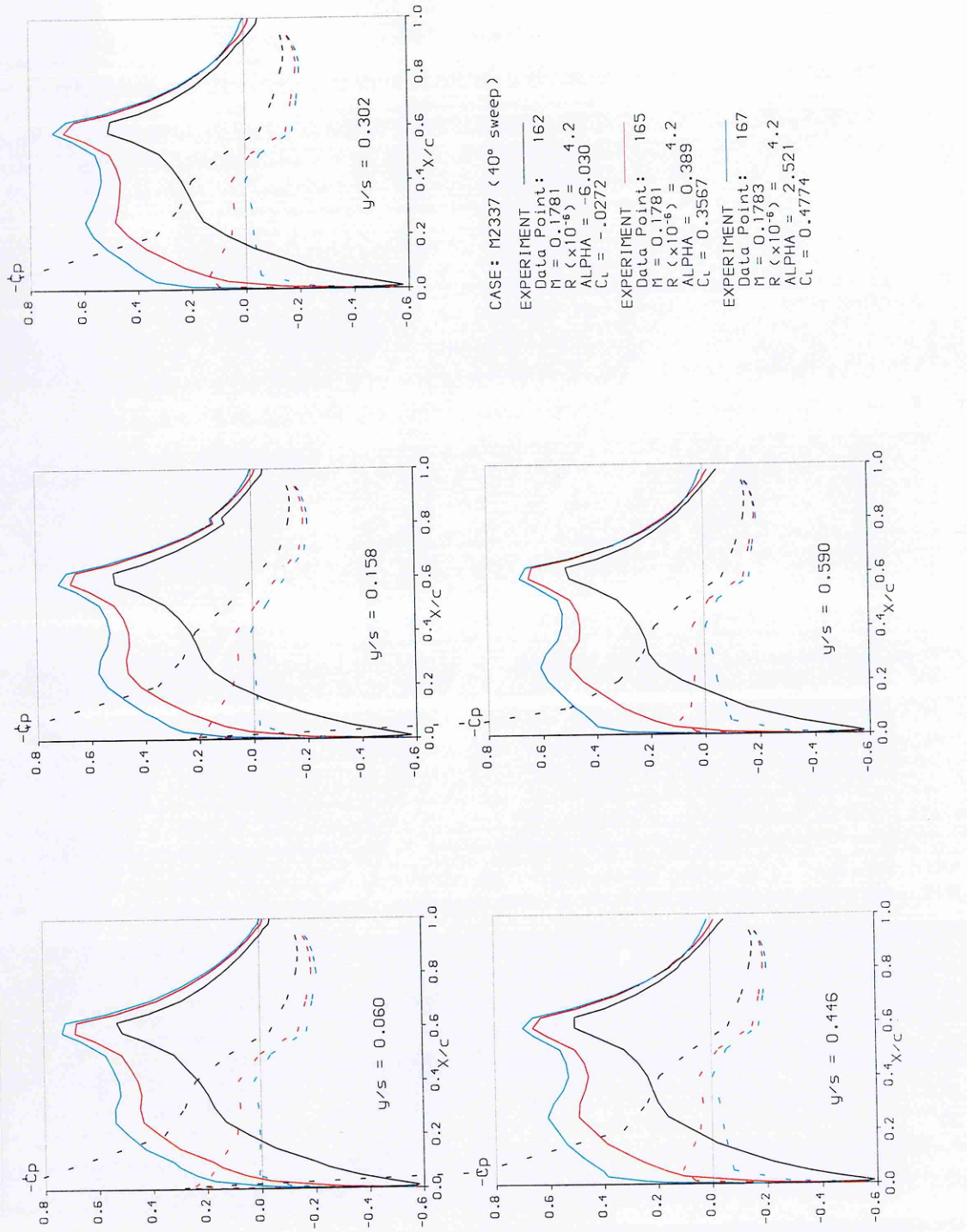

Figure: 7-13
Experimental pressure coefficient distributions, $\Lambda = 40°$, V = 60m/s.

Figure: 7-14
Experimental pressure coefficient distributions, $\Lambda = 40°$, V = 60m/s.

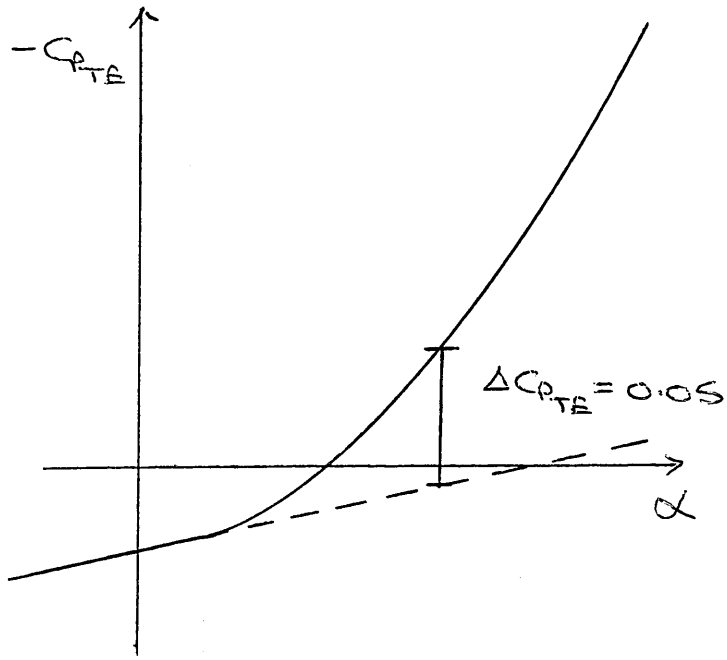

Figure: 7-15
Sketch showing criterion for the onset of flow breakdown.

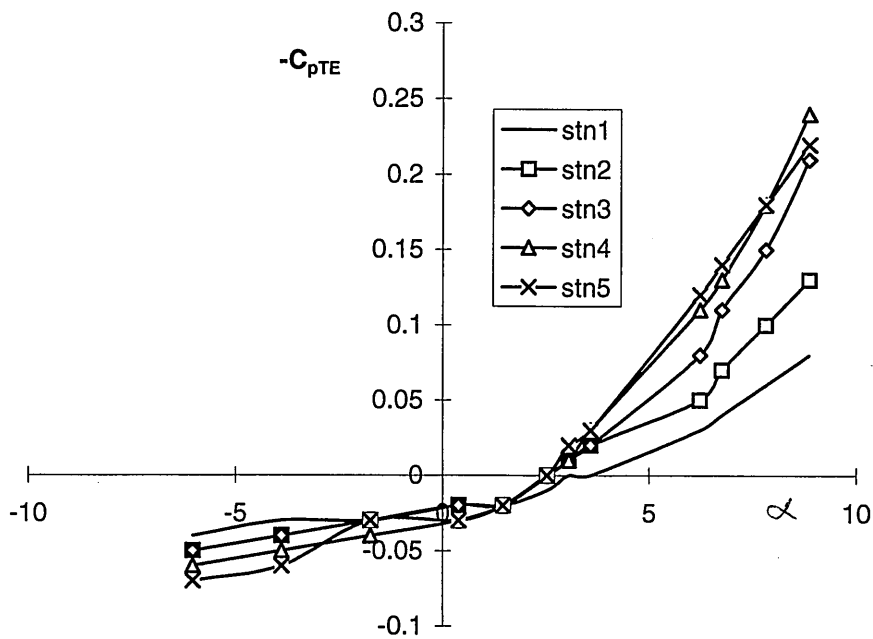

Figure: 7-16
Variation of measured trailing edge pressure coefficient with angle of incidence.

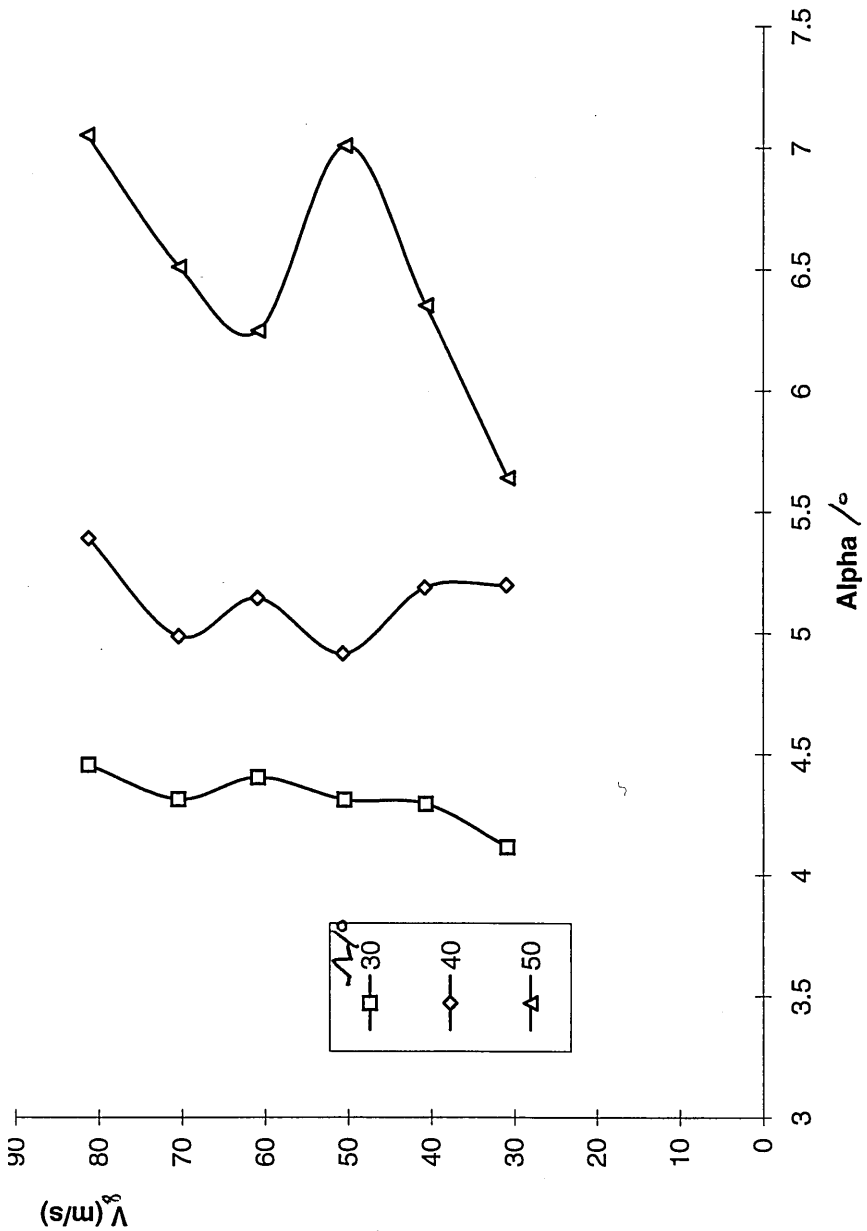

Figure: 7-17
Boundaries for the onset of flow breakdown.

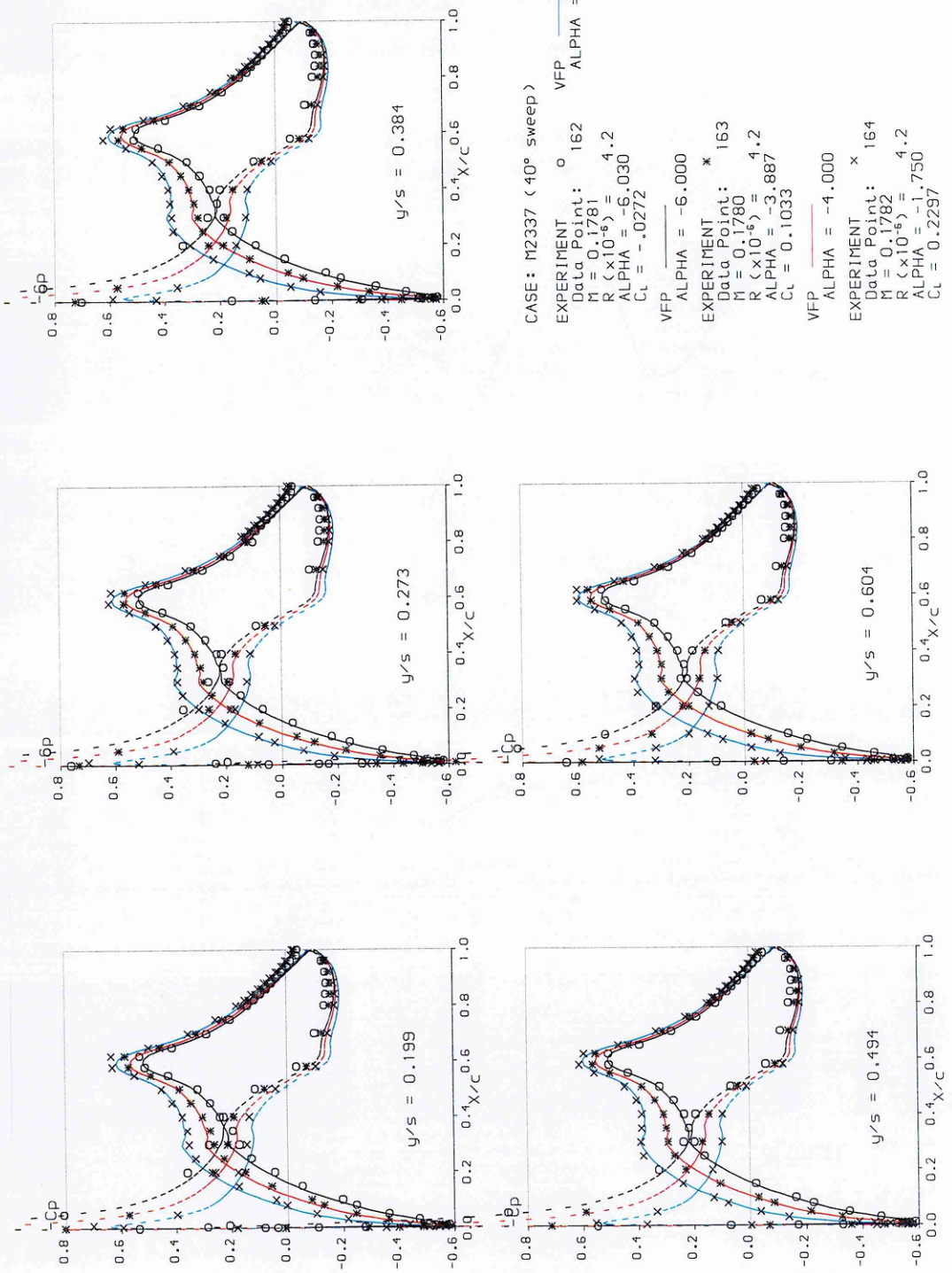

Figure: 7-18
Experimental and VFP pressure coefficient distributions, $\Lambda = 40°$, V = 60m/s.

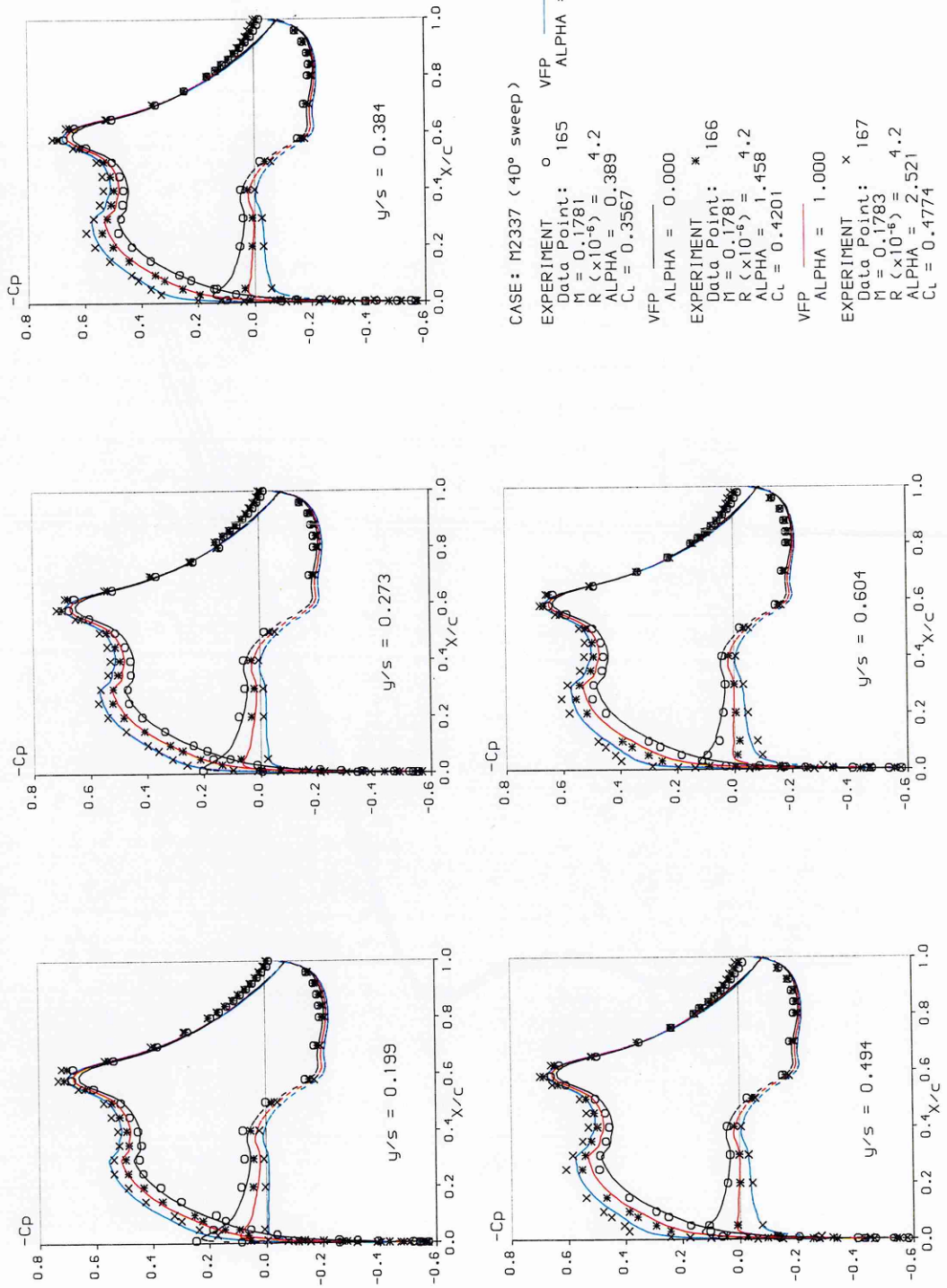

Figure: 7-19
Experimental and VFP pressure coefficient distributions, $\Lambda = 40°$, V = 60m/s.

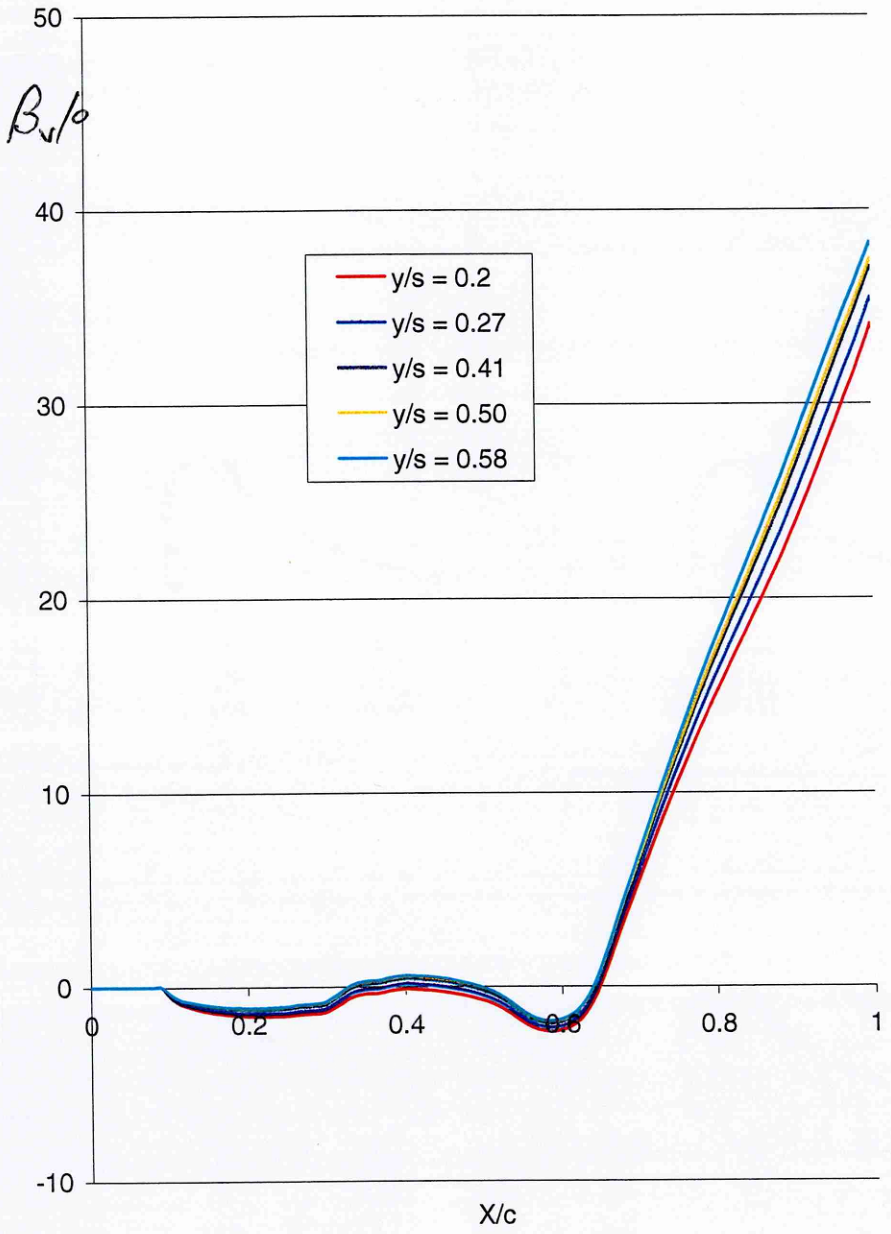

Figure: 7-20
Predicted (VFP) boundary layer curvature, $\Lambda = 40°$, V = 60m/s, α=2°.

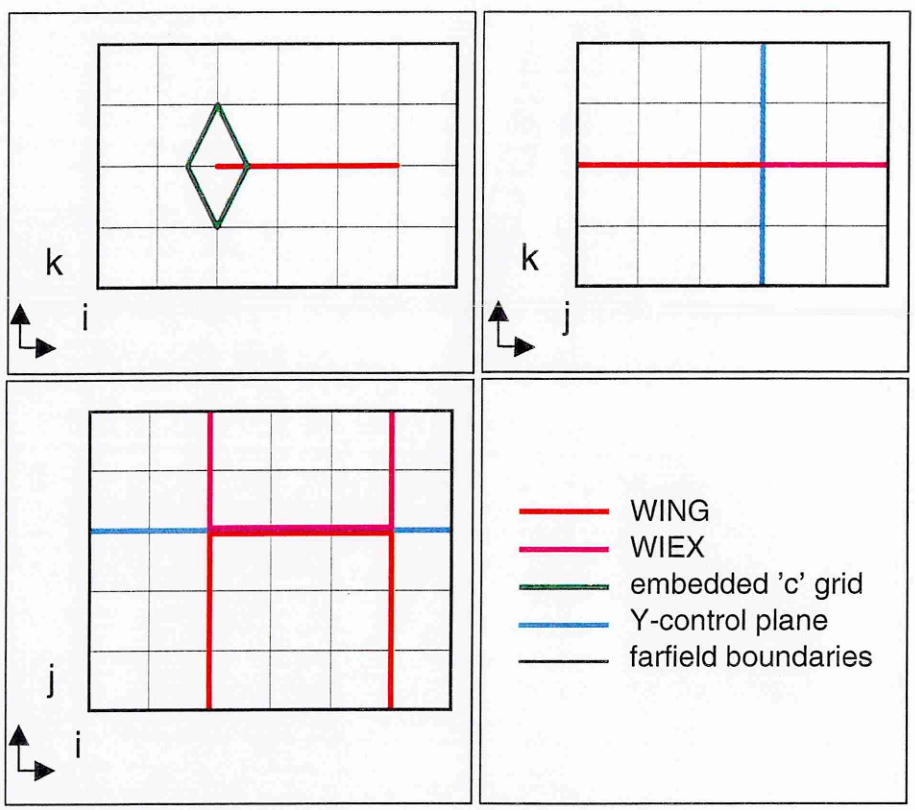

Figure: 7-21
SAUNA topology schematic for grid 1.

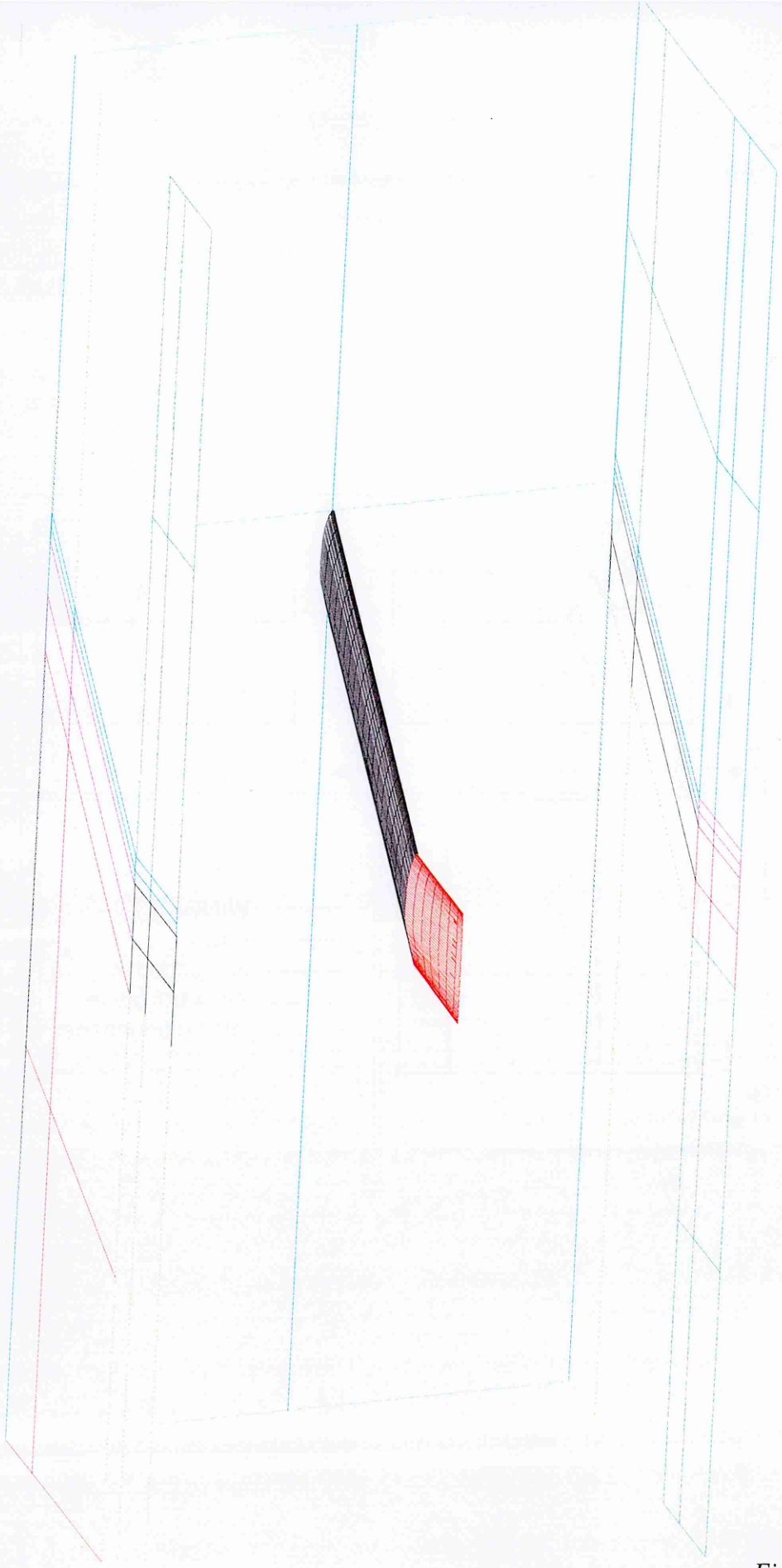

Figure: 7-22
Geometry of the wing, wing extension and shadow planes.

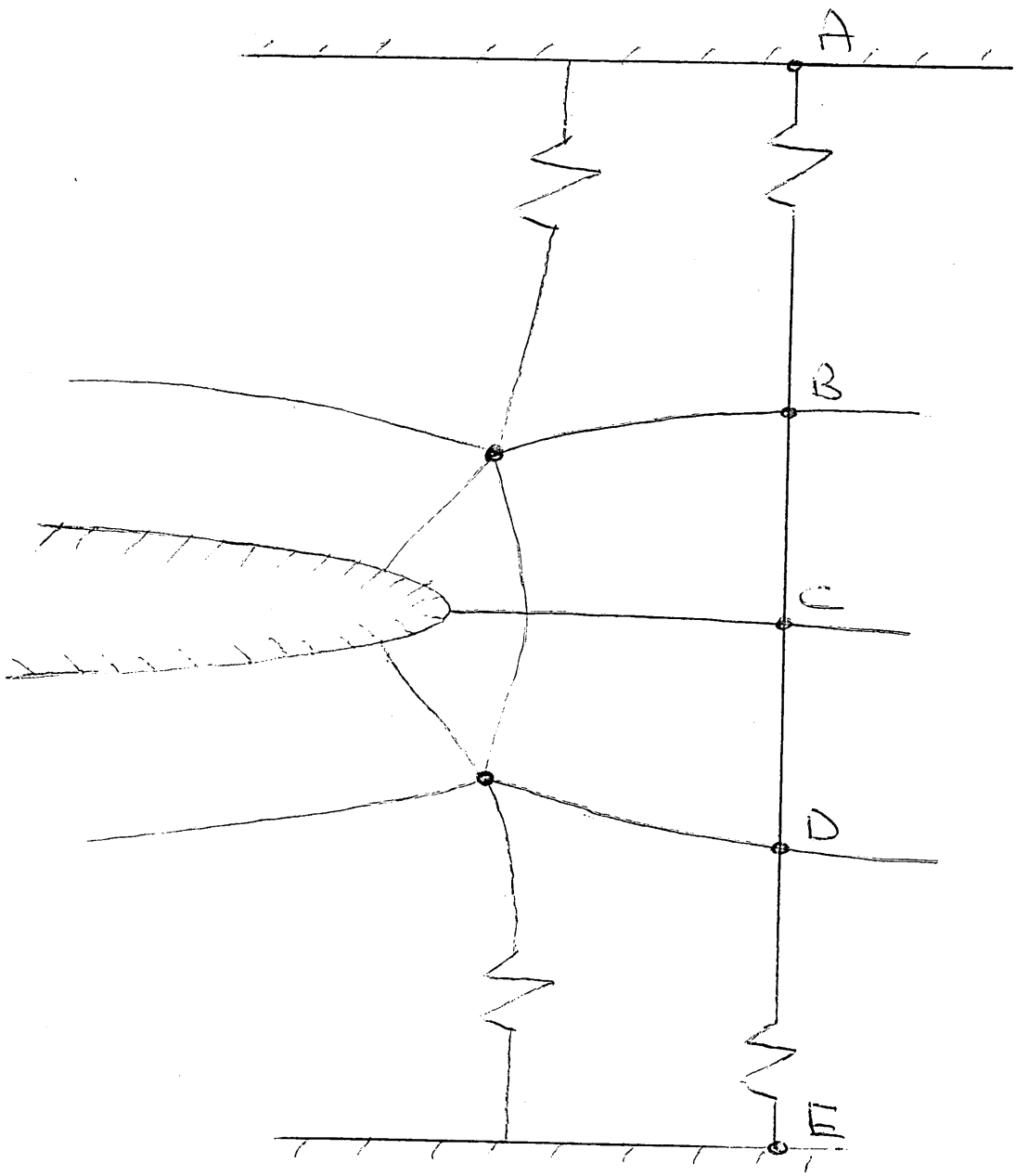

Figure: 7-23
Sketch illustrating grid edits to control C-grids.

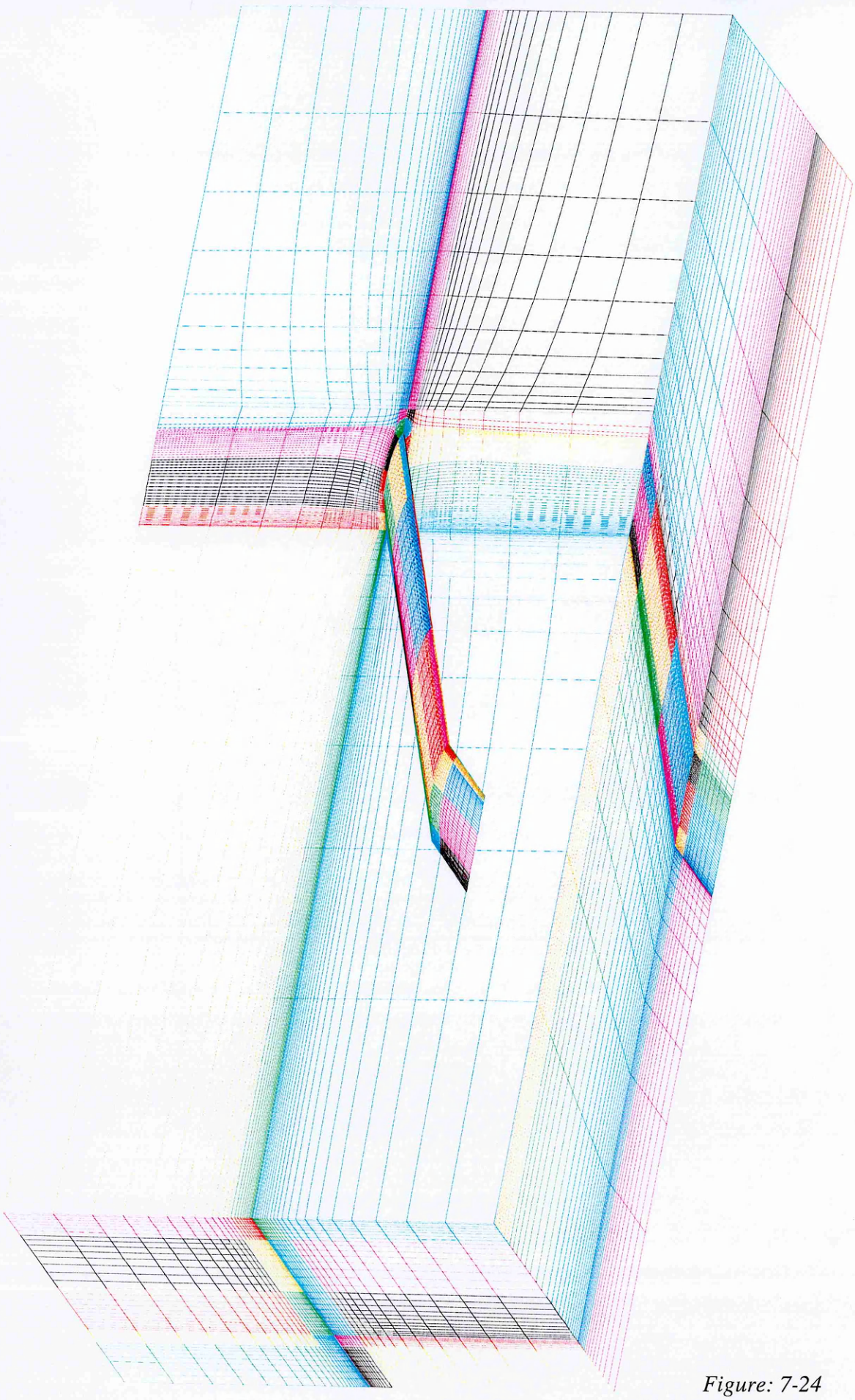

Figure: 7-24
SAUNA surface grids.

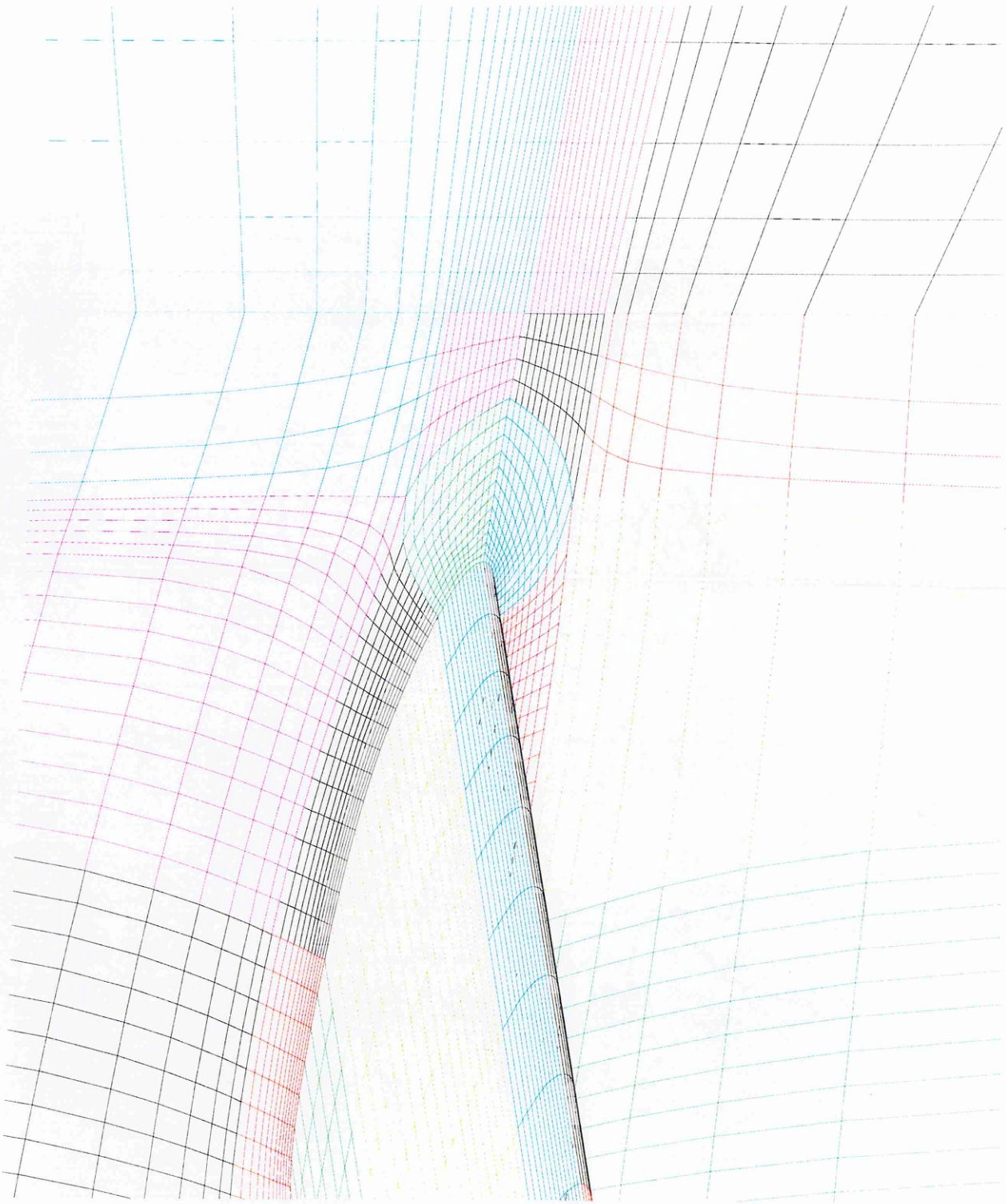

Figure: 7-25
SAUNA surface grids (close-up of figure 7-24).

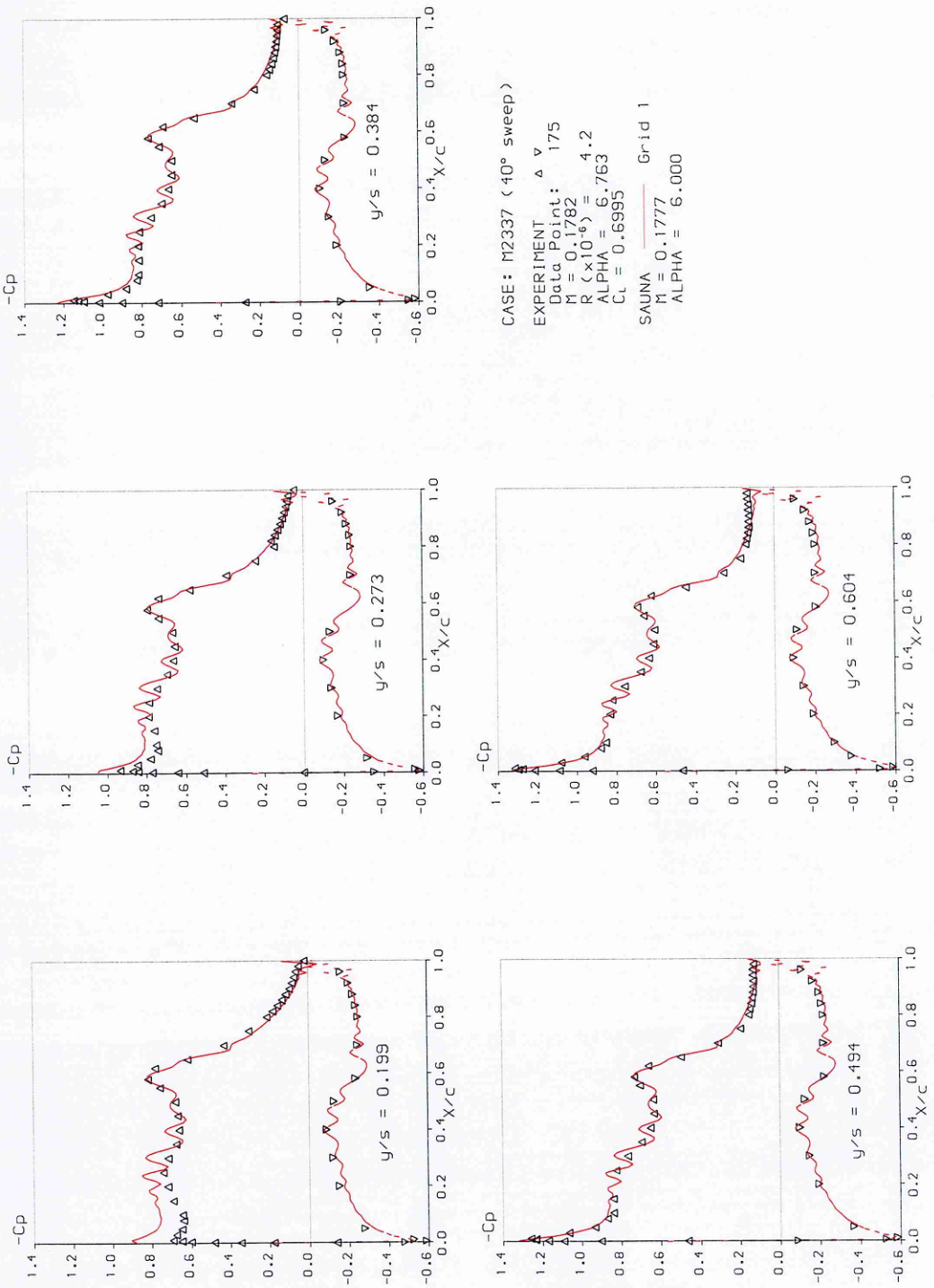

Figure: 7-26
Experimental and SAUNA pressure coefficient distributions, $\Lambda = 40°$, V = 60m/s.

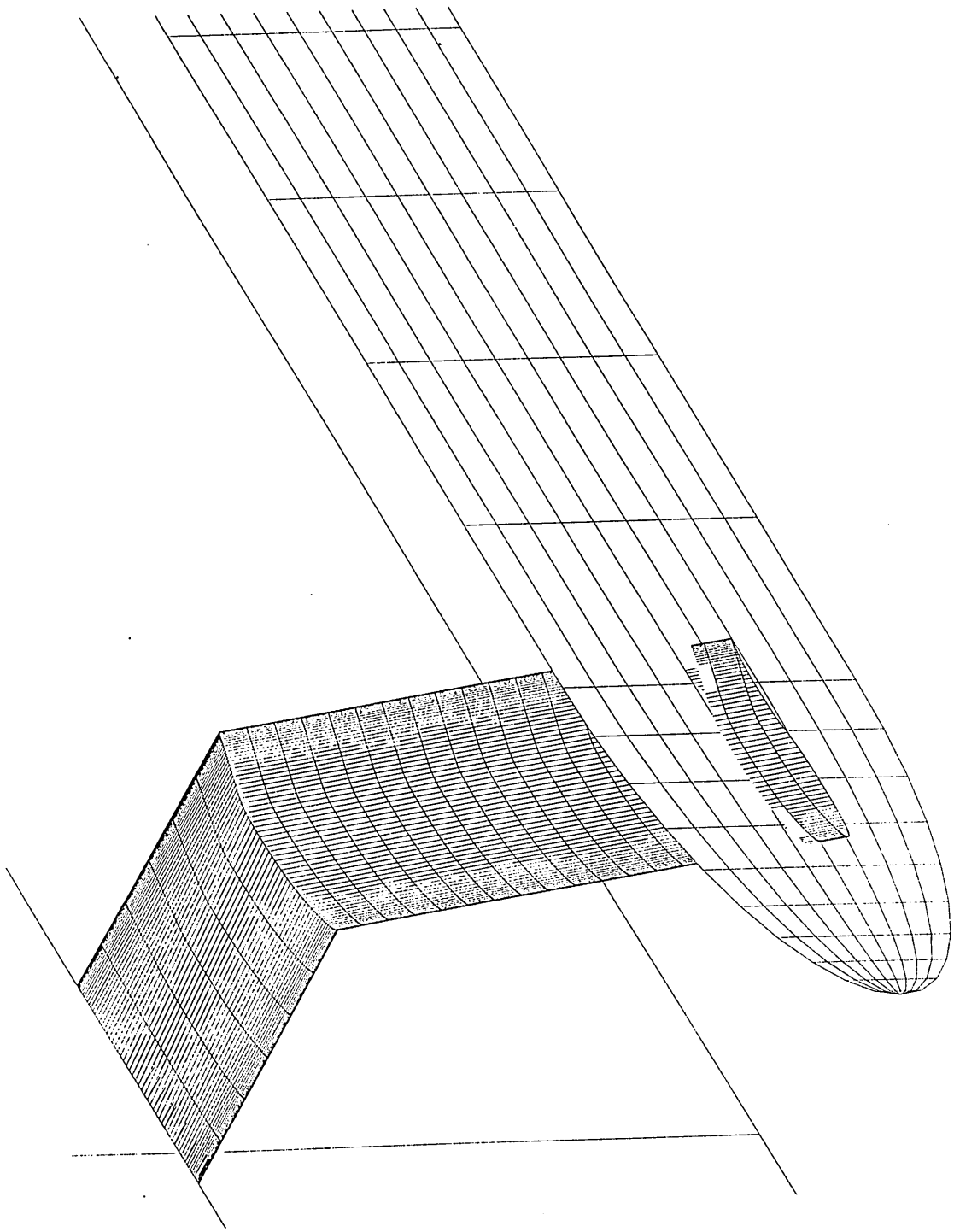

Figure: 7-27
Geometry of wing and end-plate.

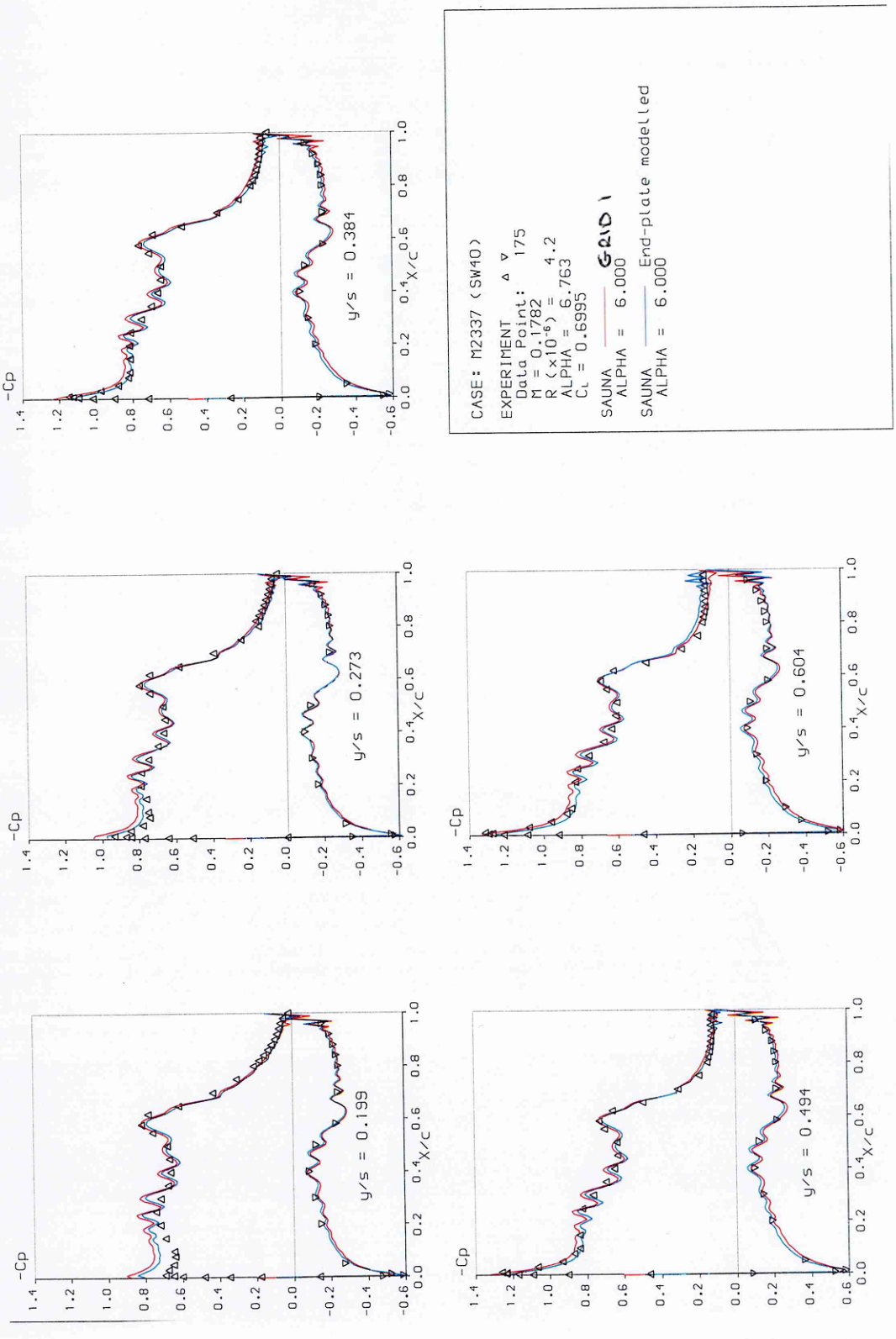

Figure: 7-28
Experimental and SAUNA pressure coefficient distributions, $\Lambda = 40°$, V = 60m/s.

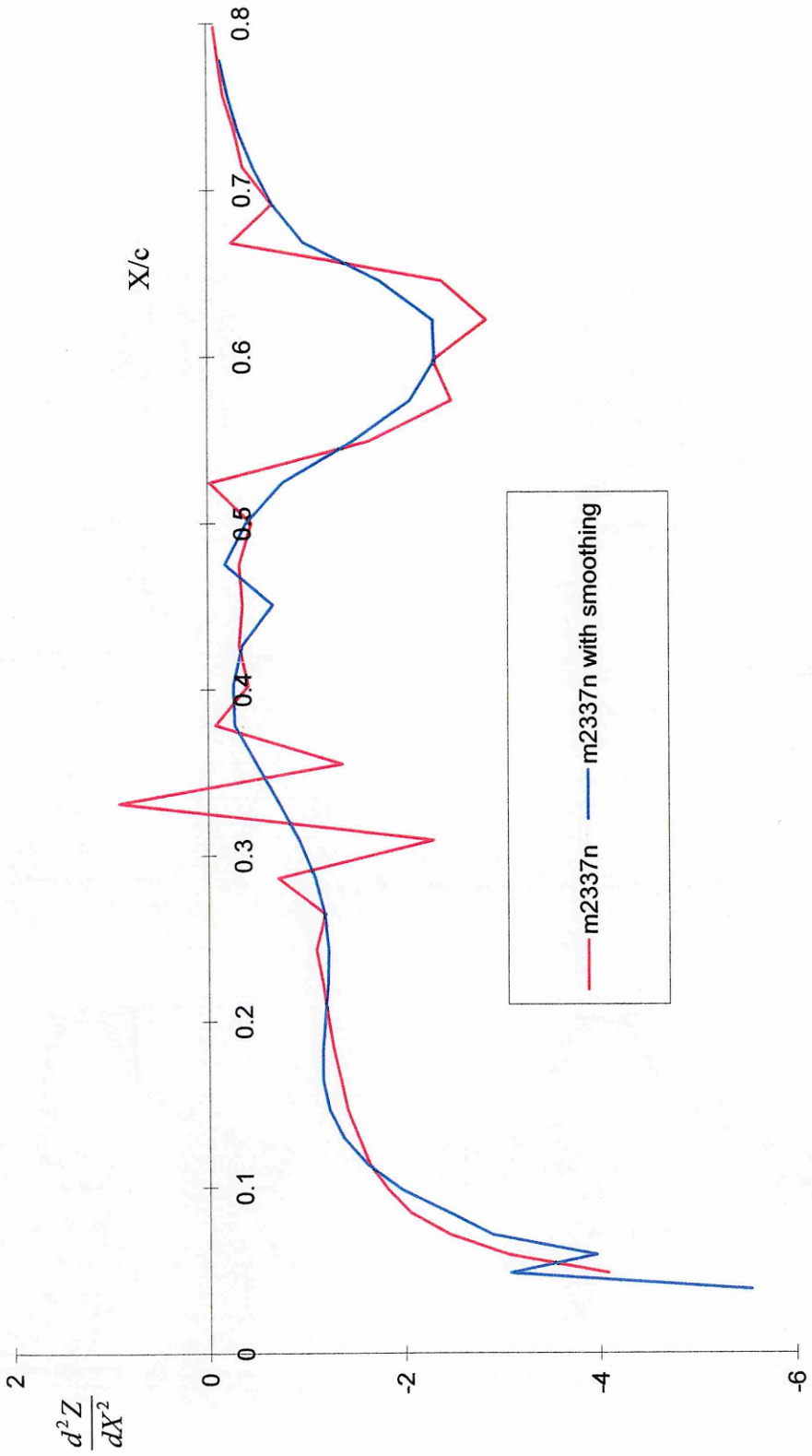

Figure: 7-29
Upper surface curvature distribution before and after smoothing.

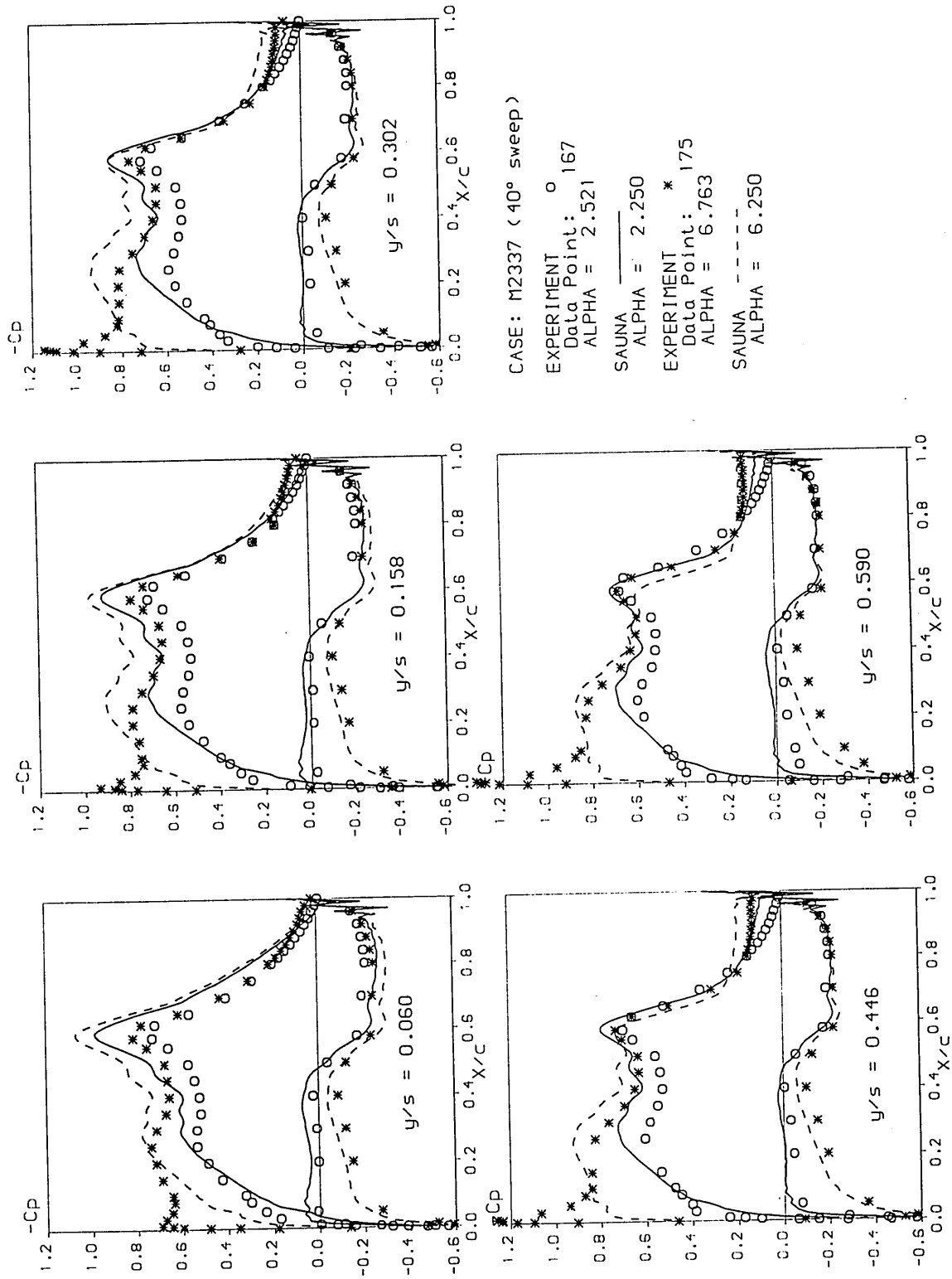

Figure: 7-30
Experimental and SAUNA pressure coefficient distributions, $\Lambda = 40°$, V = 60m/s.

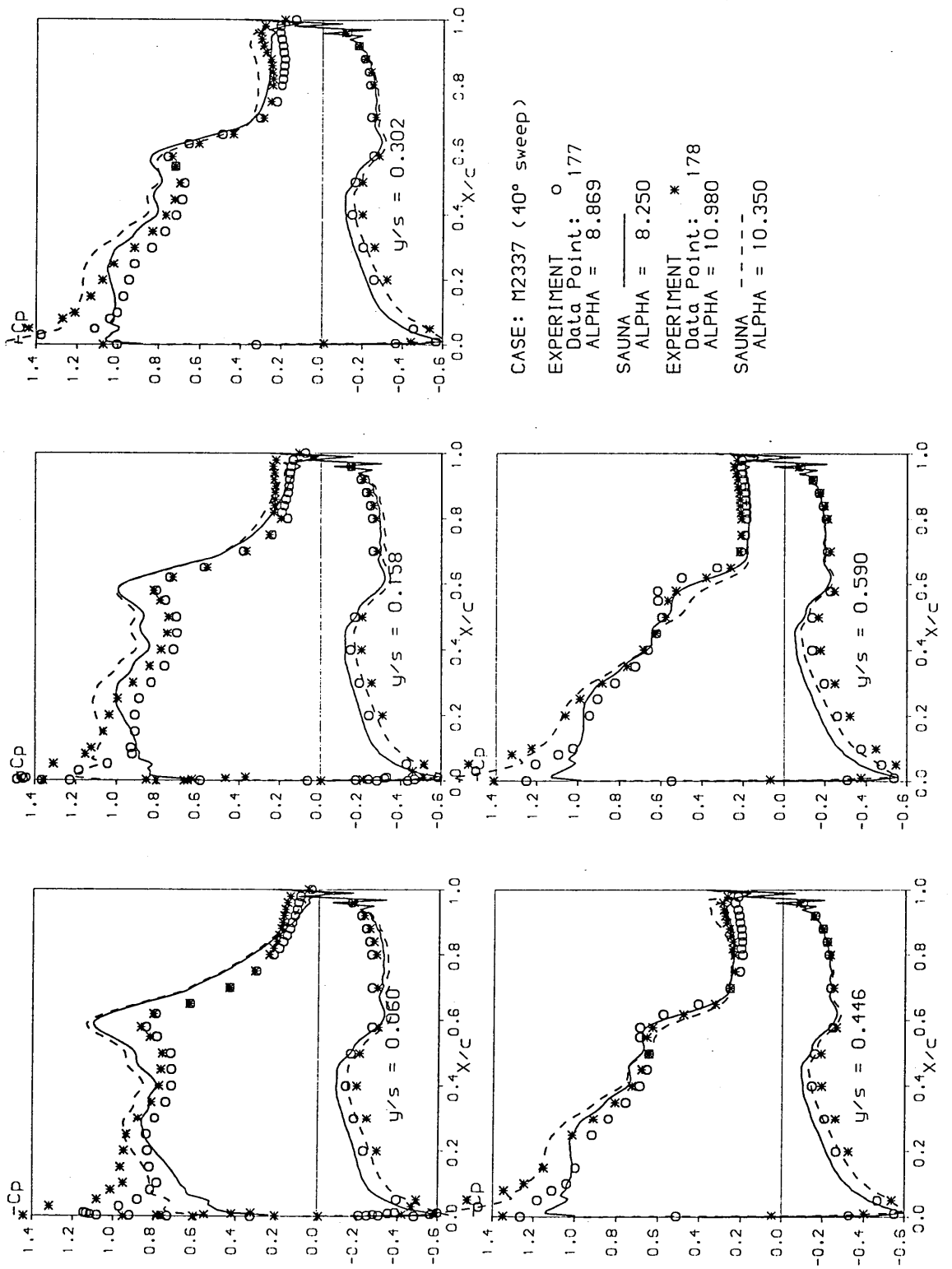

Figure: 7-31
Experimental and SAUNA pressure coefficient distributions, $\Lambda = 40°$, V = 60m/s.

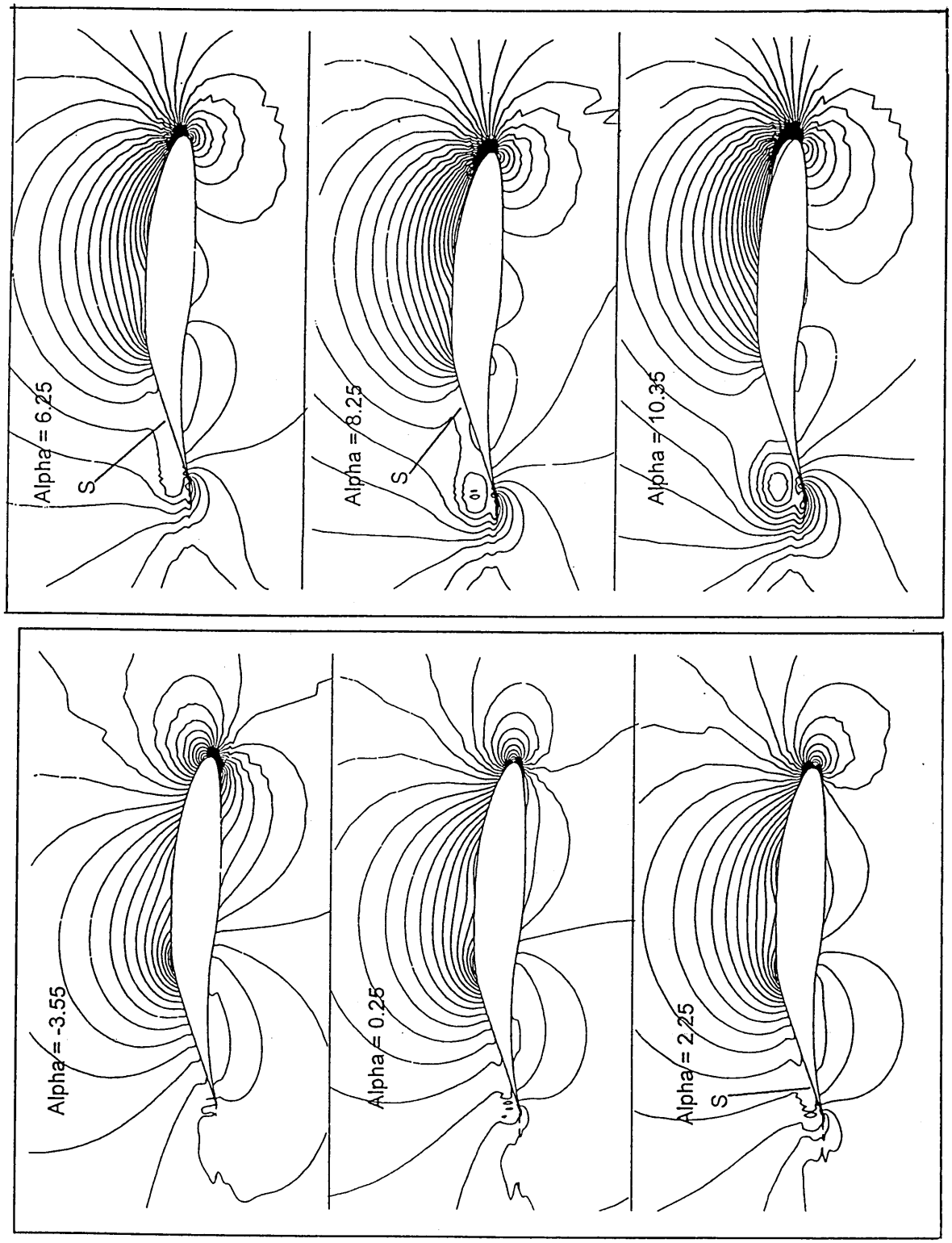

Figure: 7-32
SAUNA pressure coefficient contours ($\Delta Cp = 0.05$), $\Lambda = 40°$, $V = 60m/s$.

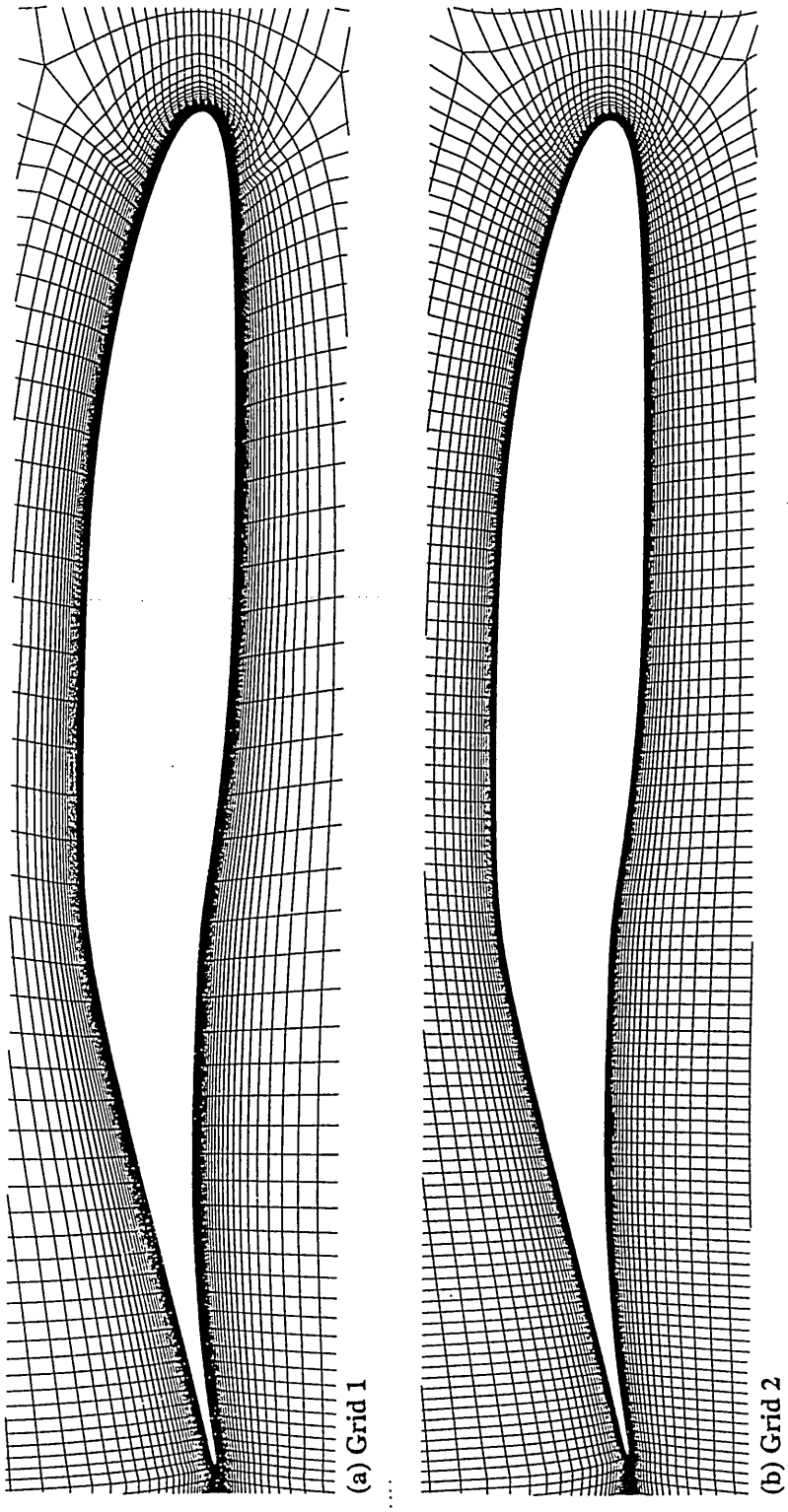

Figure: 7-33
Comparison of SAUNA surface grids.

Figure: 7-34
Experimental and SAUNA pressure coefficient distributions, $\Lambda = 40°$, V = 60m/s.

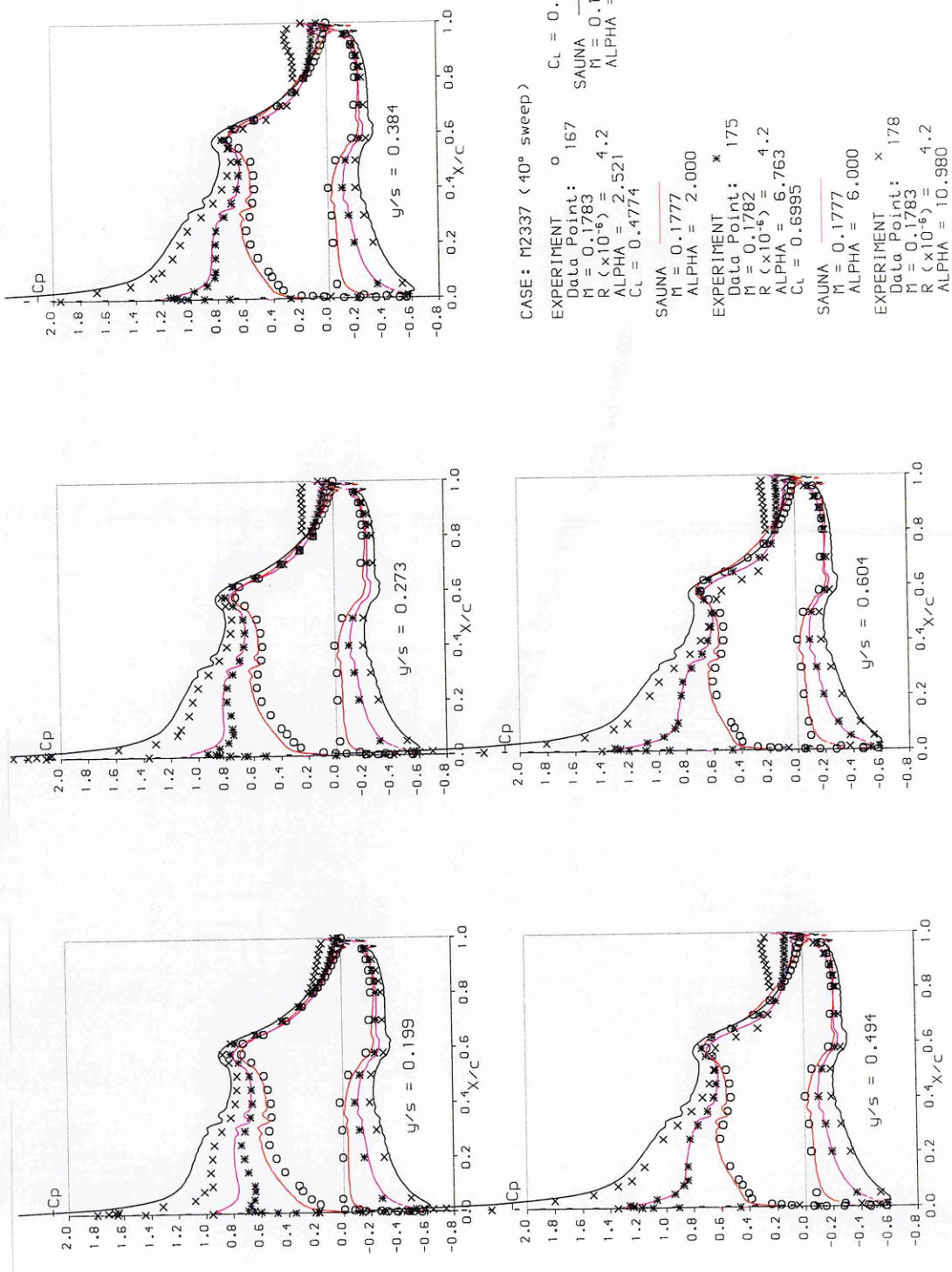

Figure: 7-35
Experimental and SAUNA pressure coefficient distributions, $\Lambda = 40°$, $V = 60m/s$.

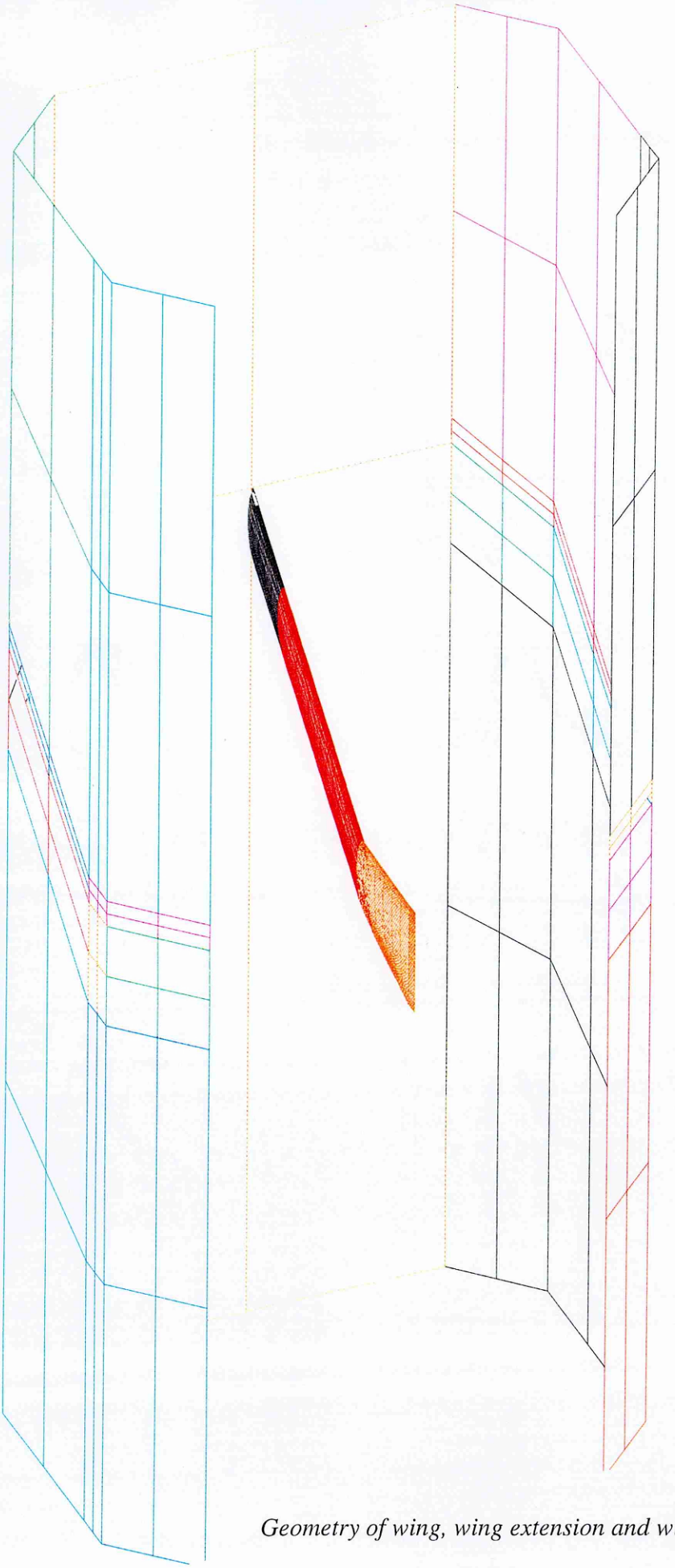

Figure: 7-36
Geometry of wing, wing extension and wind tunnel walls.

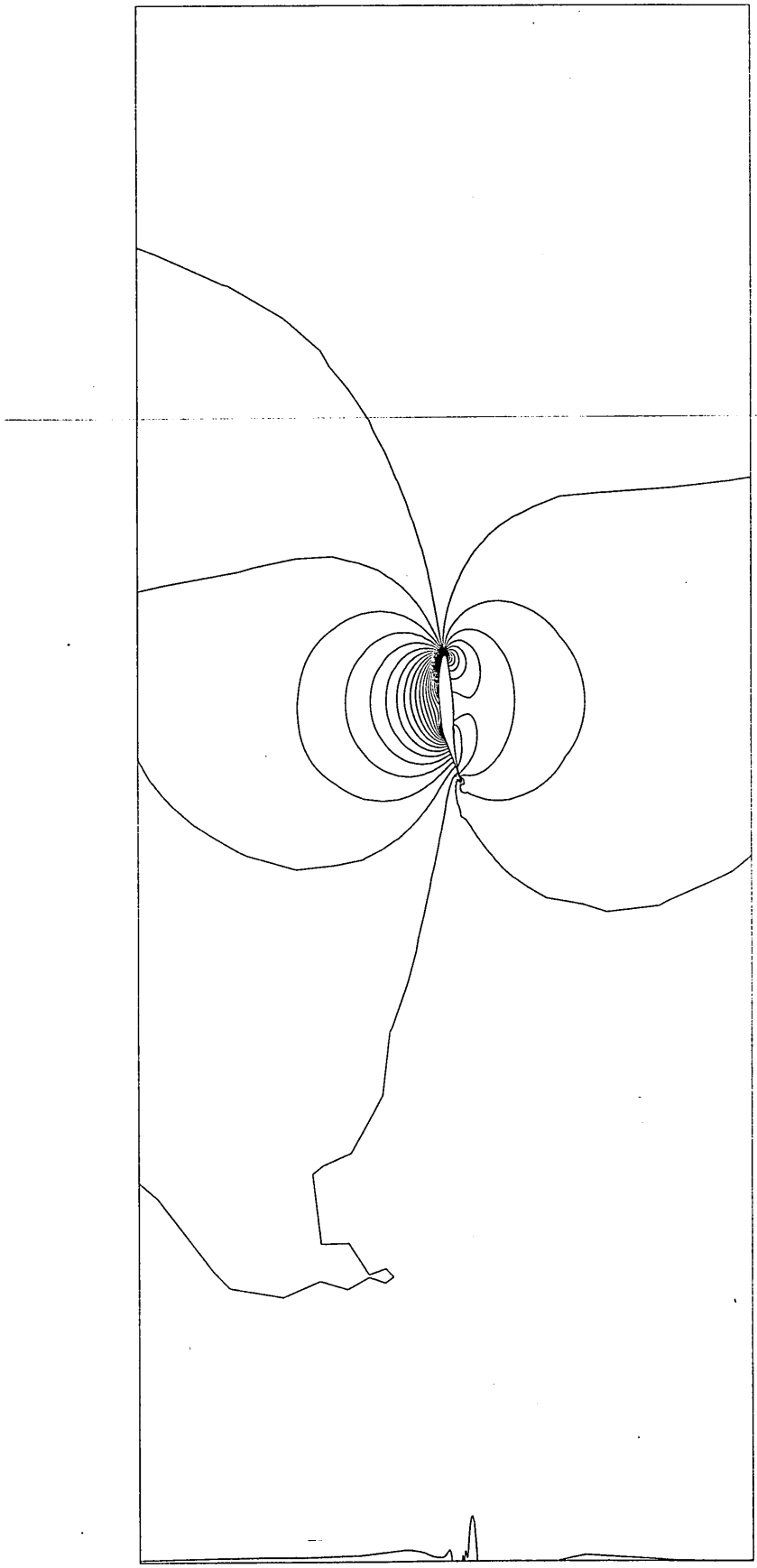

Figure: 7-37
Predicted pressure coefficient contours on a cut through the wind tunnel centre line.

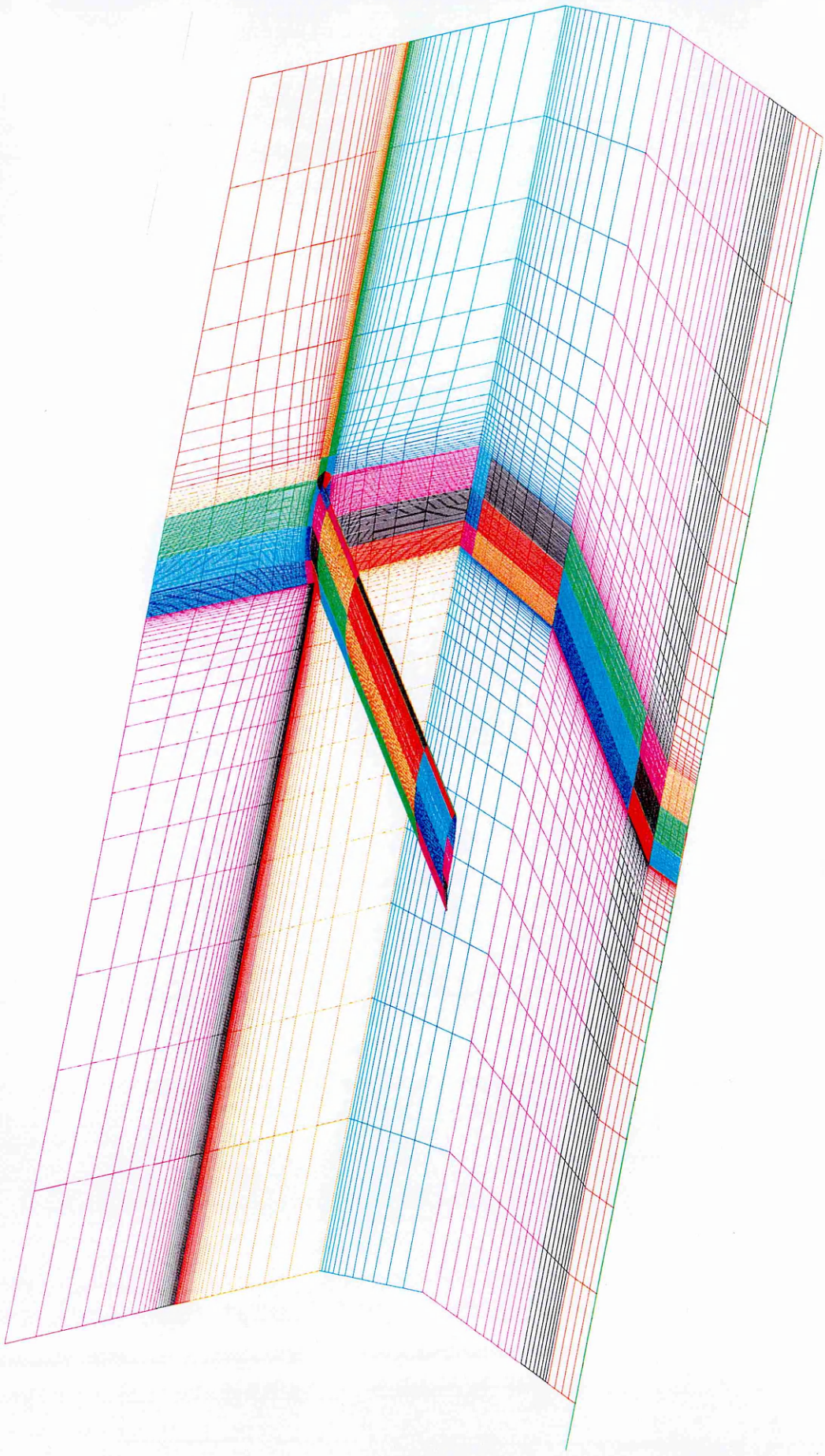

Figure: 7-38
SAUNA surface grids on wing, wing extension and wind tunnel walls.

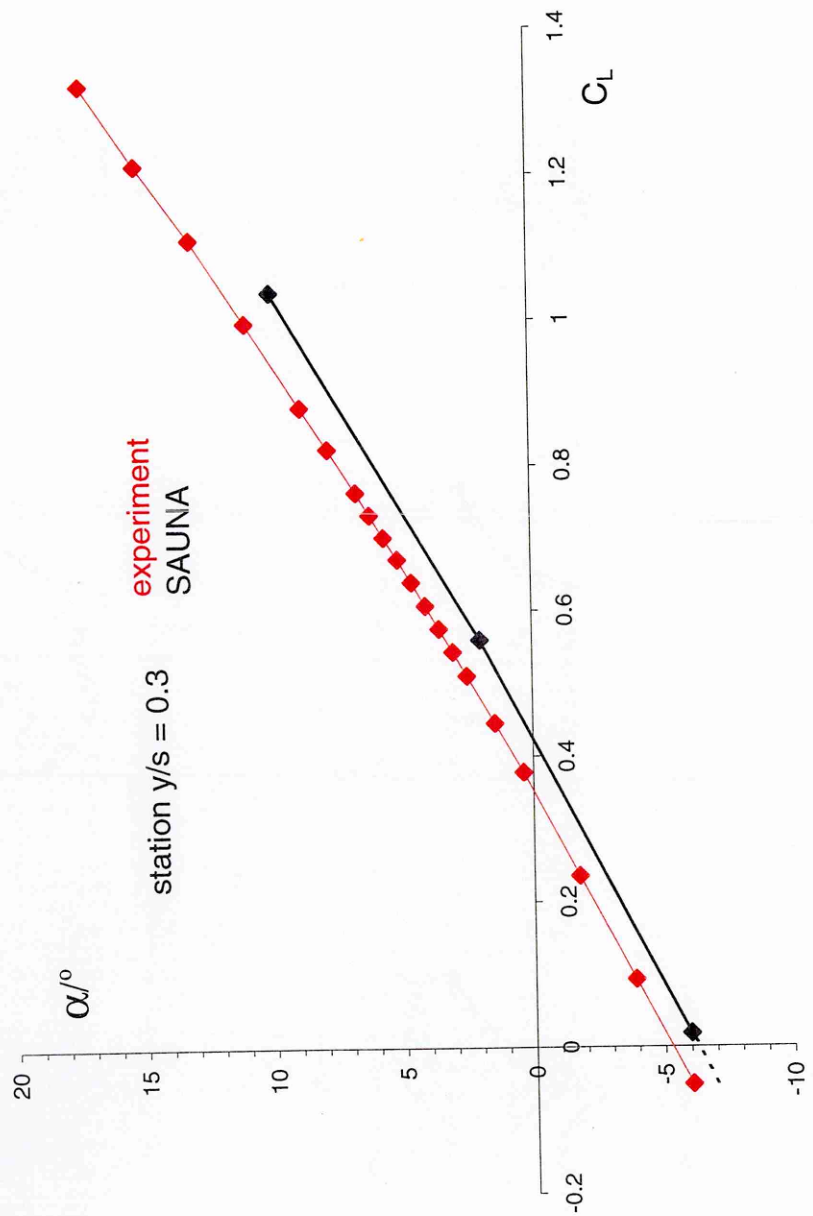

Figure: 7-39
Variation of experimental and SAUNA local lift coefficient with angle of incidence.

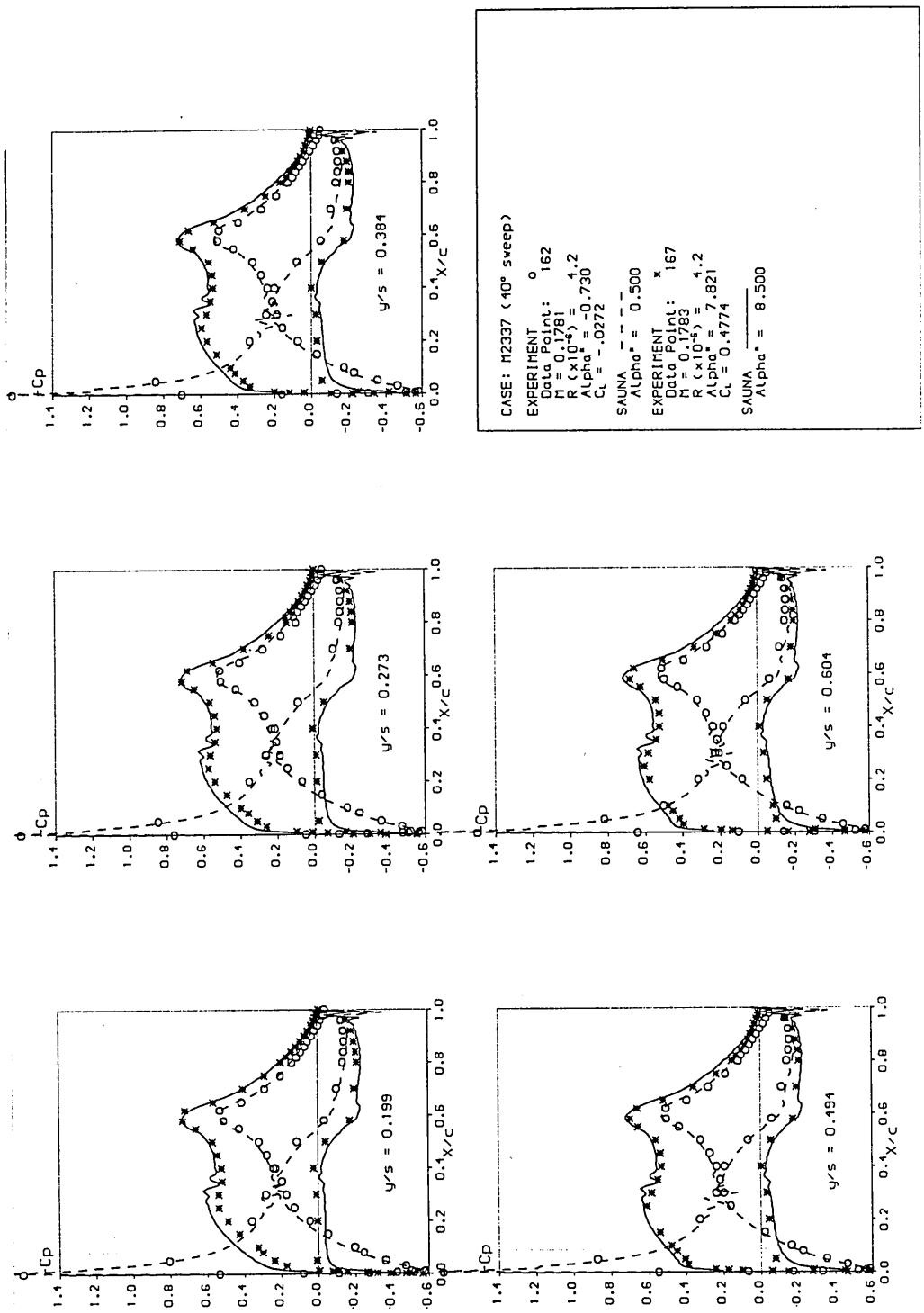

Figure: 7-40
Experimental and SAUNA pressure coefficient distributions, $\Lambda = 40°$, V = 60m/s.

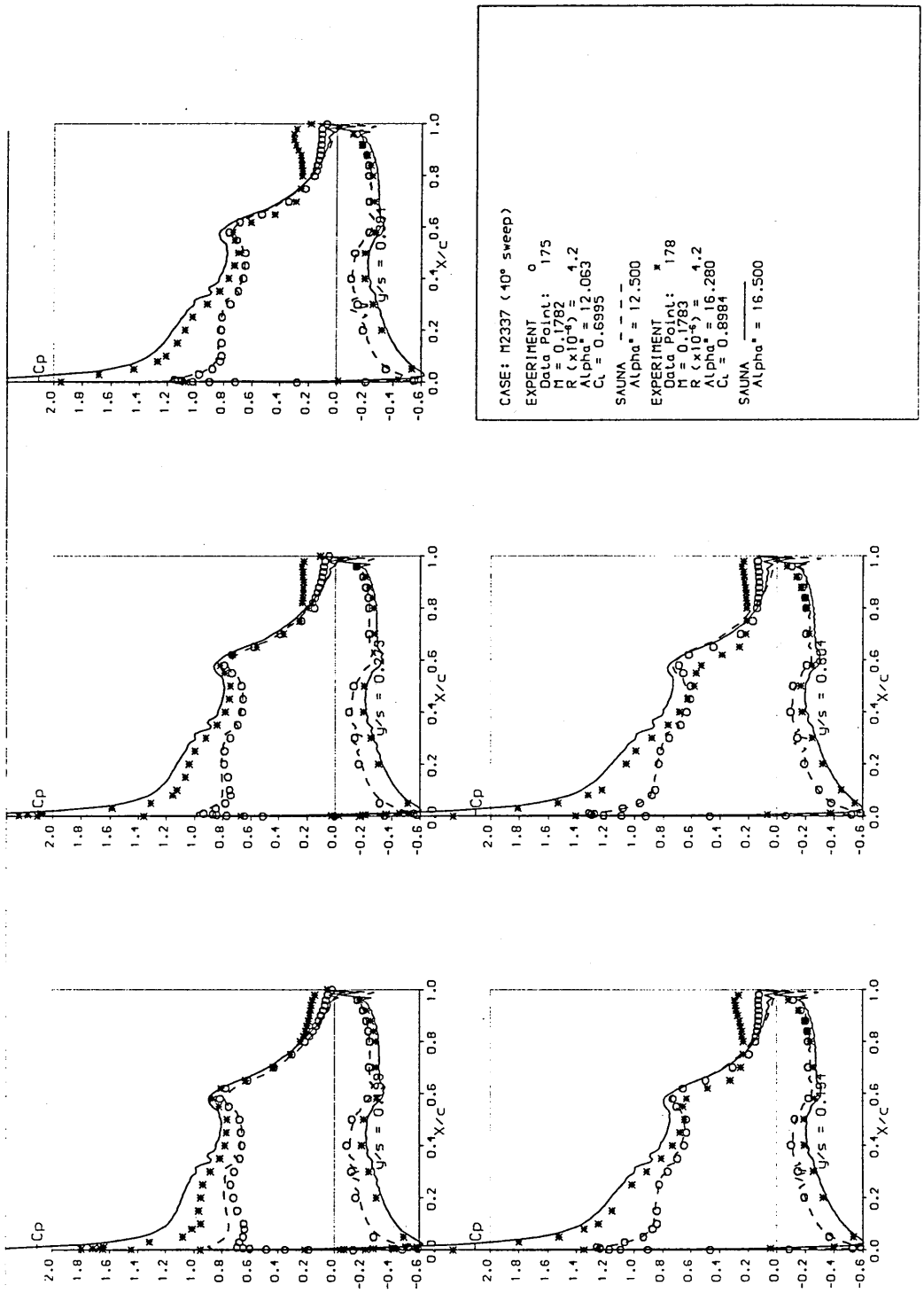

Figure: 7-41

Experimental and SAUNA pressure coefficient distributions, $\Lambda = 40°$, V = 60m/s.

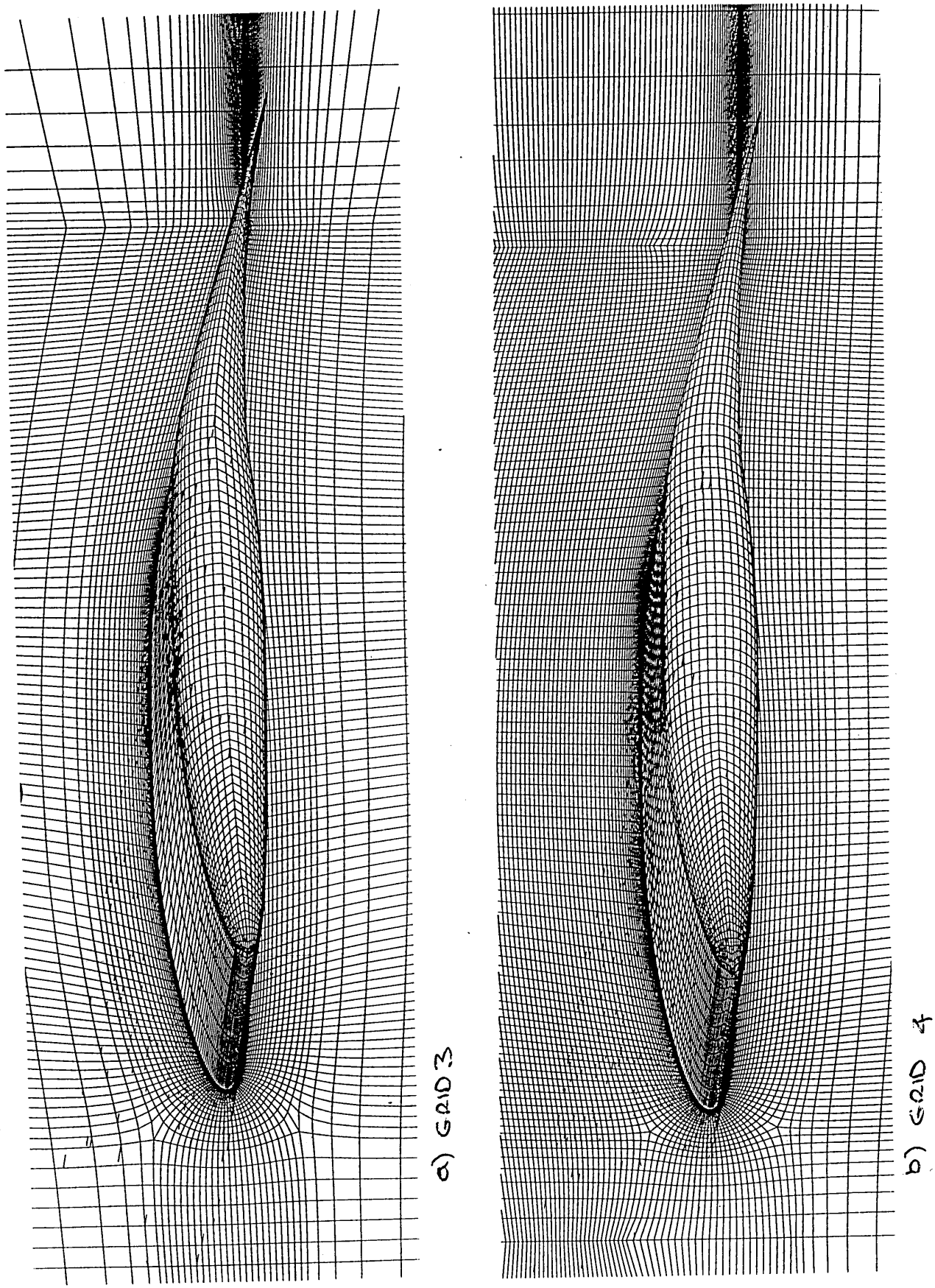

Figure: 7-42
Comparison of SAUNA surface grids.

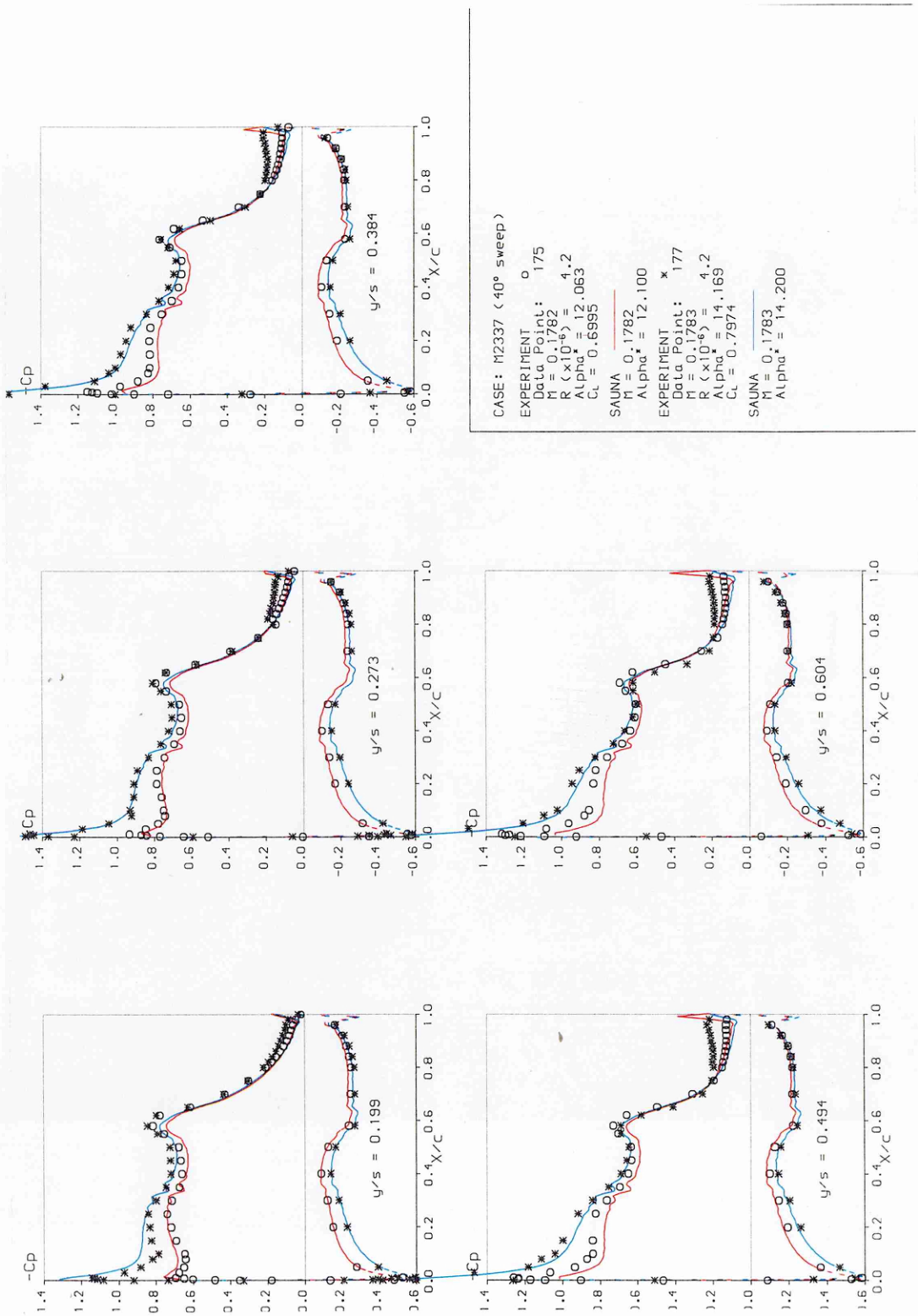

Figure: 7-43
Experimental and SAUNA pressure coefficient distributions, $\Lambda = 40°$, V = 60m/s.

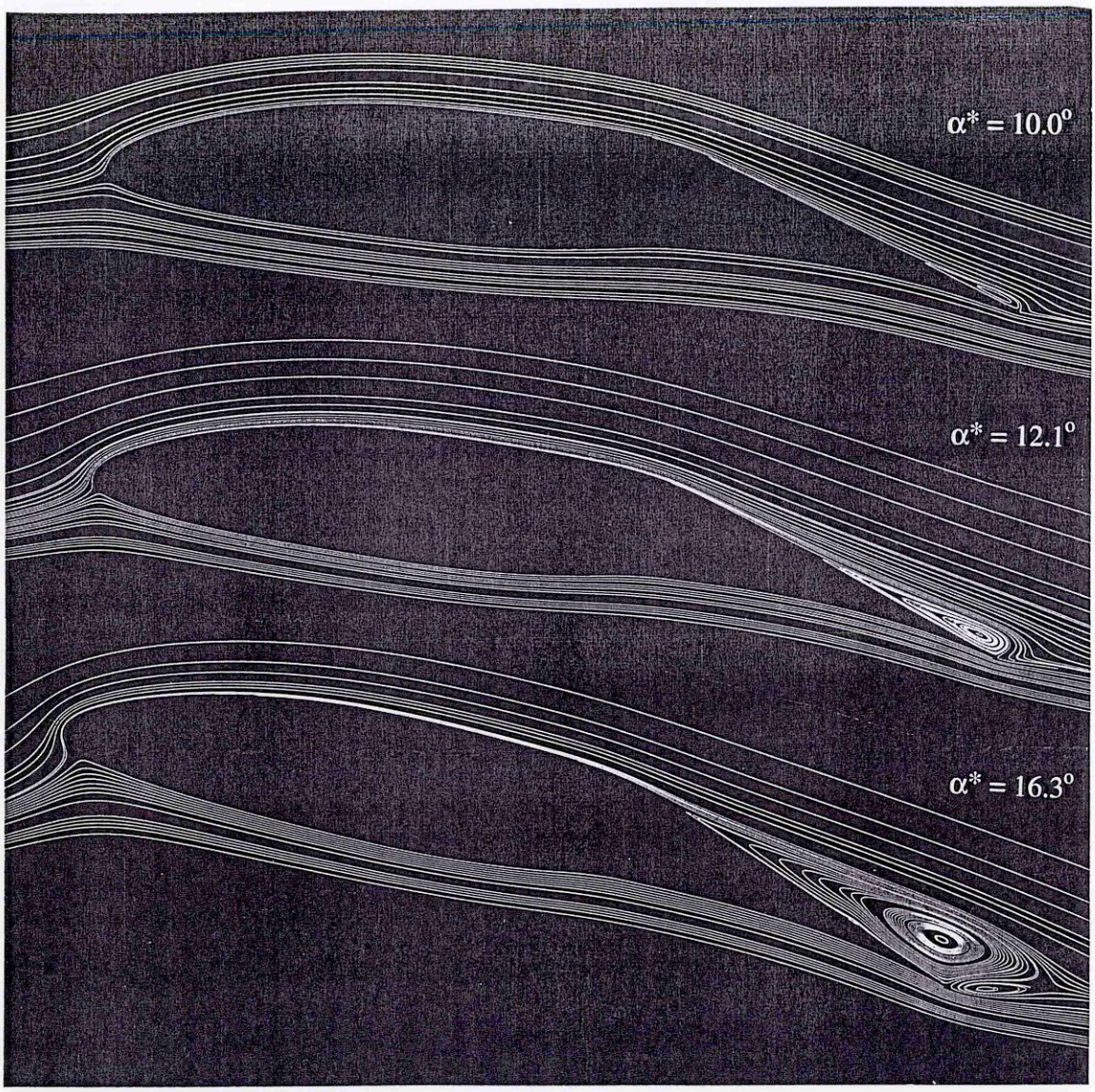

Figure: 7-44
SAUNA streamlines on a cutting plane normal to sweep ($y/s \approx 0.5$), $\Lambda = 40°$, $V = 60m/s$.

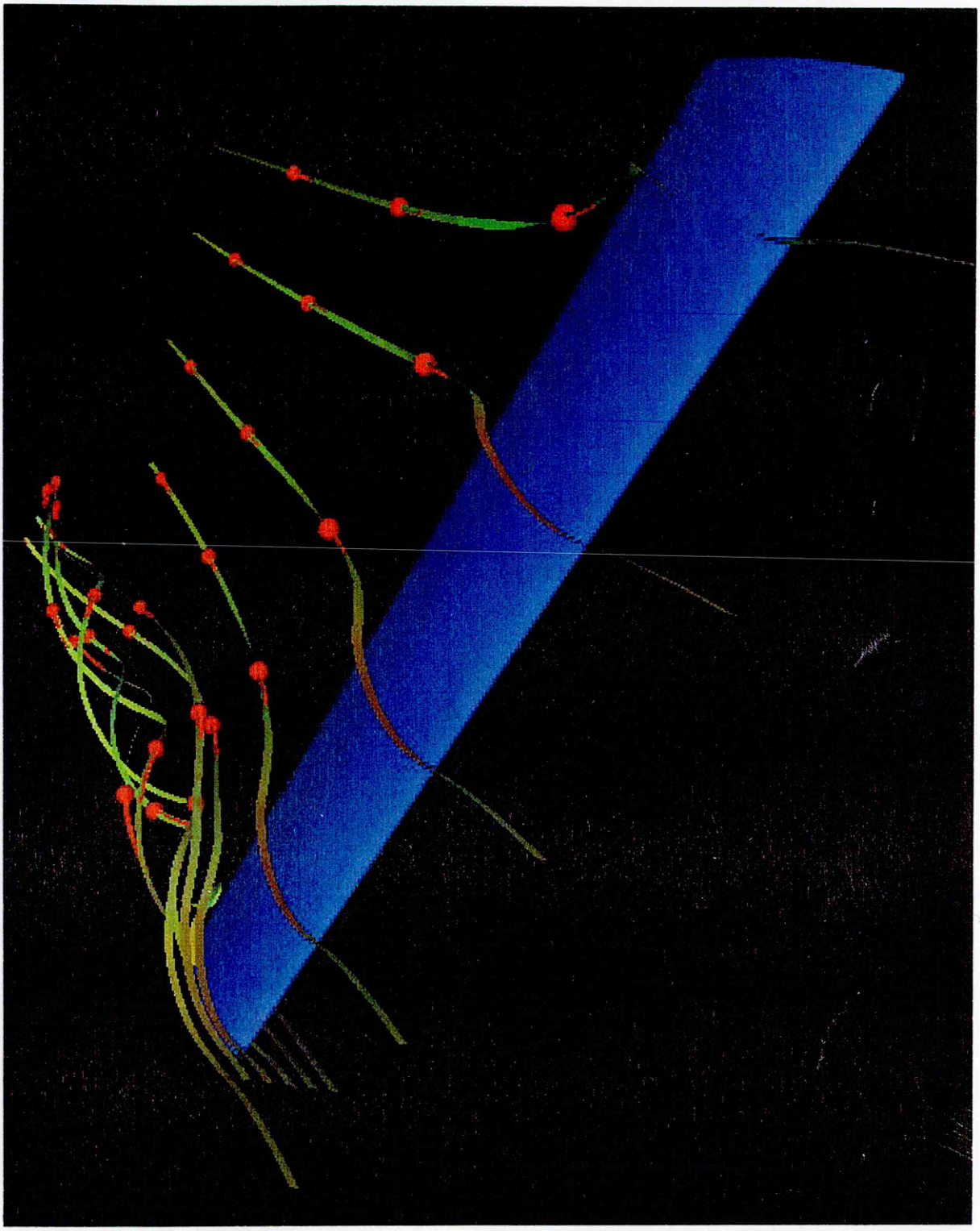

Figure: 7-45
SAUNA stream ribbons, $\Lambda = 40°$, V = 60m/s, $\alpha^* = 12.1°$.

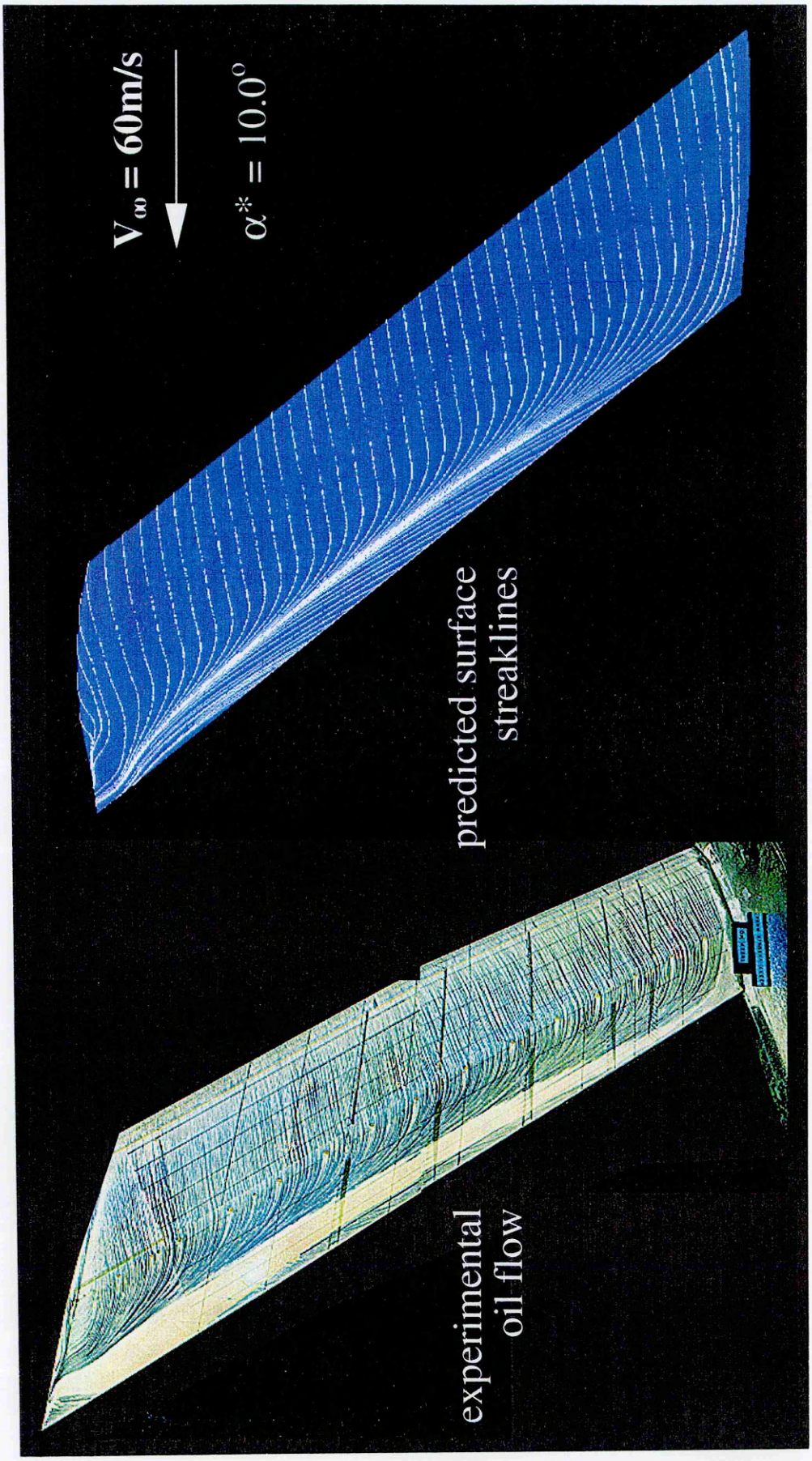

Figure: 7-46
Comparison of experimental and SAUNA surface streaklines, Λ = 40°, V = 60m/s, α^* = 10.1°.

Figure: 7-47
Comparison of experimental and SAUNA surface streaklines, Λ = 40°, V = 60m/s, α^* = 12.1°.

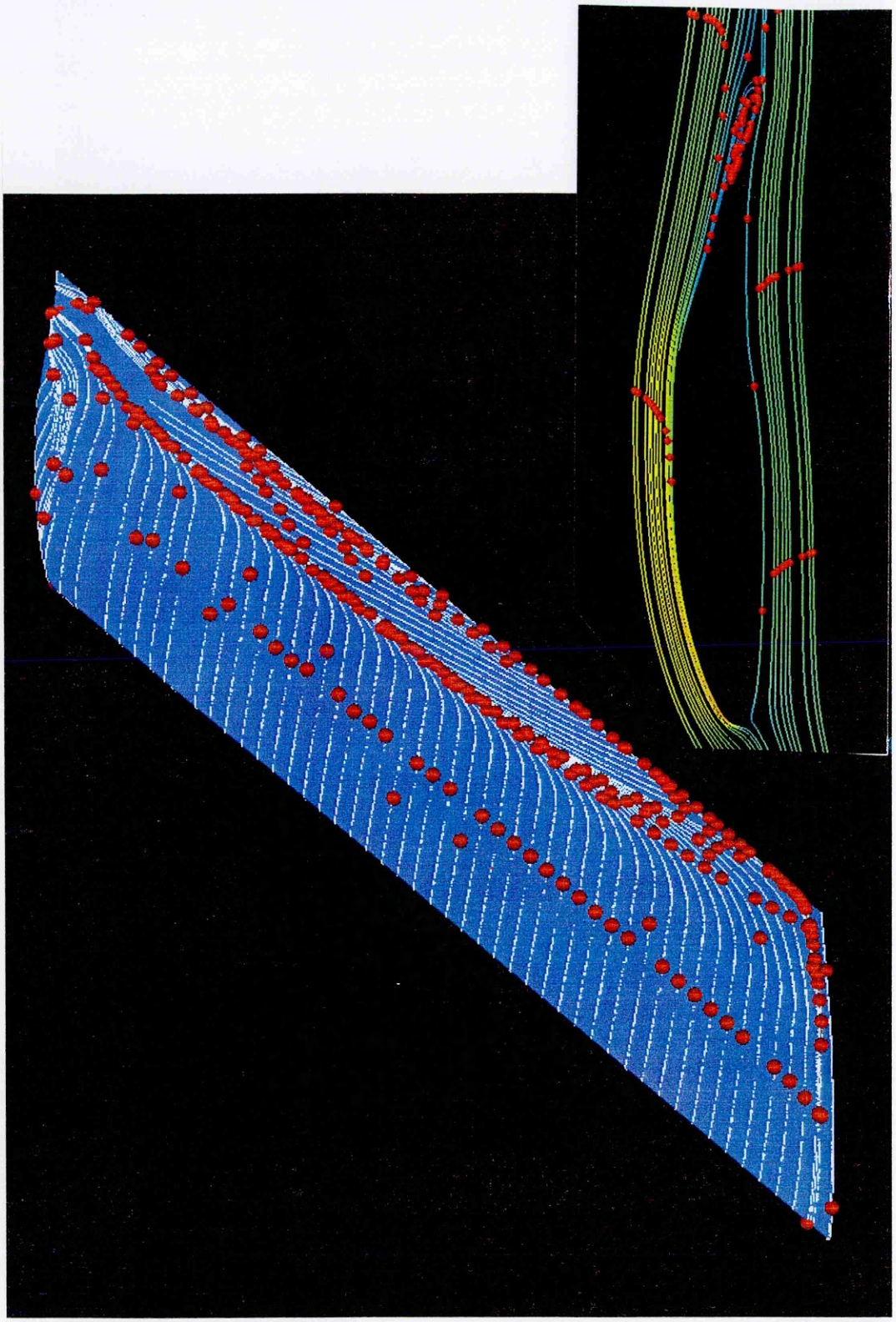

Figure: 7-48
Illustration of predicted streamline animations, $\Lambda = 40°$, V = 60m/s, $\alpha^* = 12.1°$.

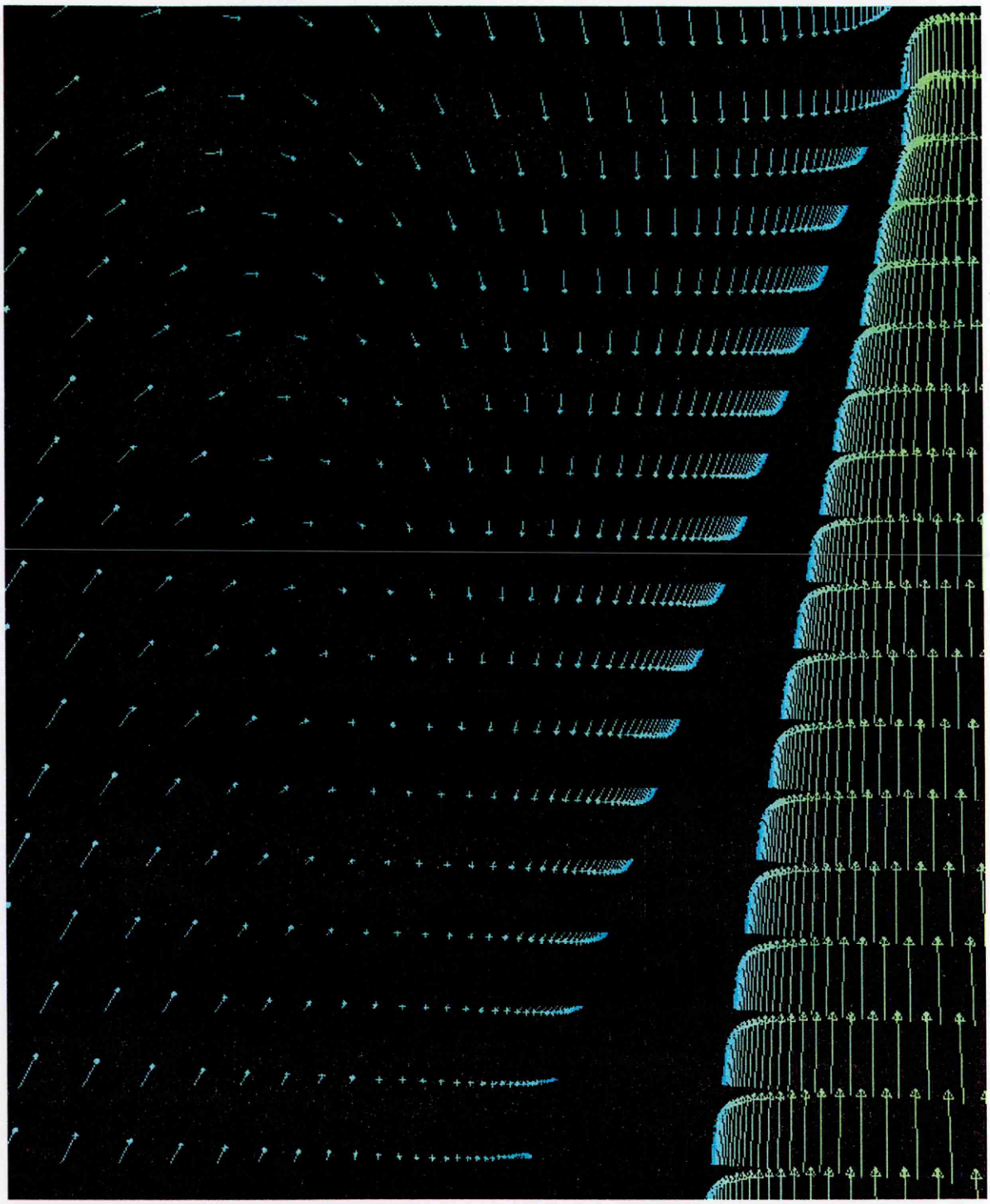

Figure: 7-49
Illustration of predicted vector arrows near the wing trailing edge, $\Lambda = 40°$, V = 60m/s, $\alpha^* = 12.1°$.

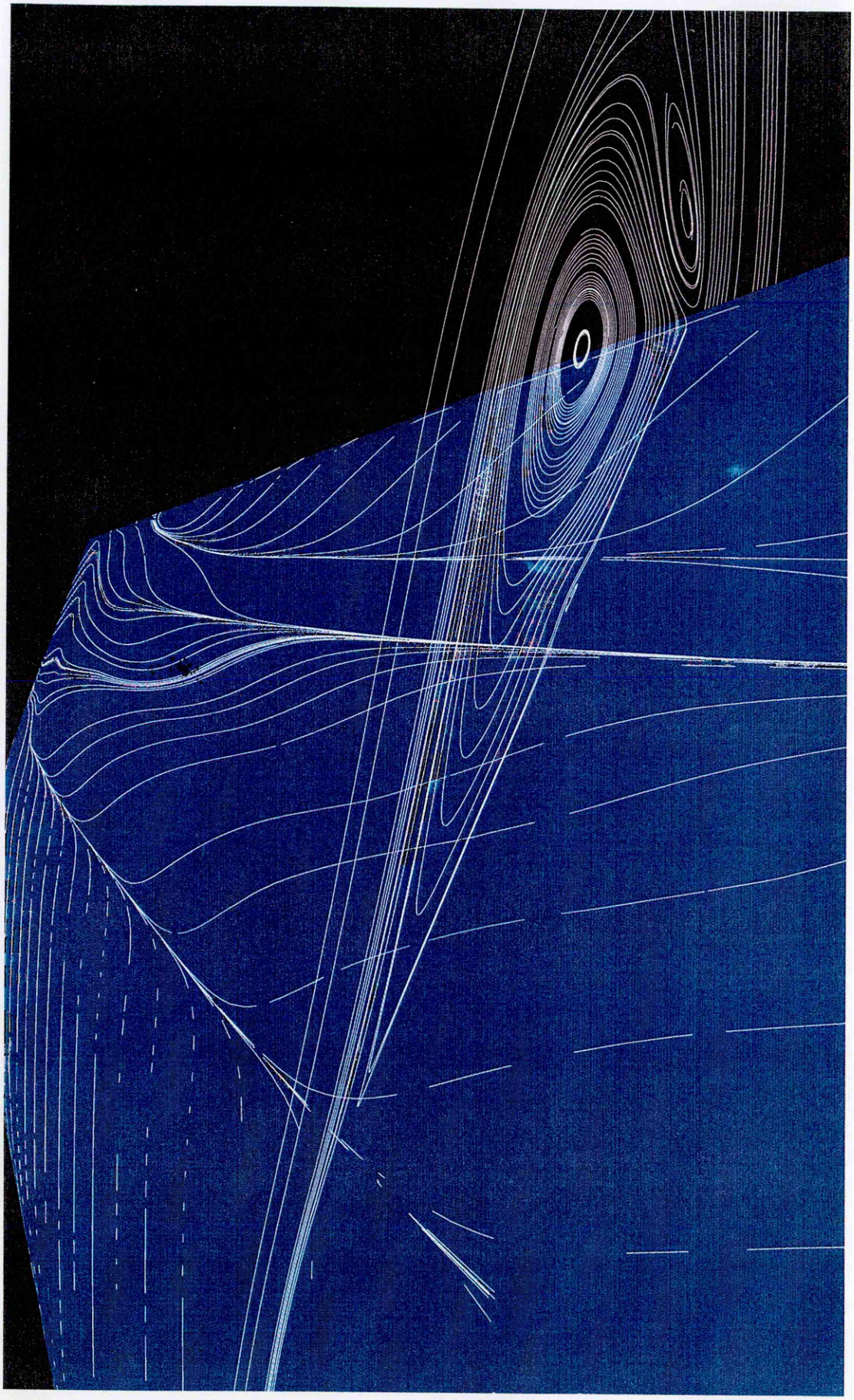

Figure: 7-50
Prediced streamlines on the outer wing upper surface and a cutting plane normal to sweep, $\Lambda = 40°$, V = 60m/s, $\alpha^* = 16.3°$.

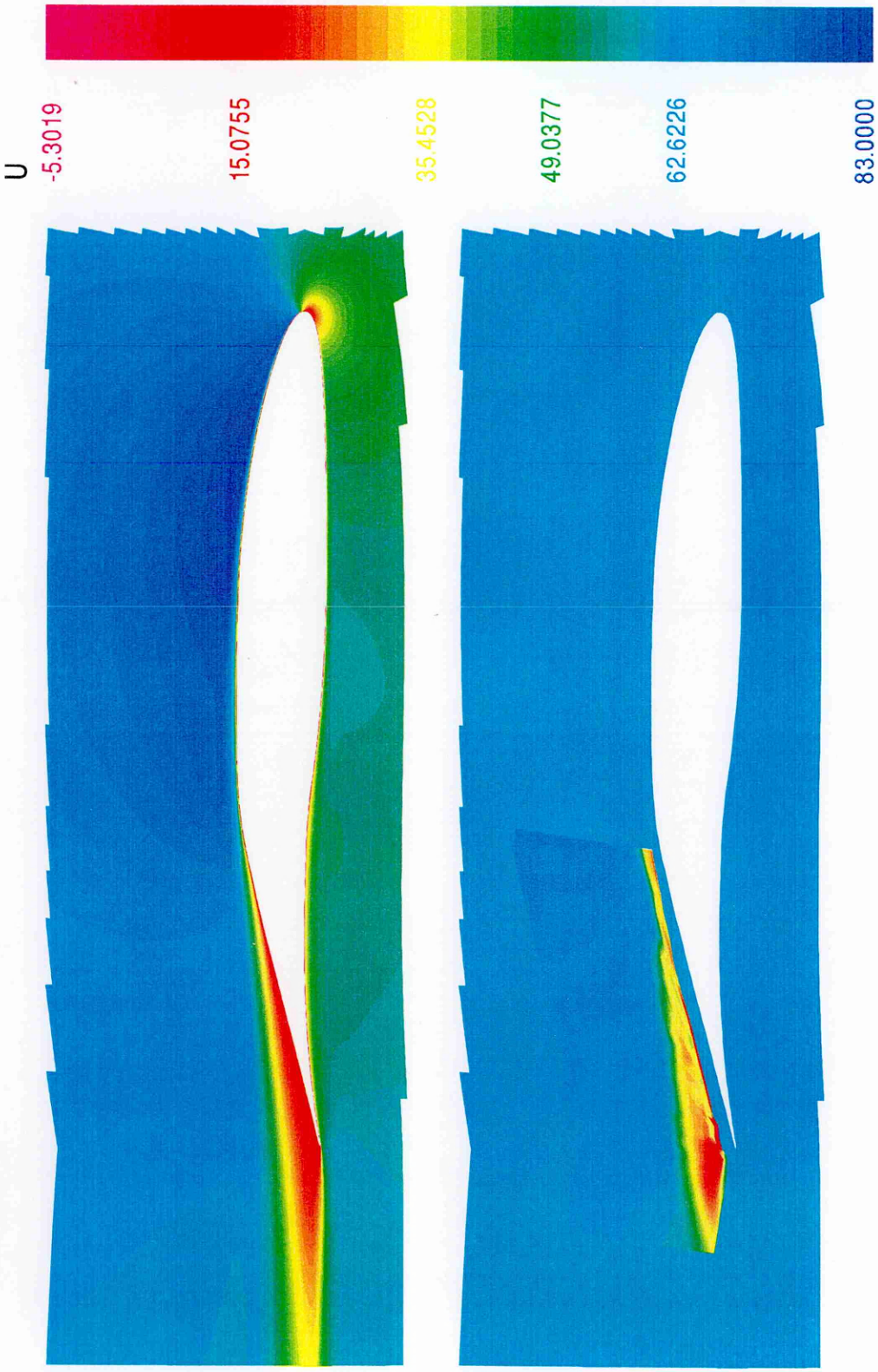

Figure: 7-51
Predicted (top) and measured (bottom) colour shaded contours of u-velocity component (m/s) on a streamwise plane, $\Lambda = 40°$, V = 60m/s, $\alpha^* = 14.2°$.

Figure: 7-52
Predicted (top) and measured (bottom) colour shaded contours of v-velocity component (m/s) on a streamwise plane, $\Lambda = 40°$, V = 60m/s, $\alpha^* = 14.2°$.

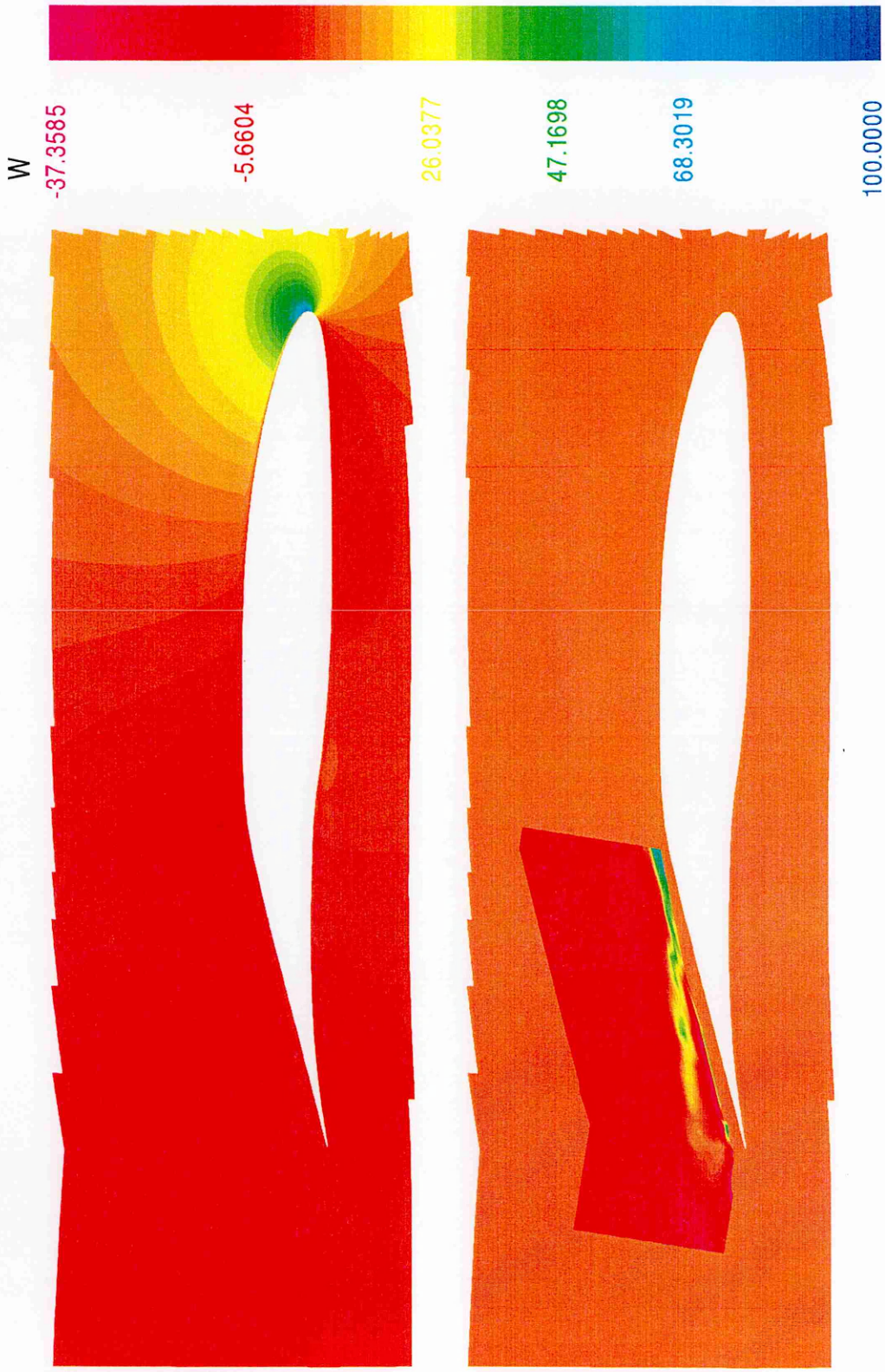

Figure: 7-53
Predicted (top) and measured (bottom) colour shaded contours of w-velocity component (m/s) on a streamwise plane, $\Lambda = 40°$, V = 60m/s, $\alpha^* = 14.2°$.

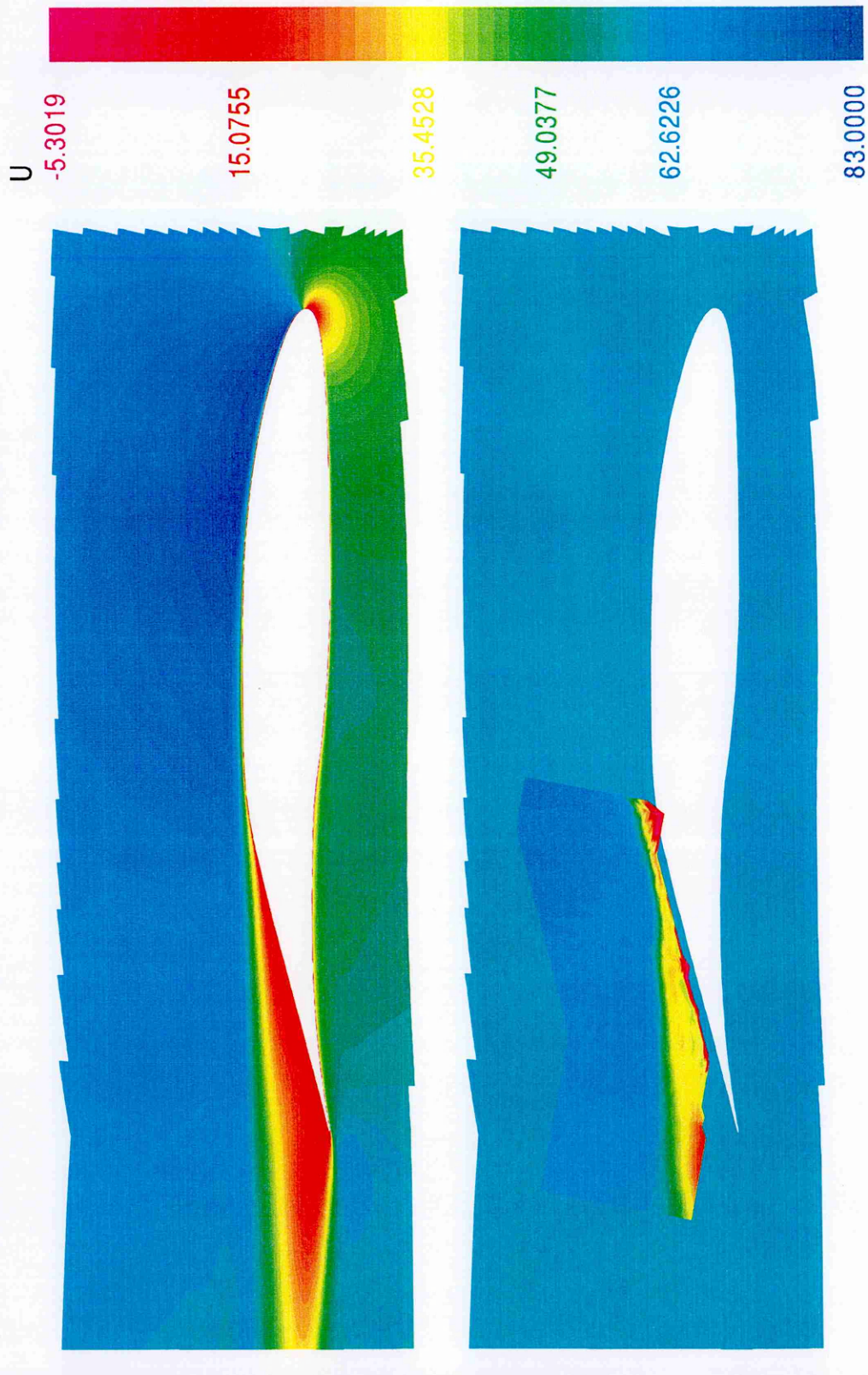

Figure: 7-54
Predicted (top) and measured (bottom) colour shaded contours of u-velocity component (m/s) on a streamwise plane, $\Lambda = 40°$, V = 60m/s, $\alpha^* = 16.3°$.

Figure: 7-55
Predicted (top) and measured (bottom) colour shaded contours of v-velocity component (m/s) on a streamwise plane, $\Lambda = 40°$, $V = 60$m/s, $\alpha^* = 16.3°$.

Figure: 7-56
Predicted (top) and measured (bottom) colour shaded contours of w-velocity component (m/s) on a streamwise plane, $\Lambda = 40°$, V = 60m/s, $\alpha^* = 16.3°$.

Figure: 7-57
Experimental and SAUNA pressure coefficient distributions, $\Lambda = 40°$, V = 60m/s.

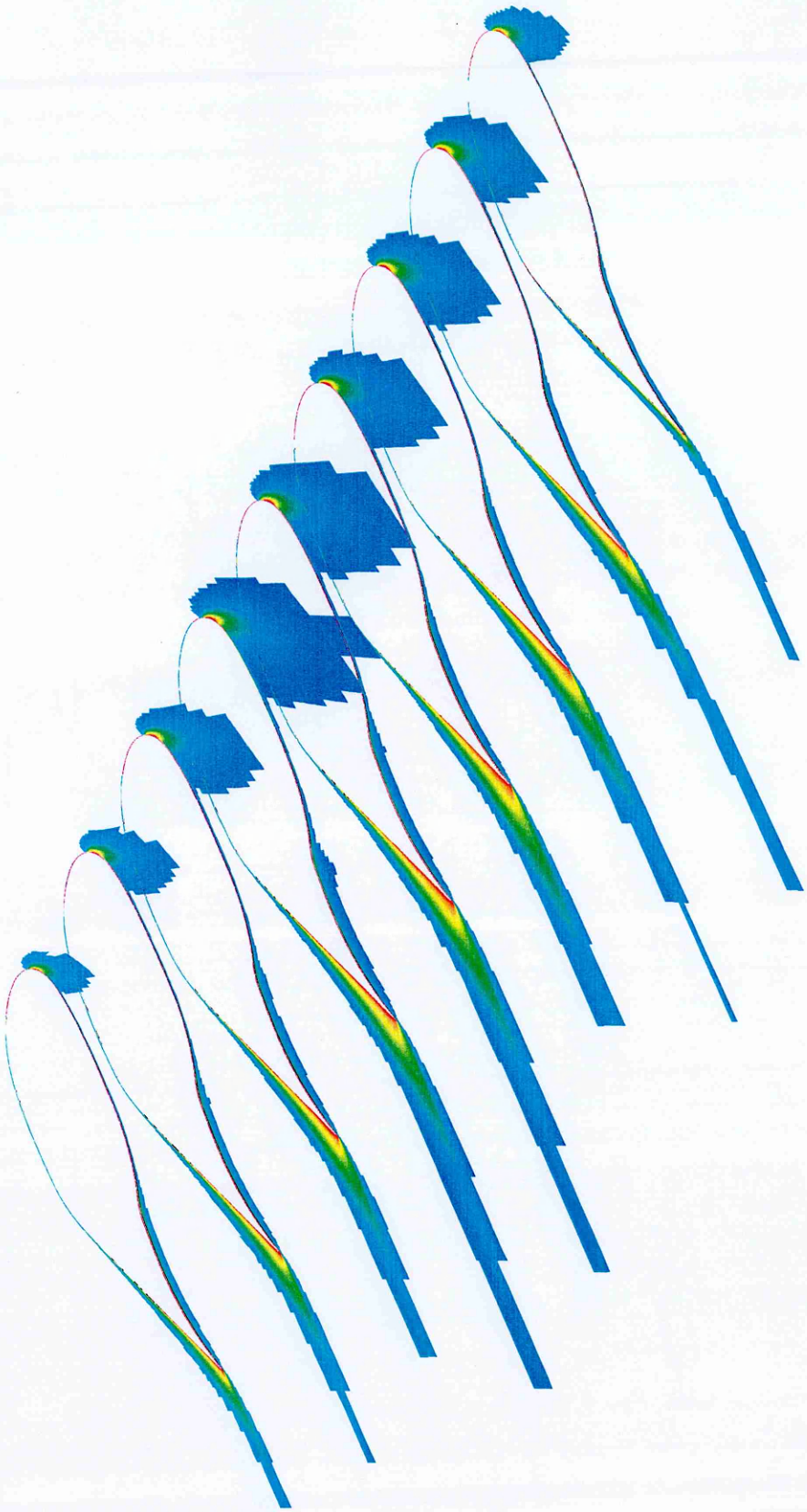

Figure: 7-58
Predicted colour shaded contours of u-velocity component on several streamwise planes, $\Lambda = 40°$, V = 60m/s, $\alpha^* = 14.2°$.

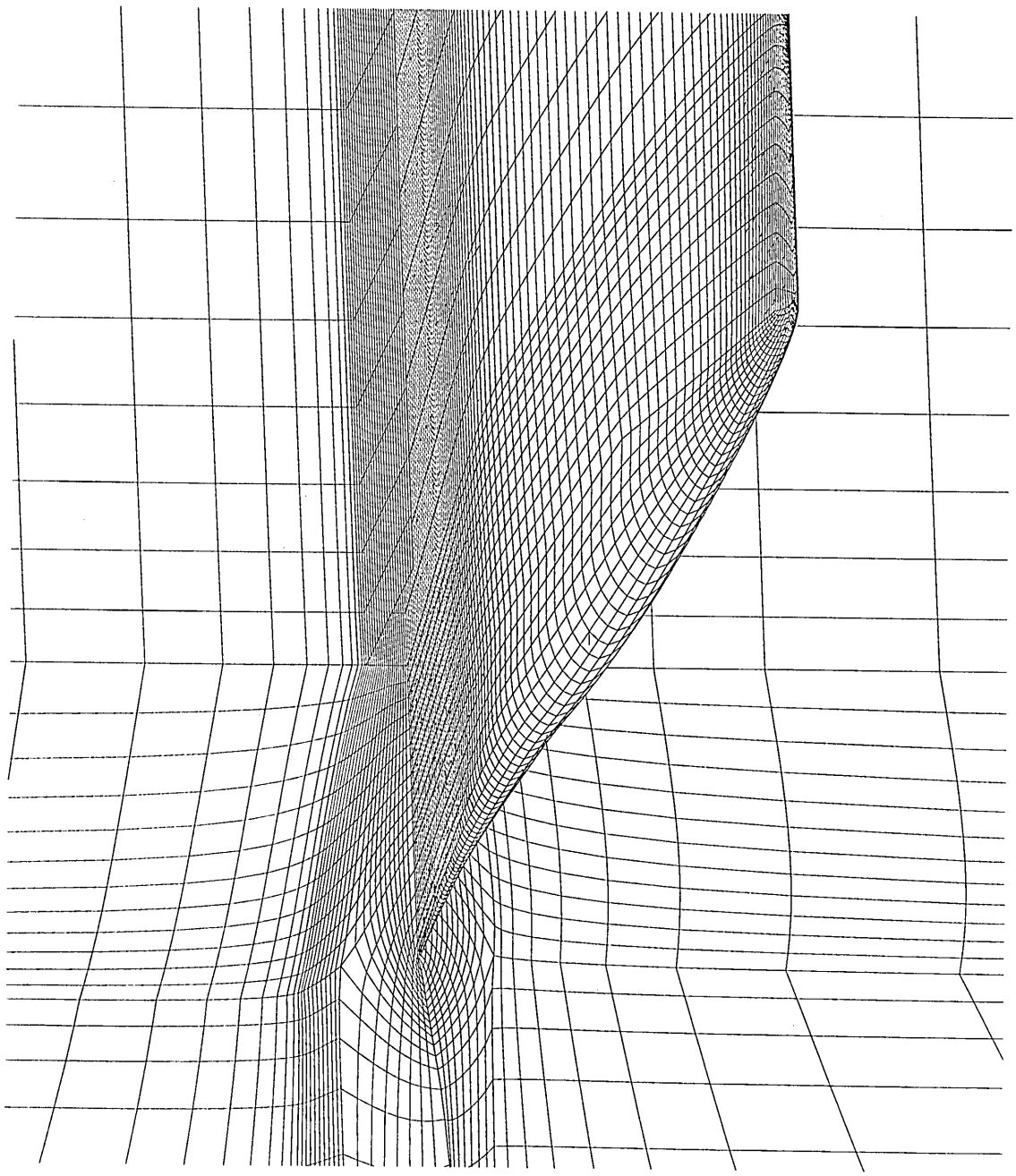

Figure: 7-59
SAUNA surface grids on the wing, shear layer boundary and control planes.

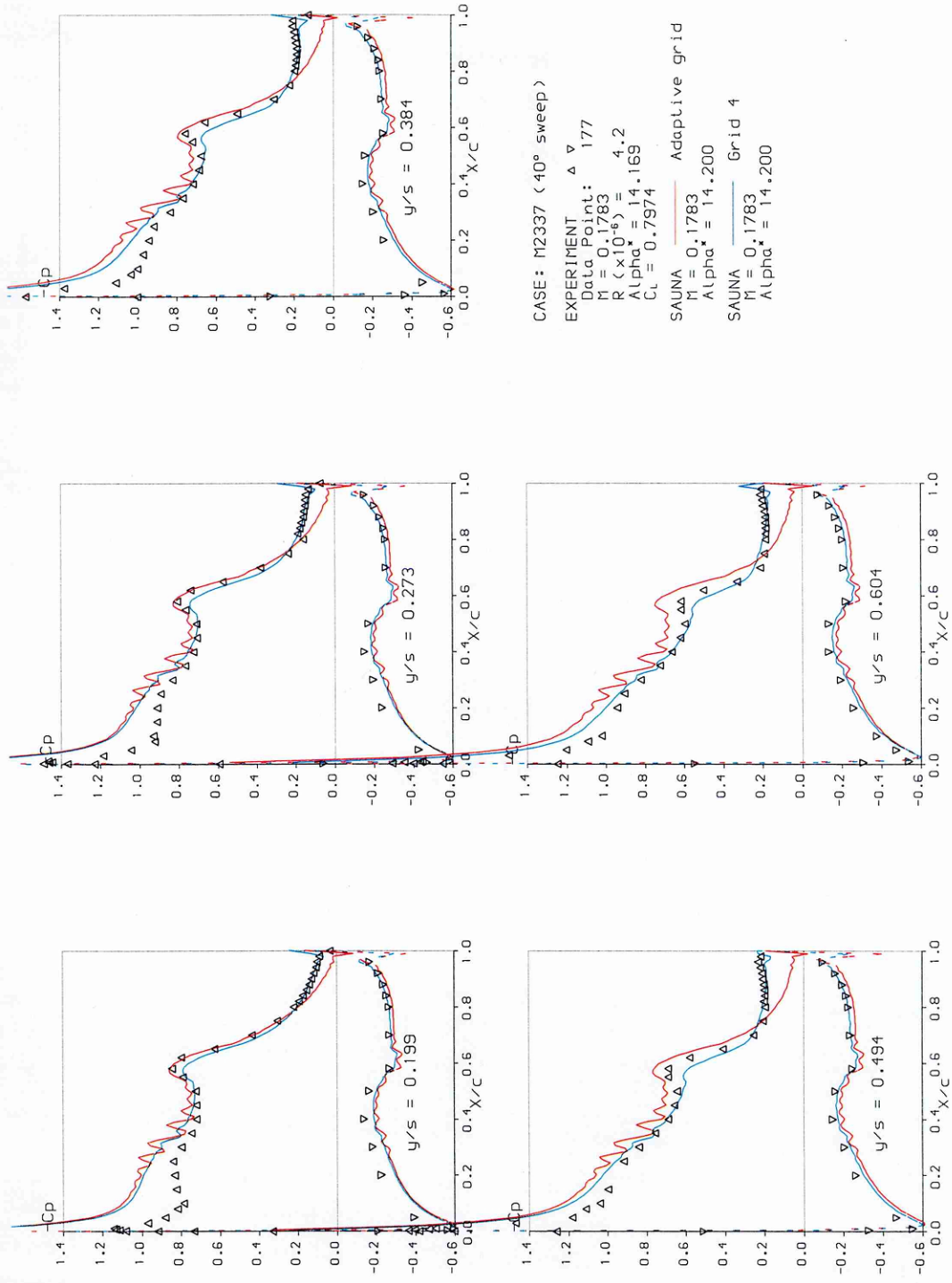

Figure: 7-60
Experimental and SAUNA pressure coefficient distributions, $\Lambda = 40°$, V = 60m/s.

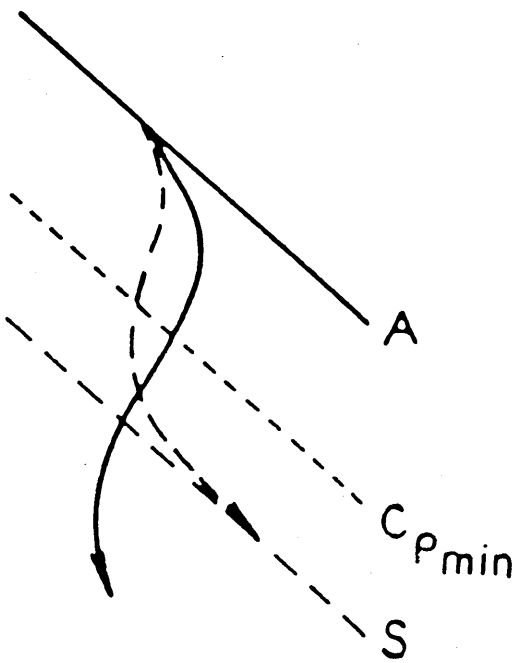

Figure: 8-1
Flow behaviour over swept wings (Kuchemann[22]).

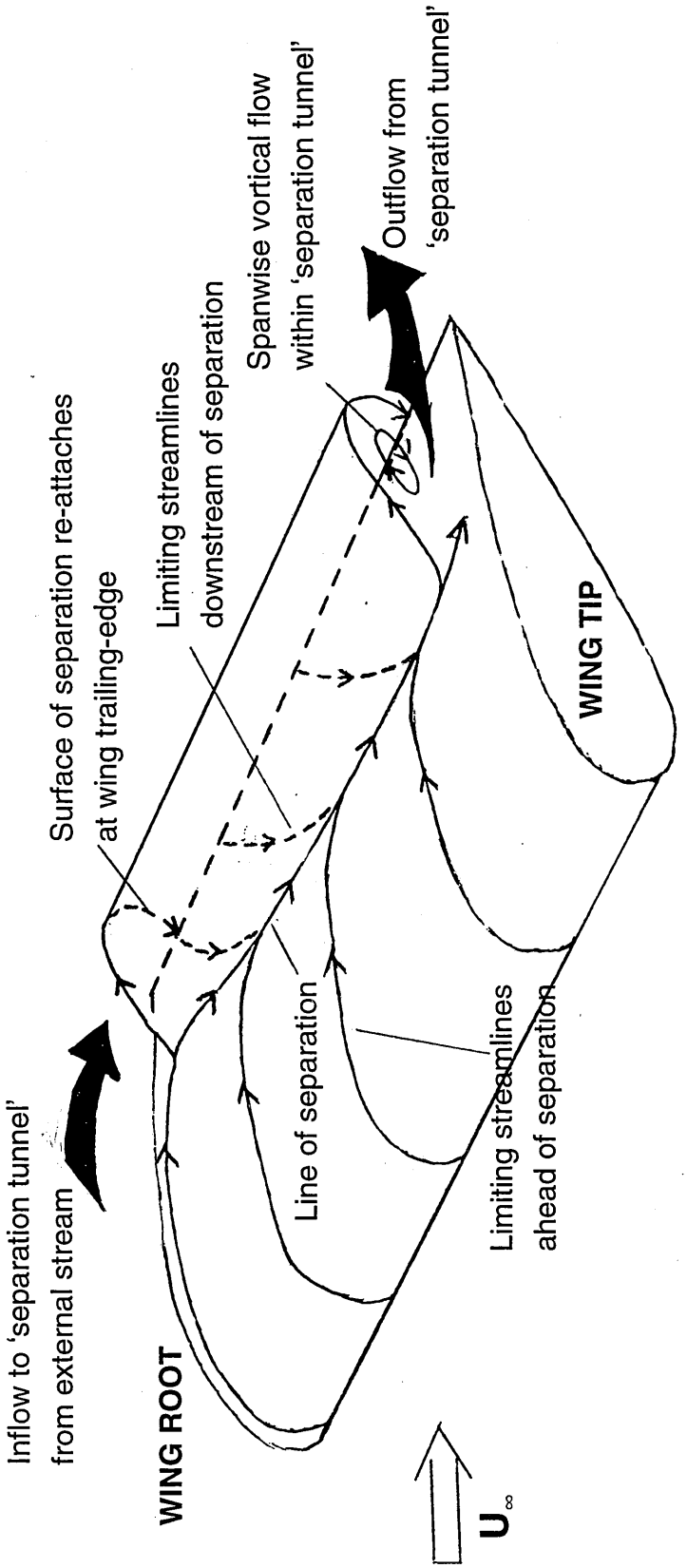

Figure: 8-2
Sketch to illustrate the swept wing separation mechanism.

Appendix A

Wing section co-ordinates for model 2337

Upper surface	
X/c	Z/c
0.000000	0.000006
0.000602	0.003317
0.002407	0.006715
0.005413	0.010176
0.009607	0.013688
0.014984	0.017251
0.021530	0.020860
0.029228	0.024520
0.038060	0.028228
0.048005	0.031989
0.059039	0.035798
0.071135	0.039643
0.084265	0.043504
0.098397	0.047353
0.113495	0.051158
0.129524	0.054883
0.146446	0.058489
0.164221	0.061944
0.182803	0.065207
0.202150	0.068247
0.222215	0.071032
0.242949	0.073533
0.264302	0.075722
0.286222	0.077573
0.308658	0.079062
0.331556	0.079988
0.354858	0.080931
0.378510	0.081556
0.402455	0.082038
0.426636	0.082374
0.450991	0.082556
0.475466	0.082581
0.500000	0.082445
0.524534	0.082145
0.549009	0.081677
0.573364	0.080520
0.597545	0.078329
0.621490	0.075085
0.645142	0.070722
0.668444	0.065532
0.691342	0.060156
0.713778	0.054674
0.735698	0.049168
0.757051	0.043701
0.777785	0.038331
0.797850	0.033096
0.817197	0.028023
0.835779	0.023142
0.853554	0.018470
0.870476	0.014026

Lower surface	
X/c	Z/c
0.000000	0.000006
0.000602	-0.003140
0.002407	-0.006040
0.005413	-0.008670
0.009607	-0.011040
0.014984	-0.013160
0.021530	-0.015040
0.029228	-0.016700
0.038060	-0.018170
0.048005	-0.019470
0.059039	-0.020640
0.071135	-0.021690
0.084265	-0.022620
0.098397	-0.023460
0.113495	-0.024210
0.129524	-0.024860
0.146446	-0.025410
0.164221	-0.025870
0.182803	-0.026240
0.202150	-0.026510
0.222215	-0.026700
0.242949	-0.026820
0.264302	-0.026850
0.286222	-0.026820
0.308658	-0.026710
0.331556	-0.026500
0.354858	-0.026280
0.378510	-0.025670
0.402455	-0.024720
0.426636	-0.023410
0.450991	-0.021740
0.475466	-0.019690
0.500000	-0.017230
0.524534	-0.014370
0.549009	-0.011100
0.573364	-0.007440
0.597545	-0.004550
0.621490	-0.002720
0.645142	-0.002010
0.668444	-0.001330
0.691342	-0.000740
0.713778	-0.000290
0.735698	-0.000026
0.757051	0.000020
0.777785	-0.000170
0.797850	-0.000590
0.817197	-0.001230
0.835779	-0.002090
0.853554	-0.003120
0.870476	-0.004320

0.886505	0.009819		0.886505	-0.005630
0.901605	0.005855		0.901605	-0.007040
0.915735	0.002150		0.915735	-0.008510
0.928865	-0.001270		0.928865	-0.010020
0.940961	-0.004390		0.940961	-0.011540
0.951995	-0.007220		0.951995	-0.013060
0.961940	-0.009730		0.961940	-0.014520
0.970772	-0.011940		0.970772	-0.015910
0.978470	-0.013850		0.978470	-0.017180
0.985016	-0.015460		0.985016	-0.018310
0.990393	-0.016780		0.990393	-0.019270
0.994587	-0.017800		0.994587	-0.020030
0.997593	-0.018530		0.997593	-0.020580
0.999398	-0.018970		0.999398	-0.020920
1.000000	-0.019120		1.000000	-0.021030

Appendix B

Method for sizing transition particles

$$R_k = 42.6(R_{xk})^{1/4}\,(1+0.2M^2)$$

Where,

k	particle size for fixing transition
xk	streamwise position of the transition trip
R_k	Reynolds number based on the particle size for fixing transition
R_{xk}	Reynolds number based on length xK
M	local Mach number